

Seismic attributes, well correlation and geostatistical analysis for sequence variability prediction in the Sleipner area

Andreas H. Hagset

GEO-3900 Master thesis in Geology

May 2016



Abstract

The upper Cenozoic stratigraphy in the northern North Sea (Sleipner area) have been investigated, using high quality 3D seismic data and five exploration wells. Interpretation of the seismic data, have indicated six distinct sequences (S1-S6). These sequences have been classified according to reflection configuration, and well log characteristics. Based on the seismic data, a simple model have been constructed for the upper Cenozoic succession. The model form the basis for co-kriging interpolation, which have been used to interpolate the petrophysical data from the well logs in each sequence. This gives the possibility to predicate how the petrophysical properties change laterally within the study area.

The upper most sequences (S1 – S3) is deposited from Pliocene to Holocene. These sequences have continuous reflections, with a parallel to subparallel reflection geometry. This configuration is often seen in sediments derived from glacio-marine processes. The well logs indicate that these sequences consist of shale, and the co-kriging interpolation, indicate that this lithology is dominant in the entire Sleipner area.

Sequence S4 correspond to the Utsira formation, which is currently used as a Co^2 storage. The Utsira formation consist of well-sorted sands, from Upper Miocene to Lower Pliocene. The seismic response, is characterized by low amplitudes, discontinuous reflections. This reflection configuration can be seen in relation to the shelf dominated, shallow marine environment, which the sequence was deposited in. The well logs clearly indicate a sand interval, and can be strongly correlated between the five wells. The co-kriging interpolation technique, indicated that the Utsira formation is present in the whole study area.

Sequence S5 was deposited during Middle Miocene. The sequence comprises several discontinuous reflections, with a disrupted configuration. Numerous anticlinal features have been observed at the base of the sequence, possibly caused by mobilized sediments, injecting into the sequence. The reflection configuration is highly affected by these features. The well logs indicate a shale dominated interval, with a few thin-layers of sand. The co-kriging interpolation, confirms a shale dominated lithology with localized sands in the study area.

Sequence S6 is deposited during Lower Miocene, and show a shale dominated lithology. The sequence comprise several high amplitude, discontinuous reflections. This configuration is related to extensive polygonal faulting of the sequence. The co-kriging results, suggest that sequence S6 consist of shale in major parts of the study area.

Acknowledgement

This research is funded by ARCEX partners and the Research Council of Norway (Grant number 228107).

Først vil jeg takke mine veiledere, Alfred Hansen og Iver Martens. Takk for god veiledning og godt samarbeid. Takk for entusiastisk undervisning i statistikk og oppfølging i Petrel. Takk for inspirasjon og kunnskap - jeg innser nå hvor kult romlig statistikk kan være!

Takk til alle venner og bekjente i Tromsø, dere har alle gjort studietiden til en fin tid. En spesiell takk til Bendik og Frank, som alltid har smilet lett tilgjengelig. Takk for at dere alltid belyser den humoristiske siden av verden og takk for at dere kommer meg gode råd og kritiske spørsmål. Vi holder kontakten!

Jeg vil også takke alle ved ARCEX og IG. Takk for hyggelige samtaler, god kaffe og en kjempe fin tid i Tromsø!

Takk til mor og far som har støttet meg igjennom all skolegang. Takk for at dere alltid stiller opp når jeg trenger hjelp og råd. Takk til brødre og søstre som har holdt meg på bakken og hjulpet meg igjennom studietiden.

Takk til min kjære Camilla, du har gjort dette året fantastisk. Takk for fine samtaler, latter, gode middager og lange skiturer. Gleder meg veldig til vår nye hverdag i Oslo.

Tusen takk alle sammen!

Andreas H. Hagset

Tromsø, 15. Mai 2016

Table of contents

1	Introduction	1
1.1	Objectives.....	1
1.2	Sedimentary principles	1
1.2.1	Seismic sequence stratigraphy	1
1.2.2	Seismic facies	3
1.3	Tectonic development	8
1.3.1	Faults	8
1.3.2	Rift basins.....	9
1.4	Well logs	13
1.4.1	Gamma ray logs (HGR)	13
1.4.2	Sonic or acoustic logs (HDT).....	14
1.4.3	Density logs (HRHOP).....	16
1.4.4	Neutron logs (HNPHI)	17
1.5	Geostatistics	19
1.5.1	Correlation and covariance.....	19
1.5.2	Semivariograms.....	21
1.5.3	Kriging and cokriging	24
2	Study area.....	27
2.1	Introduction	27
2.2	Location and structural outline.....	27
2.3	Geological evolution of the Norwegian North Sea	30
2.3.1	Paleozoic	31
2.3.2	Mesozoic	33
2.3.3	Cenozoic.....	37
3	Data and methods	45
3.1	Dataset.....	45
3.1.1	Polarity standard.....	45
3.2	Seismic resolution	46
3.2.1	Vertical resolution	47
3.2.2	Horizontal resolution.....	48
3.2.3	Artifacts and noise.....	51
3.3	Petrel - Interpretation and visualization	52
3.4	Seismic sequence classification	52
3.5	Seismic attributes	53

3.6 Well data	56
3.6.1 Well position	56
3.6.2 Well logs	57
3.6.3 Well seismic	60
3.7 Petrophysical modeling	61
3.7.1 Up-scaled well logs	62
3.7.1.1 Gamma ray logs (HGR)	63
3.7.1.2 Sonic logs (HDT)	65
3.7.1.3 Density logs (HRHOB)	67
3.7.1.4 Neutron logs (HNPHI)	69
3.7.2 Semivariogram fitting and co-kriging	71
4 Results	73
4.1 Seismic sequences	73
4.1.1 Seismic overview	73
4.1.2 Horizons	79
4.1.3 Age and thickness.....	80
4.2 Reflection configuration, well logs and features	86
4.2.1 Sequence S1	90
4.2.2 Sequence S2	91
4.2.3 Sequence S3	93
4.2.4 Sequence S4	94
4.2.5 Sequence S5	95
4.2.6 Sequence S6	96
4.2.7 Features	98
4.3 Seismic sequences: Summary tables	101
4.3.1 Reflection configuration summary	101
4.3.2 Well log summary	102
4.4 Co-kriging results	103
4.4.1 Sequence S1	104
4.4.2 Sequence S2	104
4.4.3 Sequence S3	105
4.4.4 Sequence S4	107
4.4.5 Sequence S5	109
4.4.6 Sequence S6	110
4.5 Inserting hypothetical wells	112

4.5.1 Predicting physical properties for hypothetical wells	113
5 Discussion	115
5.1 Sequence interpretation	115
5.2 Sequence variability	117
5.2.1 Sequence S1	117
5.2.1.1 Reflection configuration and features	117
5.2.1.2 Petrophysical data and distribution	117
5.2.1.3 Depositional environment	118
5.2.2 Sequence S2	119
5.2.2.1 Reflection configuration and features	119
5.2.2.2 Petrophysical data and distribution	120
5.2.2.3 Depositional environment	121
5.2.3 Sequence S3	123
5.2.3.1 Reflection configuration and features	123
5.2.3.2 Petrophysical data and distribution	123
5.2.3.3 Depositional environment	125
5.2.4 Sequence S4	127
5.2.4.1 Reflection configuration and features	127
5.2.4.2 Petrophysical data and distribution	127
5.2.4.3 Depositional environment	128
5.2.5 Sequence S5	130
5.2.5.1 Reflection configuration and features	130
5.2.5.2 Petrophysical data and distribution	131
5.2.5.3 Depositional environment	132
5.2.6 Sequence S6	134
5.2.6.1 Reflection configuration and features	134
5.2.6.2 Petrophysical data and distribution	135
5.2.6.3 Depositional environment	136
5.3 Correlation between well logs and seismic horizons	138
5.4 The co-kriging interpolation method.....	139
5.4.1 Correlation coefficient.....	139
5.4.2 Fitting the semivariogram	140
5.4.3 Hypothetical wells.....	141
6 Summary and conclusion	142
7 References	145

- 8 Appendix A 155
 - 8.1 Attributes composite line 1a..... 155
 - 8.1.1 Envelope..... 155
 - 8.1.2 Cosine of phase 156
 - 8.1.3 Dominant frequency 157
 - 8.1.4 Variance 158
 - 8.1.5 Variance with envelope 159
 - 8.1.6 RMS amplitude 160
 - 8.2 Attributes crossline 2875..... 161
 - 8.2.1 Envelope..... 161
 - 8.2.2 Cosine of phase 162
 - 8.2.3 Dominant frequency 163
 - 8.2.4 Variance 164
 - 8.2.5 Variance with envelope 165
 - 8.2.6 RMS amplitude 166

1 Introduction

1.1 Objectives

The tectonic and sedimentary development of the Cenozoic stratigraphy in the northern North Sea have been discussed by numerous authors (Jordt et al., 1995; Henriksen & Vorren, 1996; Michelsen et al., 1999; Eidvin et al., 2000; Jordt et al., 2000; Eidvin & Rundberg, 2001; Faleide et al., 2002; Eidvin & Rundberg, 2007). The seismic survey used for this study, contains high resolution 3D seismic that covers the uppermost Cenozoic deposits. The objectives for this thesis will be to identify and map the uppermost Cenozoic seismic sequences in the southern Viking Graben, and classify them according to reflection configuration, using high quality seismic data and attributes. The physical properties attained from five exploration wells, will aid in lithological and sequential classification. Furthermore, by using co-kriging interpolation, petrophysical data can be distributed in each corresponding sequence. This will give a good indication on how the lithology change laterally in the study area.

1.2 Sedimentary principles

Sedimentary facies is a stratigraphic unit with specified characteristics that reflect the conditions under which it was formed. These characteristics include the dimensions, sedimentary structures, grain size/shape, color and biogenic content etc. (Nichols, 2009). The term “Lithofacies” is a used if the description is confined to the physical and chemical aspects of transport and deposition of the sedimentary unit (Nichols, 2009; Veeken et al., 2013). The facies concept not only describes the rock types but forms the basis for facies analyses, and could be used to reconstruct paleo-environments (Nichols, 2009). The characteristic of an environment is determined by the processes that are present there, and as the environment change and fluctuate, it will give different facies.

1.2.1 Seismic sequence stratigraphy

Fundamental to sedimentology is the effect of tectonic uplift/subsidence, eustatic sea-level changes, and sedimentation characteristics (Nichols, 2009). The relationship between these, result in depositional sequences, and is defined as genetically related units bounded by unconformities and/or their correlative conformities (Mitchum et al., 1977; Vail, 1987; Veeken et al., 2013). The sedimentary fill of a basin is normally subdivided into different depositional cycles, in the same way that seismic sections are subdivided into depositional sequences based on unconformities and terminations (Mitchum et al., 1977; Veeken et al.,

2013). In seismic stratigraphy, the aim is to divide the sedimentary units into sequences based upon their termination such as onlap, toplap and downlap truncations (Vail, 1987; Catuneanu et al., 2011). Figure 1.1 show stratigraphic reflection terminations, in an idealized seismic sequences. Truncation implies that the reflection is cut by an unconformity. Toplap is a termination of reflections against an overlying surface as a result of non-deposition. Base discordant relations include onlap and downlap. Onlap is when seismic reflections are interpreted as horizontal, and terminate progressively against an incline surface. Downlap is when reflections are initially incline, and terminate down-dip against a horizontal or incline surface (Mitchum et al., 1977).

Depositional sequences can be further subdivided into seismic facies, and several seismic facies can be present within a single depositional sequence. The further focus of seismic stratigraphy studies, is to interpret these seismic facies with the aim to interpret the depositional environment and the distribution of lithofacies (Vail, 1987; Veeken et al., 2013).

The depositional sequences is composed of several stacks of system tracts, and the characteristics of these system tracts are based on relative sea-level changes (Brown & Fisher, 1977). If the sea-level rises faster than the supply of sediments towards the coastline the term “transgression” is used, and the depositional pattern is known as retrogradational. If sediments are supplied to a coastal area with a relative slow sea-level rise, it is called regression and the sediments built out, this pattern is called progradational. If the sea-level fall, the result is forced regression and the pattern is retrogradational, and may include erosion surfaces. If the sea-level and sediment supply remain relatively constant, a aggradational pattern could occur (Nichols, 2009).

In the transition from continental to marine conditions, there exist a number of different depositional environments and processes. For example; delta, alluvial fans, channels, floodplains, levees and overbanks, swamps, and many more. These depositional environments are found adjacent laterally to each other. These show different seismic expressions, and in the seismic section systematic reflections should be distinguished and classified if they are sedimentary reflections, unconformities, artefacts or non-sedimentary reflections like fault planes or fluid contacts (Veeken et al., 2013). Reflections are also observed to cross depositional environments, it is therefore assumed that the fluid content as well as cementations influence the acoustic impedance contrast. Reflections are also seen in nearly homogenous shales, this may also be related to fluid content and cementation (Veeken et al., 2013).

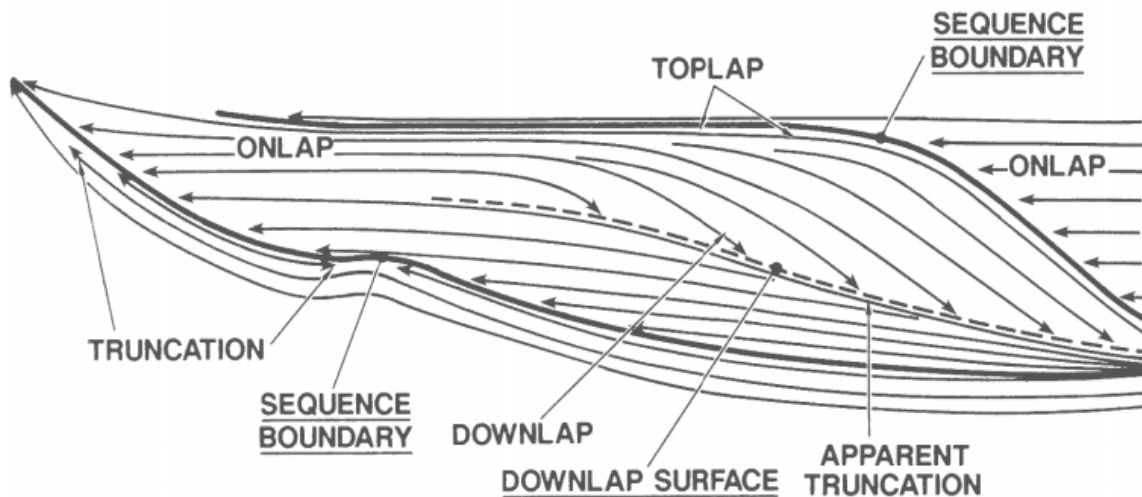


Figure 1.1: The main reflection terminations that is used in sequence stratigraphy classification. Figure is modified after Vail (1987).

1.2.2 Seismic facies

Seismic facies units is defined by Mitchum et al. (1977) to be mappable, three-dimensional seismic units which comprise groups of reflections whose characteristics differ from the adjacent units. When the internal reflection characteristics, external form and three-dimensional associations of these units are delineated, an interpretation of the processes, environmental setting and lithology can be made. By grouping reflections in a seismic sequence together based on common characteristics or parameters such as reflection continuity, reflection amplitude, frequency and geometry, seismic facies can be outlined (Mitchum et al., 1977; Veeken et al., 2013). Table 1.1 summarize the geological interpretation can be done based on the reflection parameters. These are important parameters which is fundamental for further seismic attribute generation and classification. Each parameter could give essential information about the geology in the subsurface (Mitchum et al., 1977). Figure 1.2 show examples of different seismic facies based on their reflection geometry and amplitude characteristics.

Reflection Parameter	Geological Interpretation
Configuration	<ul style="list-style-type: none"> • Bedding patterns • Depositional properties • Erosion and paleotopography <ul style="list-style-type: none"> • Fluid contacts
Continuity	<ul style="list-style-type: none"> • Lateral continuity of strata • Depositional process
Amplitude	<ul style="list-style-type: none"> • Velocity and density contrast of individual interfaces <ul style="list-style-type: none"> • Bed spacing • Bed thickness
Frequency	<ul style="list-style-type: none"> • Bed thickness • Fluid content
Interval velocity	<ul style="list-style-type: none"> • Lithofacies estimations • Porosity estimations <ul style="list-style-type: none"> • Fluid content

Table 1.1: An overview of the different reflection parameters and what kind of geological interpretation could be done based on each parameter. These are the reflection parameters used in seismic stratigraphy. Modified after Mitchum et al. (1977).

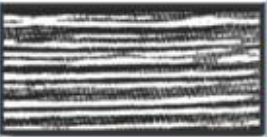
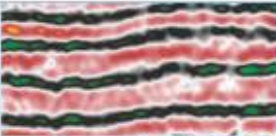

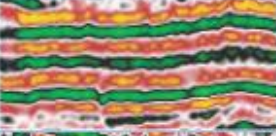
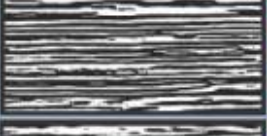
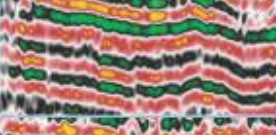
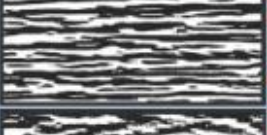


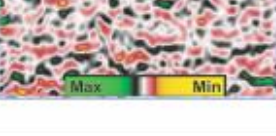
Seismic facies	Reflection geometry	Amplitude Characteristic	Seismic facies after Veeken et al. (2013)	Example from Survey ST98M3.3D
a)	Parallel continuous	Medium amplitude		
b)	Parallel continuous	High amplitude		
c)	Parallel continuous	High frequency & high amplitude		
d)	Subparallel discontinuous	High amplitude		
e)	Chaotic	Medium amplitude		

Figure 1.2: Examples of different seismic facies based on continuity, frequency, amplitude and configuration, a-e). Examples is used from the seismic survey in this study. There is no vertical scale attached to the examples, but each examples is approximated 100ms (TWT). The reflection amplitude is indicated in the bottom right corner. The figure is modified after Veeken (2007).

The geometry of a seismic facies consist of both the internal reflection configuration, and the external shape of the facies unit (Mitchum et al., 1977). The internal reflection configuration is often clearly seen in the seismic section, assuming good quality seismic data. The reflection configuration provides the foundation for basic facies analysis. The reflection configuration gives important information the conditions under deposition and distribution of the seismic units. An overview of some of the different reflection configuration is given in figure 1.3.

Parallel reflection patterns

The continuity of the layer is directly related to the sedimentary process that dominated, and may also reflected the depositional environment (Veeken et al., 2013). The reflection continuity is according to Mitchum et al. (1977) closely associated with the continuity of the stratigraphy, and therefore a good indicator of a uniform and parallel stratified deposit, expanding laterally.

The acoustic impedance provides information about the velocity as well as the density contrast between interfaces. lithological contrast and the spacing between different beds, is also important information provided by the reflection amplitude (Table 1.1) (Mitchum et al., 1977; Veeken et al., 2013).

The divergent reflection show a lateral thickening of the sediments, this indicates an asymmetrical sedimentation. These wedge-shaped bodies can be caused by variations in sedimentation rate and subsidence (Veeken et al., 2013). The wedge-shape of the deposit may indicate syn-depositional conditions and may show great lateral variability (Prosser, 1993; Veeken et al., 2013).

Discontinuous reflection patterns

Chaotic reflections are discontinuous and discordant reflections with an irregular pattern. Chaotic reflections also show a variable amplitude and frequency (Veeken et al., 2013). These reflections indicate according to Mitchum et al. (1977) sediments deposited in variable and high energy setting that could disturbed the layers. Channel fills, slumped deposits, olistostromes and over pressured shales are some of the different depositional environments and processes suggested by Veeken et al. (2013).

Disrupted reflections show a semi-continuous reflection patter, while the Hummocky reflection configuration show Irregular and discontinues reflections. The configuration has a variable amplitude and is characterized by regular reflection terminations (Veeken et al.,

2013). The hummocky configuration may indicate cut-and-fill geometries and contorted bedding. The contorted bedding is according to Veeken et al. (2013) the result of water escape under compaction and burial of the sediments, and is characterized in the seismic section by over steepening of sedimentary layers (Veeken et al., 2013).

Clinoforms

One of the most common features seen in regional seismic sections, is layers prograding and progressive developing on a gently dipping surface. These prograding patterns are called clinoforms, and are deposits that dip towards the basin center. They build out and deposit towards the architectural elements seen in deltaic to continental successions (Mitchum et al., 1977). There is a number of different configurations based upon variations in water depth and sediment deposition rate. Paleo-water depth can be interpreted from the height of prograding clinoforms (Mitchum et al., 1977).

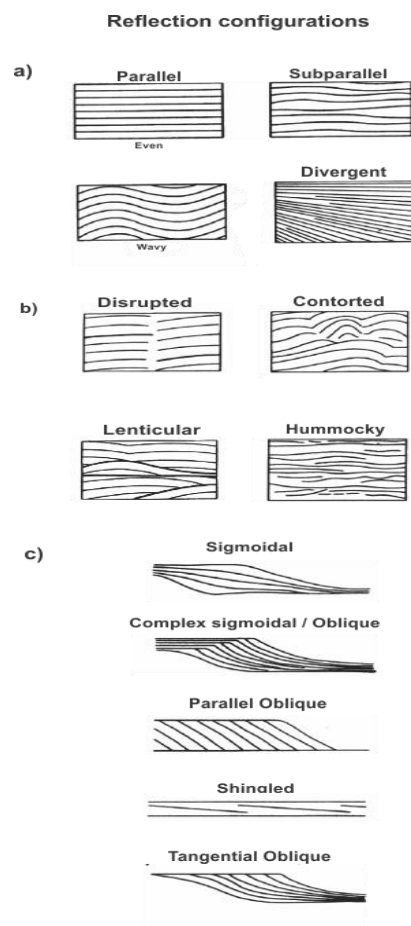


Figure 1.3: The common reflection configurations. a) Parallel, Subparallel and Divergent reflection configurations. b) Discontinuous reflection patterns. Disrupted, Contorted, Lenticular and Hummocky reflection configurations. c) Prograding clinoforms. Figure is modified after Mitchum et al. (1977).

External geometry of seismic facies

An understanding of how the sequences expands in three dimensions laterally throughout the basin is important. These external forms include a number of different shapes and geometries, and can be subdivided based upon the internal reflection configuration (Mitchum et al., 1977). These are the most common shelf seismic facies units, and their internal reflection configuration comprise a variety of parallel and divergent patterns that may indicate prograding sedimentary units (Mitchum et al., 1977). Figure 1.4 show the most common external geometries. The Sheet and sheet drape mainly consist of parallel internal reflections, indicating low-energy and uniform sedimentation. This relates to deep-marine conditions and should be mentioned (Mitchum et al., 1977). The sheet drape consist generally of fine grained sediments (Veeken et al., 2013). The wedge shape indicate a break in the sedimentation pattern, and on a smaller scale they represent a gradual change in depositional environment, and deposition rates. (Veeken et al., 2013). The bank or monoclinical geometry have an elongated shape and may also show substantial variations in the sedimentation pattern. They are associated with local high energy conditions (Veeken et al., 2013). Lenses can occur in many different facies configurations. However, they are most common as external forms seen in association with prograding clinofolds (Mitchum et al., 1977). Another type of external form, is the Mound configuration. These are build-ups of sediments either from clastic, volcanic or organic processes. The origin of mounds is very diverse and can therefore show different external shapes and internal seismic configuration (Mitchum et al., 1977). Lobes, deep sea fans, and contourite deposits are some of the deposits that could show mound geometries (Mitchum et al., 1977).

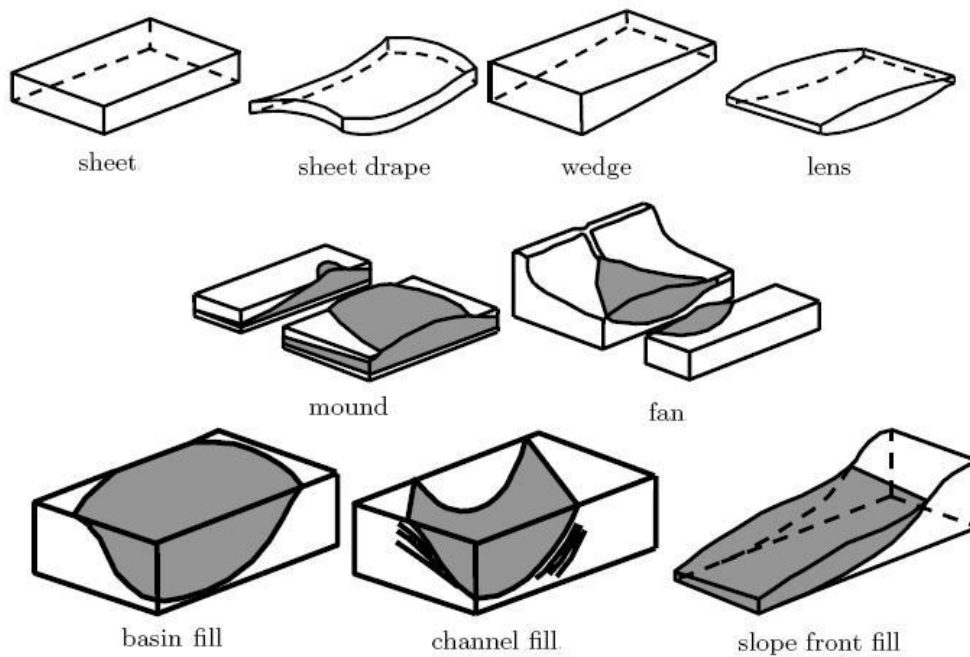


Figure 1.4: Overview of the different external geometries. Figure is modified after Mitchum et al. (1977).

1.3 Tectonic development

This chapter will provide background information towards the current configuration of the North Sea basin. The North Sea basin is a failed rift system that comprise a system of normal faults. These normal faults form the structural outline of the basin, and is essential in basin geometry seen today. The seismic used in this study only covers the post-rift section of the basin. However, a good understanding about the basin development and geometry is important in regard to the distribution and accumulation of sediments.

1.3.1 Faults

Figure 1.5 show the common fault types. Normal faults are dip-slip faults that form under extensional tectonic regimes. Normal faults is characterized by the downward movement of the hanging wall relative to the footwall, generally in a steep 60° angle (Twiss & Moores, 2007). This is a response to the stretching that occurs in brittle lithosphere. Normal faults often occur in systematic arrays or populations, associated with a tectonic extensional events. Structures common in these settings are horst and graben (Twiss & Moores, 2007). The horst and graben configuration is show in figure 1.6, and is characterized by an uplifted horst and a down-faulted graben. While grabens are bounded by two large conjugated faults, the half-grabens are only bounded by only one (Twiss & Moores, 2007). Horst and graben and half-grabens, are structures that dominate the North Sea basin.

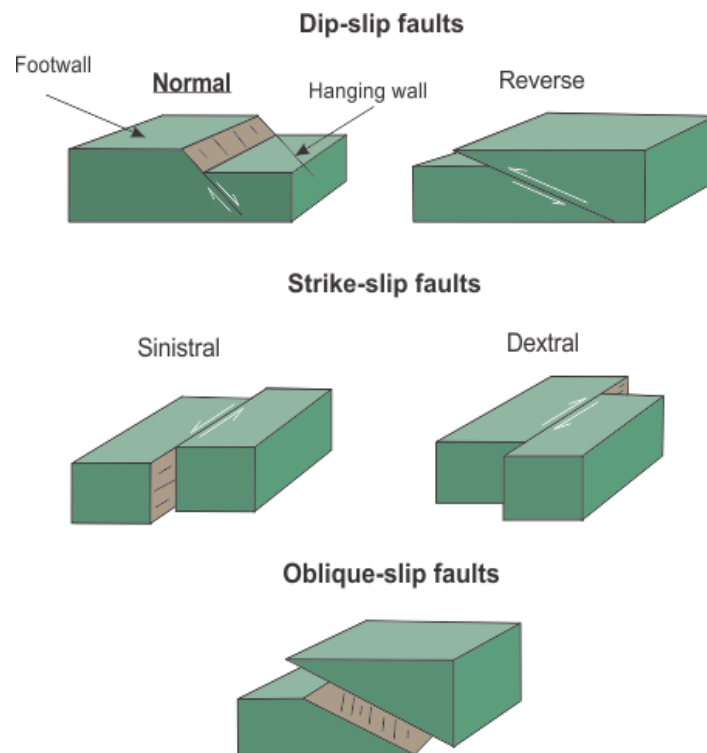


Figure 1.5: The different fault types (Dip-slip, Strike-slip and Oblique-slip) with their relative movement indicated with white arrows. Modified after Twiss and Moores (2007).

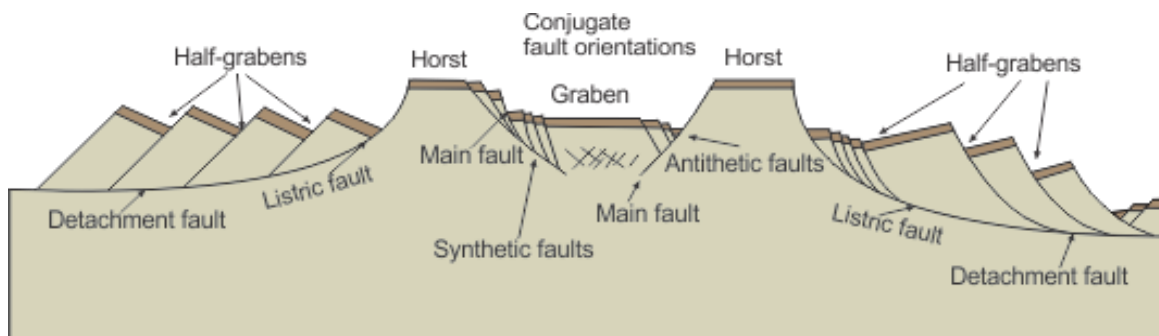


Figure 1.6: System of normal faults in an extensional tectonic regime. These normal faults occur with associated subsidiary faults. This simplified sketch represent the main structural outline of the North Sea. Modified after Twiss and Moores (2007).

1.3.2 Rift basins

Gawthorpe and Leeder (2000) implemented the initiation and growth of normal faults, and including the sedimentary response. This tectono-sedimentary model may accurately

represent the subsurface in an extensional setting. Figure 1.7 show the development of a fault array. The evolution and growth of the normal faults is subdivided into the Initiation stage, the interaction and linkage stage, and the through-going fault zone stage (Gawthorpe & Leeder, 2000). This development is central for the present day configuration of the North Sea basin.

The initiation stage is characterized by a larger number of fault segments, which show relatively small displacement. Low lying topography with isolated depocentres are developed by the early extension regime (Fig 1.7, A). Fault segments will eventually interact and link together as extension continue. In this stage the deformation is being localized along major faults, and the rate of displacement increases(Fig 1.7, B) (Gawthorpe & Leeder, 2000).

Following the interaction and linkage stage is the through-going fault zone stage. In this stage the deformation is localized in very few major faults, these faults form major half-graben and graben depocentres(Fig. 1.7, C) (Gawthorpe & Leeder, 2000). This development correspond to the basic development of the North Sea. The present day outline of the North Sea is mostly resulted from the extensive rifting events seen both in the Permo-Triassic transition and in the Mid -Jurassic to Early Cretaceous rifting phase (Zanella & Coward, 2003).

Figure 1.8 show these rifting phases under marine conditions. The initiation stage under these conditions is also dominated by a number of segment that form low-lying topography and creates several isolated depocentres (Fig. 1.8, A) (Gawthorpe & Leeder, 2000). These are early syn-rift depocentres and will show a great variation in sedimentary lithology, depending on sediment sources and position to the sea-level. This is seen in the Interaction and linkage stage both during highstand and lowstand (Fig. 1.8, B-C). The fault segments interact and propagate, resulting in an increase in displacement. Which further leads to the enlargement of depocentres as more accommodation space is created (Gawthorpe & Leeder, 2000).

Localization of deformation along the major fault zones will lead to an increase in subsidence rate. Subsidence rate might outpace the sediment input from drainage catchments and antecedent drainage, which will result in an overall deepening of the basin (Gawthorpe & Leeder, 2000). In the through-going fault stage, there is a high displacement rate on the active faults, as deformation is concentrated to a very few major faults. Displacement might outpace sediment input, and fault scarps is now areas with chutes and slumps scars. There is also a reversal in drainage, as footwalls are uplifted (Fig 1.8D) (Gawthorpe & Leeder, 2000).

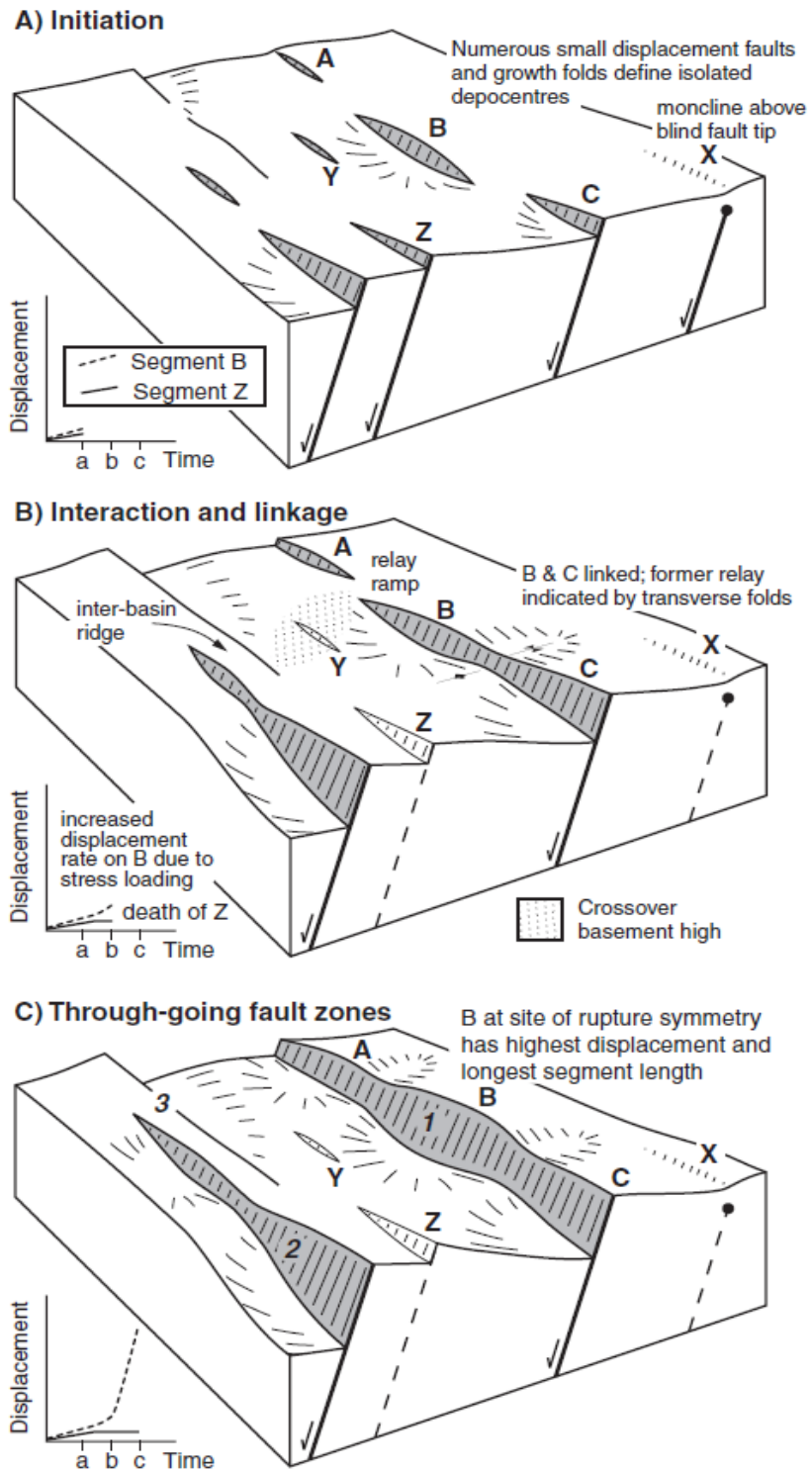


Figure 1.7: Schematic three-dimensional development of a fault array. There are three stages: A) Initiation stage B) Interaction and linkage stage C) Through-going fault stage. This development corresponds to the extensional development of the North Sea seen in Mesozoic. Figure is modified from Gawthorpe and Leeder (2000).

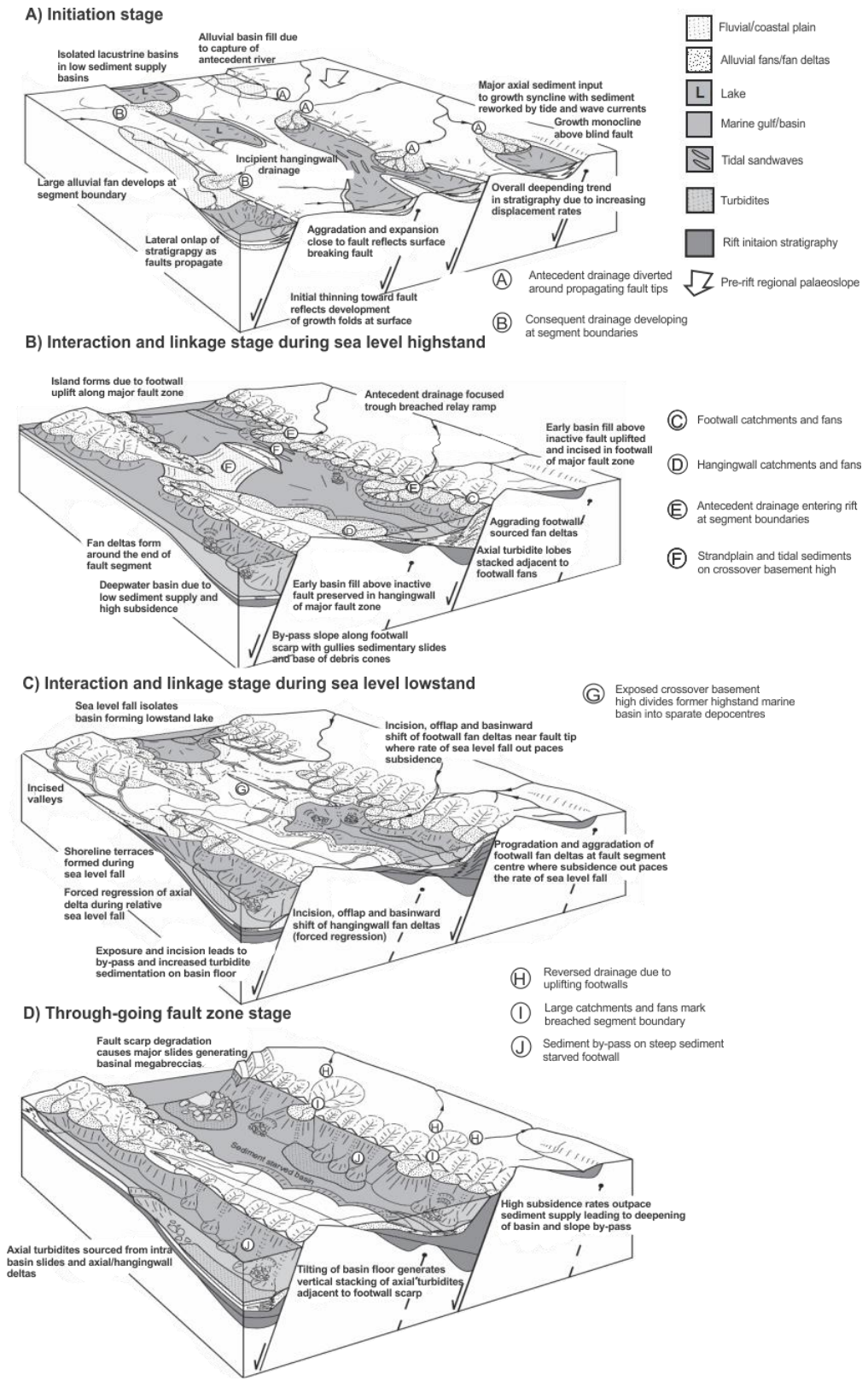


Figure 1.8: Tectono-sedimentary development of normal faults in marine conditions. A) Initiation stage, several small segments, with relative small displacement. B) Interaction and linkage stage during sea level highstand. C) Interaction and linkage during sea level lowstand. D) Through-going fault zone stage. Modified after Gawthorpe and Leeder (2000).

1.4 Well logs

There is a total of five wells in the study area, each of these contain logs that contain valuable physical data. Some of the well data only partly covers our seismic. Each well contain five logs; Gamma ray, density, sonic, and the neutron log. The function of these logs will be described in this chapter. This chapter is mainly based on the book “The Geological Interpretation of Well Logs” by Rider and Kennedy (2011).

1.4.1 Gamma ray logs (HGR)

The gamma ray log and some typical lithological responses is shown in figure 1.9. The gamma ray log measures the formations natural gamma radioactivity from uranium, thorium and potassium. A simple gamma log however, can't distinguish between these three individual elements, and simply gives a total count rate. Most rocks natural contain some amounts of gamma-emitting elements, metamorphic and igneous rocks contains more than sedimentary rock. However, among the different lithologies comprising sedimentary rocks, shales have the highest amounts. The gamma logs is often called the “Shale-log” as it is relative easy to distinguish shales from different lithologies such as sands and carbonates.

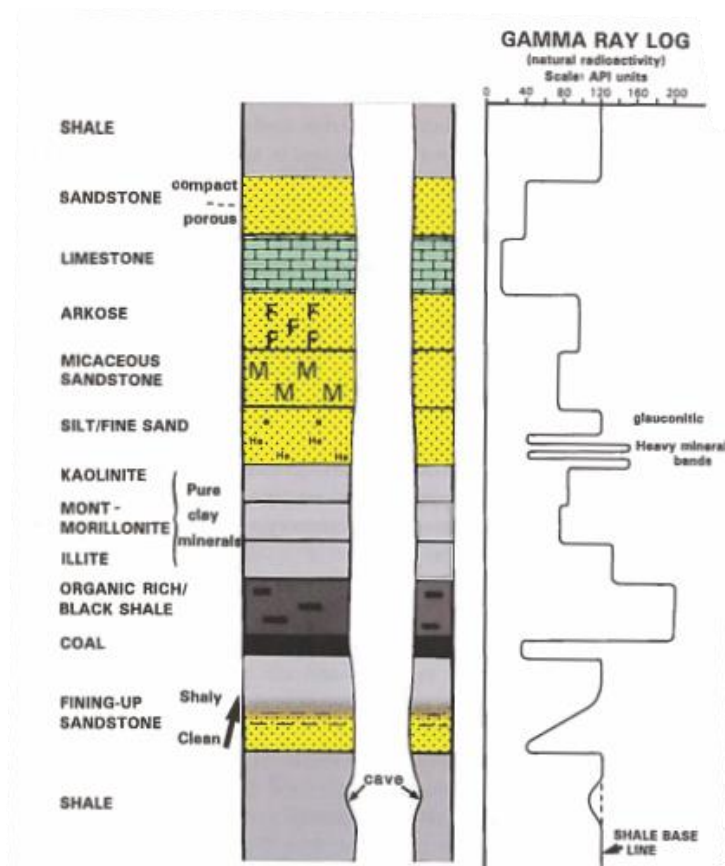


Figure 1.9: The gamma ray log and some typical lithological responses. Figure modified after Rider and Kennedy (2011).

The gamma ray logs is used in correlation of different data. During drilling, it is common practice to pick formation tops, especially in the overburden where it may be the only log available. The gamma ray log is a very good shale indicator. Based on the quality of the data it can be useful to identify lithology, and help suggest facies and key stratigraphic surfaces. Logging while drilling (LWD) gamma rays can be used to derive mineral volume and shale volume. It can detect the dominant clay minerals, give indications of depositional environment.

Gamma rays are highly energetic rays created in nuclear reactions either natural or artificial. Natural gamma radiation from rocks comes from as mention above uranium, thorium and a single isotope of potassium. As radiations from these elements pass through material their kinetical energy is effected and changed. The unit used for radioactive logging is the API (American Petroleum Institute) unit. And is defined at the University of Houston, an API unit is 1/200 of the difference between two radioactive reference units. The scale in the gamma ray log is usually designed so that an average shale reads about 100 API units.

The gamma ray is as an excellent indicator of shales, and an increase in API is often thought of as an Increase in shale content. However, radioactivity from other lithologies other than shales should be considered. Thus, lithologies indicated by the gamma ray log should be confirmed by using different logs.

Sandstones in general show low API values in the gamma log. This is related to the large amounts of non-radioactive quartz that comprise sandstones. However, associated with sandstones is also feldspars, mica, heavy minerals and lithic fragments. These contain different amounts of potassium, thorium, and uranium. Giving sandstones high to moderate API values. Marine sandstones could also have high API values related to the amount of Glauconite.

1.4.2 Sonic or acoustic logs (HDT)

The sonic log and some typical responses is illustrated in figure 1.10. By measuring the velocity of the formation, the slowness or the interval transit time can be established. The interval transit time (Δt) is found by measuring the time difference between a soundwave traveling from the top of the equipment through the drilling mud and the formation. As soundwaves tend to travel faster in the formation than the drilling mud, the interval transit time can be established (Selley, 1998; Rider & Kennedy, 2011). Sonic logs are principally used as an aid with seismic investigation. By tying the sonic log to the seismic, accurate depth

conversions and velocity profiles can be calculated. And by combining the sonic log with the density log, the acoustic impedance log can be produced, which is the first step in producing a synthetic seismogram.

The sonic log measures velocity, however the sonic log is common expressed as the interval transit time or slowness (Δt) as discussed above. Hence, slowness is the reciprocal of velocity. The standard unit of the log is either $\mu s/ft$ or $\mu s/m$, and typical values for different formations in the subsurface range from 50-150 $\mu s/ft$ (150-450 $\mu s/m$). The recorded slowness of a formation, especially from the compressional wave, is not a diagnostic tool for lithology. However variations are observed, and may indicate textural changes as well as changes in carbonate and quartz content. This can show a very distinct stratigraphic interval in the subsurface despite differences in depth. This makes the sonic log very good for correlating and may even be used to define fine grained stratigraphic intervals.

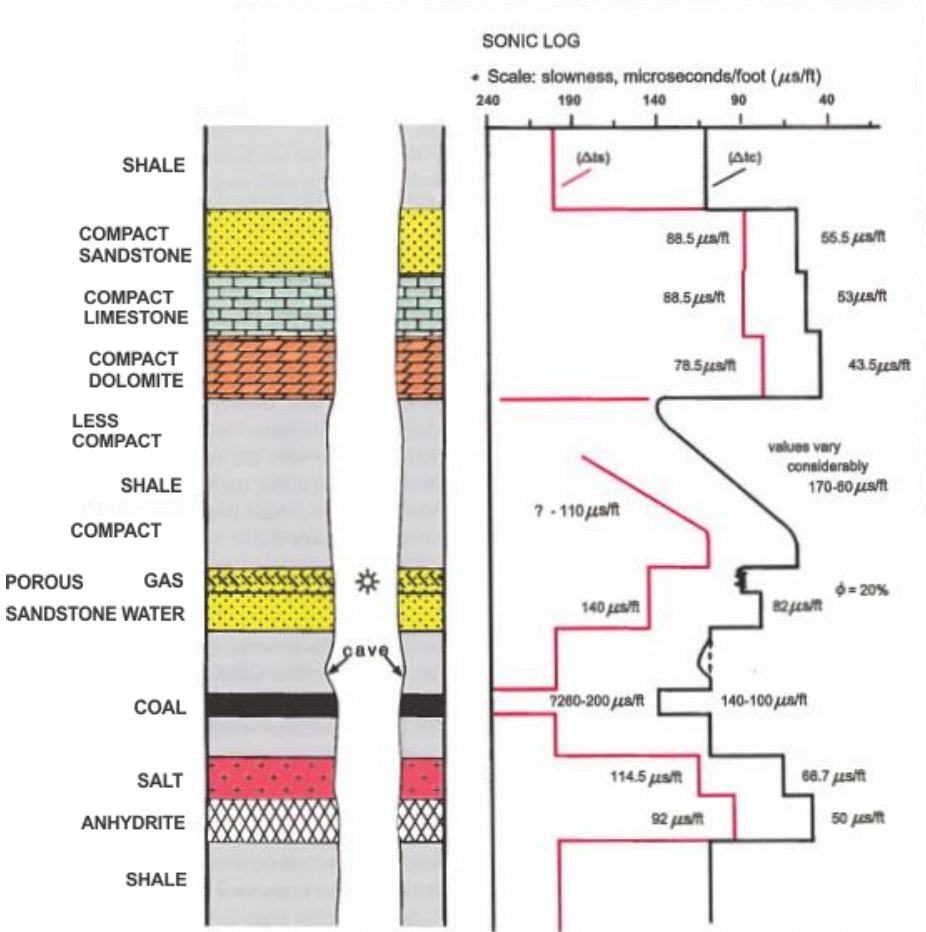


Figure 1.10: The sonic log and some typical responses to different lithologies. The red log is the primary compressional slowness, and black line is the secondary. The figure is modified after Rider and Kennedy (2011).

1.4.3 Density logs (HRHOP)

Figure 1.11 show the density log and some typical responses. The density log measures the formations bulk density. This includes the density of the formation and the density of the free fluids within the pore spaces. The density have an excellent vertical resolution compared to other logs. The density measurement tool is designed to operate in densities between 2 to 3 g/cm^3 with an accuracy of $0.01 g/cm^3$. The density log is used together with the sonic log to produce the acoustic impedance log, which is used to model seismic responses. The density log also provides good lithology indicators and could be helpful to identify different minerals. The organic content of source rocks and the quantity could also be estimated using density logs. Density could also be used to identify overpressure and is often combined with the neutron log.

The density log works by emitting gamma radiation into the formation, and measure the returning radiation. The emitted gamma rays scatter, this scattering is called Compton scattering. In high density formation the Compton scattering attenuation is high, and a lower amount of gamma rays have the energy to reach the measuring device. And in lower density formations the amount is higher. This change in count, correspond to density exponentially over the range of average density. The scale of the density log is usually plotted in a linear scale of bulk density in g/cm^3 . Different lithologies such as shale, sandstones, and carbonates are rarely defined by using density logs alone. The different lithologies show a great variability in composition and texture, making density logs a poor indicator of lithology. However, in combination with the neuron log it becomes probably one of the best indicators for general lithology

As shale gets buried further down in the subsurface, it is subjected to compaction. This correspond to a gradual decrease in porosity and an increase in density. Non-compacted shales at shallower levels normally show densities around $2.0 g/cm^3$. With depth the density gradually increases to $2.6 g/cm^3$. Mechanical compaction is dominant in the near sub-surface at low temperatures, while chemical compaction dominates further down. Compaction of shales is also an indication of age, as more compacted and older shales tend to be more dens than younger less compacted shales. However, the density of shales is closely connected to the mineral assemblage. For example, the presence of carbonates within the pore spaces can give high density values.

In sandstones variations in density is often associated with porosity changes, however this is not the case if taken into account the changes in grain density. Pure sands (orthoquartzites) has a grain density of 2.65 g/cm^3 , this is the ideal sand, and will change with the mixture of non-quartz components. Sand are often mixed with lignite fragments ($0.5\text{-}1.8 \text{ g/cm}^3$), micas ($2.82\text{-}2.99 \text{ g/cm}^3$) and feldspars ($2.52\text{-}2.74 \text{ g/cm}^3$). Heavy minerals may also be present ($3.0 - 4.19 \text{ g/cm}^3$). Hence, by measuring the density, mineral content could be estimated.

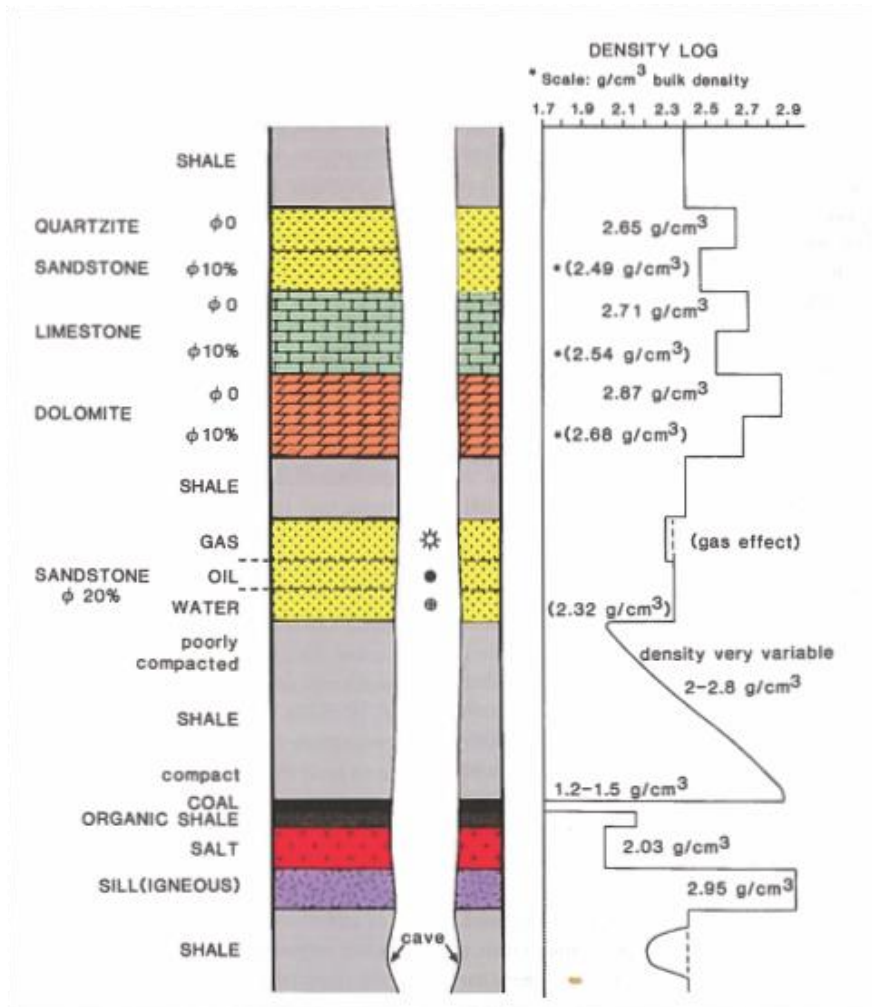


Figure 1.11: The density log and some typical responses. The density log shows the bulk density. Figure is modified after Rider and Kennedy (2011).

1.4.4 Neutron logs (HNPHI)

The density log with some typical lithologic response is shown in figure 1.12. The neutron log comprise a high energy radioactive source that emits neutrons. The emitted neutrons respond to the amount of hydrogen present in the formation. Hence, the count of the returning neutron is related to the hydrogen content, this count is known as the formations hydrogen index. High amounts of hydrogen in the subsurface will modify the neutron response, the neutron log is therefore an excellent tool in estimating the amount of water present in a formation. As most

of the hydrogen in subsurface environments exist as water, the hydrogen index can be used as a direct relation to porosity, and the log output will be given in neutron porosity units (ΦN), which is given as either a fraction or percentage (Selley, 1998; Rider & Kennedy, 2011). The neutron log is mostly used to calculate porosity, but in combination with the density log it is also used for the estimation of shale volume.

Variations in mineral content will give noticeable neutron responses, especially in shales, where different mixtures of quartz, carbonate and organic content could influence the log response. Clays have high hydrogen index and will show lower neutron values with an increase in quartz content, this is often seen in coarsening-upwards deltaic sequences where the mineral content varies greatly.

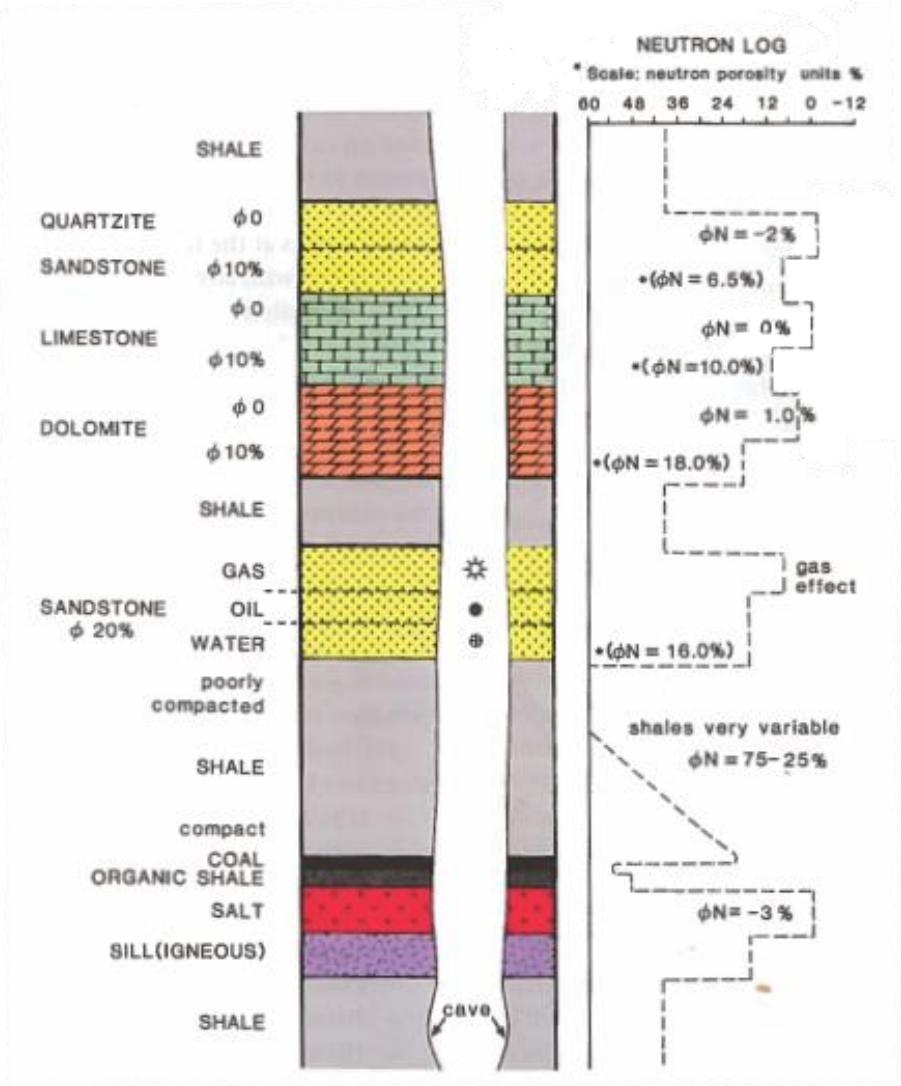


Figure 1.12: The density log with some typical lithological responses. Figure is modified after Rider and Kennedy (2011).

1.5 Geostatistics

Geostatistics is a comprehensive and complex subject. The detailed calculations and proofs are beyond the scope of this study. An introduction and description of the geostatistical tools will be given in this chapter. Geostatistics aim to provide quantitative descriptions of natural variables disturbed in space (Chiles, 2012). Such variables could be geological or petrophysical values, such as porosity or permeability. Geostatistics is used in this thesis to predict well log values in the interpreted sequences.

1.5.1 Correlation and covariance

Covariance

There is often a statistical dependence between two variables. As mentioned, two variables can be many different things, for example, seismic amplitudes and porosity values. The objective is to investigate whether there is a statistical coherence/dependence between the two variables. The covariance function represents some form of similarity, as the assumption that points close to each other are likely to have similar values. The covariance function is here given by Løvås (2013). The covariance between the two random variables X and Y is given as

$$C(X, Y) = E[(X - \mu_X)(Y - \mu_Y)] \quad (1.1)$$

where the expectation operator is given as $\mu_X = E[X]$, $\mu_Y = E[Y]$ and $E[\cdot]$ is

$$E[X] = \int_{-\infty}^{\infty} x f_x(x) dx.$$

The probability density function for the variable X is here $f_x(x)$.

To extend this equation to represent spatial similarity, some notation is necessary. Consider a random variable $Z(u)$ in a domain D. The estimated covariance of a regionalized variable is given by Sinclair and Blackwell (2002)

$$C(h) = \frac{1}{N(h)} \sum_{\alpha=1}^{N(h)} Z(u_\alpha) \cdot Z(u_\alpha + h) - m_0 \cdot m_h. \quad (1.2)$$

The vector of spatial coordinates is here u , and have components x , y and z in 3 dimensions. The variable under consideration is given as $Z(u)$, and is a function of spatial location. The lag vector h , is the separation between two spatial locations. The lagged version of the variable under consideration is then $Z(u + h)$. The number of data points separated by lag is $N(h)$. The expected values (means) are here m_0 and m_h , of the regionalized variables $Z(u)$ and $Z(u_\alpha)$. The expected values are

$$m_0 = \frac{1}{N(h)} \sum_{\alpha=1}^{N(h)} z(u_\alpha) \quad m_h = \frac{1}{N(h)} \sum_{\alpha=1}^{N(h)} z(u_\alpha + h). \quad (1.3)$$

Correlation

The correlation between two random variables is the cornerstone in geostatistics. The correlation coefficient is a measure of how well the dataset fits a linear curve (Løvås, 2013). In spatial statistics, the correlation is the covariance function over the corresponding standard deviations. The correlation coefficient is here given by Bohling (2005) to be

$$\rho(h) = \frac{C(h)}{\sigma_0 \sigma_h}. \quad (1.4)$$

The corresponding estimated standard deviations σ_0 and σ_h are

$$\sigma_0 = \frac{1}{N(h)} \sum_{\alpha=1}^{N(h)} [z(u_\alpha) - m_0]^2 \quad \sigma_h = \frac{1}{N(h)} \sum_{\alpha=1}^{N(h)} [z(u_\alpha) - m_{+h}]^2. \quad (1.5)$$

The absolute value of ρ indicates how strong the linear relationship is between two variables (Løvås, 2013). The value of ρ will always be between -1 and 1. The greater the absolute value of ρ , the stronger the correlation. If there is no correlation between the two variables, ρ will

be 0. Increasing the number of data points will increase the certainty of the correlation coefficient for the dataset. (Løvås, 2013). The correlation function is very useful, as it gives the possibility to predict values of the variables. However, the same correlation value can be seen in different datasets with a totally different data distribution. Some linear relationships are shown in different datasets in Figure 1.9. The correlation is very small for the first dataset seen in figure 1.9a. The correlation coefficient is 0 if the data points are gathered together, and show no linear relationship. If the data points is perfectly aligned the correlation is 1, and there is a perfect linear relationship (Fig. 1.9b). If the data points is spread out, and the expected value of X increases with the Y value, the correlation is positive (Fig. 1.9c). If the dataset indicate that an increases in X values, will lead to a decreases in Y values, the correlation is then negative (Fig. 1.9c).

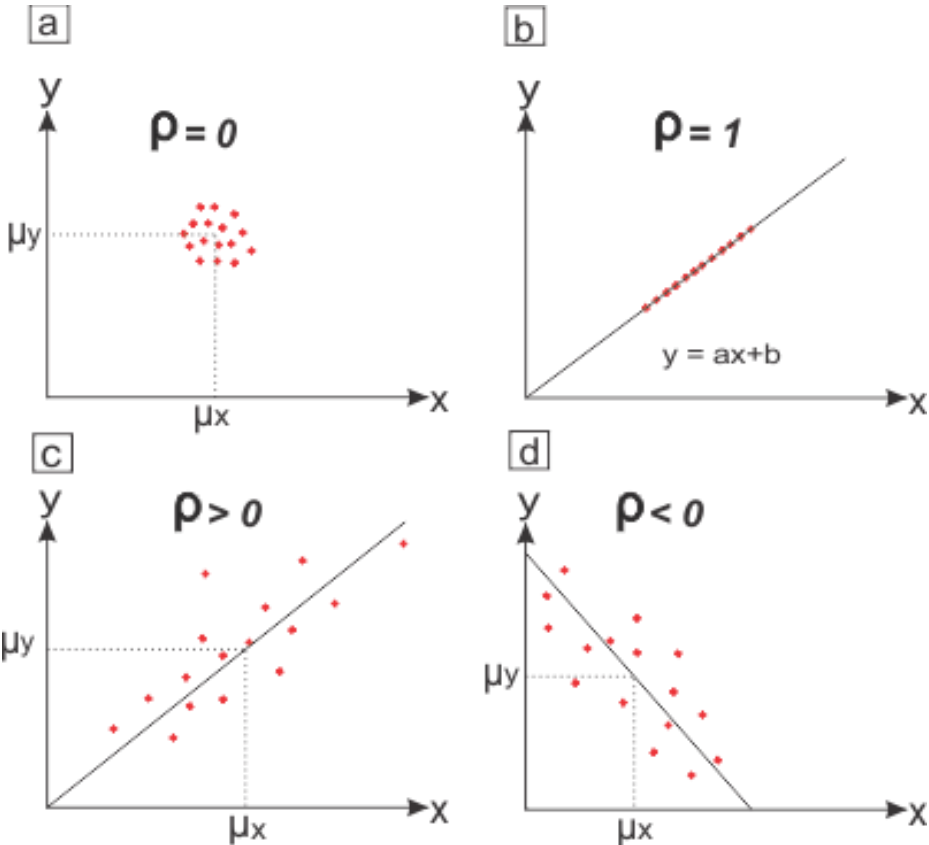


Figure 1.9 shows four datasets a-d, with corresponding correlation values. The red dots represent data points.

1.5.2 Semivariograms

Variogram, also called semivariogram and semivariance, hence, concerning the terminology there is some confusion (Bachmaier & Backes, 2008). While covariance and correlation are

measures of similarity, semivariance is a measure of dissimilarity. The experimental semivariogram is here given by Sinclair and Blackwell (2002)

$$\gamma(h) = \frac{1}{2N(h)} \sum_{\alpha=1}^{N(h)} [Z(u_{\alpha} + h) - Z(u_{\alpha})]^2.$$

(1.6)

The semivariogram is half the mean squared differences of values separated by lag (Sinclair & Blackwell, 2002). The formula denotes the regionalized random variables $Z(u_{\alpha})$ and $Z(u_{\alpha} + h)$, where u_{α} and $u_{\alpha} + h$ are the spatial position separated by the lag vector h . Hence, it is a function that relates semivariance (or dissimilarity) of all the data points, to the distance that separates them. Generally the semivariogram is an increasing function with distance h , since the further away data points are from each other, the higher the dissimilarity (Matheron, 1963). The first step when determining an experimental semivariogram, is defining a model for $\gamma(h)$. This implies to find the function that best represent the dataset (Sinclair & Blackwell, 2002). Figure 1.10 show a function determined for a hypothetical dataset, the increasing function is referred to as a model. Petrel gives the opportunity to use different models, and the modeling process is of great importance, as it directly influences the result of the kriging interpolation (Chiles, 2012).

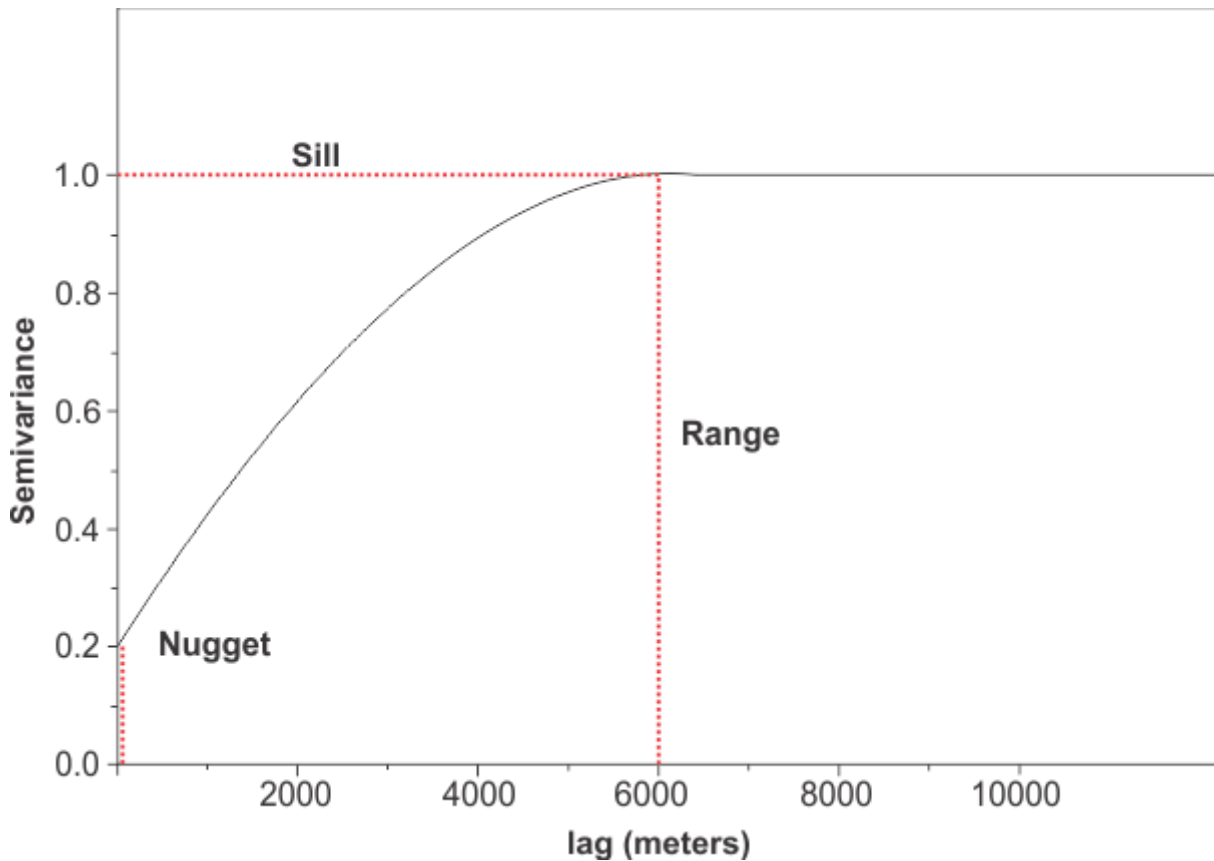


Figure 1.10: An ideal semivariogram, with semivariance $\gamma(h)$ along the y-axis and lag h along the x-axis. Nugget, Sill and range are indicated on the model. The figure is modified after Bohling (2005).

The shape of the semivariogram model is characterized in terms of specified parameters.

These are the sill, range and nugget (Fig. 1.10). Sill is the semivariance value at which the variogram levels off, and there is no correlation between data points beyond this line (Fig. 1.10) (Diggle & Ribeiro, 2007).

Range is the distance at which the semivariogram reaches the sill. There is no correlation beyond the range. Hence, the range is the distance at which there is a correlation between variables. (Fig.1.10) (Schlumberger, 2014).

The nugget effect should be zero at the origin with zero lag. However, if there are many data points close to the origin with higher semivariance values, a nugget has to be set. The nugget represents variability at small distances, smaller than the typical sample spacing in the dataset, this also included measurements errors. In practice, setting a nugget value will force spatial predictions to interpolate the data. Hence, care should be taken when fitting a nugget value to the model (Fig. 1.10) (Diggle & Ribeiro, 2007).

1.5.3 Kriging and cokriging

Kriging and cokriging are interpolation methods based on regression against observed values surrounding data points, weighted according to spatial covariance values (Matheron, 1963; Bohling, 2005; Chiles, 2012). In other words, kriging estimates spatial values between obtained data points, and data points near each other have higher covariance values than points further away, and will be weighted to a higher degree in the kriging interpolation. In many cases there is a limited number of data points available. Hence, all data points should be taken into account. And their contribution should be weighted by the strength of their correlation with prediction locations (Sinclair & Blackwell, 2002). Wells might represent these limited data points within an area. The method was first developed by Matheron (1963), who first applied it to estimate the quality of ore deposits. Figure 1.11 shows a simplified sketches of the basics of kriging and cokriging. In kriging, the prediction of the variable Z_4 at the location in the center (red dot), is a weighted sum of the three measurements Z_1 , Z_2 and Z_3 . Coefficients a_1 , a_2 and a_3 are functions of the covariance model, which describes the spatial correlation of Z . In cokriging, a secondary variable is introduced (X). Hence, the predicted value of the variable Z_4 at the center location is the weighted sum of both the three Z variables and the two X variables. Coefficients b_1 and b_2 are functions of a cross-covariance model which describe the spatial correlation between the two variables. X is used as a secondary set of measurements

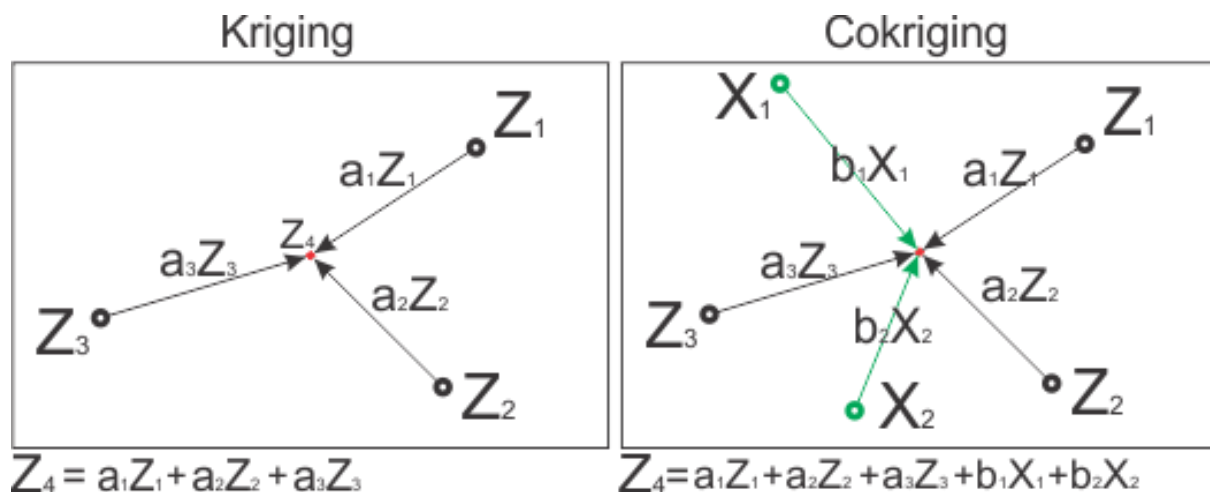


Figure 1.11: Simplified sketches of the basics of kriging and cokriging. Figure modified after Krivoruchko et al. (2014).

The simple kriging estimator of $Z^*(u)$ is here given by Bohling (2005)

$$Z^*(u) = m(u) + \sum_{\alpha=1}^{n(u)} \lambda_{\alpha} [Z(u_{\alpha}) - m(u_{\alpha})]$$

(1.7)

where u and u_{α} are location vectors, one for the estimation point and one of the neighboring data points, respectively. Furthermore, $n(u)$ is the number of data points in the local proximity used for estimation of $Z^*(u)$ and $m(u)$, $m(u_{\alpha})$ are expected mean values of $Z(u)$ and $Z(u_{\alpha})$. The weight assigned to a point $z(u_{\alpha})$ for estimation at location u is denoted $\lambda_{\alpha}(u)$. The same point will receive different weights for different estimation location. It is important to remember that kriging is a technique that uses a variogram to define the spatial variability of the input data. The objective is to pick weights that minimizes the estimated average variance. A variogram model must be defined by the user, with orientation, nugget and range. The input is given by the user and the algorithm will not calculate values larger or smaller than values defined by the input data (Schlumberger, 2014). Hence, the result of the interpolation is just as good as the input data and the variogram fitting.

Cokriging

Cokriging methods are designed to take into consideration two or more regionalized variables that are related to each other. Cokriging is especially useful when the primary attribute (well data) is sparse in the study area, but the secondary attribute (seismic data) is abundant. Cokriging requires specification of a correlation coefficient, between the primary and secondary data (Goovaerts, 1998; Chiles, 2012; Schlumberger, 2014). Cokriging is simply an extension of the kriging equation. The secondary variable or attribute is used to guide the interpolation of the primary variable known at the well location. Simple cokriging is defined by Goovaerts (1998)

$$Z^*(u) - m_1 = \sum_{\alpha_1=1}^{n_1(u)} \lambda_{\alpha_1}(u) [Z_1(u_{\alpha_1}) - m_1] + \sum_{\alpha_2=1}^{n_2(u)} \lambda_{\alpha_2}(u) [Z_2(u_{\alpha_2}) - m_2].$$

(1.8)

Cokriging models are efficient, but they require certain restricting assumptions, these include assumptions about the data normality and stationary (Krivoruchko et al., 2014). Stationary implies that the mean and variance of values do not depend on location (constant in a given

area). This is related to the term homogeneity, used by geologist to characterize similar geological characteristics (Sinclair & Blackwell, 2002). A field or volume could be called stationary if the same population is being sampled at every location in that field. This implies no trend in the data. Hence, for every location u in the domain D , the expected value of $Z(u)$ is m , the mean value of the domain (Sinclair & Blackwell, 2002).

2 Study area

2.1 Introduction

In this chapter the location of the study area will be put in a larger context with regards to the geological framework of the Norwegian North Sea. The following sub-chapters will give a more detailed description of the tectonic evolution and basin formation. The seismic data used in this study only covers the uppermost Cenozoic deposits. Hence, the stratigraphy will be given more attention in this Era.

2.2 Location and structural outline

The study area is located in the North Sea, in the Southern Viking Graben (SVG) (Fig. 2.1 & 2.2). The area has undergone several tectonic episodes, and different environmental settings. It has gone from desert to marine conditions and been subjected to volcanic influence (Fig.2.3). The North Sea rift is a complex rift system that form a triple junction system, with the Viking Graben, the Central Graben and the Moray Firth basins as the main regional rift structures (Fig. 2.2) (Ziegler, 1992; Zanella & Coward, 2003).

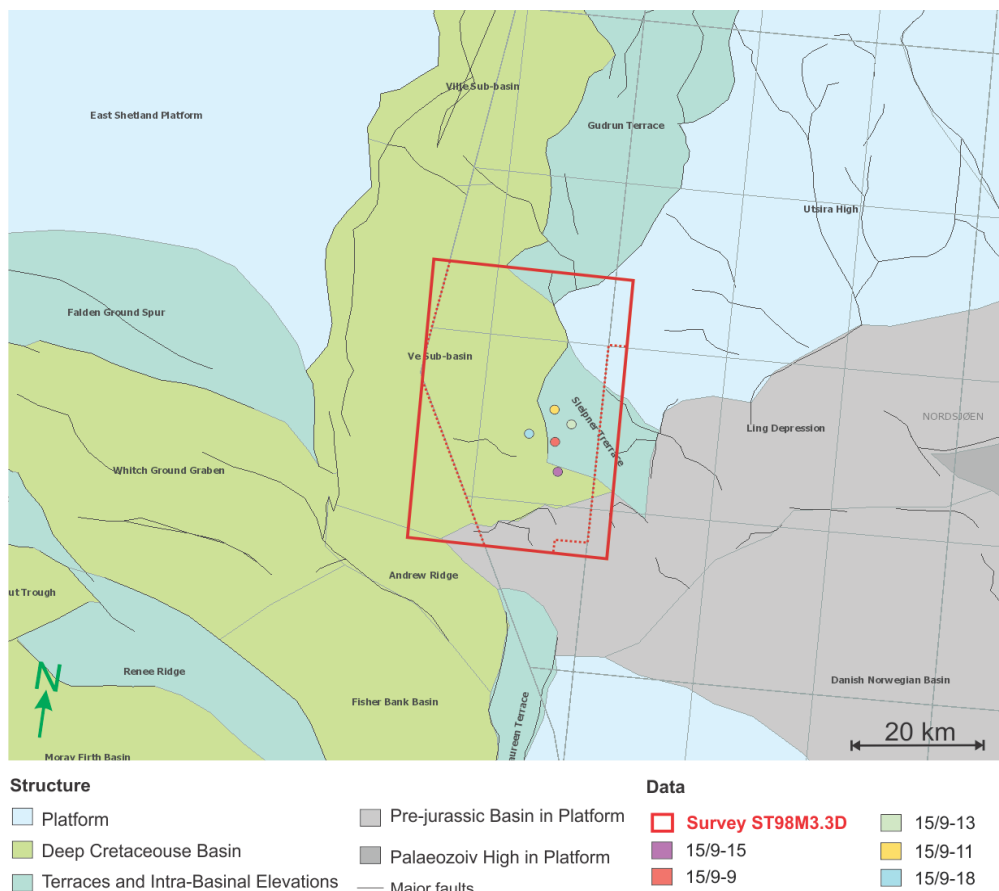
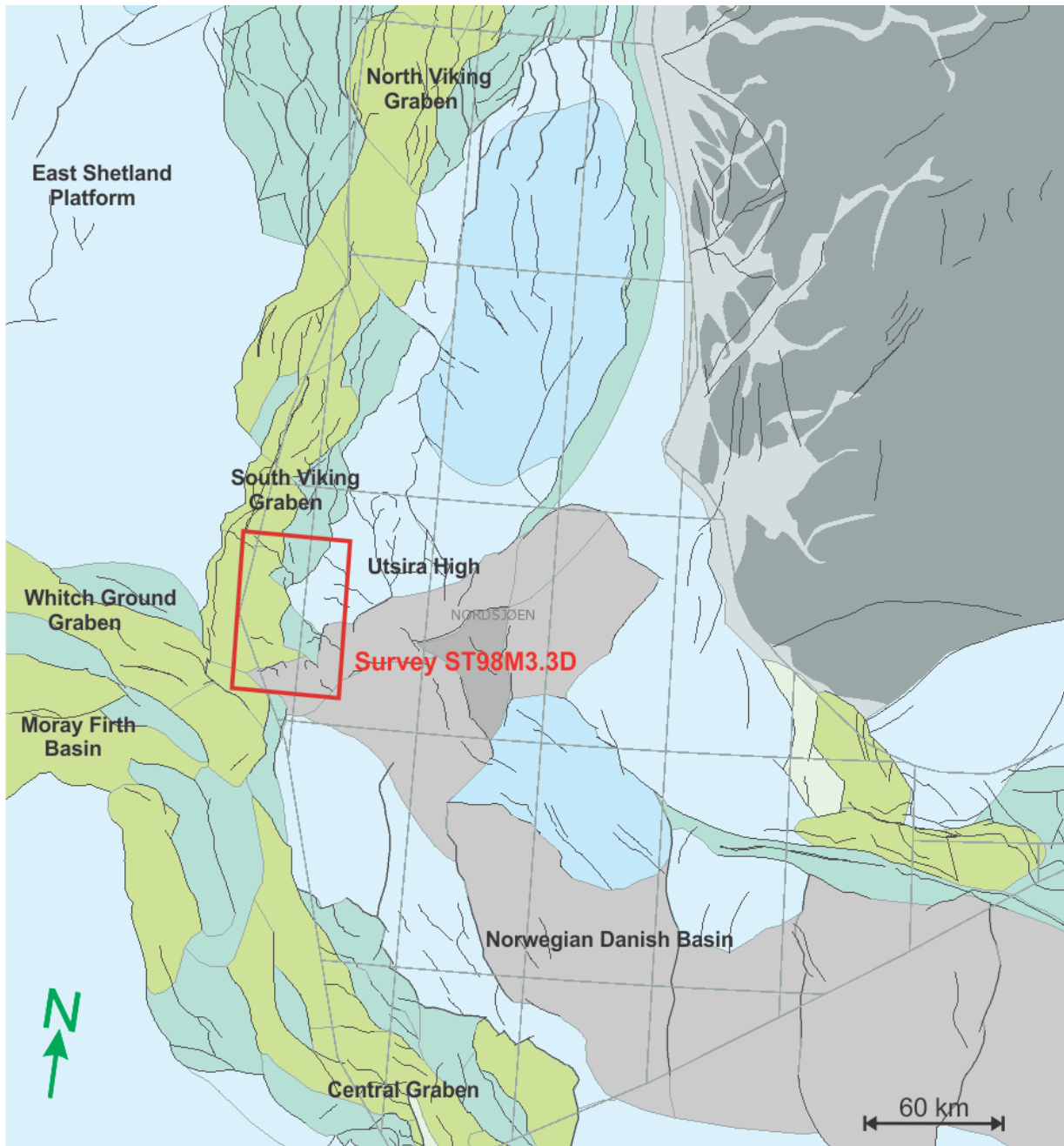


Figure 2.1: The location of the study area. The extent of the seismic data is indicated by the red dotted line within survey ST98M3.3D. Notice the location of the wells. Two of the wells are located in the Ve sub-basin and three are located on the Slepner Terrace. The Figure modified after Factmap (2016).



Structure

- | | |
|---------------------------------------|--------------------------------|
| Platform | Pre-jurassic Basin in Platform |
| Deep Cretaceous Basin | Palaeozoic High in Platform |
| Terraces and Intra-Basinal Elevations | Major faults |

Figure 2.2: Location of Survey ST98M3.3D. The main structural elements within the North Sea are included. The study area is located further towards the west, by the end of the Norwegian continental shelf (Red rectangle). The major faults in the study area are of late Jurassic age (Ziegler, 1992; Karstens & Berndt, 2015). Figure is modified from Factmap (2016).

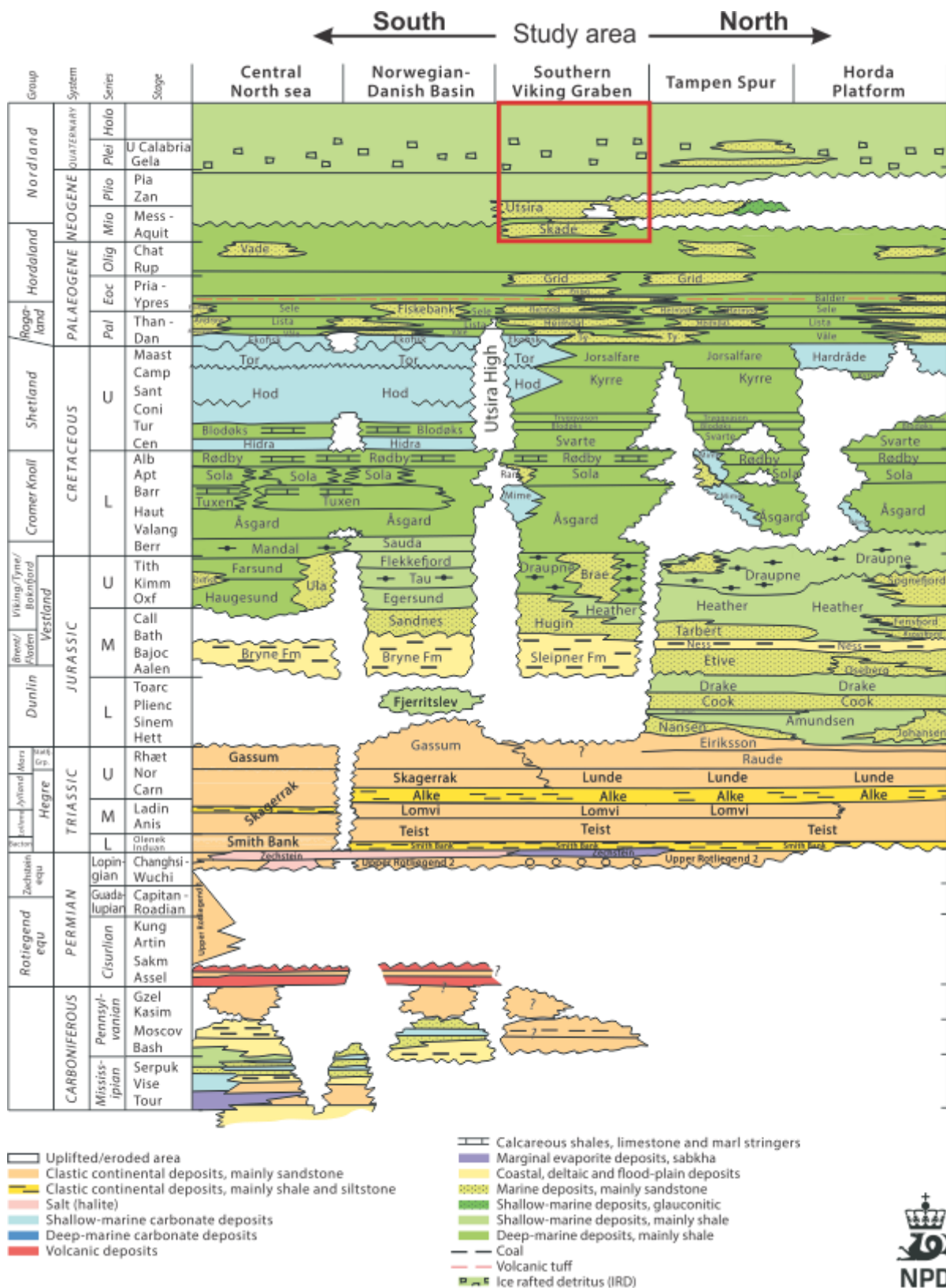


Figure 2.3: A lithostratigraphic chart of the North Sea. As mentioned, the study area is located in the Southern Viking Graben; indicated at the top of the chart, with the corresponding lithology underneath. Left from the Southern Viking Graben corresponds to south, and right corresponds to north. Notice the extent of the Nordland and Hordaland Group. Also important to notice is the Utsira Formation, as it occurs relatively localized in the Southern Viking Graben. Figure is modified from NPD (2014).

2.3 Geological evolution of the Norwegian North Sea

The North Sea has a long extensional history that began in Devonian times with the extension of the Caledonian crust. However, the present day structural framework of the North Sea is largely resulted from the extensive rifting events seen both in the Permo-Triassic transition and in the Mid -Jurassic to Early Cretaceous rifting phases (Fig 2.4 & 2.5) (Ziegler, 1975; Zanella & Coward, 2003; NPD, 2014). Following these dominant rifting phases there was a period of thermal cooling and subsidence. During Late Cretaceous to Cenozoic the basin was deformed by tectonic inversion, and the basin margins underwent substantial uplift during Cenozoic times (Glennie, 1998; Zanella & Coward, 2003). The present day configuration is characterized by an average maximum horizontal stress oriented north-west to south-east, that is consistent with the active stress field in north-western Europe (Zanella & Coward, 2003).

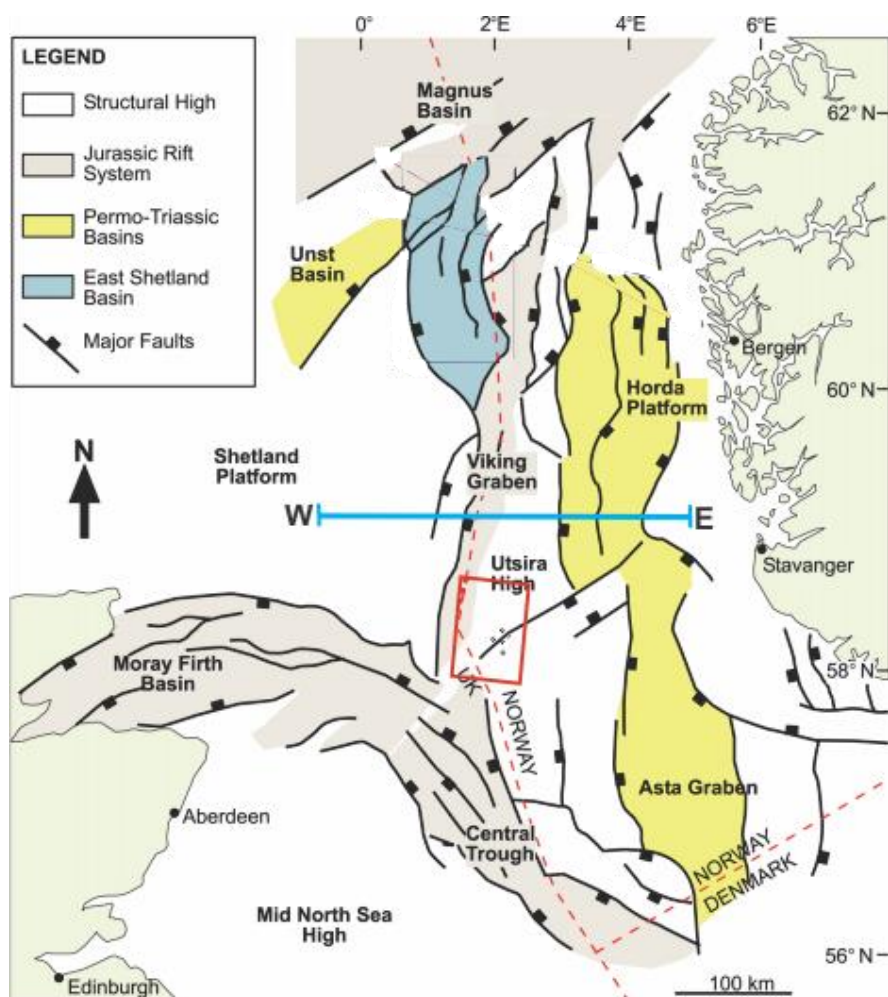


Figure 2.4: The main structural elements in the North Sea, with the corresponding Jurassic and Permo-Triassic faults. The survey is indicated with a red rectangle, and the location of the regional profile show in figure 2.5 is indicated as a blue line. The figure is modified from Faerseth (1996).

2.3.1 Paleozoic

Caledonian orogeny

The basement in the north Atlantic and in north-west Europe comprise crystalline rocks, derived from at least three tectonic domains that were accreted during Caledonian collision between Laurentia, Baltica and Avalonia (Ziegler, 1992; Coward, 1995). The Caledonian plate collision began during Ordovician times and progressively closed the Iapetus Ocean during Silurian to Early Devonian (Marshall & Hewett, 2003). Major low-angle thrusts formed in the both the Scottish and the Norwegian caledonides during the collision (Zanella & Coward, 2003). Most of the North Sea is underlain by the basement created during the Caledonian orogeny (Ziegler, 1992), and localization of the North Sea rift system is affected by the pre-existing crustal discontinuities and fault geometries created during the collision tectonics (Faereth, 1996). The Early Devonian and earlier Caledonian deformation structures, formed the Pre-Mesozoic tectonic framework, that later would be the major crustal lineaments seen today (Faereth, 1996; Zanella & Coward, 2003).

Devon

The extensive rifting seen in Devonian and Carboniferous times, is associated with large strike-slip faults (Zanella & Coward, 2003). The closure of the Iapetus Ocean created a new craton configuration known as the Old Red Sandstone Continent, named after the characteristic oxidized iron rich sandstones, which deposited under arid to semi-arid conditions (Glennie, 1998; Marshall & Hewett, 2003). Around Mid-Silurian times the tectonic regime altered and became extensional, it was under this period small local basins were formed and the first depositions of red continental sandstones were deposited (Marshall & Hewett, 2003). The extensional movement continued into Early Devonian times, giving accommodation space for thicker successions of alluvial, volcanoclastic and lacustrine sediments (Marshall & Hewett, 2003). Following in Early Devon the stress pattern changed again, leading to inversion and collapse of Caledonian compressional units (Marshall & Hewett, 2003). This movement gave a northern series of half-graben sub-basins. These basins were small with internal drainage, and dominated by rapid deposition of alluvial-fan conglomerates with small lakes (Marshall & Hewett, 2003). The sub-graben basins developed into a single system that was the main Mid-Devonian development of the Orcadian Basin (Marshall & Hewett, 2003).

Carboniferous

Tectonic extension occur during the transition from Devon to Carboniferous. Caledonian crust were reactivated in a broad diffuse system. In the southern parts of the North Sea this is gave a clockwise rotation of Caledonian basement blocks, and a reactivation of the Great Glen – Viking Graben (Coward et al., 2003). The Carboniferous is associated with a transition from continental deposits to shallow marine and deep marine depositions (Bruce & Stemmerik, 2003). Devon was dominated by continental red sandstones, while in Early Carboniferous a more diversified marine, fluvial, deltaic and continental sedimentation dominated (Bruce & Stemmerik, 2003). This transition is a direct result of marine transgression over the Old Red Sandstone Continent in Early Carboniferous, and continental drift from an arid to a more humid and tropical latitude (Bruce & Stemmerik, 2003).

In the North Sea the Carboniferous stratigraphic units are very poorly understood. The Carboniferous strata is deeply buried and have a limited distribution within the basin. However, excellent analogues are present in the adjacent onshore areas in the UK and Scotland (Bruce & Stemmerik, 2003). The tectonic framework of the North Sea is highly affected by the extension phases seen in Early Devonian and Carboniferous age. Tectonic uplift and a following phase of erosion, led to tectonic inversion of the North Sea towards the end of Carboniferous (Bruce & Stemmerik, 2003; Coward et al., 2003).

Permian

Early Permian in the North Sea is characterized by intrusions of hot asthenosphere, and regional volcanism. However, this volcanic activity was concentrated east of the Central Graben (Coward et al., 2003). The Central and southern parts of the North Sea was tectonically calm during Permian, although important reactivation of Devonian structures occurred (Glennie, 1998; Coward et al., 2003).

Permian sediments in the North Sea consist of a lower sequence named the Rotliegend Group, and comprises largely sandstones (Glennie et al., 2003). The North Sea was entering a semi-desert climate zone, and the Rotliegend sands was deposited as infill of the topography created during Late Carboniferous to Early Permian inversion and thermal-subsidence events (Coward et al., 2003; Glennie et al., 2003). Overlying the Rotliegend Group is the upper Permian Zechstein salts and carbonates. The transgression during the Permian period is related to melting of the large Gondwana ice caps, resulted in flooding of major parts of the North Sea. This gave a shallow to deep marine environment (Glennie et al., 2003). The

marine setting provided conditions for the deposition of carbonates, and in combination with the semi-desert climate gave later precipitation of evaporates in larger areas of the North Sea (Glennie et al., 2003). These carbonates and evaporates comprise the Zechstein Group and follow a three- or four cyclic pattern from basin edge to the center of the basin of limestones, anhydrites and halite (Glennie et al., 2003). These salts are widely distributed and seen deeper in the subsurface within the study area. Regional extension initiated towards the end of the Permian period, this represent the first phase of the Arctic rift system and opening of the ocean (Ziegler, 1989; Glennie et al., 2003).

2.3.2 Mesozoic

Post-dating the Caledonian orogenic extensional collapse, the lithosphere in the North Sea was affected by two major extensional phases. The Permo-Triassic and the Mid-Jurassic to earliest Cretaceous rifting phases (Ziegler, 1975, 1992; Faereth, 1996; Christiansson, 2000). The Permo-Triassic and the Late Jurassic extension phases were of approximately of same magnitude, and of equal importance in the development of the North Sea basin (Faereth, 1996). The larger master-faults in the northern North Sea are basement-involved (Fig. 2.5) and probably cut the whole upper crust, these faults are planar in geometry but changes dip from a 40-50° angle at higher Jurassic levels to a 25-35° angel in the basement (Faereth, 1996). These are major basin forming faults with several kilometers of throw, and they form half-grabens which are fundamental morphological features in the North Sea basin (Spencer & Larsen, 1990) (Faereth, 1996). Following both phases was a period of thermal cooling and regional subsidence (Christiansson, 2000).

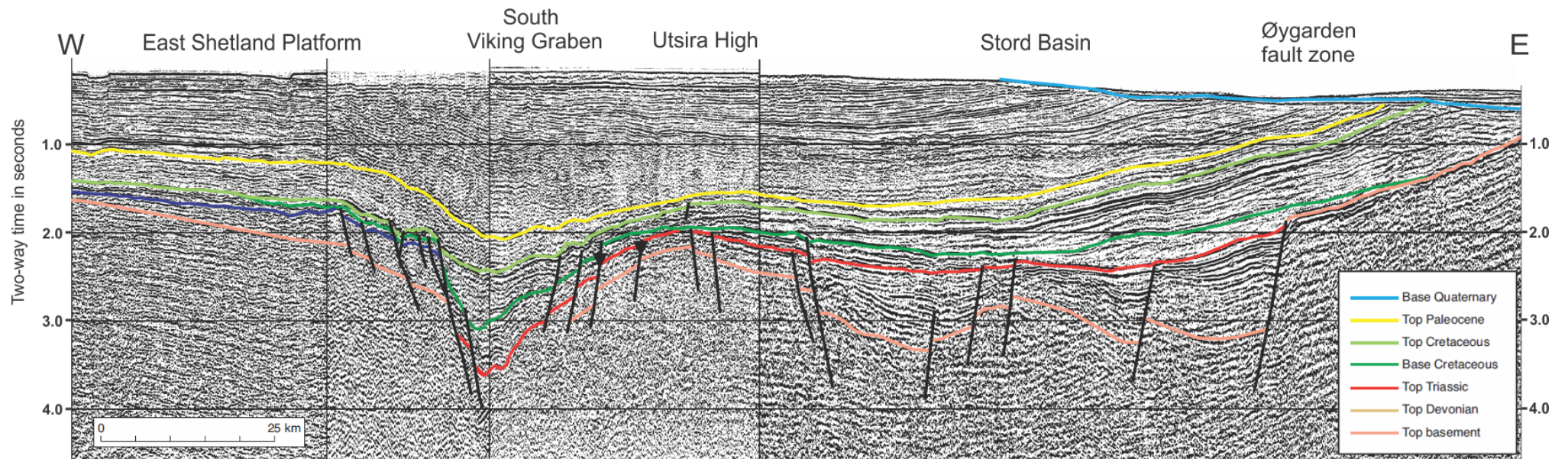


Figure 2.5: Regional seismic section from East to West. The seismic line is located just north of the study area (Fig. 2.4). The basement involved faults with origin in Mesozoic gives the basin its post-rift outline. The South Viking Graben area is highly down-faulted, giving substantial accommodation space. Notice the uplifted East Shetland Platform to the west of SVG. Also notice the deltaic outline (top Paleocene) into the South Viking Graben. Figure is modified after (Zanella & Coward, 2003).

Triassic

The Permo-Triassic rifting affected the total width of the northern North Sea, and stretching occurred as far as the West Shetland Basin, with the West Shetland Spine Fault as the main controlling segment (Faereth, 1996). The Permo-Triassic rifting events marks a change in tectonic regime in NW Europe, from plate accretion in Paleozoic, to a continental extension regime (Ziegler, 1992; Coward, 1995). The northern North Sea rift system is characterized by large rotated fault blocks with sedimentary basins in asymmetric half-grabens, these structures correlates to the major extension of the lithosphere and thinning of the crust that occurred during this rifting phase (Fig. 2.5) (Christiansson, 2000). Large N-S to NE-SW faults in a discontinuous rifting pattern and regional subsidence dominated (NPD, 2014). The fundamental impact Triassic rifting had on the development of the structural framework of north-west Europe is related to earlier Caledonian orogeny collapse, basin formation and to the closure of the Appalachian-Variscan Ocean (Coward, 1995; Goldsmith et al., 2003). The extension was multidirectional and affected major part of the wider European region (Ziegler, 1992). Rifting can clearly be seen in the marginal areas of the Viking Graben, the Horda Platform and the Magnus Basin , also seismic data taken from this area show clear wedge-shaped geometries of the deposits, indicating that the area was tectonically active during the early rift phase (Prosser, 1993; Christiansson, 2000).

There was also a return to terrestrial conditions during Triassic, as the North Sea and Viking Graben became a site for large deposits of red bed including alluvial fan, fluvial, aeolian, sabkha, lacustrine and some shallow-marine facies (Fig. 2.3) (Coward, 1995; Goldsmith et al., 2003). The extent of the different lithologies were dependent on the tectonic development and relative movement of fault blocks (Coward, 1995), and the Triassic to Middle Jurassic shows a pattern of repeating outbuilding of clastic wedges form the Norwegian and East Shetland hinterlands within an evolving post-rift basin (Christiansson, 2000).

Jurassic

The latest tectonic event that had major influence on the geometry of the North Sea, is the Middle Jurassic to Early Cretaceous rifting phase (Ziegler, 1992; Glennie, 1998). The major faults is characterized by a northeast- southwest trend, seen clearly in the study area (Fig 2.4). The initiation of this phase occurred during Late Mid-Jurassic time, with climax during the Late Jurassic (Christiansson, 2000). The Jurassic extension was concentrated mainly along the axis of the Viking and Sogn grabens (Faereth, 1996).

The faulting and rifting stages in Mid-Jurassic influenced a broader area than in the final stages of rifting (Christiansson, 2000). This corresponds to the initiation stage of fault growth, where several fault segments with minor displacement cover a larger area (Gawthorpe & Leeder, 2000). Smaller fault segments interacted and form large fault segments where most of the displacement accumulates, the continued extension was focused along these few fault segments, along the graben margins as a through-going fault zone (Christiansson, 2000; Gawthorpe & Leeder, 2000). At the same time internal graben relief became more pronounced, giving a mature graben topography with platforms and sub-platforms (Christiansson, 2000).

The present configuration and distribution of sediments is effected by a number of factors, these include pre-existing Triassic rift topography, Mid-Jurassic doming and Late Jurassic rifting and erosion (Husmo et al., 2002). There are regional differences in facies development and relative age of the facies units, and in eastern and central areas halokinesis have occurred. Lower and Middle Jurassic sediments are absent in the southern area of the North Sea (Fig. 2.3), but thicken towards north (Husmo et al., 2002). Only in the northern parts of the North Sea, at the Horda Platform, East Shetland Basin and northern Viking Graben complete conformable successions of Triassic age occur (Husmo et al., 2002). In the South Viking Graben, much of the lower and middle sediments is eroded, marked by the intra-Aalenian unconformity (Fig 2.3) (Husmo et al., 2002). The absence of stratigraphy is due to erosion of tilted footwall blocks (Husmo et al., 2002). At the Sleipner East field, the upper part of Mid-Jurassic sediments are the most present with the Sleipner, Hugin, and Heather Formations (Fig.2.3) (Husmo et al., 2002)

Cretaceous

Cretaceous post-rift setting was dominated by major structural features such as relay ramps, rotated fault blocks and sub-platforms. These structural features had a strong influence on basin configuration and therefore sediment distribution (Gabrielsen et al., 2001). According to Gabrielsen et al. (2001) the Cretaceous transition from syn- to post-rift configuration was diachronous. Evidence of this is observed as differences in early post-rift subsidence in the southern parts of the Viking Graben (Gabrielsen et al., 2001). During Cretaceous the North Sea underwent regional subsidence, with a gradual infilling of graben relief of deep-water shales and minor pelagic carbonates (Christiansson, 2000). A rise in eustatic sea level combined with regional subsidence resulted in progressive overstepping of basin edges and a

decrease in clastic influx into the North Sea basin (Christiansson, 2000). The high eustatic sea level provided good conditions for the deposition of chalk in the Late Cretaceous, these deposits are more pronounced in the southern parts of the North Sea, whereas in the north terrigenous mudstones dominate (Christiansson, 2000). The lower Cretaceous stratigraphy records a complex depositional history with post-rift thermal collapse, and long-term changes in global sea level. There is also local halokinetic and tectono-eustatic events (Copestake et al., 2003). Transgressive and regressive cycles form the basis for a number of regional sequences during the Lower Cretaceous. These cycles are a result of relative sea level change and were a controlling element in facies and sediment thickness distribution during Early Cretaceous (Copestake et al., 2003). The Upper Cretaceous succession in the study area comprises siliciclastic and clay dominated sediments, termed the Shetland Group (Surlyk et al., 2003).

2.3.3 Cenozoic

The uppermost Cenozoic stratigraphy is subdivided into the Hordaland and the Nordland Groups, their stratigraphy is extensively documented (Jordt et al., 1995; Jordt et al., 2000; Faleide et al., 2002; Rundberg & Eidvin, 2005; Eidvin & Rundberg, 2007; Gregersen & Johannessen, 2007). In Cenozoic times the epicontinental basin was bounded by the higher areas of Scandinavia, the British islands, and Central Europe (Gregersen & Johannessen, 2007). The basin fill indicates regional vertical movements, which is controlling for the basin geometry and provenance of the sediments (Christiansson, 2000). This vertical movement included regional basin subsidence and episodic marginal uplift (Jordt et al., 1995; Gregersen & Johannessen, 2007). The location of depocentres and sequence geometries indicate that vertical movements of the basin during Cenozoic are closely related to pre-existing underlying Mesozoic and Paleozoic structures within the North Sea basin (Fig 2.5) (Christiansson, 2000; Fyfe et al., 2003).

Paleocene

Paleocene sedimentary units are extensively distributed throughout the whole of the North Sea basin, and it's also one of the most prominent hydrocarbon plays (NPD, 2016). The sediments from this period are part of the largely un-faulted post-rift sequence, and are deeply buried in the central portion of the basin (Veeken, 1996). During Paleocene the North Sea changed from a basin-center to a basin margin deposition pattern (Ahmadi et al., 2003). Erosion of the uplifted areas gave a high sediment input, which further led to the cessation of

the calcareous depositions that prevailed over most of the North Sea during late Cretaceous time (Veeken, 1996). This led to the initiation of siliciclastic deposition, and the uplifted Scotland and Shetland areas acted as the primary source for the great volumes of these sediments (Fig. 2.5) (Jordt et al., 1995; Glennie, 1998). These uplifted areas gave south-easterly drainage patterns, and the deposition of a prograding shelf system that was the major source of coarse siliciclastic sediments during Paleogene (Glennie, 1998). The submarine fans that developed was a dominant transport process from shelf to basin. They occurred as confined and unconfined gravity flows derived from either a point or a line source. These fans spread out and overlapped, and they now form near-continuous sandstone bodies. These deposits become finer grained distally and eventually wedge out towards the basin center (Ahmadi et al., 2003).

Eocene

Stratigraphic units deposited during Eocene show similarities to units deposited in Paleocene, indicating a continuation of subsidence in a post-rift setting (Jones et al., 2003). This post-rift sedimentary fill is largely shale dominated, with minor sand input that decreases as sediment supply lowered in Eocene. In the study area, above the Viking Graben, deep marine sedimentary deposits dominate, while marginal to shallow-marine sedimentation is seen along the western and also the eastern margins of the basin (Jones et al., 2003).

Sea-floor spreading gave the North Sea a compressional stress field towards the Alpine mountain belt (Knott et al., 1993). This compression gave rise to uplift along the basin-margins, resulting in extensive deposition of hemipelagic sediments by submarine fans into depocentres of the Viking and Central grabens (Jones et al., 2003).

The large, stacked, submarine fans that dominated the Paleocene were now more smaller and localized fans, and Mid- to Late Eocene systems became more channelized (Jones et al., 2003). The general pattern of deposition during the Eocene shows an overall progradation from west in the North Sea basin, similar to Paleocene. The input of clastic sediments into the basin, occurred mainly during Early Eocene. This was largely controlled by the position of major rivers and delta system that supplied sediment from the East Shetland Platform and the Scottish Highlands (Glennie, 1998; Jones et al., 2003). Sediments deposited during Eocene usually have a gradual thinning eastwards trend in the central North Sea. This indicated lesser overall input of the coarser clastic sediments from the east. This is probably due to regional

subsidence of mainland Norway, and other factors such as climate change and variations in subaerial vegetation (Jones et al., 2003).

Oligocene

The uppermost sequence of Oligocene sediments is classified by Jordt et al. (1995) to be CSS-4 (Fig 2.6). The same sequence have been interpreted in more detail by Rundberg and Eidvin (2005) (UH-3). Continued post-rift and subsidence followed on in Oligocene. Basin development during this time is influence both by the closing of the Tethys Ocean and the opening of the North Atlantic Ocean. The North Sea Basin lost connection with deep waters to the south-east during Oligocene, at the same time the opening of the Atlantic Ocean gave an improvement of oceanic circulation to the basin (Fyfe et al., 2003). Tectonic movements influenced the oceanic circulation within the North Sea Basin, and may have caused local hiatus during Early to Mid-Oligocene. An abundant sediment supply together with steady regional subsidence led to huge accumulations of massive Upper Cenozoic deposits (Fyfe et al., 2003).

Figure 2.8 show the extent of the uppermost Oligocene sediments. These sediments was derived from the Fennoscandia High, which contributed with clastic sediments to the North Sea margin throughout Oligocene to Early Pleistocene times. Also clastic sediments derived from the East Shetland Platform were deposited on the north-western margin of the basin (Fig. 2.8) (Fyfe et al., 2003).

Miocene

Several authors have contributed with classification and interpretation of the uppermost sequences of Cenozoic age (Rundberg & Smalley, 1989; Jordt et al., 1995; Michelsen et al., 1999; Galloway, 2001, 2002; Rundberg & Eidvin, 2005; Eidvin & Rundberg, 2007). The stratigraphic chart presented in figure 2.6, show the sequence subdivision done by Jordt et al. (1995) in the Central North Sea. This subdivision have later been discussed by several authors, and will be implemented for this thesis. The Miocene successions have been divided into three seismic sequences CSS-5, CSS-6 and CSS-7, and the Plio-Pleistocene into CSS-8, CSS-9 and CSS-10 (Fig. 2.6). The recent work of Rundberg and Eidvin (2005) and Eidvin and Rundberg (2007) will also be central in the classification of the seismic sequence for this thesis.

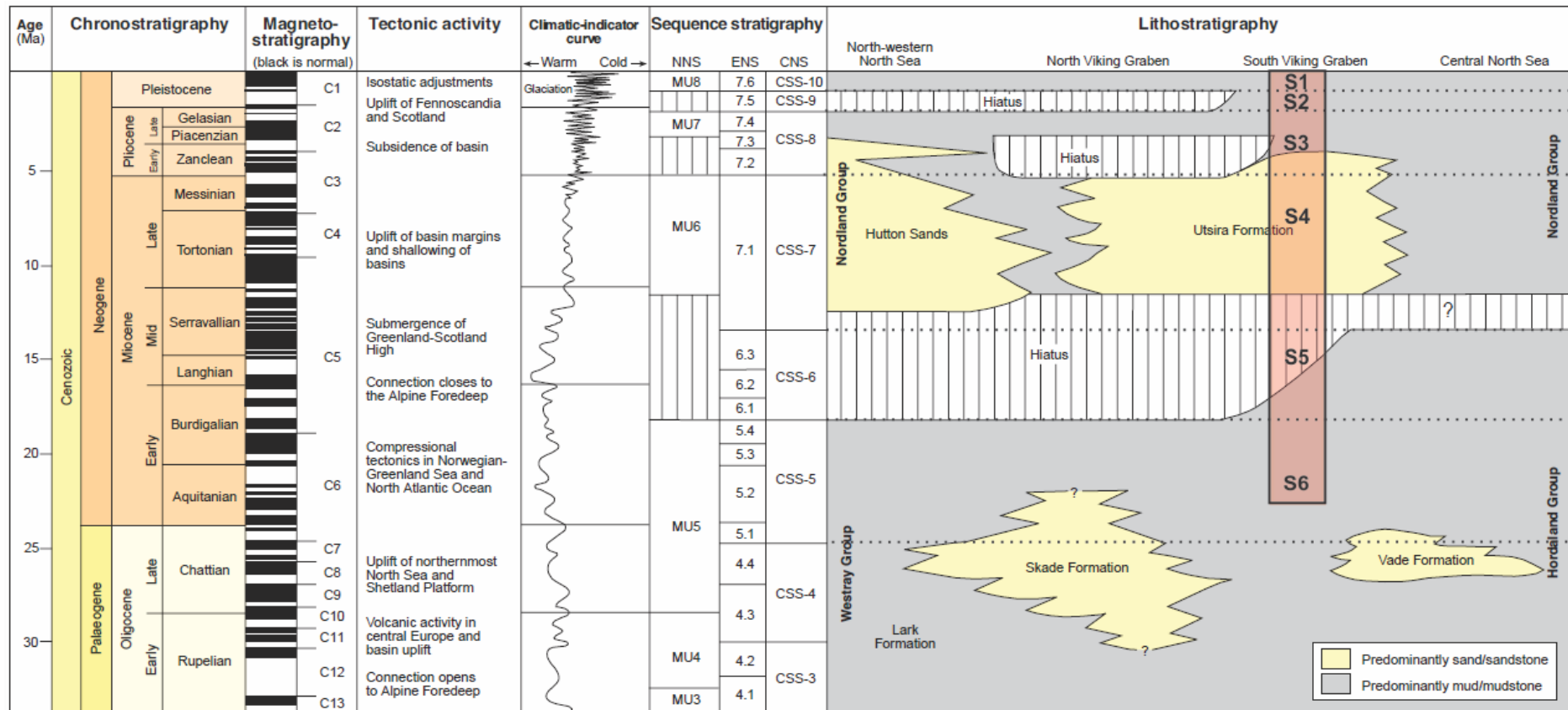


Figure 2.6: Stratigraphic correlation chart. The approximate position of the study area and seismic coverage is indicated with a red column. The sequences interpreted in this thesis is indicated in the red column. The climatic curve is based on isotope ratios in Atlantic waters after Abreu and Anderson (1998). The different sequence stratigraphy is based on different authors: The northern North Sea (NNS), Rundberg and Smalley (1989). The eastern North Sea (ENS), Michelsen et al. (1999). And the Central North Sea (CNS), Jordt et al. (1995). The lithostratigraphy is based on Isaksen and Tonstad (1989) and Knox and Holloway (1992). Dating work is performed by Eidvin et al. (2000) and Eidvin and Rundberg (2001). Figure is modified after Fyfe et al. (2003).

Figure 2.7 present a stratigraphic chart over the Southern Viking Graben area. The interpretation done by Rundberg and Eidvin (2005) indicate that the lowermost sequences in the study area, is of Lower Miocene age (UH-4). A new sequence of Middle Miocene age have been interpreted (LN-1). This sequence might correspond to sequence CSS-6, after Jordt et al. (1995). However, sequences CSS-6 is possibly eroded in the study area, and may only be present in the southern parts of the basin (Jordt et al., 1995). The Utsira Formation corresponds to sequence CSS-7 and LN-2 after Jordt et al. (1995) and Rundberg and Eidvin (2005), respectively. Figure 2.8 show the Southern Viking Graben stratigraphy, interpreted after Rundberg and Eidvin (2005). The figure indicate a regional overview of the area, and the seismic used in this thesis covers a narrow view close to 15/6-3 (Fig. 2.8).

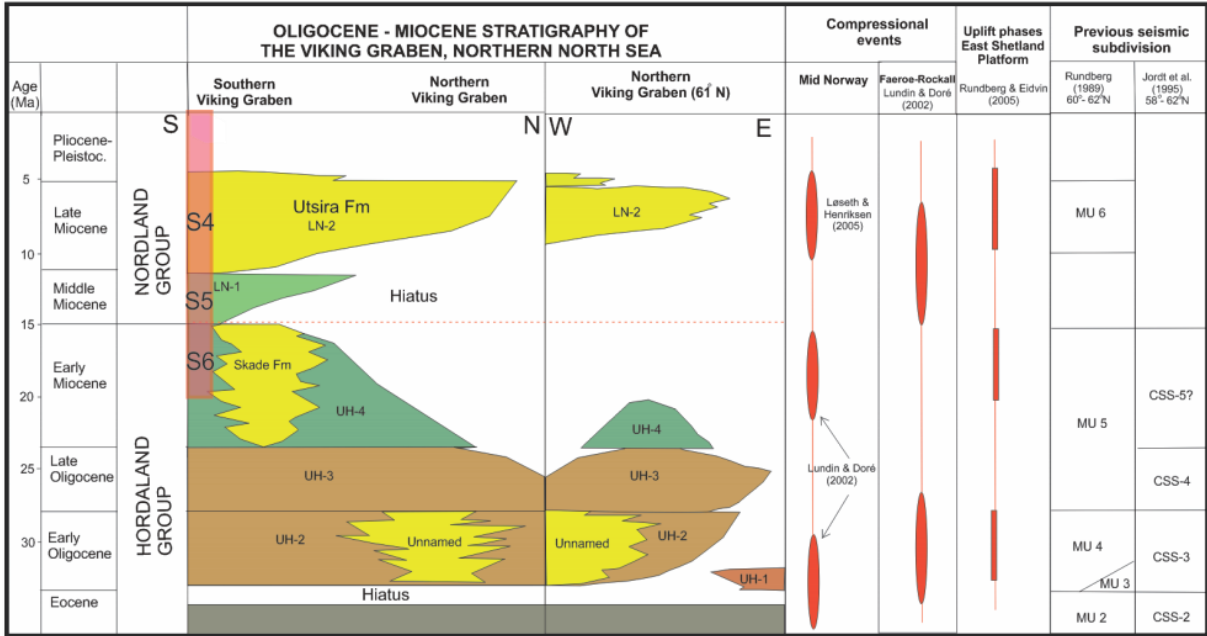


Figure 2.7: Oligocene-Miocene stratigraphy in the Viking Graben and northern North Sea. The red column indicate the approximated position of the seismic data. Compressional events after Lundin and Dore (2002) and Løseth and Henriksen (2005). Previous seismic subdivision after Rundberg and Smalley (1989) and Jordt et al. (1995). The Figure is modified after Rundberg and Eidvin (2005).

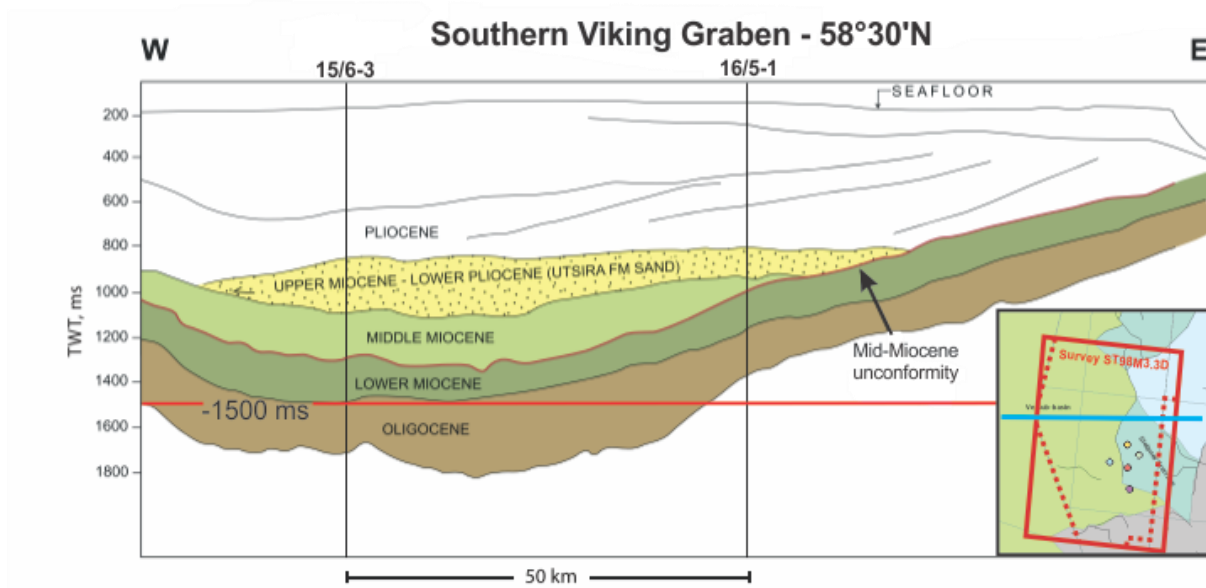


Figure 2.8 East-west section of the southern Viking Graben at approximately 58°30'N. The location of the section is indicated as a blue line in the bottom right corner, in relation to the study area. Notice the Mid-Miocene unconformity and the overlying Middle Miocene sequence (LN-1). The red line indicates the depth of the seismic data (Survey ST98M.3D). Figure modified after Rundberg and Eidvin (2005).

Lower Miocene is characterized with a slow argillaceous sedimentation, which eventually led to a sedimentation break and unconformity that occurred towards Mid-Miocene (Fig. 2.8) (Eidvin & Rundberg, 2007; Gregersen & Johannessen, 2007). The Lower Miocene sequence is interpreted by Eidvin and Rundberg (2007) to conformably overlie the Oligocene deposits, and is classified as the uppermost part of the Hordaland Group (UH-4).

The margins of the North Sea basin experienced uplift during Mid- to Late Miocene (Løseth & Henriksen, 2005; Gregersen & Johannessen, 2007). Uplift together with a gradual drop in temperature, resulted in a further restricted connection between the Norwegian-Greenland Sea and the North Sea (Fyfe et al., 2003). In the northern parts, this led to a narrow seaway that connected the North Sea with the Atlantic (Fig. 2.9a) (Galloway, 2001, 2002).

The transgression gave good conditions for progradation of deltaic complexes from the Shetland Platform and Scandinavia areas (Fig. 2.10) (Galloway, 2002). Erosion of the uplifted Shetland Platform led to depositions of the Utsira Formation (Galloway, 2001, 2002; Fyfe et al., 2003). Figure 2.10 shows a regional seismic line that shows that the Utsira sands are located in a basin restricted depocenter, east for the Shetland Platform, below the prograding deltaic

units. (Gregersen & Johannessen, 2007). The Sleipner area is considered a depocenter for the Utsira sand, with a thickness of 200m (Rundberg & Eidvin, 2005). The sand sequence have in recent times been used as a CO_2 storage reservoir (Chadwick et al., 2004; Boait et al., 2012; Chadwick & Noy, 2015). Figure 2.9 show the regional paleo-environment at the deposition of the Utsira Formation, in the Southern Viking graben. The sand has most likely been reworked within this shallow marine setting, with focused oceanic currents focused through the narrow strait (Galloway, 2002).

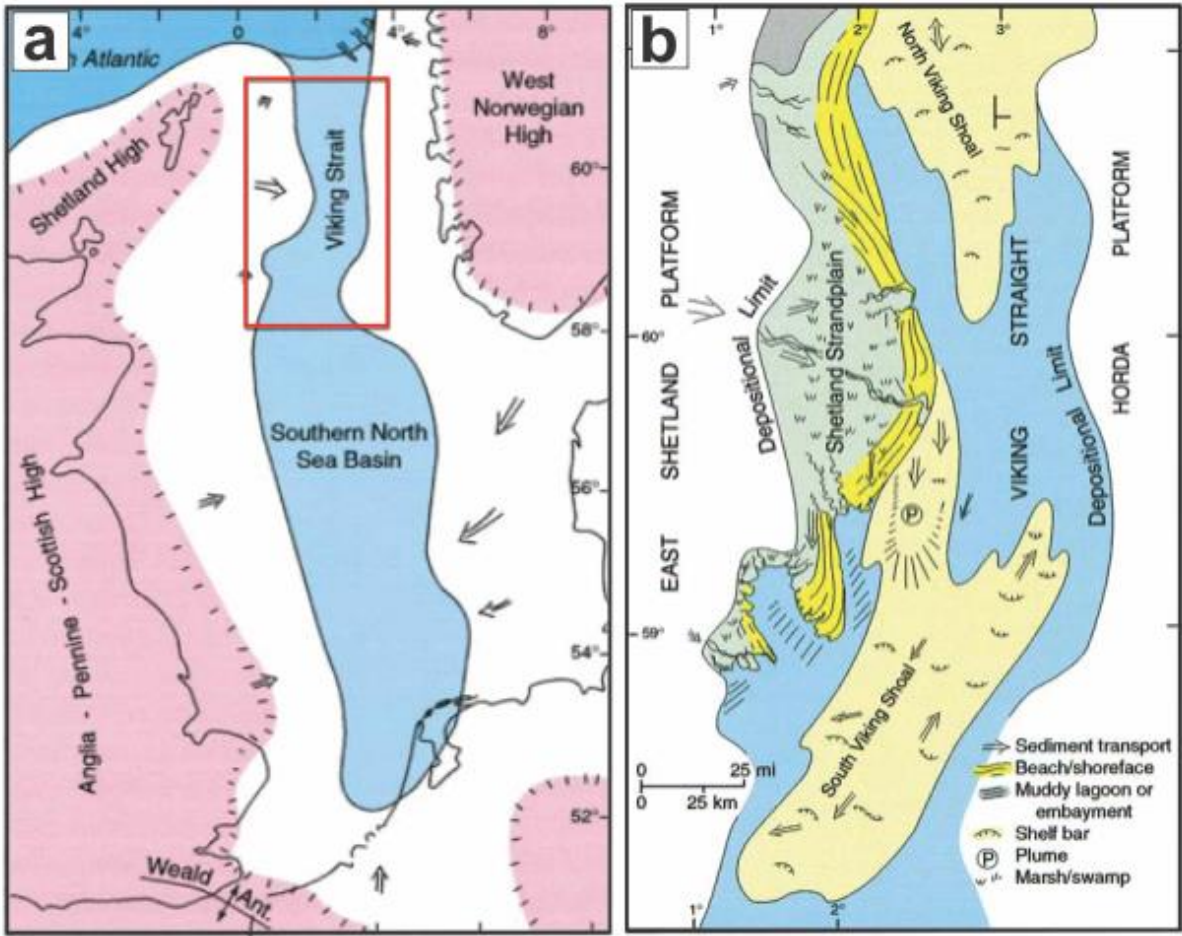


Figure 2.9a: Regional paleogeography of the northern North Sea during the Miocene epoch. The red rectangle corresponds to the location of figure 2.9b. Which is showing an interpretation of the depositional systems and paleogeography of the Utsira Formation. The study area for this thesis is located at the South Viking Shoal depocenter. Figure is modified after Galloway (2001).

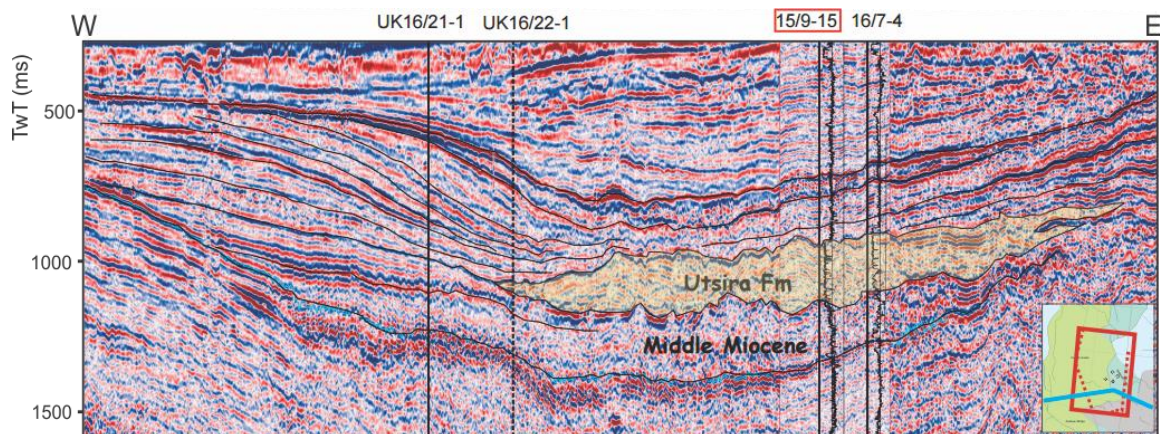


Figure 2.10 is showing a seismic section across the southern Viking graben, with the uppermost Cenozoic deposits in focus. The location of the seismic section is indicated in the bottom right corner, as a blue line running through the southern parts of the survey used in this study. The seismic section also connects with well 15/9-15, which is also used in this study. The outline of the Utsira Formation in this area is highlighted with a pale yellow color. Notice the deltaic complex to the West. Figure is modified after Eidvin and Rundberg (2007).

Pliocene

After the uplift seen in Mid- to Late Miocene, the North Sea Basin underwent subsidence. This resulted in the deposition of argillaceous sediments of great thickness (Fyfe et al., 2003). These depositions belong to a huge progradation deltaic complex (Eidvin & Rundberg, 2007). As a consequence of the Norwegian-Greenland opening and the new connection to the ocean, icebergs and glacial processes initiated. This is seen as glaciomarine drop stones in pro-deltaic deposits. (Eidvin et al., 2000; Fyfe et al., 2003). Iceberg scouring is also seen in the central part of the North Sea, indicating that the temperature and oceanic currents allowed sea ice to drift south. Seismic sequence CSS-8 might correspond to the sedimentary units deposited in the Mid- to Late Pliocene, and its main source is suggested to be from southern Norway (Jordt et al., 1995).

Pleistocene – Holocene

The uppermost sequences of Pleistocene and Holocene age, is interpreted by Jordt et al. (1995) to comprise seismic sequence CSS-9 and CSS-10. During Late Pliocene and Early Pleistocene the surrounding landmasses of the North Sea was influenced by an uplift episode that resulted in further deposition of terrigenous sediments in the North Sea. (Dore et al., 1999). Most of the Pleistocene period was dominated by glacial and glaciomarine conditions. There were also temperate periods, resulting in an advance and retreat pattern of the Scandinavian and Scottish ice sheets (Fyfe et al., 2003) This led to both erosion and deposition of glacial sediments within the North Sea Basin. The area between Norway and Scotland was probably covered by ice during different periods in Pleistocene.

3 Data and methods

3.1 Dataset

The seismic data used in this study consist of a 3D seismic cube, referred to as survey ST98M3.3D. Figure 3.1 show the location of the survey in relation to the Norwegian coast. The survey consist of 3297 Inlines and 5026 crosslines, and covers an area of $\sim 2844\text{km}^2$. The survey have relative high quality seismic, in the entire cube. The survey has been cut at - 1500ms (TWT). The survey have been merged together by several surveys, and the consequence is a series of anomalies. The signal to noise ratio is generally high.

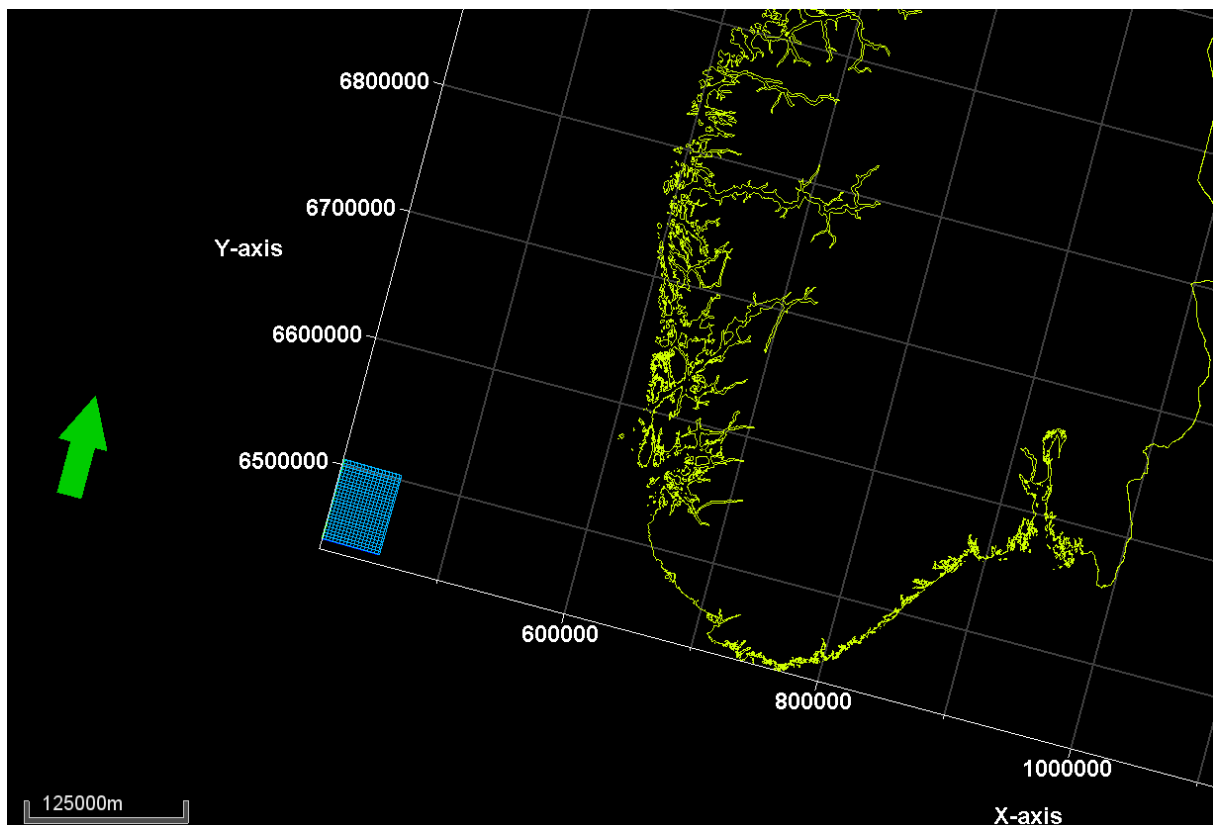


Figure 3.1: Location of Survey ST98M3.3D relative to the Norwegian coast (Blue rectangle). The x and y-axis shows distance in meters.

3.1.1 Polarity standard

In survey ST98M3.3D the polarity standard is with reference to SEG and Sheriff (2006), a zero phase signal with normal polarity. This configuration is shown in figure 3.2. Figure 3.2b, shown the seafloor reflection, which always produces a positive acoustic impedance contrast.

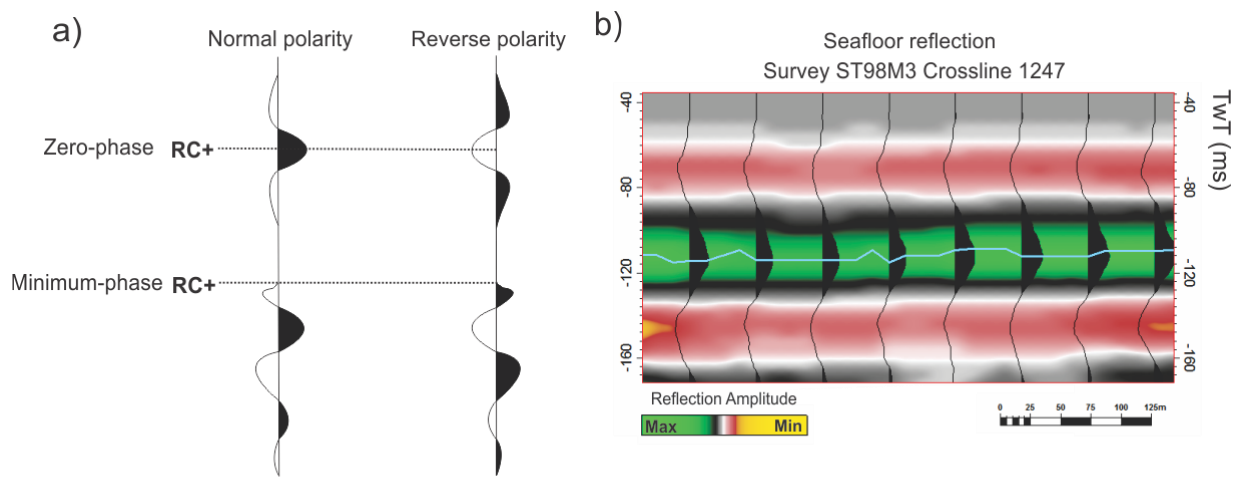


Figure 3.2 a) Polarity conventions for plotting seismic signals (SEG). In this study the seismic data has a zero-phase with normal polarity convention. b) Seafloor reflection. Zero-phase with normal polarity wavelet in survey ST98M3.3D. Notice that in this study positive amplitudes are green, and negative amplitudes are yellow. Figure modified from Sheriff (2006)

3.2 Seismic resolution

Acoustic impedance contrasts have the potential to produce seismic reflectors as the seismic waves travel through the subsurface. These contrast has to be large enough to be detected, and the ability to detect them relies strongly on the seismic acquisition and processing system. The resolution to which these contrasts can be detected has both vertical and horizontal aspects, and is defined to be the ability to distinguish between the top and base boundaries of an layer within the subsurface (Sheriff, 1985; Brown, 1999) The relationship between wavelength, velocity and frequency is given by Brown (1999)

$$\lambda = \frac{v}{f}. \quad (3.1)$$

The wavelength is denoted λ , and v is velocity. The frequency is denoted f , and given in hertz. Downwards through the subsurface, the lithology undergoes diagenesis. This leads to an increase in seismic velocity with depth, as seismic waves propagates faster in a more compacted medium. When velocity increase, a decrease in frequency is observed. This is because higher frequencies in the seismic signal, are more quickly attenuated than the lower frequencies. The result is in an drastically increase in wavelength with depth, and this in turn

makes the resolution of the seismic data much poorer (Brown, 1999). The relationship between these parameters and depth is shown in figure 3.3.

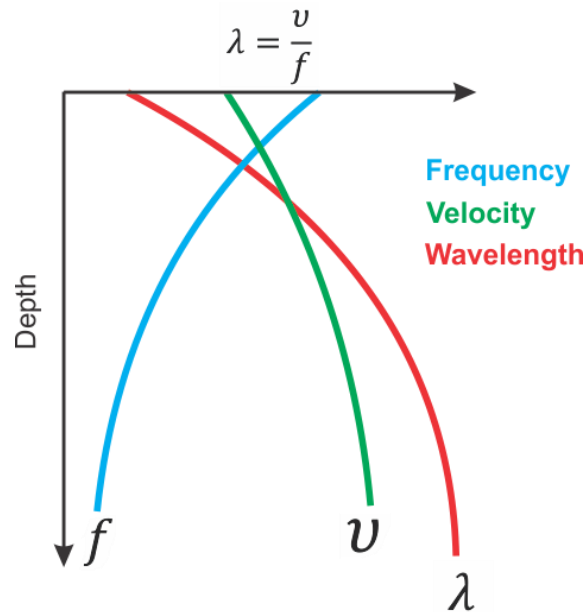


Figure 3.3: The relationship between frequency, velocity and wavelength as they propagate downwards through the subsurface. The wavelength increase drastically with depth, as frequency decreases. This reduces the resolution of the seismic data. Figure modified after Brown (1999).

3.2.1 Vertical resolution

Vertical resolution has according to Brown (1999) two limitations, the limit of visibility and the limit of separability. The limit of separability is one-quarter of a wavelength, the same as half a period, it is simply the bed thickness corresponding to the closest separation of two wavelets of given bandwidth. In other words, two reflected waves from a layer will be separated in time as long the time thickness of the layer is equal to, or larger than half of the seismic wave's period. This means that we can identify the top and bottom of the layer, as long as the thickness exceeds half the wavelength to the seismic wave. For thinner layers than this, the amplitude is progressively attenuated by destructive interference until the limit of visibility is reached. This is when the reflection signal becomes completely obscured by the background noise. The vertical resolution is given by Brown (1999)

$$Vr = \frac{\lambda}{4}. \tag{3.2}$$

The vertical resolution is here denoted as Vr , where λ is the wavelength.

By using the inspector tool in Petrel, a spectral analysis can be performed on the seismic data. The internal velocity of each layer have been obtained using the sonic logs. (Converting from $\mu\text{s}/\text{ft}$. to m/s). The vertical resolution for each sequence in survey ST98M.3D have been calculated and summarized in table 3.1. The velocities and frequencies have been measured approximately in the middle of each sequence.

Sequence	Velocity	Frequency	Wavelength	Vertical resolution
S1	1,847 m/s	41.07 Hz	44.97m	11.24m
S2	1,792 m/s	39.97 Hz	44.83m	11.20m
S3	2,032 m/s	39.57 Hz	51.35m	12.83m
S4	2,102 m/s	39.36 Hz	53.40m	13.35m
S5	2,344 m/s	39.02 Hz	60,07m	15.02m
S6	2,405 m/s	38.37 Hz	62,67m	15,69m

Table 3.1: The vertical resolution of each interpreted sequence. The internal velocity of the sequences has been obtained from the sonic logs, measured in the middle of the sequence.

3.2.2 Horizontal resolution

The horizontal resolution for unmigrated data is defined as being the radius of the Fresnel zone. Subsurface features extending beyond the Fresnel-zone, will be visible in the seismic data. Figure 3.4 illustrates waves that move in three-dimensions as they propagate in a spherical pattern from the source, these wavefronts affect a considerable large area. The area in which these waves are reflected from, and returned to the hydrophone/geophone within a half-cycle (one-quarter of a wavelength), is known as the Fresnel-zone (Sheriff, 1985). In other words, the area of the reflector that produces the reflection is limited by the wavefront arriving one-quarter of a wavelength later. Horizontal resolution of unmigrated (stacked) seismic sections is taken as being the radius of the Fresnel zone (Sheriff, 1985; Reynolds, 2011).

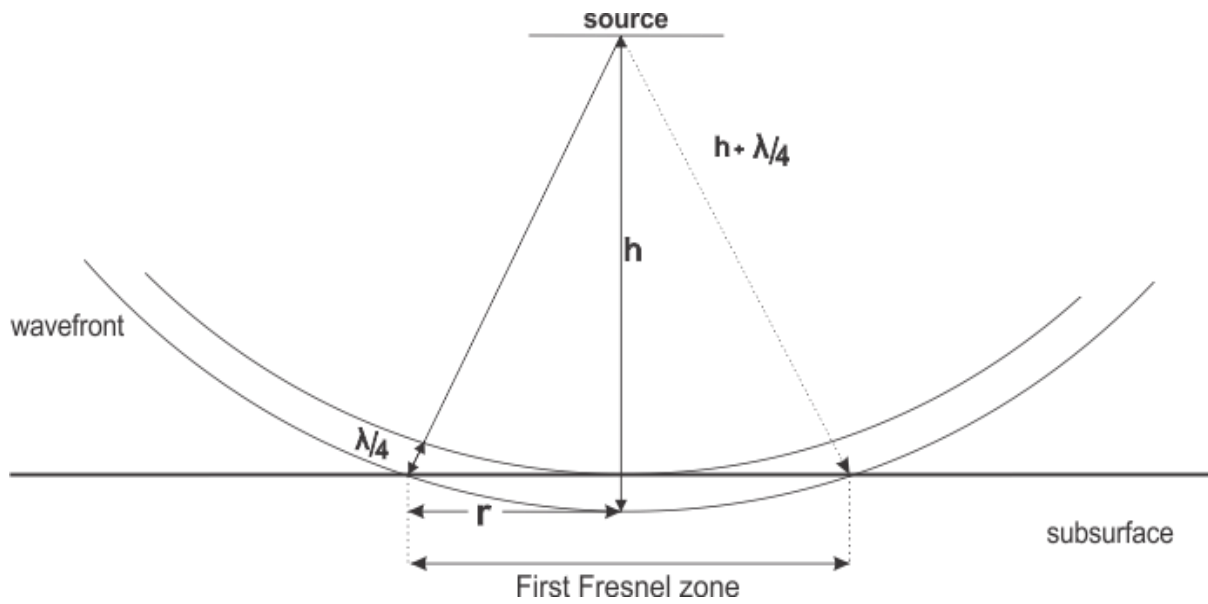


Figure 3.4: Illustrating the first Fresnel zone on a reflector at a depth of h . Figure is modified from Reynolds (2011).

The size of the Fresnel zone in unmigrated data defines horizontal resolution, and its magnitude can be calculated. The radius of the Fresnel zone increase with depth and higher frequency gives a higher radius of the Fresnel zone. The radius of the Fresnel zone is given by Sheriff (1980)

$$rf = \frac{v}{2} \sqrt{\frac{t}{f}}$$

(3.3)

The radius of the Fresnel-zone is here denoted as rf , where v is the average propagating speed of the incident wave. The two-way travel times is given as t , and f is the frequency.

Migration is a technique to improve the horizontal resolution, by reposition reflections which are out of place because of dip. It also involves focusing the energy spread over the Fresnel zone and collapsing diffractions patterns (Brown, 1999). In migrated seismic data, the horizontal resolution can be improved considerably, by collapsing the Fresnel zone. However, in two-dimensional seismic data, the migration only allows the collapse of the Fresnel zone in the inline direction. This is illustrated in figure 3.5, in the light blue colored ellipse. For three-dimensional data, the migration of data can collapse the Fresnel zone to a considerable

smaller circle. This is because seismic waves are three-dimensional, and by just applying migration in two-dimension, we can only expect part of the improvement (Brown, 1999). Horizontal resolution of migrated seismic data is given by Sheriff (1985) and Reynolds (2011)

$$Hr = \frac{\lambda}{4} \tag{3.4}$$

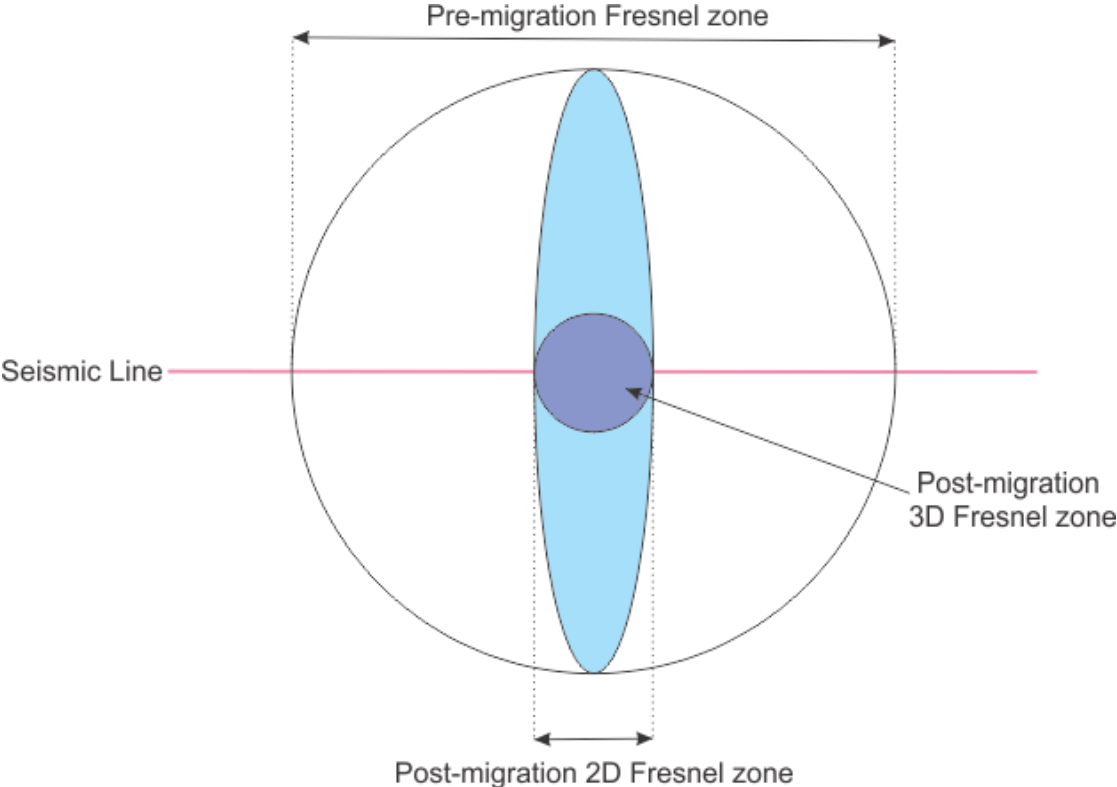


Figure 3.5: illustration of the Fresnel zone in different migration settings. The light blue ellipse show that the Fresnel zone can only be collapsed in the inline direction of the two-dimensional seismic line – perpendicular to the line for 2-D migration. In three-dimensional data, the Fresnel zone can be shrunk down to a small circle. Figure modified from (Brown, 1999).

By applying equation 3.3 and 3.4, the radius of the Fresnel zone have been calculated for each interpreted sequence. The two-way time used in these calculations, is the estimated depth to the interpreted horizons. These follow distinctive high amplitude reflections. Table 3.2 summarizes the horizontal resolutions.

Sequence	Velocity	Frequency	Two-way travel time	Horizontal resolution, pre-migration	Horizontal resolution, post-migration
S1	1847 m/s	41.07 Hz	0.35s	85m	11.24m
S2	1792 m/s	39.97 Hz	0.6s	109m	11.20m
S3	2,032 m/s	39.57 Hz	0.9s	153m	12.83m
S4	2,102 m/s	39.36 Hz	1.15s	179m	13.35m
S5	2,344 m/s	39.02 Hz	1.3s	214m	15m
S6	2,405 m/s	38.37 Hz	1.5s	237m	15.66m

Table 3.2: Summary table of the horizontal resolutions, for each seismic sequence. The velocity is obtained from the sonic logs and the two-way time is estimated based on the depth of the interpreted horizons.

3.2.3 Artifacts and noise

By interpreting the seafloor of the seismic data, a surface can be generated. These surfaces show the outline of the seafloor reflection (Fig. 3.6). The 3D survey has been merged together with different surveys and reprocessed to the current one (Basu et al., 2008; Karstens & Berndt, 2015). This is clear as the interpretation of the seafloor reflection show larger sections that represent the numerous surveys (Fig. 3.6). Regarding wavelet phase and configuration, the wavelet jumps an entire phase from different sections. The abnormal seafloor configuration is assumed to be related to the synchronization and adjustment of the seismic data during processing; as the wavelets and reflections fits in the subsurface. However, different survey sections have slightly different amplitude value distributions. In other words, some sections will appear to have stronger amplitudes than others and vice versa. This is because they show a different signal-to-noise ratio. This is important to remember when interpreting reflection configuration. Figure 3.6 show the interpreted seafloor reflector. Survey footprints are present throughout the survey, and these correlates to the acquisition geometry of our survey; as they occur parallel to the inlines direction (Chopra & Larsen, 2000).

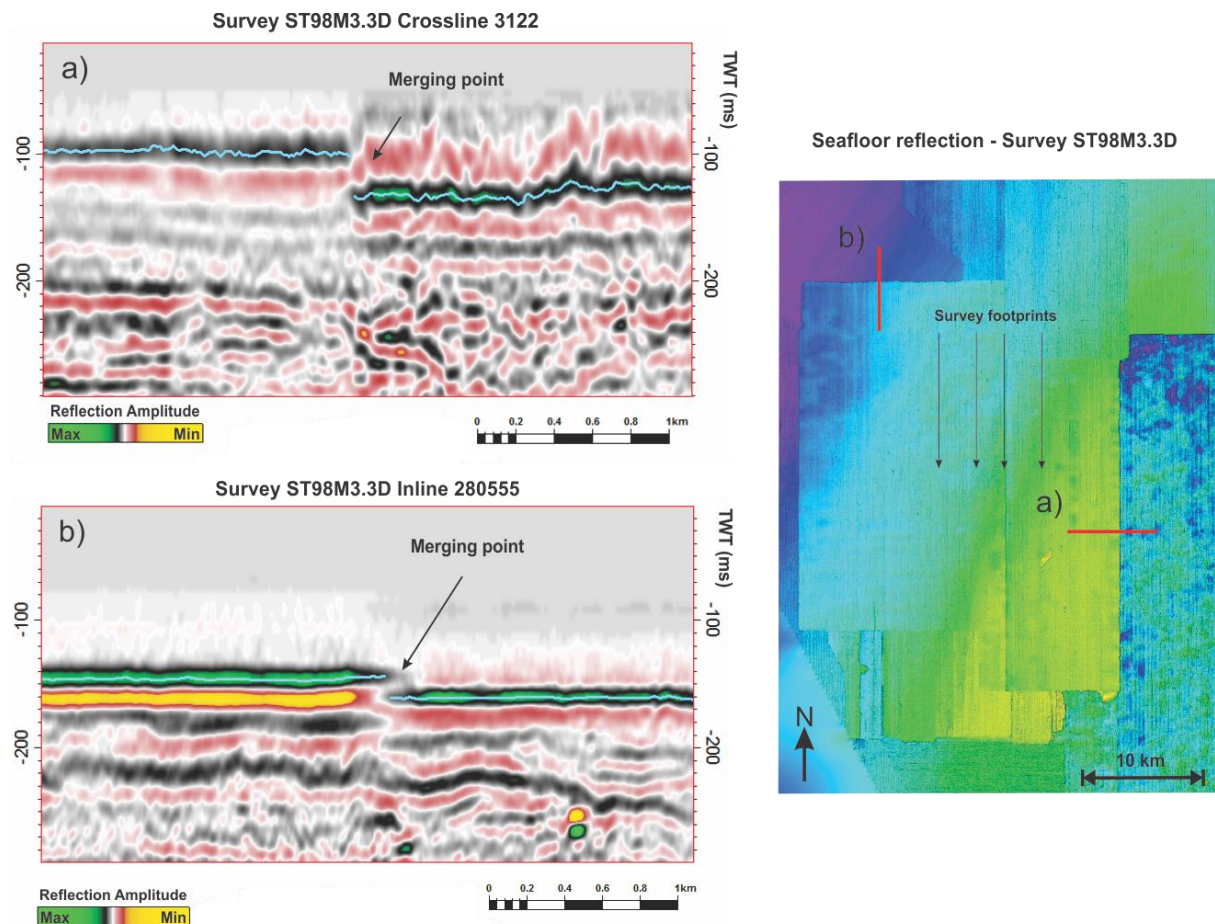


Figure 3.6: The interpreted seafloor reflection is indicated towards the right. Crossline 3122 (a) and inline 280555 (b), are illustrating the irregularities seen at the seafloor reflector. Also notice the survey footprints parallel to the inline direction, oriented N-S.

3.3 Petrel - Interpretation and visualization

The Petrel 2014 software from Schlumberger has been used during this study to interpret, visualize and manage data. The seismic depth is given in two-way time (TWT). Horizons have been interpreted by using seeded 2D auto tracking and guided auto tracking. Petrel has also provided a platform to investigate seismic sequences in depth, by using volume attributes and modelling tools.

3.4 Seismic sequence classification

Based upon the reflection configuration, continuity as well as amplitude characteristics, seismic sequences will be mapped and delimited. Each seismic sequence within survey ST98M3.3D, show a different configuration. And in order these sequence in three dimensions throughout the survey, interpretation of key reflectors will be prioritized.

3.5 Seismic attributes

Seismic attributes was introduced in the early 1970's. These attributes was based on complex seismic traces and provided an important tool for interpreting data in a qualitative way (Odoherthy & Anstey, 1970; Balch, 1971). Since then, seismic attributes have become an important and central tool in lithology predication and reservoir characteristics (Taner, 2001; Chopra & Marfurt, 2005). One of the early contributors on seismic attributes, Taner, M. T., defines a seismic attribute as “all the information obtained from seismic data, either by direct measurements or by logical or experienced reasoning” (Taner, 2001). However, seismic attributes is not new information. Attributes represent different methods and ways to present basic information from the seismic data (Brown, 2001). Classification of different seismic attributes can be done in many different ways (Taner, 2001). The basic overview given by Brown (2001) is presented in figure 3.7. Time, Amplitude, Frequency, and Attenuation are the main aspects, and different attributes of these can be used pre- or post-stack (Brown, 2001). By selecting the right attributes, important information can be extracted from the seismic data. Some authors have suggested to select attributes that are independent of one another, and to avoid false correlations, attributes should be confined to physical properties (Barnes, 2000; Chopra & Marfurt, 2005). This thesis aims to identify reflection configuration in relation to well data. Hence, the following attributes will be used.

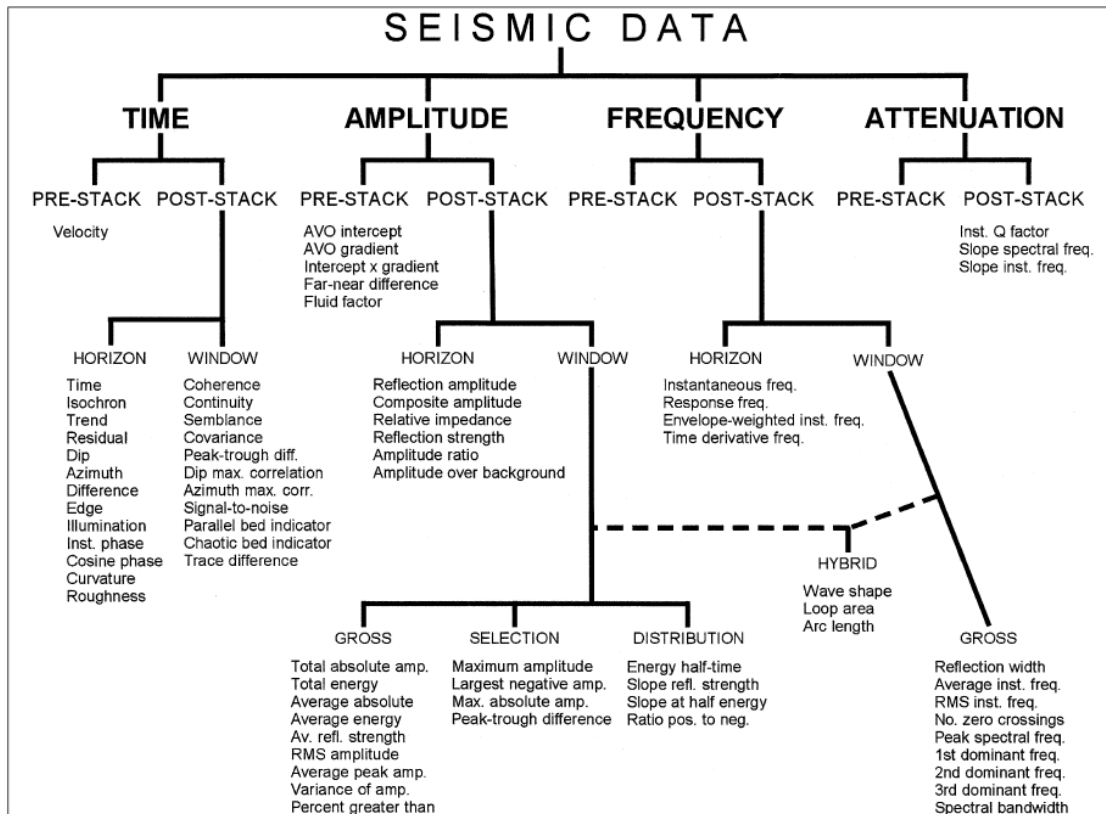


Figure 3.7: Classification scheme of seismic attributes, from basis seismic information of time, amplitude, frequency and attenuation. Figure from (Brown, 2001).

The Trace Envelope

Also called “Instantaneous amplitude, magnitude or reflection strength. The trace envelope attribute, represent the envelope of the seismic trace. It occur with relative low frequency and consist of only positive amplitudes. The envelope can be referred to as the instantaneous energy of the seismic trace, and its magnitude is proportional to the reflection coefficient (Subrahmanyam & Rao, 2008) The envelope attribute is important for detecting bright spots, often caused by shallow gas accumulations. It can also detect major lithological changes related to strong reflections and boundaries. The envelope is calculated by taking the square root of the sum of the squares of the real and imaginary amplitudes (Chopra & Marfurt, 2005).

Cosine of phase

The cosine of phase is a good indicator of the lateral continuity of layers, sequences boundaries, faults, and on-lap patterns. This attribute is independent from the amplitude, and is therefore very useful in the interpretation of reflectors who show great variability in their

amplitude (Subrahmanyam & Rao, 2008). It shows variations in energy of different reflectors, as it mainly represent the acoustic impedance contrast (Taner, 2001).

Dominant frequency

The dominant frequency is further defined by Barnes (1993) as the square root of the sum of squares of the instantaneous frequency and bandwidth. Dominant frequency is essentially the hypotenuse between instantaneous frequency and instantaneous bandwidth (Barnes, 1993). The dominant frequency attribute can indicate bed thickness and even lithology parameters. These will appear as contrast between different frequency values. Edges of low acoustic impedance thin layers can also be detected. Furthermore, higher frequencies can indicate sharp interfaces or thinner layers of shale, lower frequencies can indicate sand rich bedding (Subrahmanyam & Rao, 2008).

Variance

The variance attribute represent the trace-to-trace variability calculated in three dimensions in a particular interval, it then produces lateral changes in acoustic impedance that can be interpreted. In other words, traces similar to each other in three dimension will produce a low variance coefficients, and traces that are discontinuous will produce large variance coefficients. Hence, features such as channels, faults and abrupt lithology/geometry changes will be clearly seen in the seismic section.

RMS

The root mean squared (RMS) attribute calculated the square root of the sum of squared amplitudes, and divided it by the number of samples within a specific time window (Schlumberger, 2014). The RMS attribute is use in order to highlight abnormal high amplitudes, both negative and positive. The RMS attribute is a good indicator of acoustic contrasts, which could indicate a change in lithology and hydrocarbons.

3.6 Well data

3.6.1 Well position

Five wells has been used in this study. These are exploration wells drilled in the Sleipner area during the 1980s (NPD, 2016). Figure 3.8 indicate the position of each well. The wells are located in the Sleipner East field in the North Sea. They comprise both wildcat wells and appraisal wells (NPD, 2016). The exact coordinates of the wells is summarized in table 3.3. The coordinate system is ED50-UTM31.

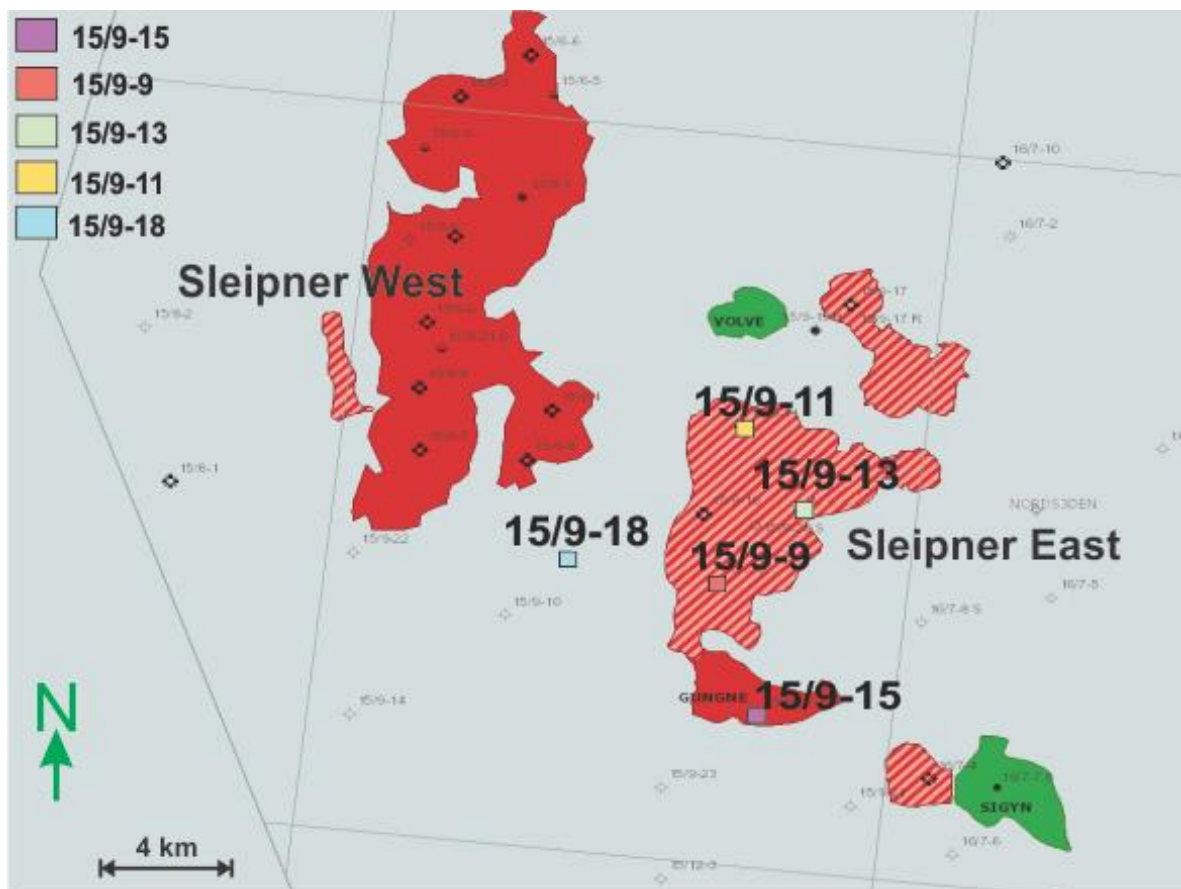


Figure 3.8: Map of the Sleipner gas field (Block 15/9). The wells used in this study are shown in relation to the Sleipner field. Red zones are gas fields, striped red is gas/condensate, green is oil fields. The Norwegian border runs to the west of the Sleipner west field. Notice that well 15/9-18 is located outside the Sleipner east field. The map is modified from Factmap (2016).

Well	X	Y	Latitude	Longitude
15/9-9	435038.52m	6467984.08m	58°20'47.81"N	1°53'24.97"E
15/9-11	435410.76m	6474001.57m	58°24'2.53"N	1°53'41.79"E
15/9-13	437653.7m	6470978.02m	58°22'25.96"N	1°56'2.86"E
15/9-15	436817.55m	6462991.44m	58°18'7.35"N	1°55'19.28"E
15/9-18	429961.76m	6468508.49m	58°21'1.95"N	1°48'12.26"E

Table 3.3: The location of each well. The coordinate system is: ED50-UTM31.

3.6.2 Well logs

Each well have a total of seven logs, and in the well-section window presented in figure 3.9, value ranges for each log is hard to see. Abbreviations, value ranges and units used in each log is therefore presented in table 3.4. Each well log have their lowest value to the left, in their respective column. The acoustic impedance log (AI) and reflection coefficient (RC), have been constructed using the sonic and density log, by simply multiplying the density log with the sonic log. The corresponding reflection coefficient is extracted from the acoustic impedance log.

Some of the well logs don't cover the uppermost section of seismic data in survey ST98M.3D. The well log coverage towards the seismic data is indicated in figure 3.9. The gamma ray and sonic logs cover the entire upper seismic section. The density, caliper, acoustic impedance and reflection coefficient logs starts in the middle of the Nordland Group. The neutron logs generally starts at the Hordaland Group, and extends further down (Fig. 3.9)

Three well-tops are located in the seismic area used in this study. The well tops marks the beginning of a Formation or a larger Group. In this study, the well-tops marks the beginning of the Nordland Group, Utsira Formation and the Hordaland Group. The wells are calibrated and time converted using check-shot. The depth of the well tops (NPD, 2016) is summarized in table 3.5. In the well-section windows the dotted lines of surfaces and well tops, show their relative position at the exact interaction point between the well log and the interpreted seismic reflection. This can be misleading, as the data resolution of the well logs is several times

higher than the seismic (Fig 3.9). The well-section windows further used in the thesis will have color tables, to better visualize the different log values.

Log type	Abbreviations	Value range and units
Gamma ray	HGR	0-120 API
P-sonic	HDT, HAC	30-230 us/ft.
Density	HRHROB, DEN	1-3 g/cm ³
Neutron	HNPFI, HCNC	0-1 m ³ /m ³
Caliper:	HCALI	0.10-0.80 in
Acoustic impedance	AI	0-8000 kPa s/m
Reflection coefficient	RC	-0.1 - 0.1

Tabell 3.4: All the different logs used in this thesis. The table gives an overview of the abbreviations, value ranges and units used in the well-section windows for each log.

WELL	Nordland GP		Utsira Fm		Hordaland GP	
15/9-9	-165.10ms	108m	-886.06ms	844m	-1128.99ms	1092m
15/9-11	-185.93ms	113m	-867.96ms	823m	-1341.03ms	1311m
15/9-13	-220.54ms	106m	-912.60ms	869m	-1178.93ms	1143m
15/9-15	-107.79ms	108m	-922.83ms	884m	-1156.58ms	1129m
15/9-18	-203.69ms	120m	-919.04ms	866m	-1246.40ms	1210m

Table 3.5: The depth of the different well-tops in our study area (NPD, 2016). The depth corresponds to the start of the Formation/Group. By using check-shot calibration, the depths of the wells-tops can be given both in two-way-time (TWT), and meters.

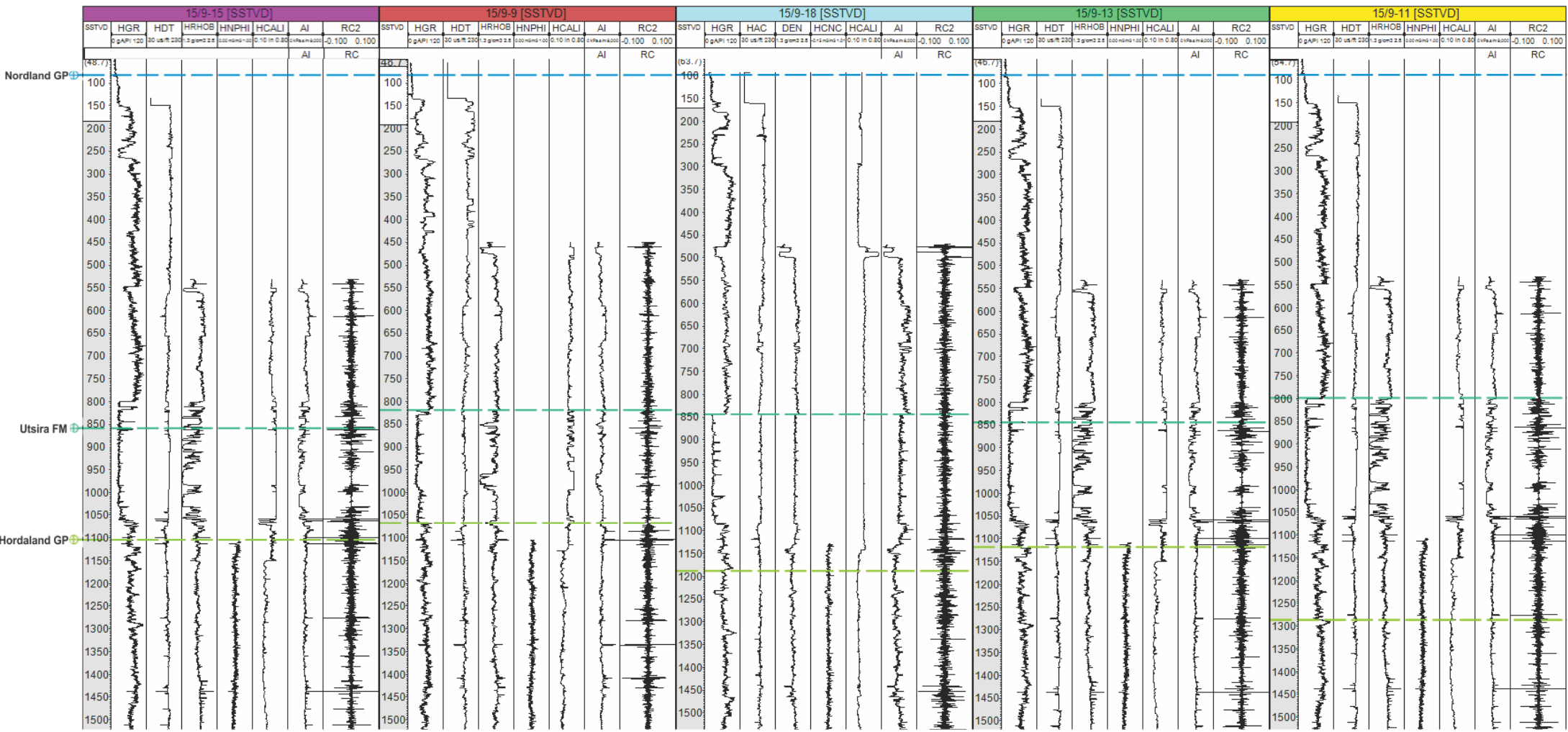


Figure 3.9: Well section window with all the wells and corresponding well logs used in this study. The position of the well tops is indicated according to NPD (2016). The well logs are flattened on the Nordland GP well top. Value ranges for each log is summarized in table 3.4.

3.6.3 Well seismic

In order to compare the seismic data with the different log responses, seismic adjacent to the well have been extracted. Figure 3.10 show a principle sketch of orbital extraction. By using a positive and negative azimuth of 180° the seismic can be extracted in a circle, centered on the well track for each time step. This has been done for all the wells and corresponding seismic/attributes.

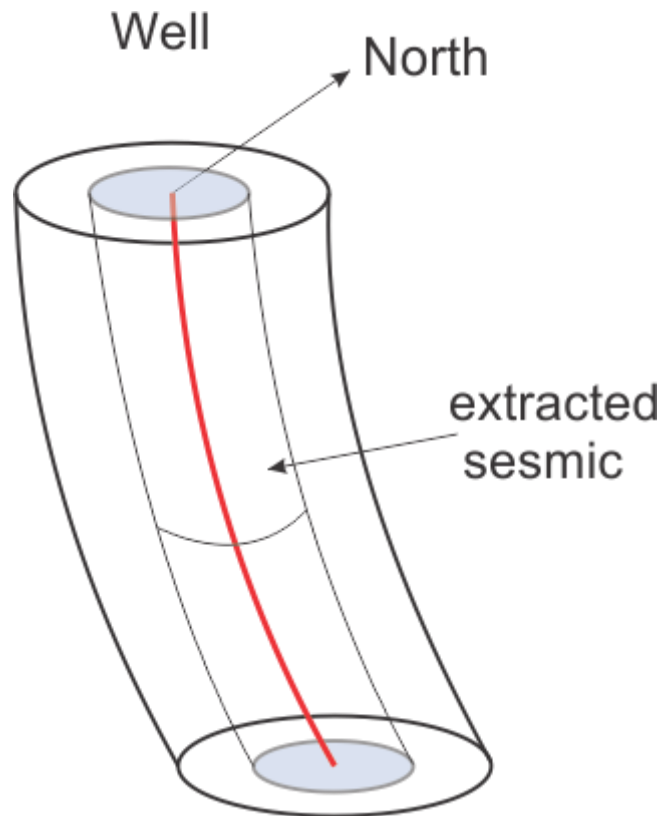


Figure 3.10: Principle sketch of the orbital extraction of well seismic. The red line is the well track, and the shaded blue circles indicate the seismic volume that have been extracted. Figure is modified after (Schlumberger, 2014).

3.7 Petrophysical modeling

By using the grid tool in Petrel, a simple model of Survey ST98M3.3D have been constructed. This involve building the model according to the interpreted horizons and then adjusting the depth, using well-tops from NPD (2016). The model consists of zones or volumes in-between the horizons. These zones represent the different sequences, and will be populated with physical properties from wells and resampled seismic from the survey. This is done by using the co-kriging interpolation method. Co-kriging will primary be used on each individual sequence, and presented along the interpreted horizons. Co-kriging will also be used on the entire model, in order to insert a hypothetical well and predicate how the petrophysical values change laterally. Figure 3.11 show a sketch of the model and summarize the most important steps that have been done towards co-kriging. Table 3.6 and 3.7 summarized the location, orientation and amount of grid cells in the model. The variable depth within the model is captured by the interpreted horizons. As the seismic covers only post-rift sediments, and generally show continuous bedding, no faults have been included in the model. There are no major tectonic faults in the seismic data.

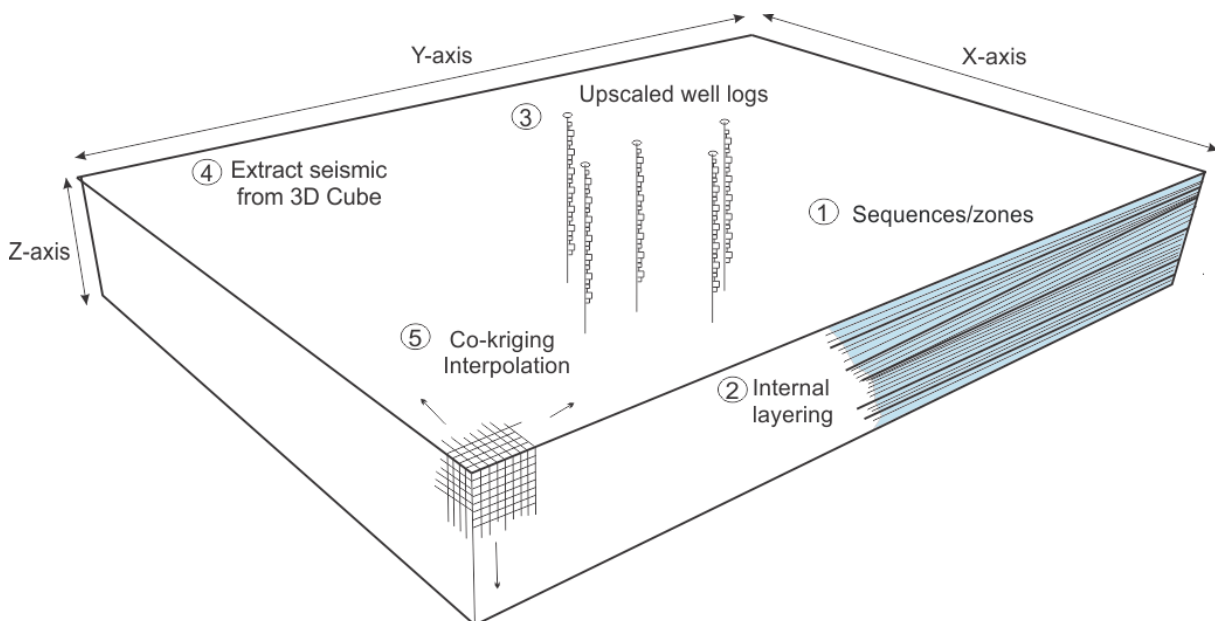


Figure 3.11: Sketch of the simple grid model, and the different processes related to building the model and co-kriging. 1. The interpreted horizons subdivided the model into sequences. (“Zones” in Petrel”). 2. The sequences are adjusted to well tops and given internal layering. Every sequences have 20 layers, expect for sequences S2 (25 layers). The internal layering set the vertical resolution for the well logs. 3. The original well logs are up-scaled after the internal layering of the model. 4. Seismic data will be extracted from the original seismic 3D cube (Survey ST98M3.3D). The seismic data will act as the secondary variable under the co-kriging interpolation. 5. Co-kriging interpolation is used to distribute the petrophysical data from the up-scaled well logs in each cell. The co-kriging algorithm uses specific semivariogram parameters (see chapter 3.7.2.). The petrophysical data from the well logs is the primary variable.

Axis	Min	Max	Delta
X	412583m	448883m	36300m
Y	6451052m	6501452m	50400m
Z (TWT)	-1500ms	-65.93ms	1434.07ms
Latitude	58°11'26.51"N	58°38'56.35"N	0°27'29.84"N
Longitude	1°29'38.38"E	2°07'49.72"E	0°38'11.34"E

Table 3.6: Extent and location of the model, given both in meters and latitude, longitude. The coordinate system is: ED50-UTM31.

Description	Value
Grid cells	363 x 504 x 6
Total number of 3D grid cells	1097712
Total number of 3D grid nodes	1286740
Number of horizons	6

Table: 3.7: The amount of grid cells, nodes, and horizons used in the model.

3.7.1 Up-scaled well logs

By giving these zones multiple layers, the final vertical resolution of the model can be set. The well log graph can be commonly seen as an irregular line extending downwards. In Petrel, this graph consist of a large number of data points, where each point represent a sample. In order to do modeling with the well logs, they have to be normalized. By giving the model layers, Petrel subdivide the well-logs into sections, were the average value is used. This operation is called “up-scaling”, and is a method to get the detailed data from the well-logs into the model. The up-scaled well logs has to be representative, and a quality check should be performed in Petrel, by comparing the original data with the up-scaled data. This is done by using the histogram function, which compares the original data and the up-scaled data. The distribution of values is plotted towards the percentage of occurrence in the model. The up-scaling process is essentially a coarsening of the data, and is an important step in modeling.

The gamma ray, sonic, density and neutron logs have all been up-scaled, and will be further used in the co-kriging interpolation. In the following subchapters, the original well logs are presented towards the up-scaled well logs.

3.7.1.1 Gamma ray logs (HGR)

Figure 3.13 show the up-scaled gamma ray values (blue) compared to the original well logs (red). The histogram show values for the whole model, and the values used in the model is indicated as green. The histogram show a relative good fit between the up-scaled logs and the original data. The well section window in figure 3.14, show the up-scaled and the original well logs. The vertical resolution within the up-scaled logs, is set by the layers given to each sequence in the model. The well section window also indicates a relative good correlation.

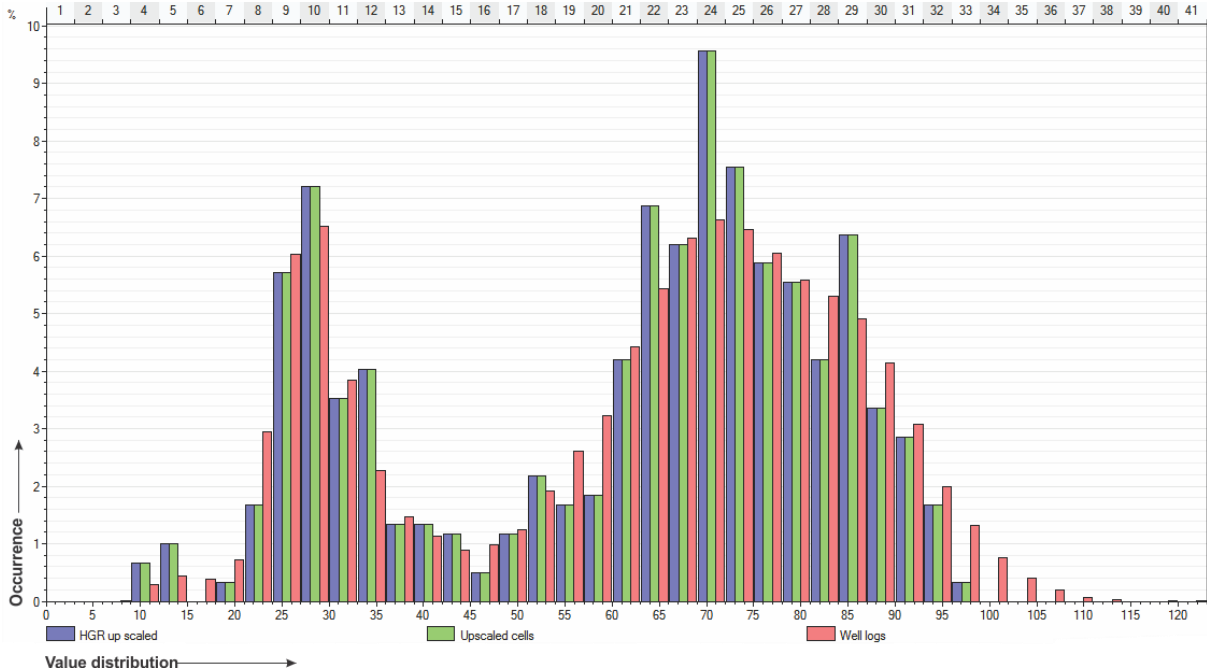


Figure 3.13: Histogram showing the gamma ray values plotted along the X-axis, and the percentage of occurrence in the model plotted in the Y-axis. The X-axis is subdivided into intervals, indicated at the top of the figure. Blue columns are the up-scaled values. Green columns are the values used in the model, and corresponds to blue. Red columns are the original data from the well logs.

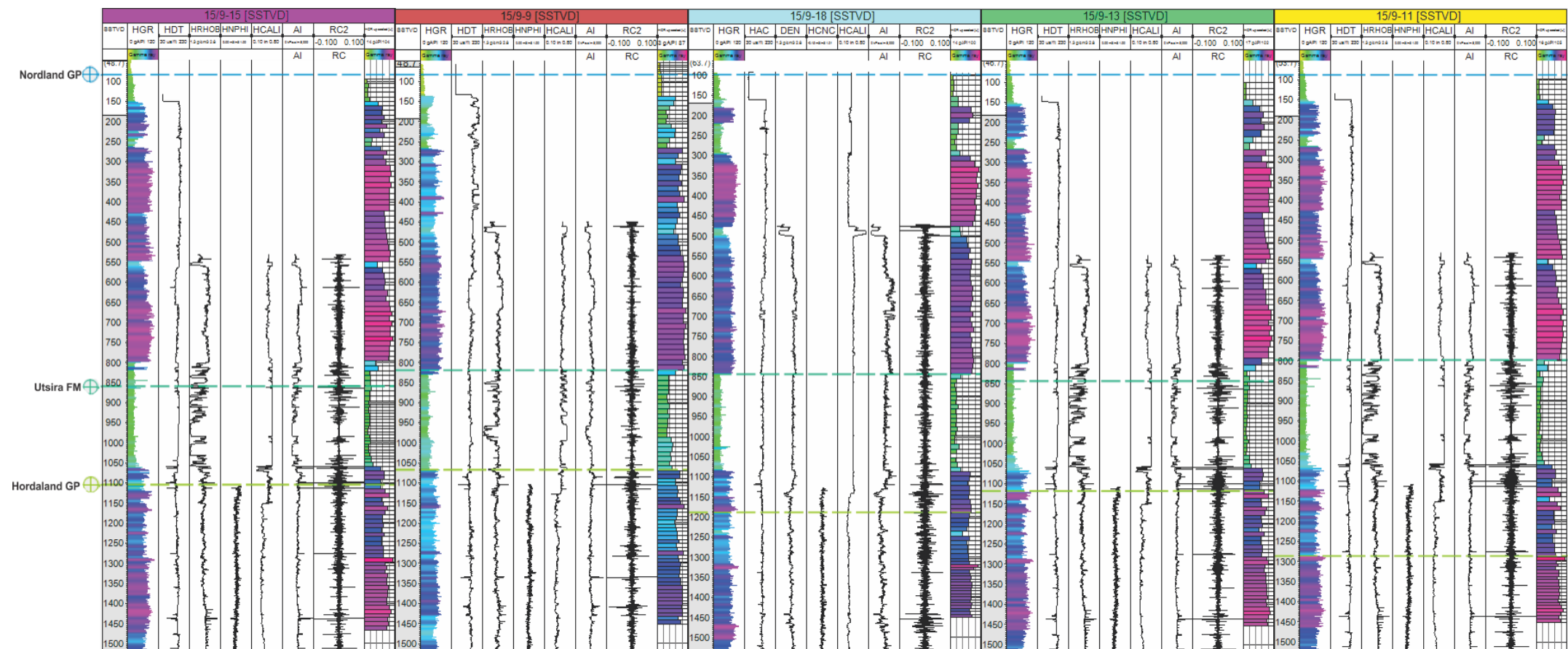


Figure 3.14: Well section window that indicates the relationship between the gamma ray log and the corresponding up-scaled logs. The original logs is shown to the left in the wells, and the up-scaled logs to the right. The vertical resolution of the up-scaled logs is indicated as layers within the logs, these corresponds to the layers given to the model. Value ranges for the color table is shown in table 3.4.

3.7.1.2 Sonic logs (HDT)

Figure 3.15 show the histogram for the original data in the sonic logs and the corresponding up-scaled logs, in the entire model. The histogram indicates a relative good fit, but some deviations are present. Figure 3.16 show a well section window that show the resolution of the up-scaled well logs towards the original data. It is clear from the well section window, that the upscaling processes averages values, and details from the original logs is lost. However, the well section window indicates an overall good fit towards the original data.

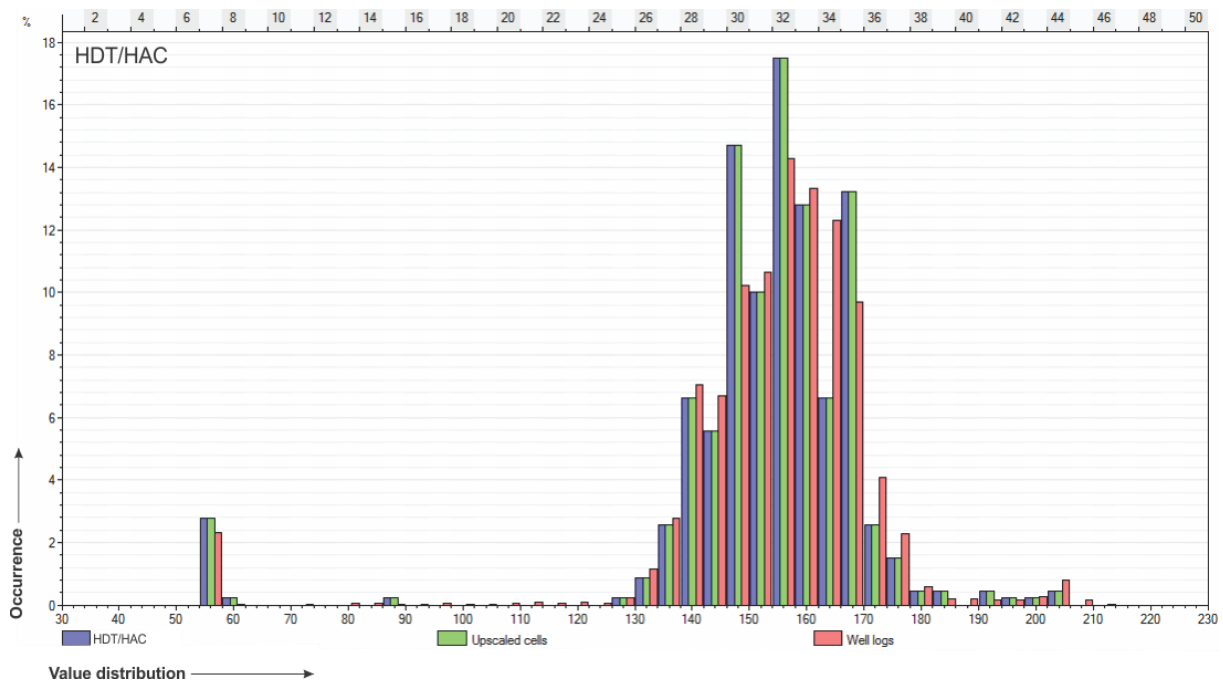


Figure 3.15: Histogram showing the Sonic values plotted along the X-axis, and the percentage of occurrence plotted in the Y-axis. The X-axis is subdivided into intervals, indicated at the top of the figure. Blue columns are the up-scaled values. Green columns are the values used in the model, and corresponds to blue. Red columns are the original data from the well logs.

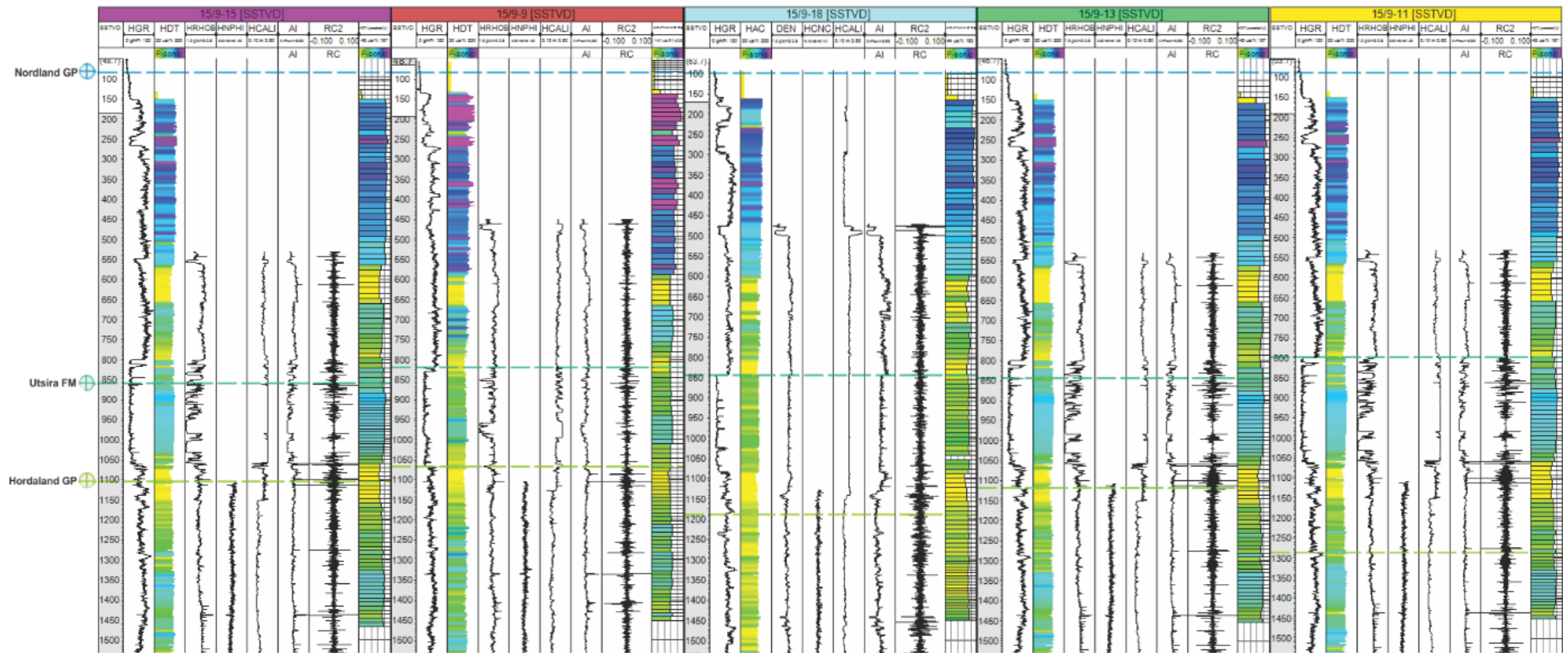


Figure 3.16: Well section window that indicates the relationship between the sonic logs and the corresponding up-scaled sonic logs. The original logs is shown to the left in the wells, and the up-scaled logs to the right. The vertical resolution of the up-scaled logs is indicated as layers within the logs, these corresponds to the layers given to the model. Value ranges for the color table is shown in table 3.4

3.7.1.3 Density logs (HRHOB)

The density logs start in the middle of the Nordland Group. This implies that the uppermost sequences, will not be interpolated using the density logs. The histogram shown in figure 3.17, indicate the relationship between the original data and the up-scaled logs. The histogram indicate a relative good fit between the two datasets. The well section window in figure 3.18 indicates the same. However, interlayers with spikes in the density logs are seen. These spikes are averaged within the up-scaled well logs.

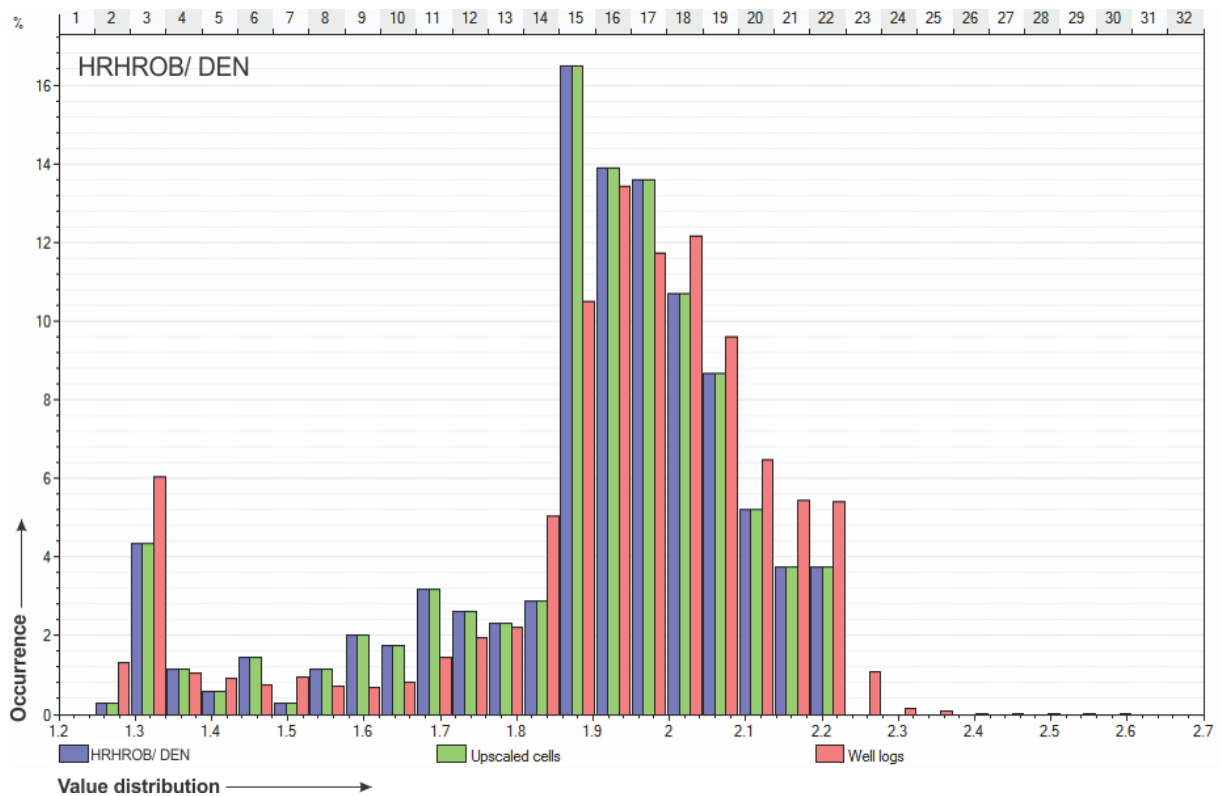


Figure 3.17: Histogram showing the Density values plotted along the X-axis, and the percentage of occurrence plotted in the Y-axis. The X-axis is subdivided into intervals, indicated at the top of the figure. Blue columns are the up-scaled values. Green columns are the values used in the model, and corresponds to blue. Red columns are the original data from the well logs.

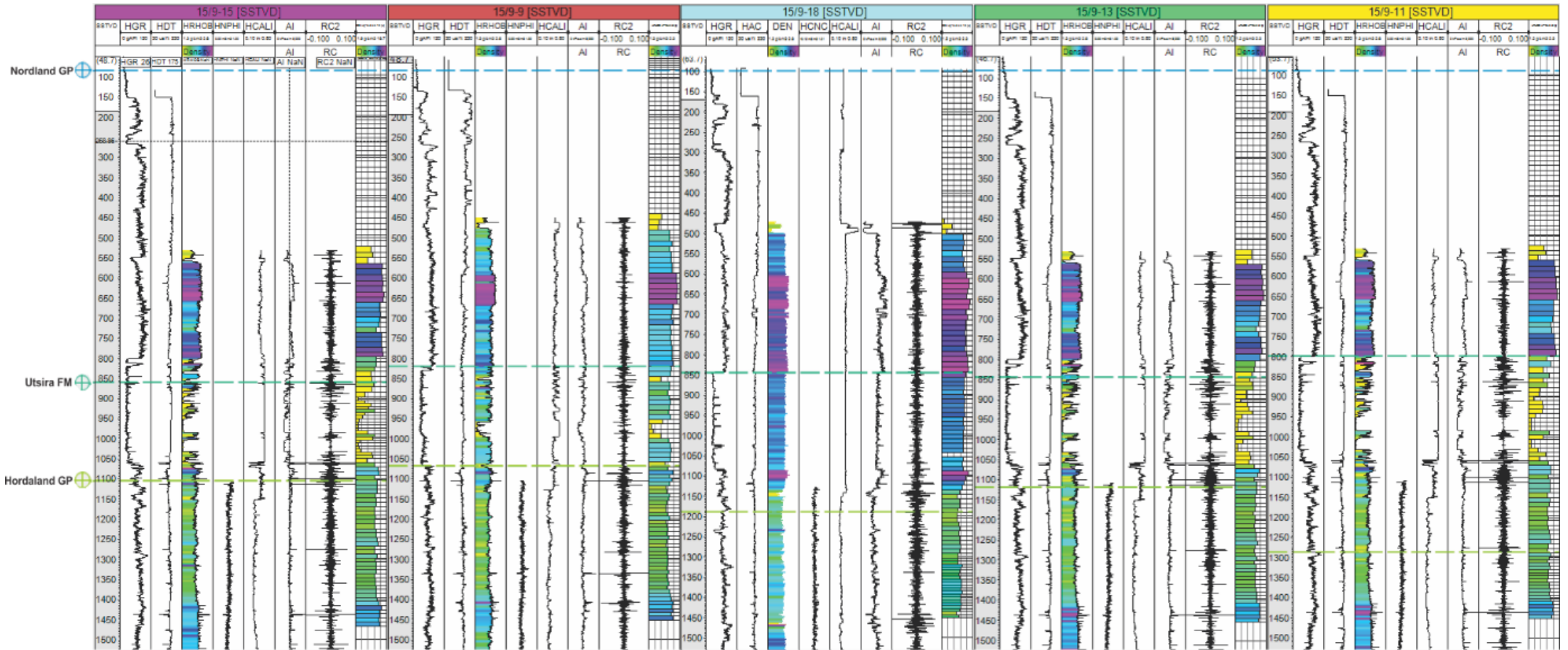


Figure 3.18: Well section window that indicates the relationship between the density logs and the corresponding up-scaled density logs. The original logs is shown to the left in the wells, and the up-scaled logs to the right. The vertical resolution of the up-scaled logs is indicated as layers within the logs, these corresponds to the layers given to the model. Value ranges for the color table is shown in table 3.4.

3.7.1.4 Neutron logs (HNPHI)

The neutron log only cover the lower part of the seismic data. The histogram in figure 3.19, indicate that most of the neutron values are located between 0.42 and 0.60 m³/m³. The up-scaled well logs represent this value distribution, as values located further away from this interval is neglected. These values represent a very small portion of the original logs. However, it is still a clear loss of detail. The well section window in figure 3.20, indicates both the original data and the up-scaled logs, and the extent of the logs is clearly seen. Both the histogram and the well section window, indicate that the up-scaled logs fit the original data.

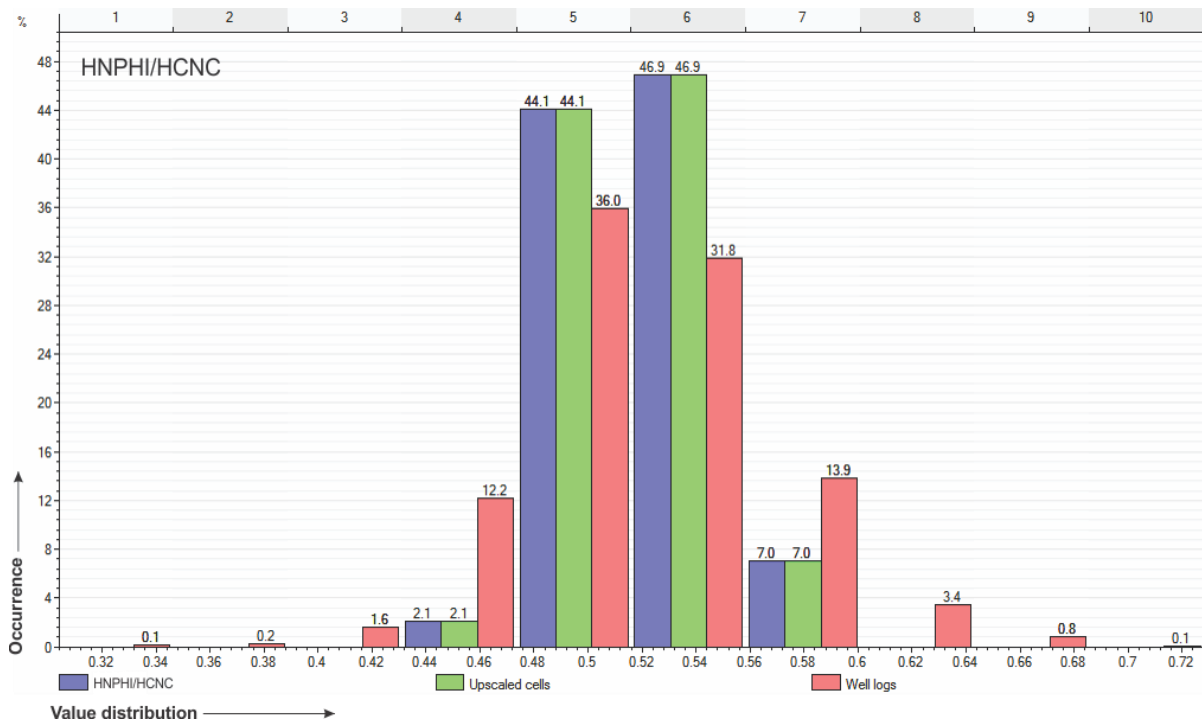


Figure 3.19: Histogram showing the neutron values plotted along the X-axis, and the percentage of occurrence plotted in the Y-axis. The X-axis is subdivided into intervals, indicated at the top of the figure. Blue columns are the up-scaled values. Green columns are the values used in the model, and corresponds to blue. Red columns are the original data from the well logs.

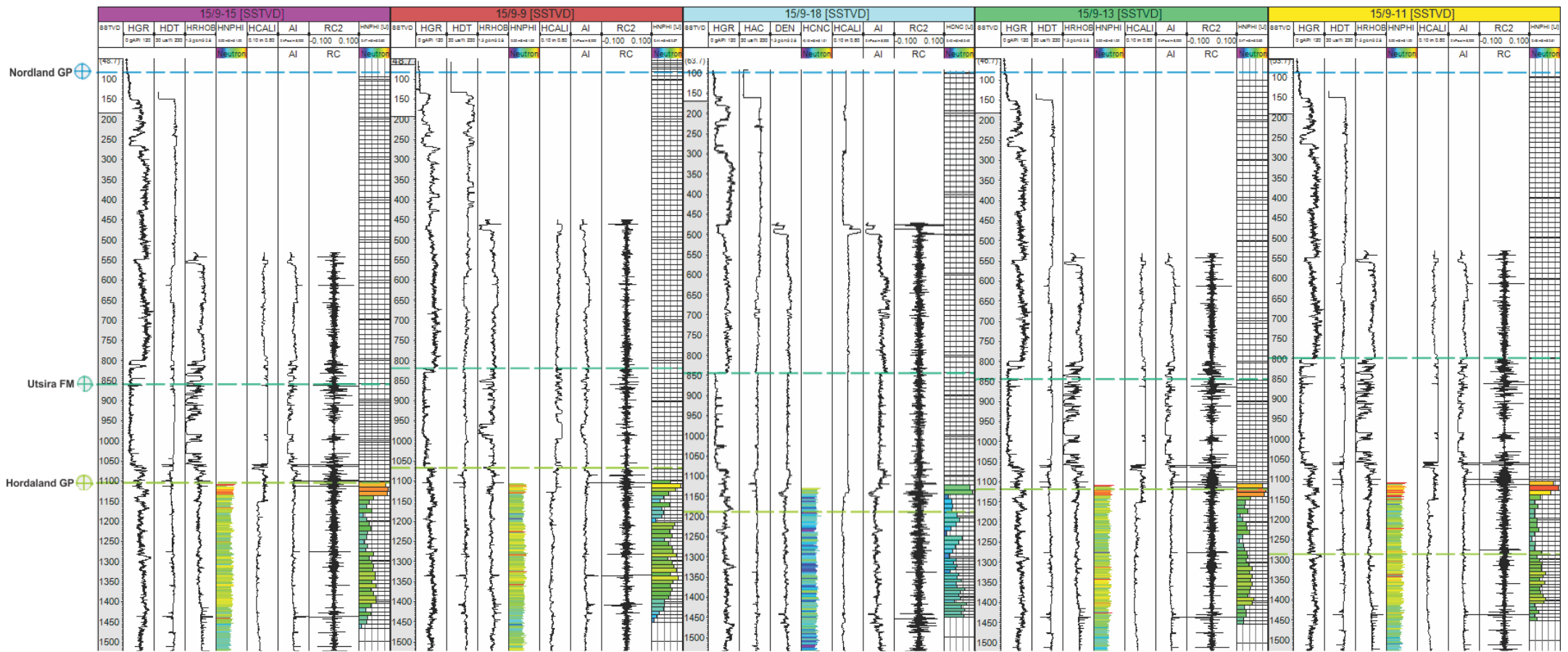


Figure 3.20: Well section window that indicates the relationship between the neutron logs and the corresponding up-scaled neutron logs. The original logs is shown to the left in the wells, and the up-scaled logs to the right. The vertical resolution of the up-scaled logs is indicated as layers within the logs, these corresponds to the layers given to the model. Value ranges for the color table is shown in table 3.4

3.7.2 Semivariogram fitting and co-kriging

The wells are located in a relatively small area, compared to the size of the model. The data analysis tool in Petrel is used in order to find the limits of the semivariogram. Figure 3.21 show the semivariograms used for modeling gamma values in the model. The major and minor direction semivariograms is used for every sequence and property. In the major and minor direction, the range is set to 12000 and 8600 meters, respectively. This implies that there is a correlation between the well logs in this area, and that there is no correlation outside these ranges (Fig. 3.21). This gives the possibility to compare each sequence according to the same parameters, after the co-kriging interpolation. Table 3.8 summarizes the spherical semivariogram parameters used in the co-kriging interpolation for each well log.

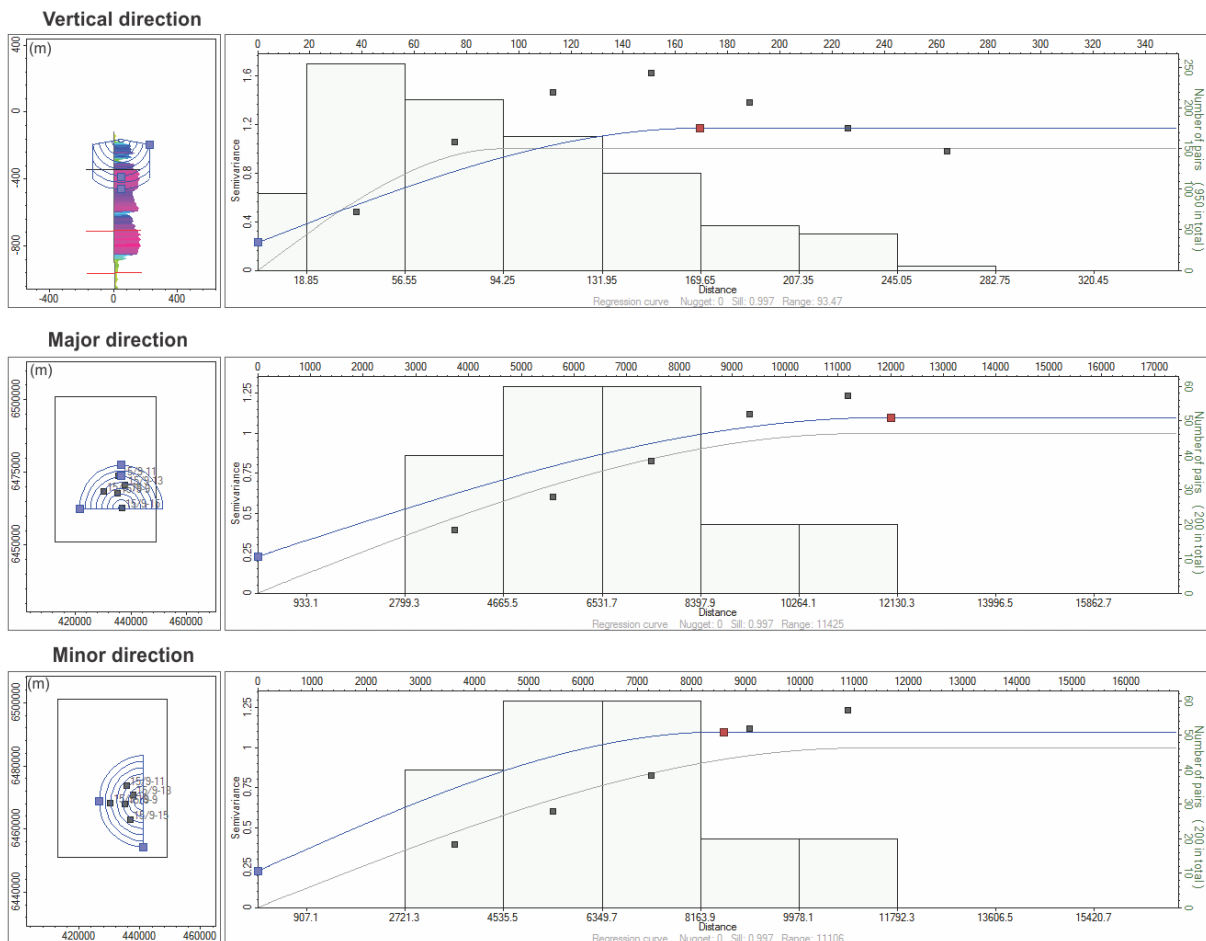


Figure 3.21: Semivariograms used in co-kriging interpolation. The major and minor direction semivariograms, is used for all the sequences and properties. The histogram shows number of data points within each lag. The grey line is the regression curve. The blue line is the semivariogram model used. The windows to the left show the extent of the semivariogram in the model, wells are indicated as black points.

Well log	Sill	Major range	Minor range	Vertical range	Nugget
HGR	0.8931	12000m	8600m	170m	0
HDT	0.9981	12000m	8600m	213m	0
HROB	0.6527	12000m	8600m	41m	0.4043
HNPHI	1.0152	12000m	8600m	48.376m	0.1909

Table 3.8: Semivariogram parameters used in the co-kriging interpolation.

4 Results

This chapter presents the different findings and interpretations done from survey ST98M3.3D and the five wells. The 3D grid model can be considered an interpretation, as its outline is based on the classification of seismic sequences and well data. The co-kriging results presented, are just one realization of many different outcomes, as the outcome of the model is strongly influenced by the modelling phase. The sequences will be interpreted and discussed from youngest to oldest.

4.1 Seismic sequences

Survey ST98M3.3D comprises several strong lateral continuous reflectors. By subdividing the seismic cube into seismic sequences based upon different reflection configurations, geological assumptions about the depositional area and conditions can be made. By using seismic adjacent to the wells, good correlations can be done. In order to illustrate the distribution and outline of the seismic sequences, seismic lines that cover the length and width of survey ST98M3.3D are first shown. Figure 4.1 shows the study area and the location of the overview seismic sections.

4.1.1 Seismic overview

Figure 4.2 and 4.4 show two un-interpreted seismic sections, inline 795155 and crossline 3038. These lines provide a good overview of the seismic trend in the study area. The inline extends through the entire survey from south to north, and the crossline from east to west. Both lines run through the Sleipner east field (Fig.4.1). The inline shows numerous strong reflections and also several irregular areas. The length of the inline is 62.8 km and most of the reflections are horizontal. However, inline reflections are clearly visible along the entire length of the seismic section. Crossline 3038 is 37.5 km long and also shows several strong reflectors (Fig.4.4). However, all these reflectors remain relatively horizontal compared to the inline.

The interpretation of Inline 795155 is shown in figure 4.3. The interpreted horizons are following strong positive continuous amplitudes. These horizons are corresponding with the well-tops and well data. The horizons sub-divide the seismic section into sequences, and each sequence shows a different reflection configuration and geometry. The interpreted crossline 3038 indicated in Figure 4.6, shows generally horizontal reflectors. However, areas where the reflector is highly disturbed are present, and makes interpretation very difficult.

Both the crossline and inline show features and anomalies that indicate that the stratigraphy has been subjected to different mechanical forces. These features are present in larger parts of the survey, and highly disrupt and contort the seismic data. Some of these features will be briefly discussed.

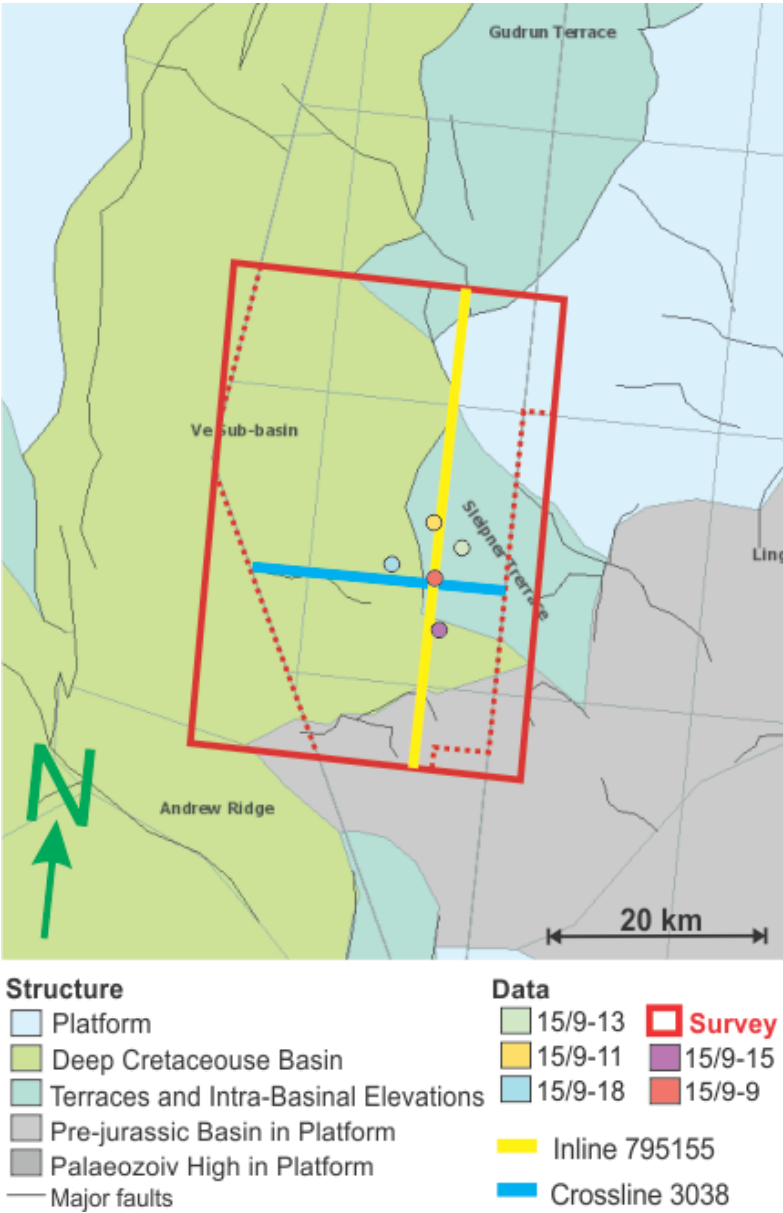


Figure 4.1: location of Inline 795155 and Crossline 3038. These lines provide a good overview over the configuration and distribution of the different sequences in the study area. Figure is modified from Factmap (2016)

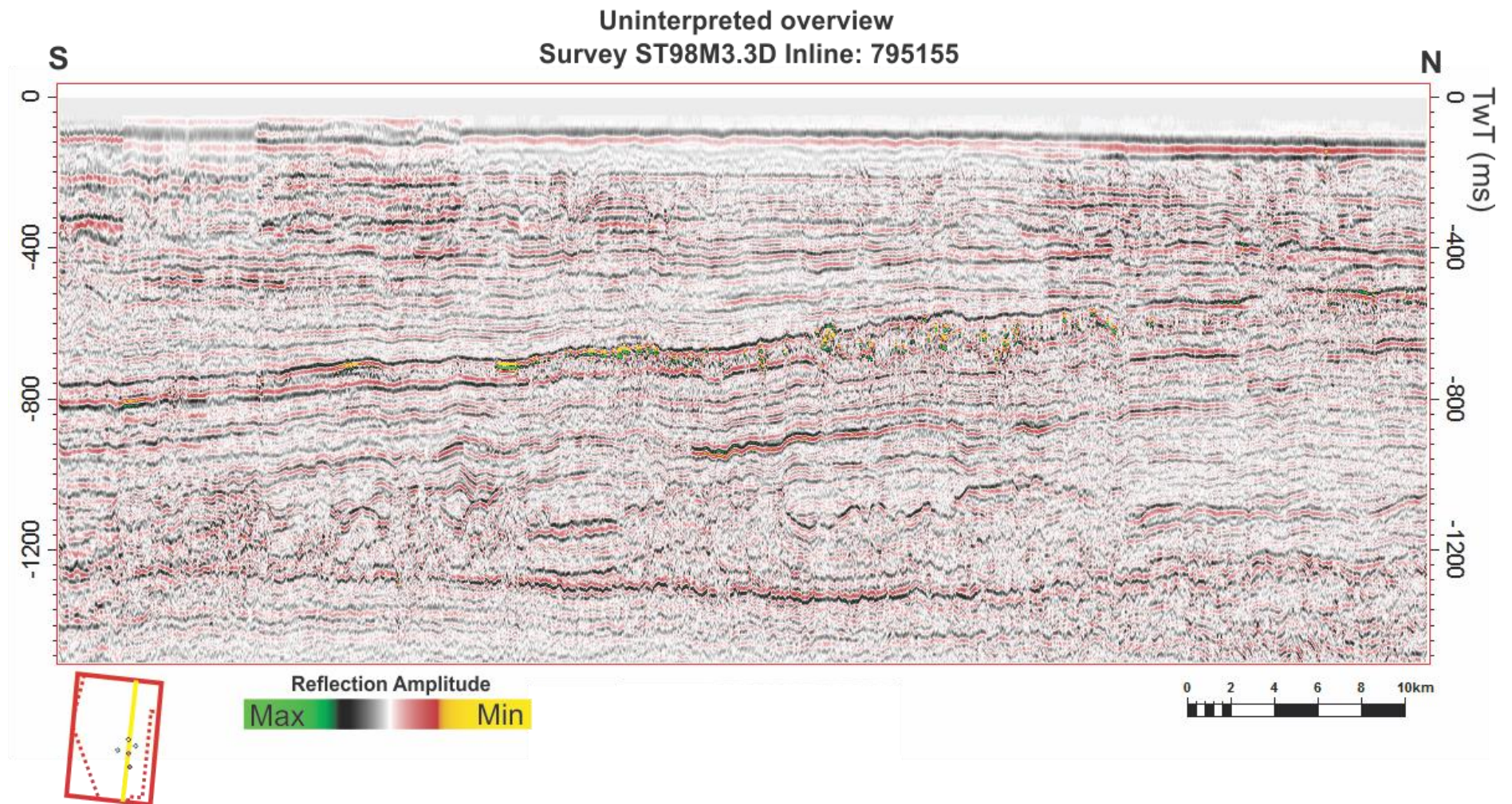


Figure 4.2: Inline 795155 which stretches from south to north within survey ST09M3.3D. This seismic section covers the entire north-south length of the survey. The yellow line within survey ST98M3.3D is indicating the location of the seismic section. Detailed location is shown in figure 4.1.

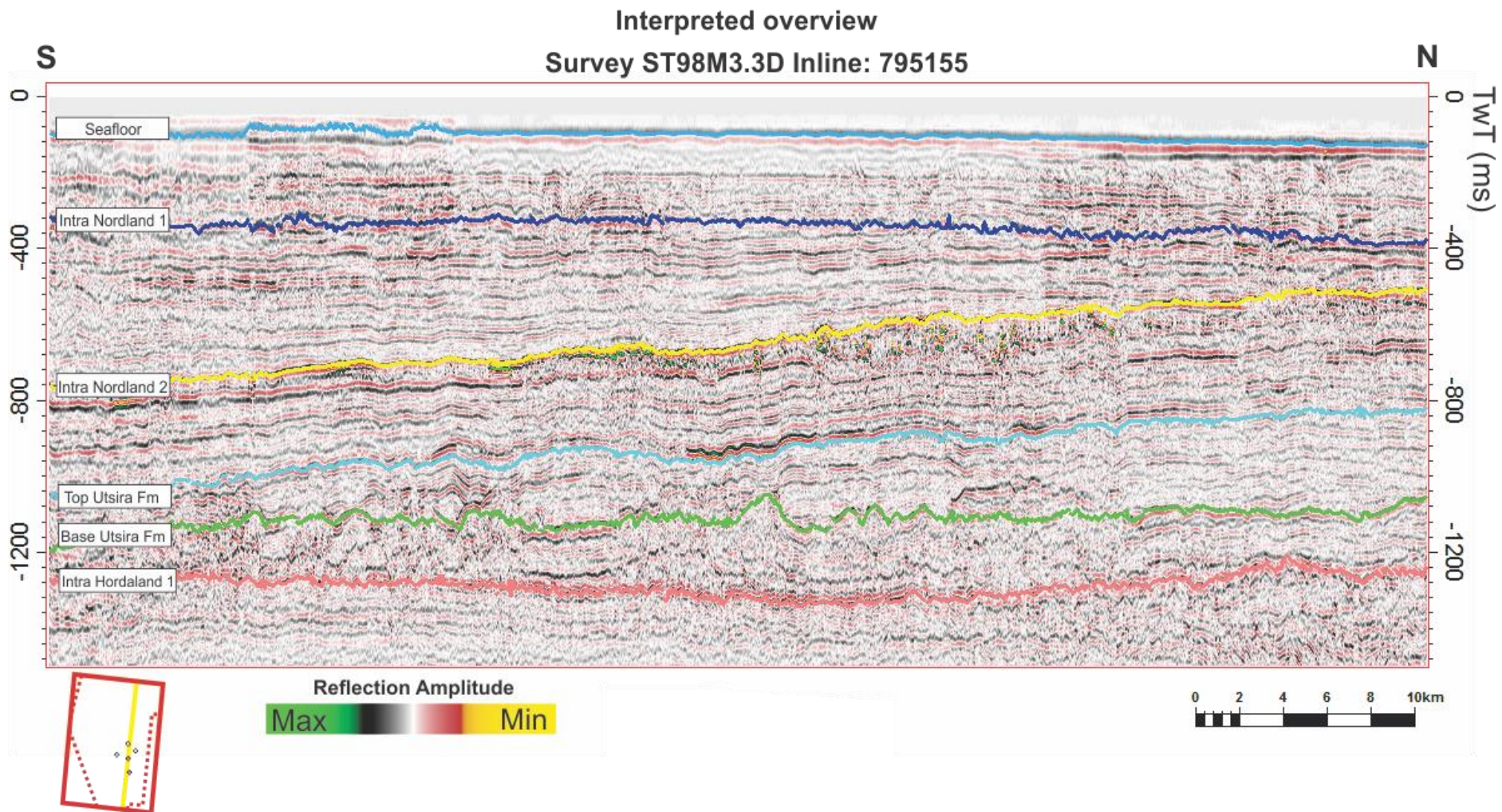


Figure 4.3: The interpreted seismic horizons along inline 795155. The Interpreted horizons are marked with names on the left side of the seismic section. Detailed location is shown in figure 4.1.

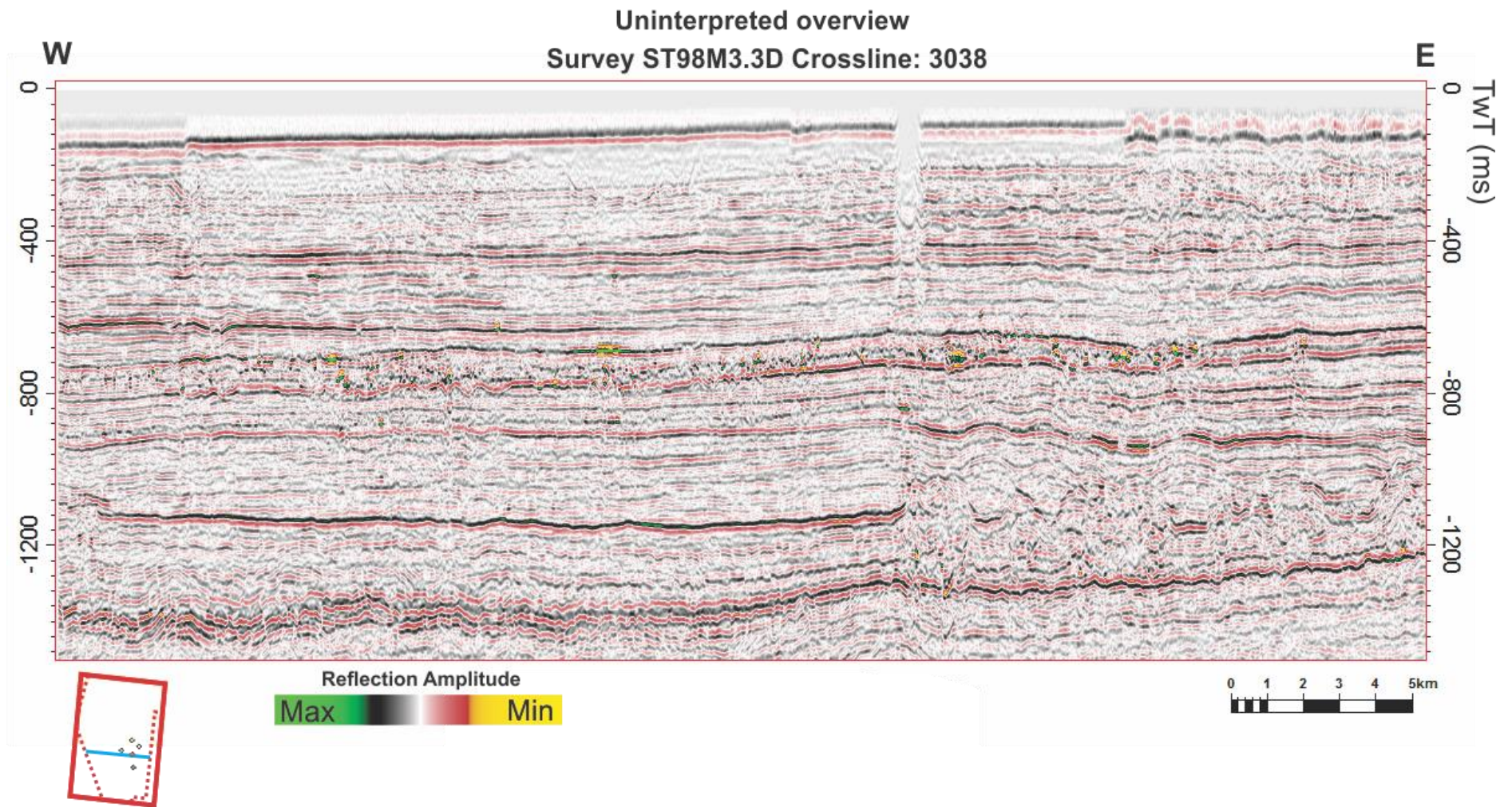


Figure 4.4: Seismic section of crossline 3038. The crossline is oriented east-west and covers the width of the survey. Crossline 3038 is a good representation of the seismic data orientated west-east. Detailed location is shown in figure 4.1.

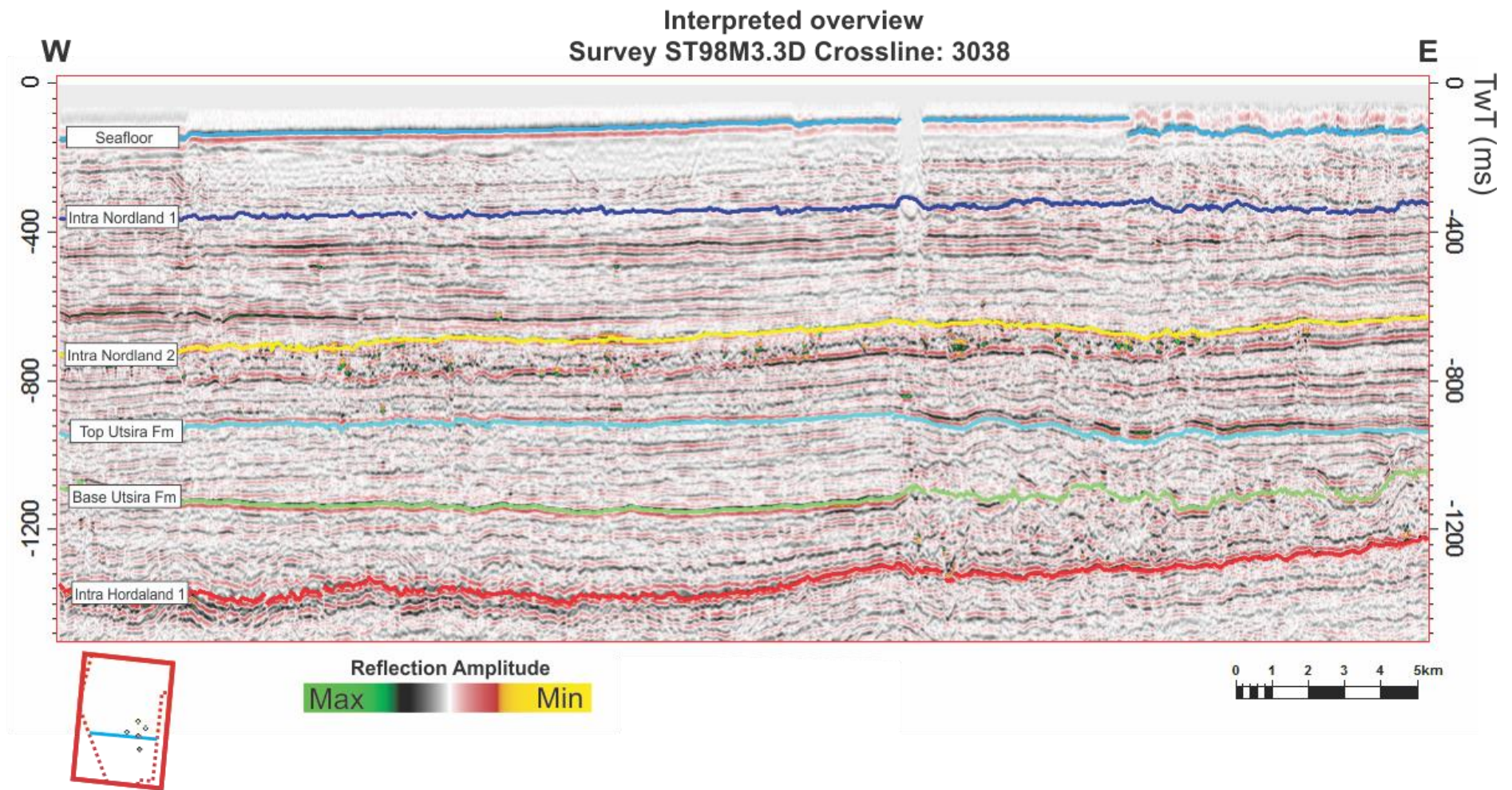


Figure 4.5: Illustrates the interpreted seismic horizons on crossline 3038. Notice the artifacts located at the seabed, towards the upper east side of the seismic section. Detailed location is shown in figure 4.1

4.1.2 Horizons

Each interpreted horizon will to some degree show a variability in depth throughout the survey. However, the general trend of the interpreted horizon is captured in the inline and crossline presented in figure 4.3 and 4.5.

The seafloor horizon (SF) is the top of the Nordland Group, and is following a strong and continuous reflection. The reflection jumps upwards and downwards in time when it enters irregular areas with artifacts. These areas are most likely related to the processing phase of the survey and are seen in the whole survey, but they mainly disturb the seafloor reflection (Fig. 3.6). In figure 4.5 the crossline show clearly one of these artifacts, located at the seabed towards the eastern parts of the seismic section. It cuts the seafloor reflection and disturb the underlying seismic.

Intra Nordland 1 (IN1) is following a weaker positive reflection. The horizon may be following an erosional surface. The horizon is corrected and correlated with well logs. This horizon delimits the upper section of the seismic data, corresponding to the first sequences.

Intra Nordland 2 (IN2) is the most continuous horizons that has been interpreted. The reflection is high amplitude and is seen throughout the entire survey. The reflection is generally dipping towards the south (Fig. 4.3). The horizon varies in depth, between -500ms (TWT) in the northern parts and -760ms (TWT) in the southern parts. The horizon subdivide the lower parts of the Nordland Group into sequence 2 and 3.

Top Utsira Fm (TUFm) marks the beginning of the Utsira Formation and the horizon correlates strongly in-between wells (NPD, 2016). The reflection is continuous with a strong positive amplitude. The interpreted horizon is dipping towards the south, and seem to be sub-parallel to the overlying horizon (IN2) (Fig. 4.3). The horizon varies in depth from about -800ms (TWT) to -1000ms (TWT).

Base Utsira Fm (BUFm) marks the end of the Utsira Formation and start of the Hordaland Group. The horizon is interpreted along a strong positive reflection, which is semi-parallel to TUFm. The reflection is in some areas highly contorted and discontinuous. These areas are very chaotic, and it can be difficult to trace the horizon. The horizon varies in depth from -1100ms (TWT) to -1200ms (TWT).

Intra Hordaland 1 (IH1) is the deepest interpreted horizon. The horizon follows a strong positive discontinues reflection. The reflector is abruptly cut and tilted to the side in a series

of sections. This horizon varies in depth from -1200ms (TWT) to about -1400ms (TWT). The horizon have been interpreted to be the Mid-Miocene unconformity, after (Rundberg & Eidvin, 2005) (Fig. 2.8).

4.1.3 Age and thickness

Figure 4.9 and 4.10 show sequence 1-6. The sequences and their configuration may represent different conditions under deposition, and each sequence have a different shape and orientation. The uppermost sequence (S1) is delimited by the seafloor reflection and the underlying interpreted horizon (IN1). The time thickness of the sequence is indicated in figure 4.6. However, the uppermost units of the seismic is highly disturbed. This is apparent in the time thickness maps, as the interpreted horizon jumps in time at disturbed areas. The sequences varies between -180ms and -300ms (TWT) in time thickness. S1 appears to extend laterally without any major changes in dip, both in the north-south and east-south direction. The sequence might be thinning towards the south, indicated as lower values in the time thickness map (Fig.4.6.). The uppermost and first sequence (S1) is interpreted to be sequence CSS-10 after Jordt et al. (1995), and consist mostly of Late Pleistocene to Holocene age.

The second sequence (S2) is delimited by the underlying horizon (IN2) and show a very distinct dipping trend towards the south (Fig. 4.9). The upper horizon (IN1) remains horizontal while the underlying horizon (IN2) dips. By that reason, the thickness of the seismic sequence varies greatly in the north-south direction across the survey. This is clearly seen in the time thickness map in figure 4.6. In the northern part, the sequence can be -120ms (TWT) thick, and in the southern parts it can increase to -450ms (TWT). In the east-west direction the sequence show little to no variability in thickness. The sequence might be dipping a few degrees towards the west (Fig. 4.10). S2 is interpreted to be sequence CSS-9 after Jordt et al. (1995), and mostly of Pleistocene age (Fig 4.9 and 4.10).

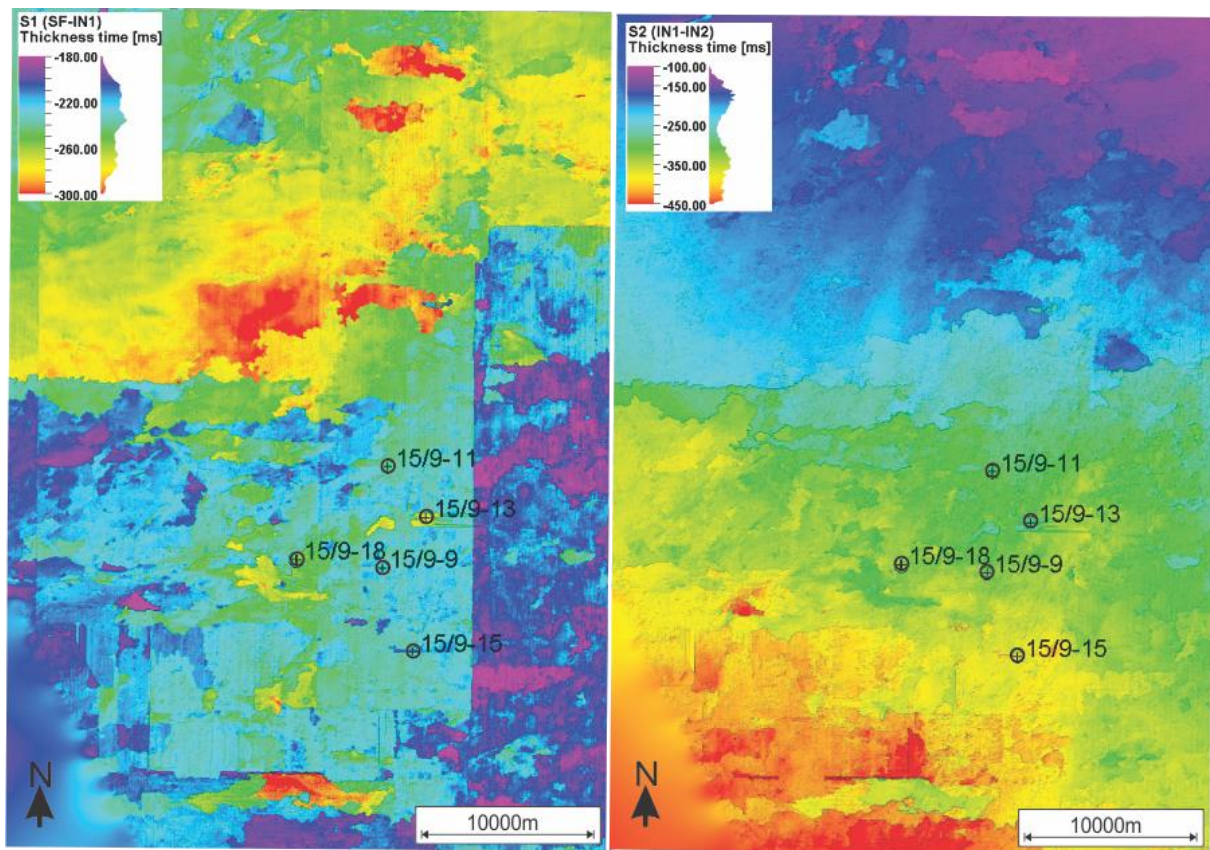


Figure 4.6: Time thickness map of the first and second sequence. The thickness is derived between the interpreted horizons SF-IN1 for the first sequence, and IN1-IN2 for the second sequence. Thickness is given in milliseconds (TWT). These thickness maps are highly disturbed by artifacts and irregular seismic data. The graph to the right of the legend, indicates the value distribution.

The third sequence (S3) is overlying the Utsira Formation, and show a clear dip towards the south (Fig. 4.9). Figure 4.7 indicates that the sequence is narrowing towards the south-east. The greatest thickness is confined to the north-west in the survey, where the thickness can get up to -340ms (TWT). Towards the southern parts the sequence, the thickness can narrow down to almost -200ms (TWT). In the east-west direction (Fig. 4.10) the sequence appear to be more horizontal oriented, compared to the north-south direction (Fig. 4.7). However, a low angle dipping trend towards the west is observed. S3 is interpreted to be sequence CSS-8 after Jordt et al. (1995), and the sequence is most likely deposited during Pliocene.

The fourth sequences (S4) comprise the Utsira Formation. Figure 4.9 show that the sequence have a low angle dip towards the south. Figure 4.7 indicates that the sequence might decrease in thickness towards the south. Generally the sequence appear show greater thicknesses at local points within the survey (Fig. 4.7). These areas seem to be delimited by areas with lower thicknesses. The average thickness of the sequence is approximately -220ms (TWT), and appear to be thicker in the northern parts. The sequence can narrow down to only -50ms (TWT) in the southern parts. This might indicated that the sequence pinches-out further south.

The sequence is relative horizontal in the east-west direction (Fig. 4.10), and thickness seem to decrease towards the east. However, the eastern part of the seismic section show high levels of noise and contorted reflections. S4 have been interpreted to be sequence CSS-7 after Jordt et al. (1995). And LN-2 after Rundberg and Eidvin (2005). The age of deposition was first established by Isaksen and Tonstad (1989) to be Late Miocene (Fig 4.9 and 4.10).

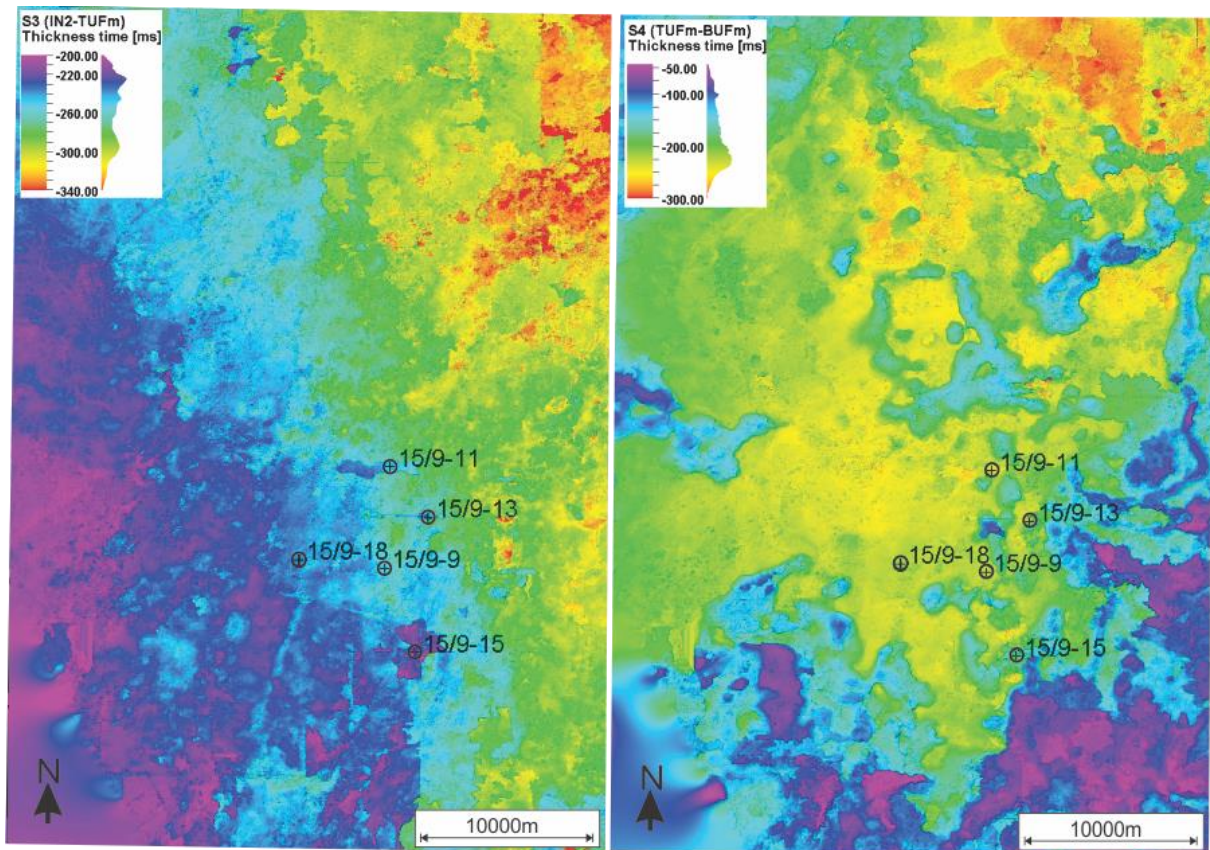


Figure 4.7: Thickness maps of sequence S3 and S4. The thickness is derived between the interpreted horizons IN2-TUFm for S3, and TUFm-BUFm for the S4. Thickness is given in milliseconds (TWT). The graph to the right of the legend, indicates the value distribution.

The fifth sequence (S5) comprise the upperparts of the Hordaland Group, and is located beneath the Utsira Formation (S4). The top horizon of the sequence (BUFm) is affected by several anticlinal features. These can be seen in figure 4.8 as elongated ridges. This phenomenon makes the thickness deviate from other areas. The thickness of the sequence is on average around -220ms (TWT). The sequence seem to have a lower thickness to the north-west, and a higher thickness to the south-east. Along the east-west direction the sequence show a relative horizontal orientation with a low angle dip towards the west (Fig 4.10). The sequence is interpreted to be LN-1 after Rundberg and Eidvin (2005) and is most likely deposited during Middle Miocene (Fig 4.9 and 4.10).

The sixth sequence (S6) show gradual thinning towards the south-east. This can be seen in the time thickness map in figure 4.8. However, the base of the sequence is defined at -1500ms (TWT). This implies that the true thickness of the sequence is unknown. The thickness map gives a relative thickness towards the defined base. The thickness is only -75ms (TWT) in the south-east. A thickness up to -325ms (TWT) is observed in the edges of the survey (Fig. 4.8). S6 have been interpreted to represent CSS-5 after Jordt et al. (1995), and UH-4 after Rundberg and Eidvin (2005)The age of the sequence is Lower Miocene (Fig 4.9 and 4.10).

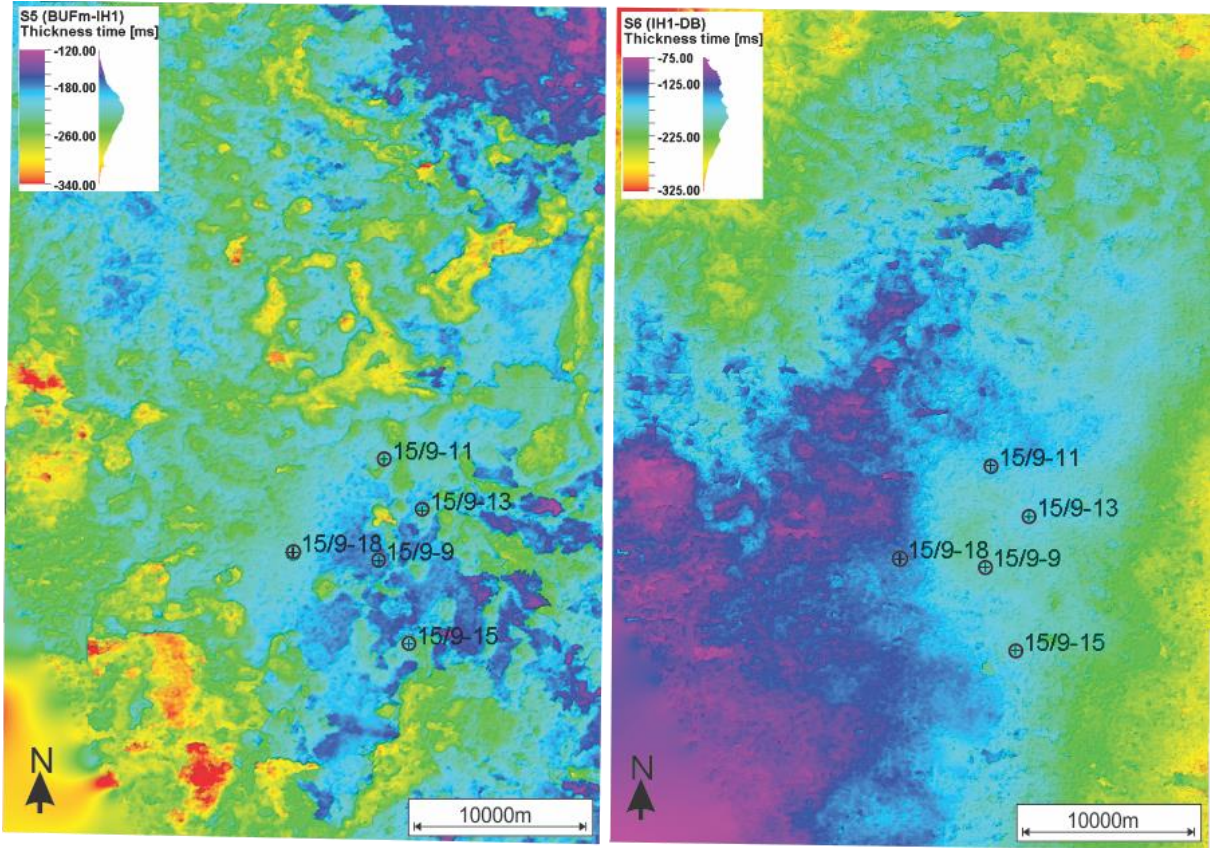


Figure 4.8: Thickness maps of sequence S5 and S6. The thickness is derived between the interpreted horizons BUFm-IN1 for S5, and IH1-DB for the S4. Thickness is given in milliseconds (TWT). The graph to the right of the legend, indicates the value distribution.

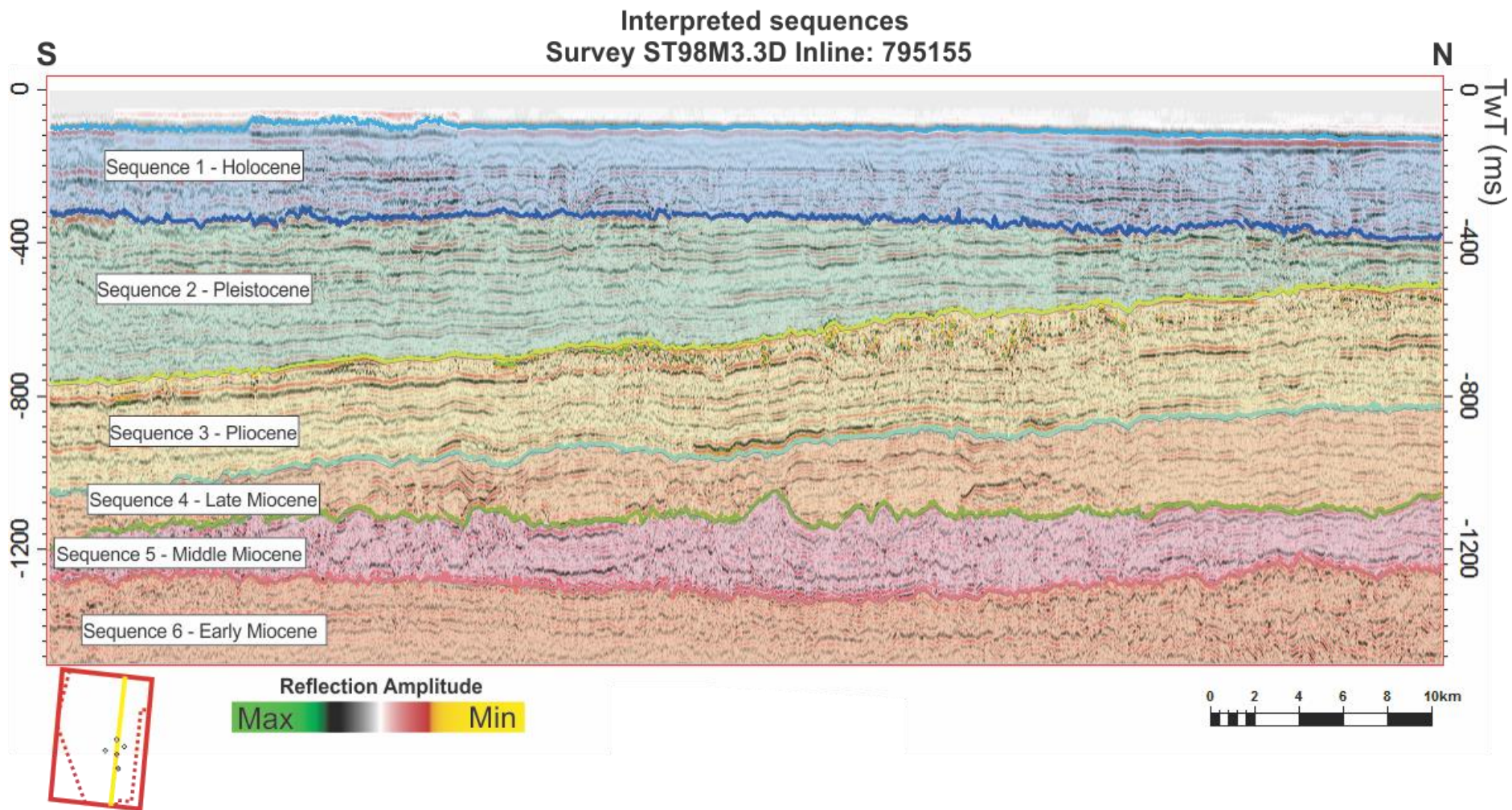


Figure 4.9: Seismic section showing sequence 1-6 in the north-south direction. Detailed location is shown in figure 4.1.

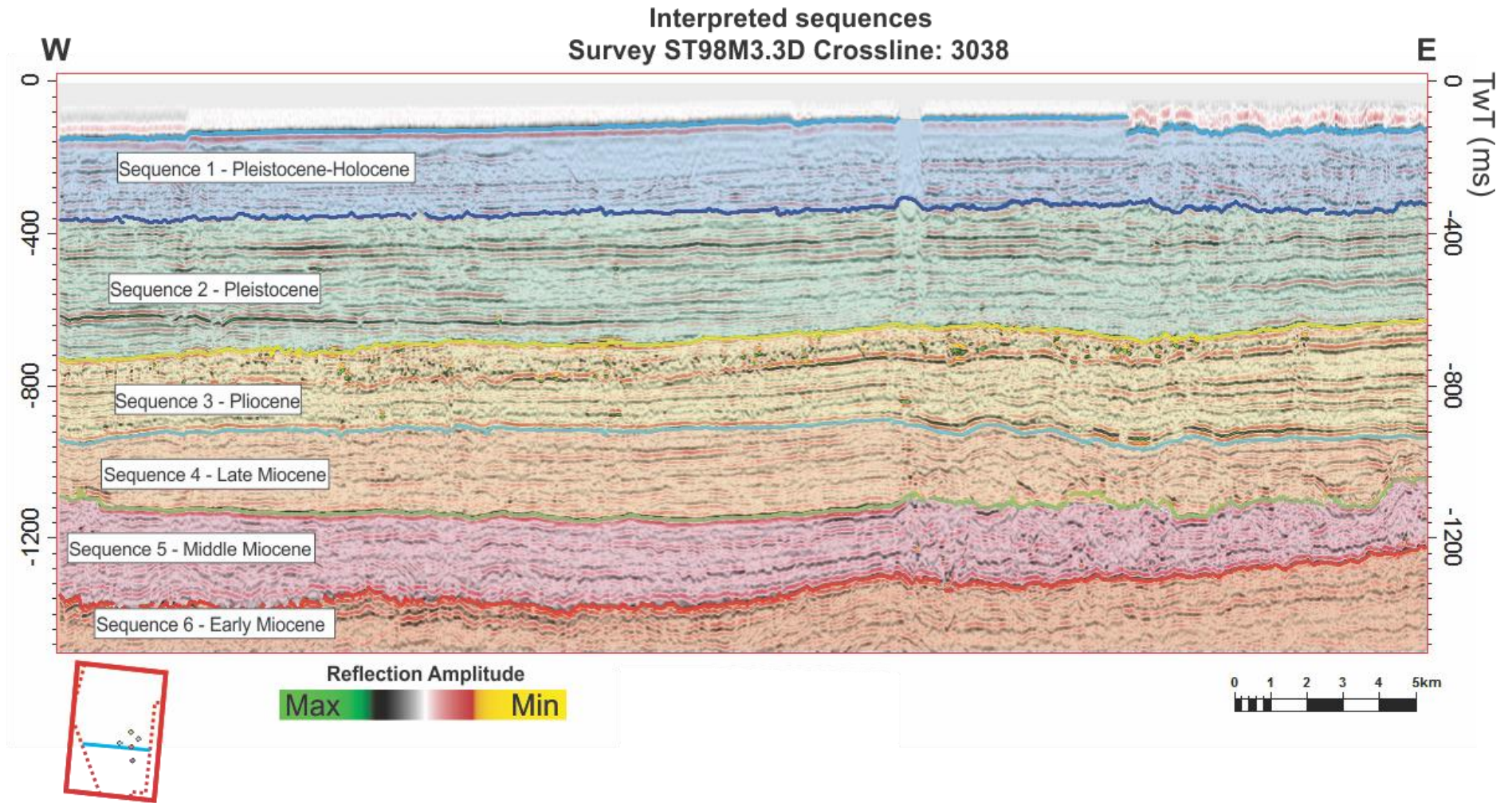


Figure 4.10: Seismic section showing sequence 1-6 in the east-west direction. Detailed location is shown in figure 4.1.

4.2 Reflection configuration, well logs and features

The sequences will be further described using a composite line and crossline. The location of these lines is shown in figure 4.11. The composite line covers most of the wells in an approximately north-south orientation, while the crossline covers the east-west orientation. The composite line with corresponding wells is shown in figure 4.12, and the crossline in figure 4.13. The reflection configuration will be interpreted based on these lines, and the corresponding attributes provided in Appendix A. All the attributes will be located in this appendix, and will be referred to by the figure number. The seismic attributes provide critical insight towards the reflection configuration, and numerous attributes have been produced for both the composite line and crossline. The well logs are given in figure 4.14, with the corresponding sequences indicated. The well logs will provide useful petrophysical insight for each sequence. There are numerous interesting features in the study area. Detailed descriptions of polygonal faults, sand-injection and gas-chimneys have been given by authors such as Lonergan et al. (1998); Løseth et al. (2012); Karstens and Berndt (2015). Some of the features observed in the composite and crossline is shown in figure 4.15 and 4.16.

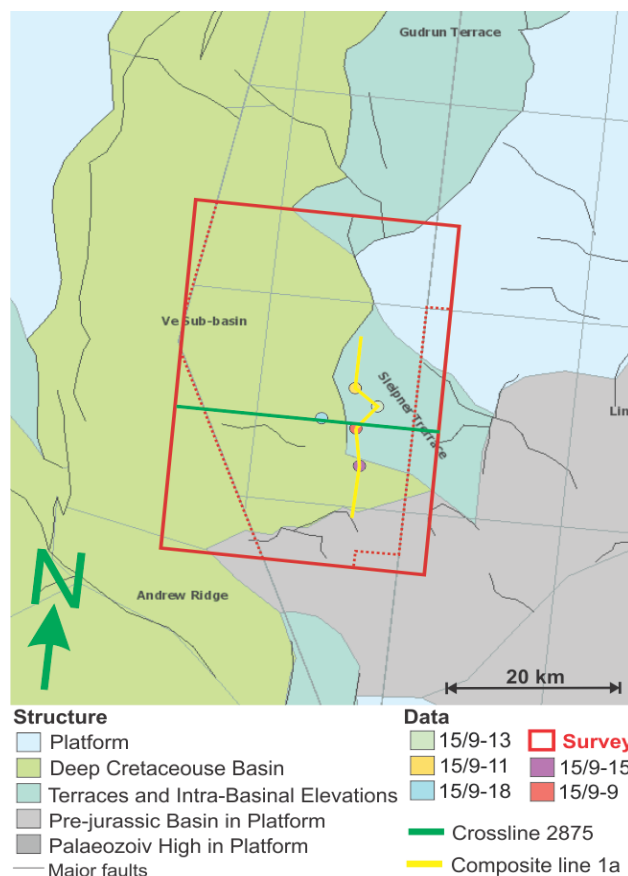


Figure 4.11: Location of composite line 1a and crossline 2875. These are used in the interpretation of reflection configuration.

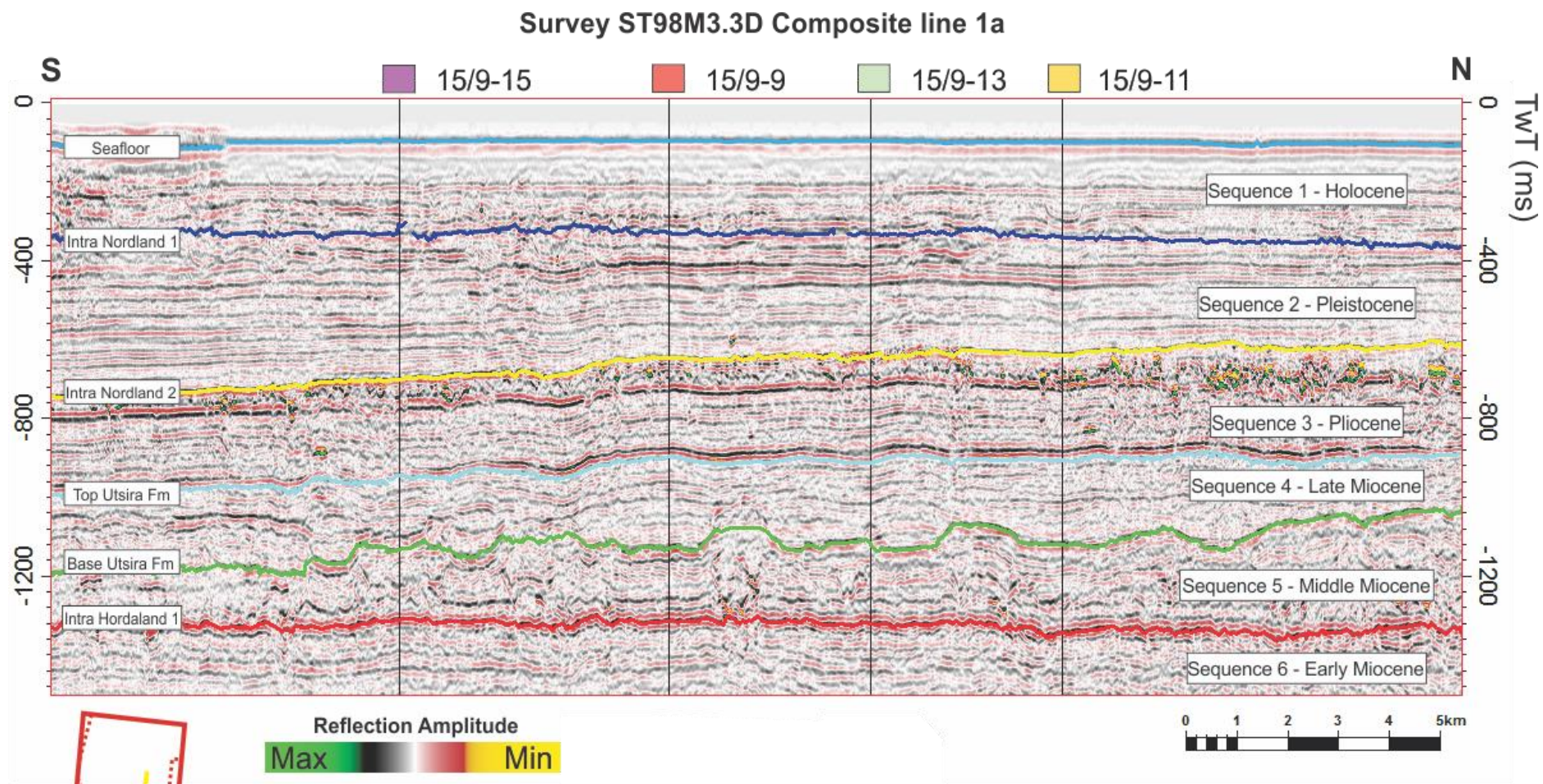


Figure 4.12: Seismic section of composite line 1a. The overall orientation is north-south, but deviates slightly between wells. Location and orientation is shown more clearly in figure 4.11. The interpreted horizons is shown to the left, and the sequences with age to the right.

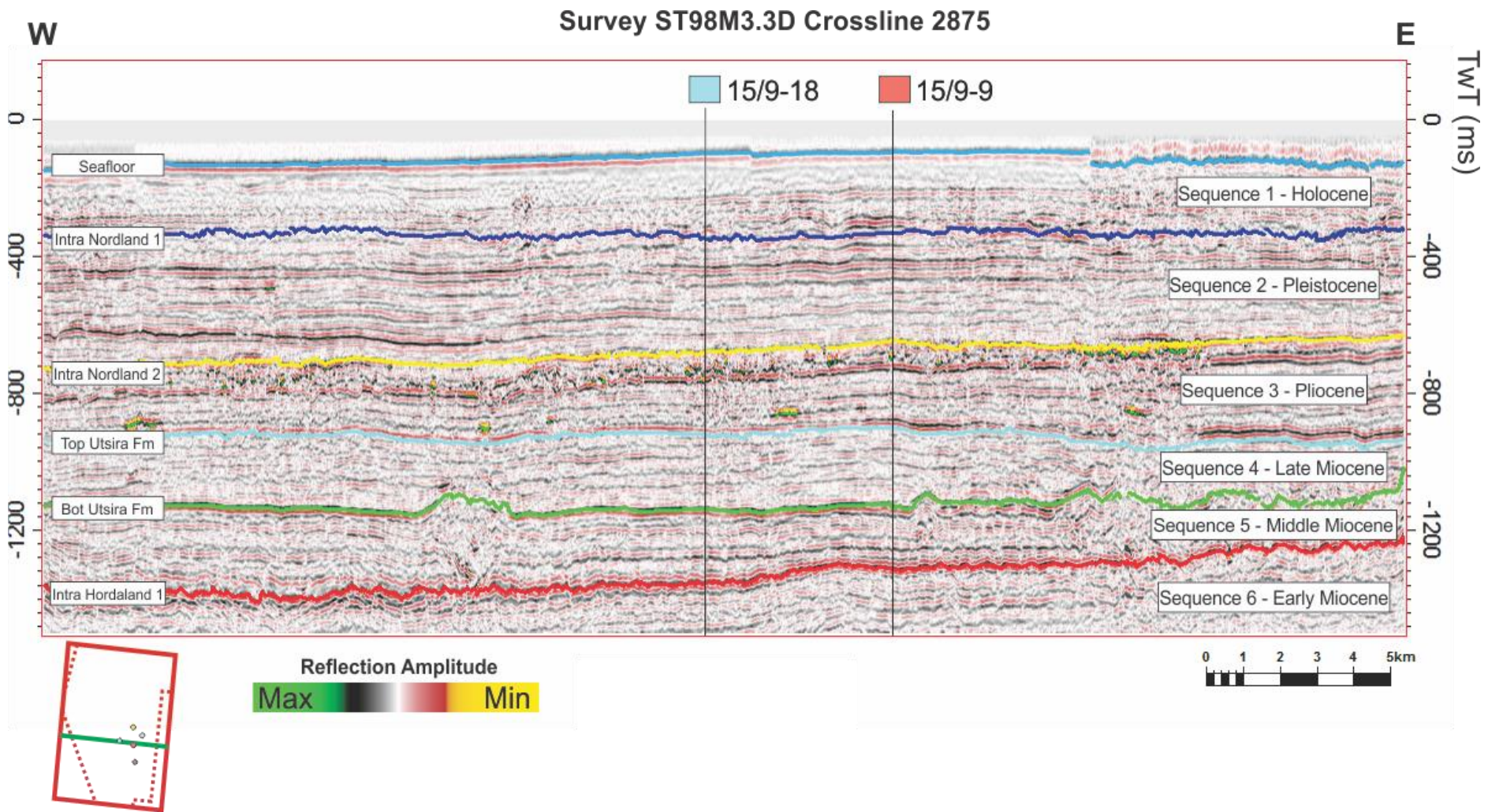


Figure 4.13: Seismic section of crossline 2875. The location and orientation is indicated in figure 4.11. The interpreted horizons is shown to the left, and the sequences with age to the right.

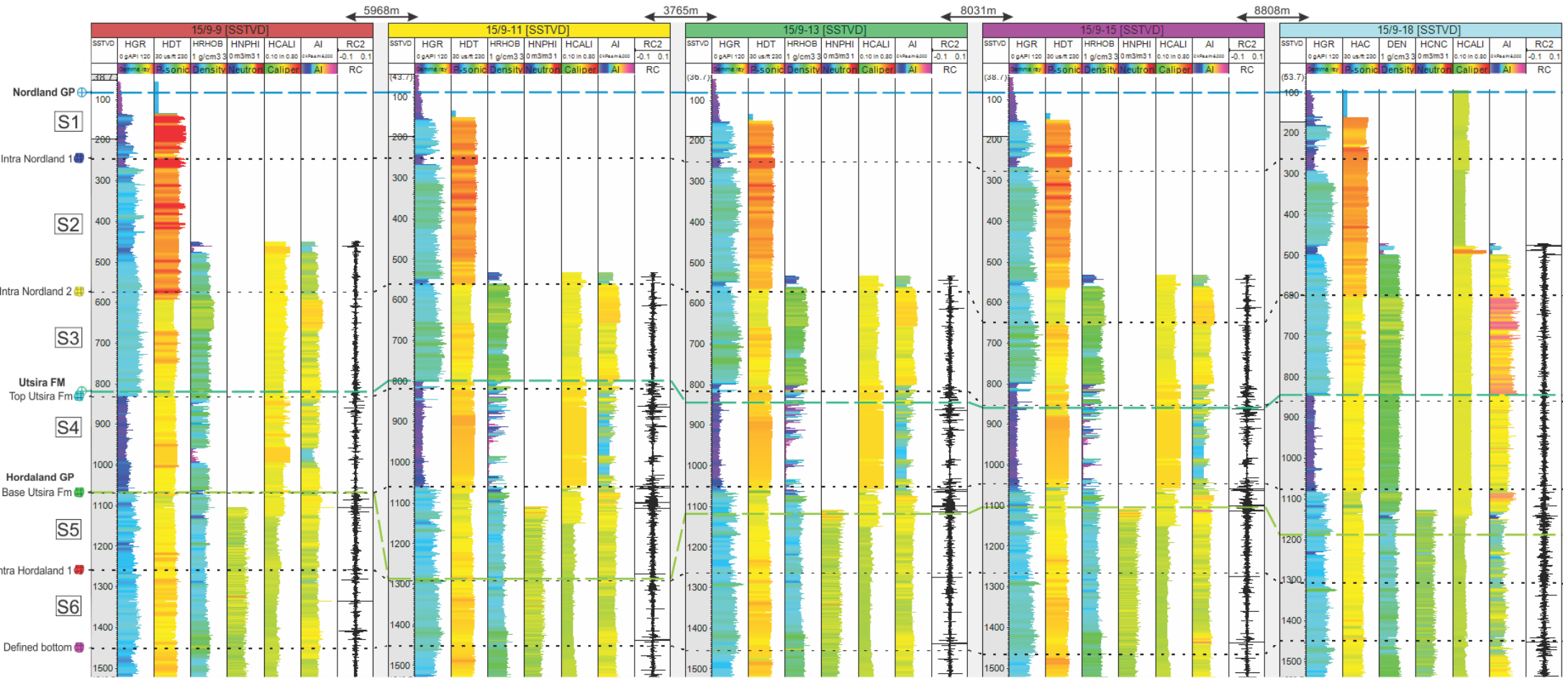


Figure 4.14: Well section window with all the wells and the corresponding logs. The wells are adjusted to the Nordland GP well top. The sequences, well tops and horizons is indicated in the left margin, these can be traced by their black lines (horizons/surfaces) across the well logs. The lateral distance between the wells is indicated at the top. A total of seven logs is shown for each well, they have the following abbreviations, value ranges and units; Gamma ray: HGR (0-120 API), P-sonic: HDT, HAC (30-230 us/ft.), Density: HRHOB, DEN (1-3 g/cm³), Neutron: HNPPI, HCNC (0-1 m³/m³), Caliper: HCALI (0.10-0.80 in), Acoustic impedance log: AI (0-8000 kPa s/m), Reflection coefficient: RC (-0.1 - 0.1). Values stretch from left (low value, blue) to right (high value, red) in their respective column.

4.2.1 Sequence S1

In figure 4.12 and 4.13 the uppermost sequence (S1) show a very variable reflection configuration, as the uppermost part of the seismic data is to some degree disturbed by processing and merging. The general trend is a presence of a few reflections, which show a subparallel geometry. These reflections are often disrupted by chaotic areas that cut the reflection.

The cosine of phase attribute show a strong continuous reflection in the middle of the sequence (Fig. 8.2). This reflection is also vaguely seen in the frequency attribute. In the variance attribute, there is a low variance interval extending laterally both in the composite line and crossline (Fig. 8.4 and 4.10). This low variance interval most likely correspond to the middle reflection of the sequence. The envelope attribute highlights this reflection, which seem subdivide the sequence into a lower and upper section (Fig. 8.1 and 8.7). This subdivision is supported by values observed in the well logs (Fig. 4.14).

In the lower part of the sequence, reflections show a subparallel configuration, from the base of the sequence (IN1) and upwards to the middle of the sequence. The cosine of phase attribute show these very clearly (Fig. 8.2 and 8.8), while the envelope attribute show an irregular configuration of several stronger amplitudes (Fig. 8.1 and 8.7). The cosine of phase attribute suggest that these few reflections are discontinuous, and the envelope seem to support this. The attributes and seismic seem to agree that the lower part of the sequence is disturbed and locally contorted. In addition, the lower part of the sequence is associated with higher gamma ray values than the overlying deposits. The gamma ray values is averaging 55 API in this section, while the sonic log show high values ranging from 170 to 210 $\mu\text{s}/\text{ft}$. (Fig. 4.14). The log values and the stronger continuous reflection in the middle of the sequence seem too correlated.

The uppermost part of the sequence show weaker reflections, and seem to be dominated by noise and disturbed seismic (Fig. 4.12 and 4.13). This might be related to the processing of seismic data. The cosine of phase attribute show that these reflections are discontinues as they are disrupted at several locations (Fig 8.2. and 8.8). The envelope attribute show no clear positive amplitudes in the upper parts of the sequence.

The well logs show that the upper section of the sequence, is associated with very low gamma ray values (Fig. 4.14). Gamma ray values is averaging 35 API in this interval. The sonic logs also show very low values averaging 60 $\mu\text{s}/\text{ft}$.

A few channel features are located in this sequence. They occur as concave or synclinal features in the seismic section (Fig.4.15). The cosine of phase attribute show these features very clearly in the sequence, at the location of well 15/9-11.

Generally the sequence is dominated by low amplitude reflections that appear to be subparallel. These reflections can to some degree be traced in the lower parts of the sequence, but are often cut and disrupted. At the location of survey transitions and areas with high signal to noise ratio, the reflections is hard to trace. The reflection in the middle of the sequence is continuous and with a relatively strong amplitude. Both the gamma log and sonic log show a very distinctive increase in values at this point. This supports the likelihood that this reflector marks the transition from the upper unconsolidated sands to the more compacted marine shales (Rider & Kennedy, 2011), as the gamma log increase to 65 API, and the sonic log increases to 165 $\mu\text{s}/\text{ft}$.

The sequence is classified with a low amplitude discontinuous, disrupted configuration which is highly disturbed by noise and artifacts. The reflectors are hard to trace laterally throughout the survey. The sequence is also highly affected by the merging process (Basu et al., 2008).

4.2.2 Sequence S2

The second sequence (S2) show a similar reflection configuration in the composite line and the crossline. The general trend in the sequence is several incline medium to low amplitudes. The cosine of phase show relative good continuity, suggesting a steady depositional environment (Fig 8.2 and 8.8). A few positive amplitudes is shown by the envelope attribute, some of these are larger than the adjacent reflections (Fig. 8.7). The extent of these envelope amplitudes, is largest in the upper part of the sequence. In the crossline, they occur both in the upper and lower parts. The variance attribute, show distinguishable low values along these reflections. The thicker envelope reflection seen in the upper part of the sequence, is also highlighted as a lower frequency layer.

The envelope and variance attribute together, might show indications of bedding both in the composite line and crossline, where the variance attribute show higher values along lithological boundaries (Fig. 8.5 and 8.11). These boundaries are clearly seen in the cosine of phase attribute, which indicate numerous reflections with a relative good continuity over larger parts of the sequence.

Some of the reflections are disrupted and cut, both in the composite line and crossline. The envelope attribute also indicate several lower magnitude reflections, present in most of the

sequences. These are also seen in the frequency attribute as several lower frequency reflections within the sequence.

The reflection configuration of the sequence consist of mostly medium amplitude parallel continuous reflections with medium to high amplitude. The majority of the reflections are continuous, but can be locally disrupted. The sequence increase in thickness towards the south (Fig. 4.6), and the incline reflections in the composite line might indicate a divergent reflection configuration.

The gamma ray logs show that the sequence mainly contain high values, suggesting a shale lithology (Fig 4.14). several spikes in the gamma ray values are observed, and these might correspond to higher shale content and might indicate a lower energy regime (Rider, 1990). The spikes have an average value of 95 API, while most of the sequence show values around 60 to 80 API. The gamma logs show a distinctive trend. In the lower parts of the sequence, the gamma logs are showing gradual lower values upwards in the borehole. These trends might correspond to a funnel shape (Rider, 1990). The overlying interval might correspond to a cylindrical shape.

The sonic logs is averaging 170 $\mu\text{s}/\text{ft}$. Several spikes are present in the logs, which seem to correlate to the gamma logs. These spikes are measured to 187 $\mu\text{s}/\text{ft}$.

The density logs starts at the lower parts of the sequence, and show low values at 1.4 g/cm at the beginning. Downhole, the density log increase to 2.0-2.1 g/cm . The caliper logs shows an average value of 0.50in. The acoustic impedance show a lower value at the beginning of the logs that seem to correlate to the lower values seen in the gamma and density log. The acoustic impedance values averages 3,600 $\text{kPa s}/\text{m}$. The reflection coefficient corresponds to the acoustic log, and show lower values at lower acoustic impedance values (Fig. 4.14).

4.2.3 Sequence S3

The third sequence consist of several incline reflections with medium to high amplitude (Fig. 4.12 and 4.13). The higher amplitude reflectors are located in the upper and lower parts of the sequence, while the medium reflectors are located in the middle of the sequence (Fig. 4.12). The higher positive amplitude reflections clearly stand out in the envelope attribute (Fig. 8.1 and 8.7). These reflections also have low variance. The cosine of phase attribute show several reflections within the entire sequence. These reflections can be traced laterally, but are often disrupted (Fig 8.2 and 8.8).

The variance with envelope, and RMS attribute highlights several bright spots in upper parts of the sequence (Fig. 8.6 and 8.12), these bright spots are overlying zones with acoustic masking, this could indicated that the bright spots are accumulations of shallow gas (Andreassen et al., 2007). The bright spots also distort the high amplitude continuous reflections, which is seen both in the composite line and crossline (Fig. 4.15 and 4.16).

The sequence mostly show a subparallel reflection configuration. The high amplitude reflectors are confined to the upper and lower part of the sequence, while the majority of the reflections have medium amplitude. The reflections are usually locally disrupted, by zones of acoustic masking and associated bright spots. The discontinuities within the sequence is highlighted by the cosine of phase attribute. The location were the reflections are disrupted, is better visualized in the RMS amplitude attribute. The middle part of the sequence show numerous medium amplitude reflections. These have a subparallel reflection configuration and can be traced laterally. Layering can be vaguely seen in the dominant frequency attribute (Fig 8.3 and 8.9). This might correlate to the thickness of the sediment units (Mitchum et al., 1977). The variance attribute, indicate that the strong amplitudes seen in the envelope attribute have low variance.

The well logs indicated that the sequence can be subdivided into an upper and lower part (Fig. 4.14). The sonic log show lower values in the uppermost interval. The density log show a slightly elevated values in the corresponding interval. Hence, the acoustic impedance also indicates this subdivision (Fig. 4.14). This interval contain most of the bright spots seen in the RMS and envelope with variance attributes. The gamma log show no anomalies, and show an average value of 85 API, suggesting that the lithology is shale. The sonic log show values down to 140 μ s/ft in this interval, while the density show 2.2 g/cm³.

The lower parts of the sequence show gamma ray values averaging 90 API. Smaller spikes are present, and these show values around 100 API. In well 15/9-11, 15/9-13, and 15/9-15 the shape of the gamma ray graph, might indicate a fining upwards trend (Fig 4.14). The sonic log show higher values, ranging from 160-170 us/ft. The density log then show lower values in the lower parts of the sequence, averaging 2.0 g/cm³. The caliper log shows relatively steady values, averaging 0.50 in in the sequence. The acoustic impedance log show higher values in the uppermost section, corresponding to the other logs, ranging from 4,500 to 4,800 kpa s/m. The acoustic log then show an average value of 3,700 kpa s/m with smaller spikes in values (Fig. 4.14).

4.2.4 Sequence S4

The fourth sequence corresponds to the Utsira Formation and show a number of low amplitude reflections that show a local chaotic configuration. The envelope attribute indicate that there is no lateral continuity between positive amplitudes within the sequence. Positive amplitudes occur, but these are seen sporadic and irregular (Fig. 8.1 and 8.7). In addition, the cosine of phase attribute show that the reflections within the sequence are discontinuous with a disrupted configuration (Fig 8.2 and 8.8). Compared to the other sequences, the dominant frequency show no indication of layering. The frequencies appear sporadic and irregular in an interval of 60Hz to 20Hz (Fig 8.3. and 8.9). The variance attribute show no pattern in dissimilarity within the sequence. However, localized areas with higher variance is present within the sequence.

The lower parts of the sequence show anticlinal features that cut the lower reflection. These features cut the well-defined base of the Utsira Formation, and distort the reflections (BUFm) (Fig 4.15). These are associated with local chaotic reflectors, seen clearly in the cosine of phase attribute (Fig 8.2). These features might be related to the underlying sediments, which have been mobilized. The features have been interpreted by Løseth et al. (2012) to be related to fluidized sand-injections. The envelope attribute indicate no strong positive amplitudes associated with these features. However, the variance attribute show higher values underneath these anticlinal features. The high RMS amplitudes seen at the top of S3 might be related to these features.

In general the seismic and corresponding attributes indicate a disrupted reflection configuration with medium-low amplitude and low frequency. The sequence also show a

localized chaotic reflection configuration, which might be related to sand injections and/or fluid migration.

The gamma ray logs have an average value of 30 API within the sequence, this is a good indication of a sand interval (Fig. 4.14). Several spikes is located within the sequence, and show values up to 60 API. The sonic logs show relatively uniform conditions in the sequence, and have values ranging from 145 to 155 $\mu\text{s}/\text{ft}$. The density logs show some different responses in this interval. Generally there is very low density in the formation with values down to $1.3 \text{ g}/\text{cm}^3$. However, the density logs show several spikes in the sequence. These spikes might represent thin-beds with high density mineral composition. They show values ranging from 1.9 to $2.1 \text{ g}/\text{cm}^3$. Well 15/9-18 and partly 15/9-9 show steady values with no spikes, averaging $2.0 \text{ g}/\text{cm}^3$. Compared to the other sequences, the caliper logs show elevated values with an average spacing 0.57 inches within the sequence. These elevated values, most likely reflect a change in borehole conditions. The acoustic impedance ranges from 3800 to 4,100 $\text{kPa s}/\text{m}$ within the sequence. But values down to 2,600 $\text{kPa s}/\text{m}$ can be observed in low density intervals (Fig. 4.14).

4.2.5 Sequence S5

The fifth sequence contain low to medium amplitude reflections with low frequency. These reflections are hard to trace laterally as they are highly disrupted by the anticlinal features seen at the base of the Utsira Formation (Fig.4.15 and 4.16). Larger parts of the sequence have a chaotic configuration related to these features. In general, the sequence show a few reflections with medium to low amplitude. These are discontinuous, with the most disturbance occurring adjacent to the anticlinal features.

The envelope attribute show several positive amplitudes within the sequence. These appear in an irregular pattern, with almost no indication of continuous bedding. The positive amplitudes are highly disturbed around the anticlinal features (Fig 8.1 and 8.7). The cosine of phase attribute show that the sequence consist of several reflections that can be traced to some degree. However, most of them are highly disturbed. The reflections are most disrupted and chaotic around the anticlinal features, and it is clear that these features cut the natural parallel bedding of the sequence (Fig 8.2 and 8.8). The reflections that is not affected by these features, are usually located in between the anticlinal features and show a subparallel configuration.

The frequency attribute indicate higher frequency bedding within the sequence. This is clearer in the crossline direction, as the composite line is more disturbed by different features and acoustic masking. The variance attribute indicate local high variance at the center of the anticlinal features (Fig 8.4 and 8.10). This is also seen in the variance with envelope attribute, as localized positive amplitudes seen in relation with the higher variance zones. The RMS attribute show small localized anomalously high amplitudes with the sequence. However, these are just seen in the composite line, and appear near the anticlinal features (Fig 8.6).

The general trend in the well logs indicate that Gamma ray values are ranging from 50 to 80 API, with an interlayering of lower and higher values (Fig. 4.14). The sonic logs show values range from 130 $\mu\text{s}/\text{ft}$. to 160 $\mu\text{s}/\text{ft}$ within this sequence. The density logs show the same interlayering as the gamma log, and values are ranging from 1.8 g/cm^3 to 2.0 g/cm^3 . The neutron logs makes it first appearance in this sequence, and show an average value of 0.40 m^3/m^3 . The caliper logs changes from an average of 0.50in to an average of 0.35in. This is most likely related to the change to a smaller diameter casing in the borehole. The acoustic impedance logs also show sections with different values. These values range from 3,800 to 4,100 $\text{kPa s}/\text{m}$. These reflections is also seen as high positive and negative spikes in the reflection coefficient logs (Fig. 4.14)

4.2.6 Sequence S6

Bellow the top of sequence 6 (IH1), there is a few very distinctive reflections. These reflections show a small degree of continuity, as they are displaced and tilted to the side. These appear to form a series of fault blocks, with an average width of 340m. These are indicated as polygonal faults in figure 4.15 and 4.16. Figure 4.17 show a dip angle map of the IH1 horizon, towards the north in the survey. The polygonal faulting can here be clearly visualized, and it appear that these don't have any dominate strike orientation.

The cosine of phase attribute suggest a subparallel reflection configuration. However, most of the reflections seen in this attribute are disrupted, although some indication of continuous reflections occur (Fig 8.2 and 8.8). The envelope attribute indicated high amplitudes confined to the top of the sequence, while medium to low amplitudes are present throughout most of the lower part of the sequence (Fig 8.1 and 8.7). Acoustic masking can be seen in association with the polygonal faulting and the migration of fluids, these areas can be classified as a chaotic reflection configuration, as there is no continuity of the reflectors in these areas (Fig

4.15 and 4.16). The variance attribute show higher variance in the zone with acoustic masking (Fig 8.4 and 8.10).

The dominant frequency attribute shows a relative low frequencies within the sequence. However, contours of higher frequency layers can be seen in the sequence. The irregular patterns of positive amplitudes seen the envelope attribute, is coherent with the reflection configuration interpreted from the original seismic amplitude.

The reflections seen in the cosine of phase attribute can be hard to trace, as they appear to be affected by the polygonal faults near IH1. The variance attribute show slightly higher variance values as lines that stretch vertical downwards from IH1. The variance with envelope and RMS amplitude attributes show no high amplitudes within the sequence (Fig. 8.2 and 8.8).

In general the sequence have medium to high amplitude reflections. These appear to be subparallel in the cosine of phase attribute. However, the reflections is affected by polygonal faulting. These faults can be clearly seen in the cosine of phase attribute of crossline 2875, along and underneath IH1, towards the west. A disrupted reflection configuration is proposed for the sequence.

Sequence 6 have generally high gamma ray values, these range from 80 to 100 API (Fig. 4.14). The sonic logs have relative uniform values, ranging from 150 to 165 us/ft. The density logs have in the uppermost part of the sequence values around 1.8 g/cm³, and 2.0 g/cm³ in the lower parts. The neutron logs show a decrease in values from 0.50 m³/m³ in the top to 0.45 m³/m³ in the lower parts. The caliper logs is averaging 0.35 in. The acoustic impedance log has an average value of 3,800 kPa s/m, with no major changes. The reflection coefficient log show several high value spikes that don't seem to correlate to any reflection. These spikes might be considered as errors.

4.2.7 Features

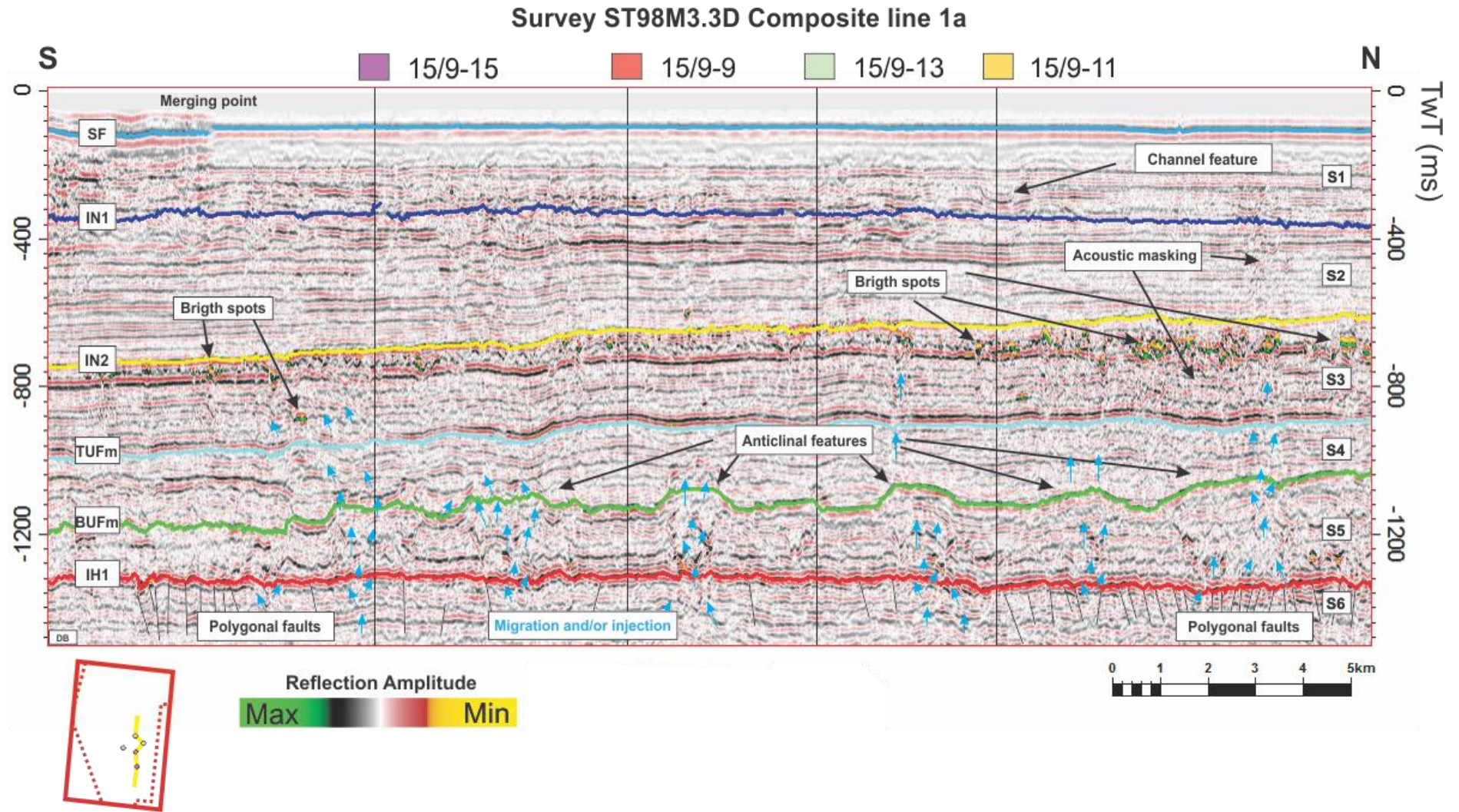


Figure 4.15: Seismic section of Composite line 1a, showing the numerous features in the study area.

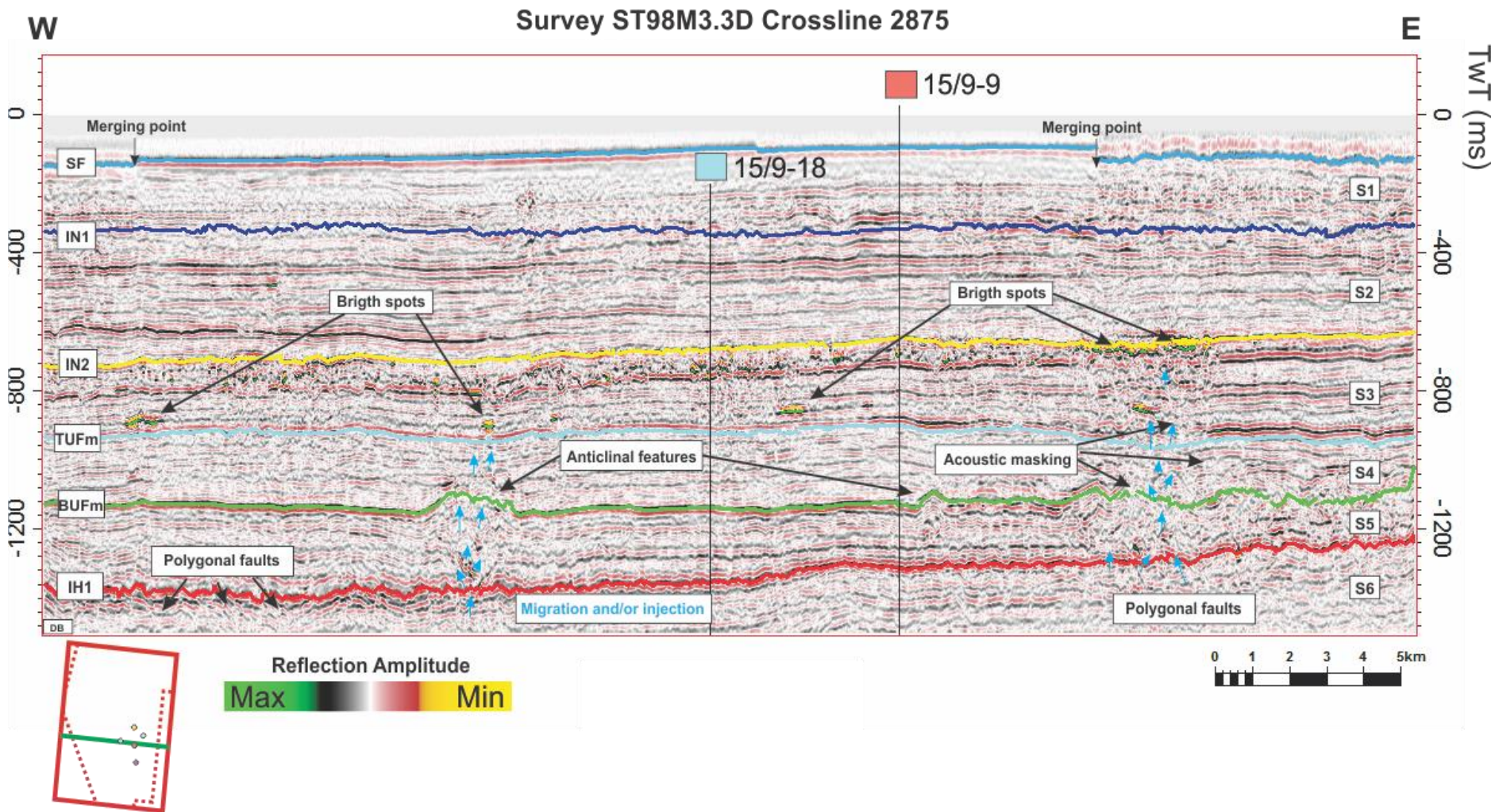


Figure 4.16: Seismic section of Crossline 2875 showing some of the characteristic features in the study area.

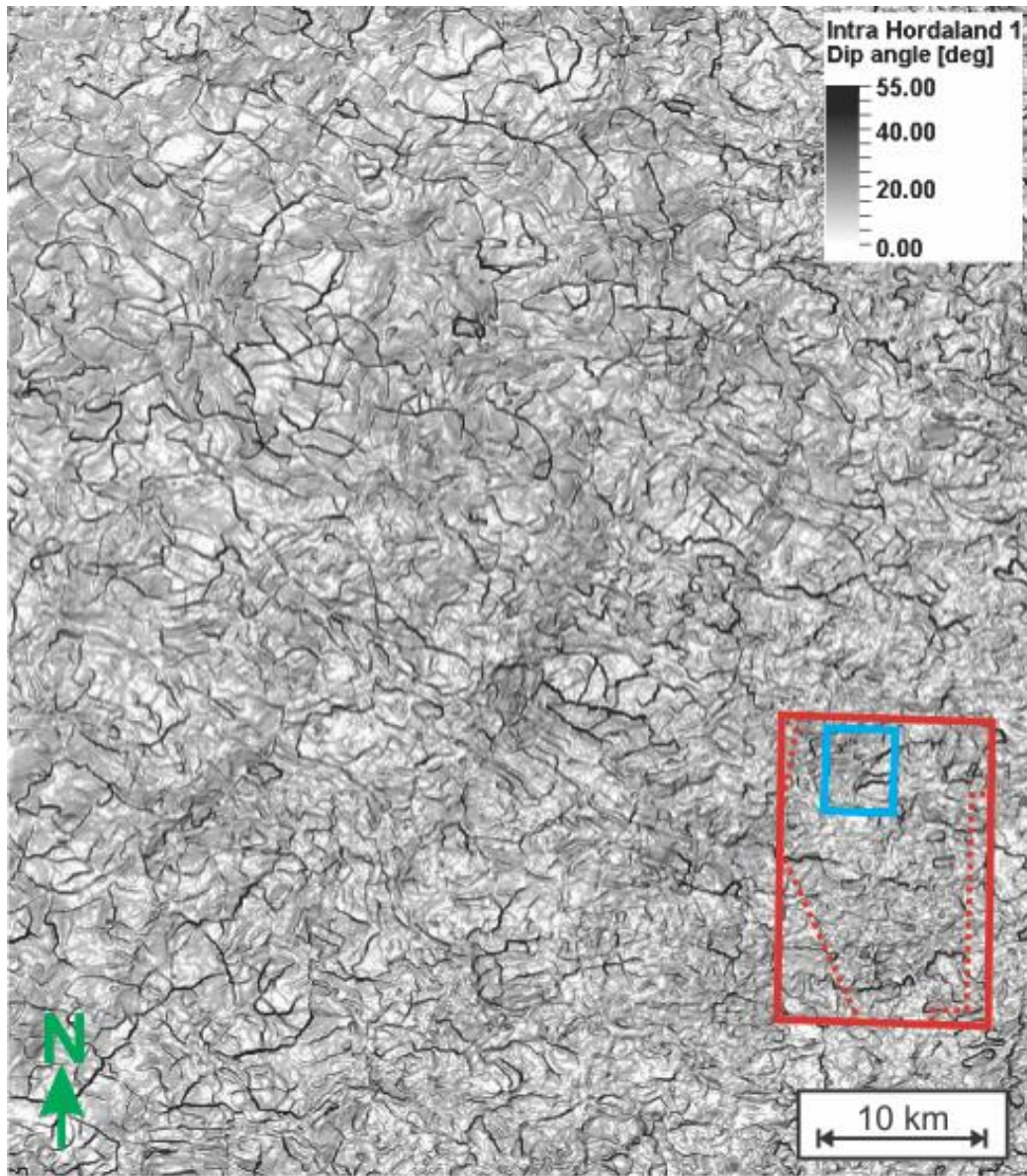


Figure 4.17: Dip angle map of the Intra Hordaland 1 horizon. Fault lines are seen as elongated black lines, as the dip angle increase towards 55 degrees.

4.3 Seismic sequences: Summary tables

4.3.1 Reflection configuration summary

Each sequence show a variable degree of a parallel to subparallel reflection configuration. However, they show distinct differences and have been summarized in table 4.1. The sequences show different amplitudes and reflection configuration. Each sequence have associated features that can disturb the seismic, and alter the reflection configuration.

Sequence	Amplitude	Reflection geometry	Associated features	Reflection configuration related to features
S1	Low-medium amplitudes	Discontinuous disrupted	Channel features and highly disturbed seismic data.	Locally contorted
S2	Medium amplitudes	Continuous-parallel	Distinct thickening towards the south.	Divergent
S3	Medium-high amplitudes	Continuous-subparallel	Bright spots – possible shallow gas accumulations?	Locally disrupted
S4	Low amplitudes	Discontinuous-disrupted	Injection and migration of fluids?	Locally chaotic
S5	Medium amplitudes	Discontinuous-disrupted	Anticlinal features	Locally chaotic and contorted
S6	High-medium amplitudes	Discontinuous-disrupted	Polygonal faults	Locally chaotic

Table 4.1: Summary of amplitude strength, reflection geometry and associated features for each sequence.

4.3.2 Well log summary

A summary table of the petrophysical properties located in each sequence is shown in table 4.2. The table show average values. Where spikes in the logs occur, a value range have been used. The interval velocity have been calculated for each sequence using the sonic logs.

	Gamma ray logs	Sonic logs	Interval velocity	Density logs	Neutron logs	Caliper logs	Acoustic impedance logs
S1	35-65API	60-165 μ s/ft.	5,080-1847m/s	X	X	X	X
S2	75API	170 μ s/ft.	1792m/s	2.0g/cm ³	X	0.50in	3600 Kpa s/m
S3	90API	150 μ s/ft.	2,032m/s	2.0–2.2g/cm ³	X	0.50in	3,700-4,700 Kpa s/m
S4	25-60API	145-155 μ s/ft.	2,102-1,966m/s	1.3-2.0g/cm ³	X	0.57in	3,800-4,100 Kpa s/m
S5	50-80API	130-160 μ s/ft.	2,344-1,905m/s	1.8-2.0g/cm ³	0.40 m ³ /m ³	0.35in	3,800-4,100 Kpa s/m
S6	80-100API	160 μ s/ft.	2,405m/s	1.8-2.0g/cm ³	0.45-0.50 m ³ /m ³	0.35in	3,800 Kpa s/m

Table 4.1: Summary table of the petrophysical properties located in each sequence. In intervals where larger spikes occur, an average minimum and an average maximum have been used. The Interval velocity for each well have been calculated from the sonic logs. The red values indicate that the values don't represent the whole sequence. X indicates the absence of well logs through the section.

4.4 Co-kriging results

A simple grid model that have been used to predict petrophysical properties within each sequences. The co-kriging interpolation method uses all the information from the up-scaled well logs (see chapter 3.7.1) and the seismic data within each sequence. The following subchapters will focus on the co-kriging interpolation, and the results will be presented along the interpreted horizons. The location of the interpreted horizons in the model is indicated in figure 4.18, which show the outline of the model.

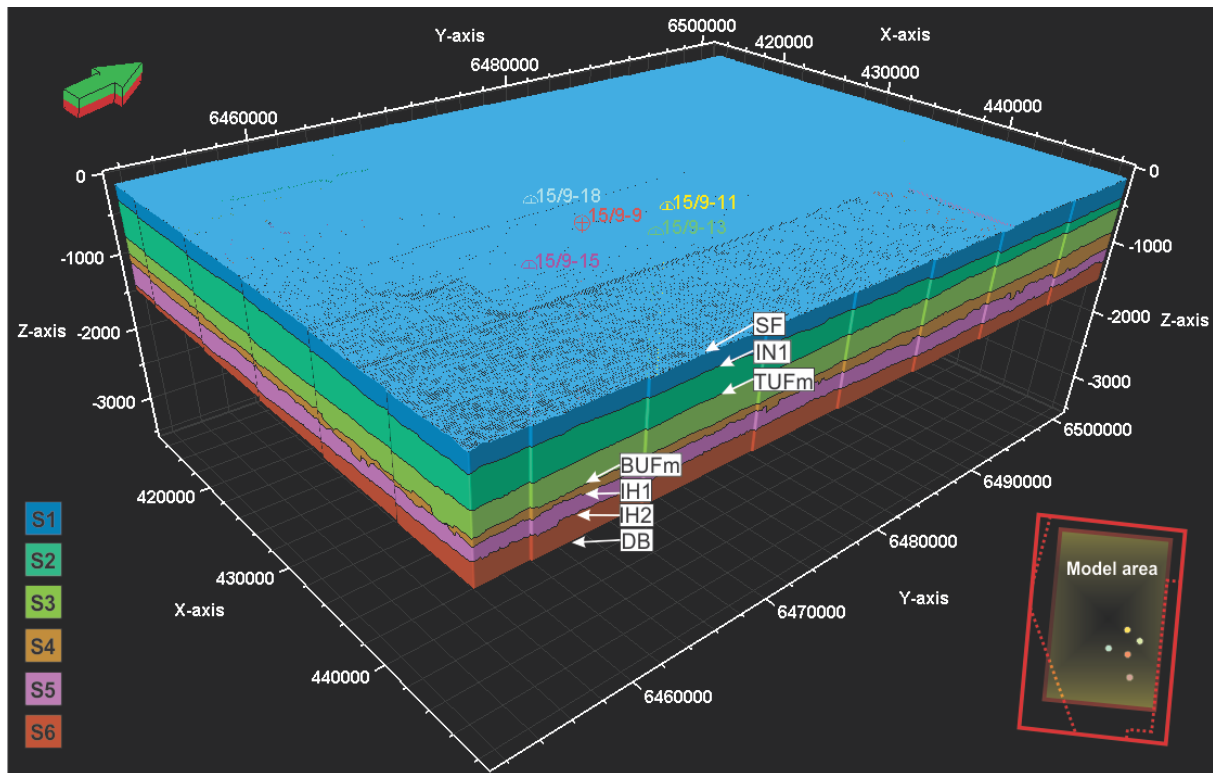


Figure 4.18: A simple grid model of the uppermost Cenozoic sequences in the Sleipner area. The model is here shown without layering in the sequences. The Z-axis is in two-way time. The X and Y-axis is in meters. The wells used in the study are indicated at the top of the model. The color codes of the sequences is indicated in the bottom left corner. The interpreted horizons is indicates with white arrows. The orientation of the model is given with the north arrow. The model area in relation to survey ST98M.3D is illustrated in the bottom right corner.

4.4.1 Sequence S1

Figure 4.19 show the distribution of gamma ray and sonic values after the co-kriging interpolation. Gamma ray values are unevenly distributed, and the result is affected by the chaotic seismic. The distribution of values correlates to the values observed in the well logs (Table 4.2), and the figure show an interaction between low values and higher values. Most of the values are located in-between 20-35 API. However, higher values towards 90 API can be observed. The interpolation of the sonic log, show some of the same trends as the gamma logs. Survey footprints and other artifacts are observed. The sonic log provides a good correlation towards the seismic data, and the distribution of values indicates this. Figure 4.19 indicate that most values are located around 170 μ s/ft.

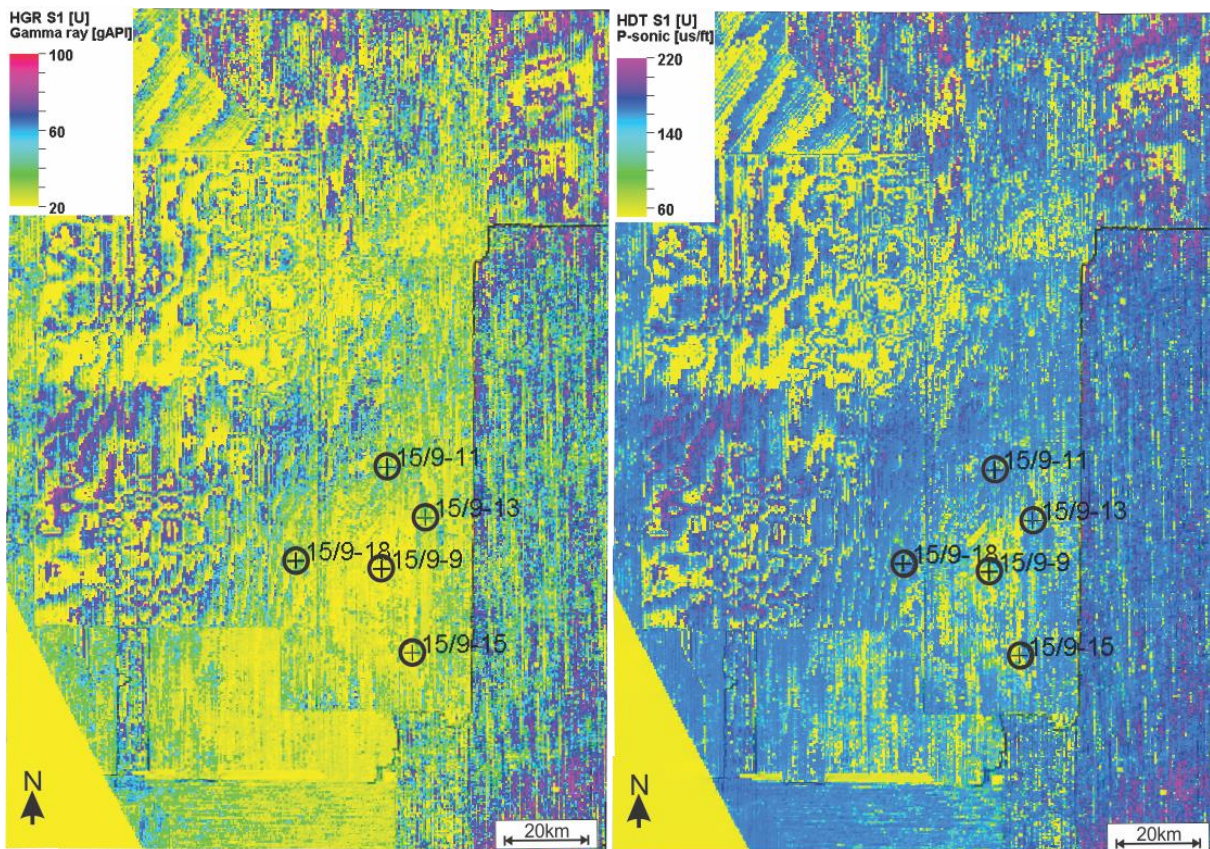


Figure 4.19: Co-kriging interpolation done between extracted seismic and the logs in sequence S1. The figure show that the Seafloor horizon (SF) is highly disturbed.

4.4.2 Sequence S2

The second sequence show gamma values distributed in the model. In figure 4.20, most of the values are located around 80 API. The value distribution observer in the co-kriging interpolation, correlates with the values observed in the well logs. The high gamma ray values indicate a shale lithology. Local areas with lower values are observed, these lower values might indicate a more sand prone lithology. Lower gamma values can be observed as

elongated features, that might possible be channel or lobe features. The sonic log show values mostly from 160 to 180 μ s/ft.

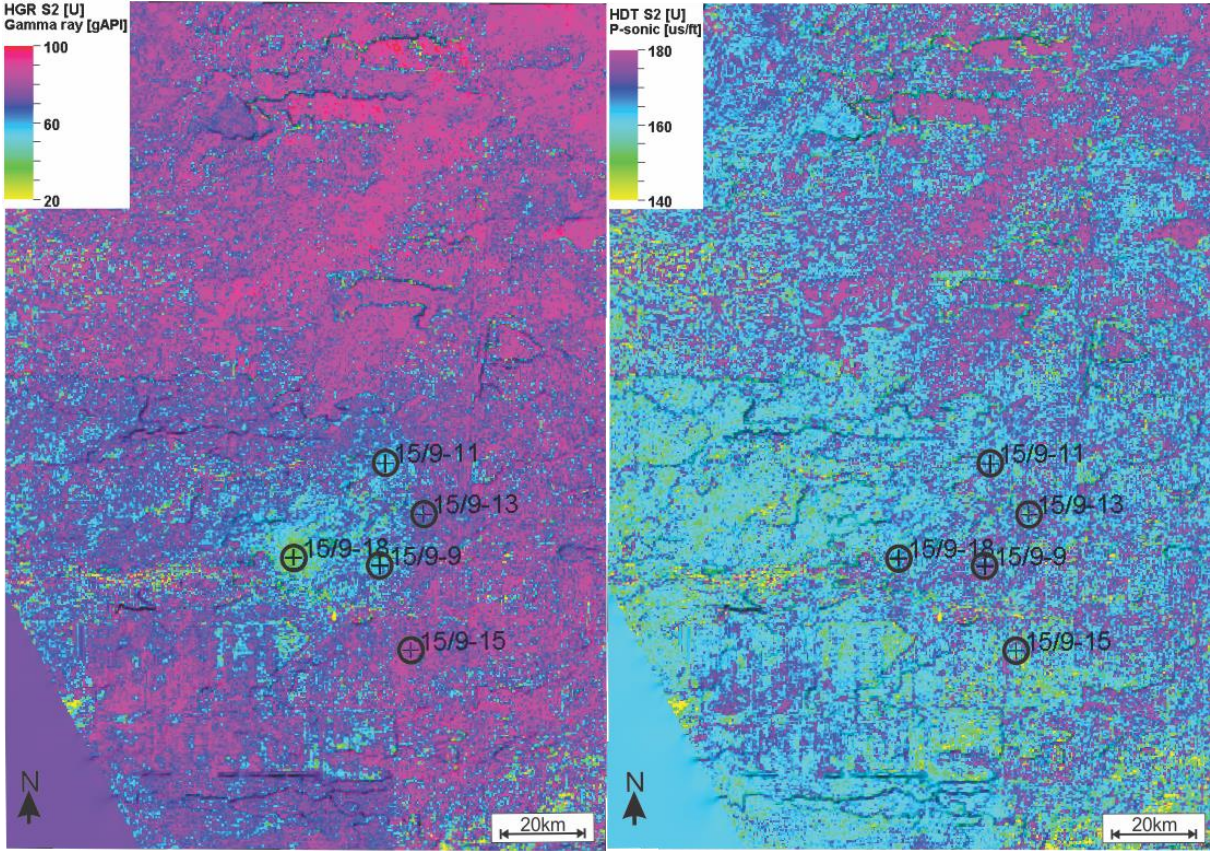


Figure: 4.20: Co-kriging interpolation done on the second sequence S2. The gamma ray distribution is shown to the left and the sonic to the right.

4.4.3 Sequence S3

The co-kriging results shown in figure 4.21, indicate a relative uniform value distribution. Most of the gamma ray values are located around 90 API, but local lower values are observed. The lower values show elongated patterns, which could indicate local deposits of sand. The sonic log show values around 150 μ s/ft. However, local higher values also occur. These higher values are seen as elongated features in figure 4.21, and might indicate a change in texture. Some of the local lower gamma values, are observed to occur with lower sonic values.

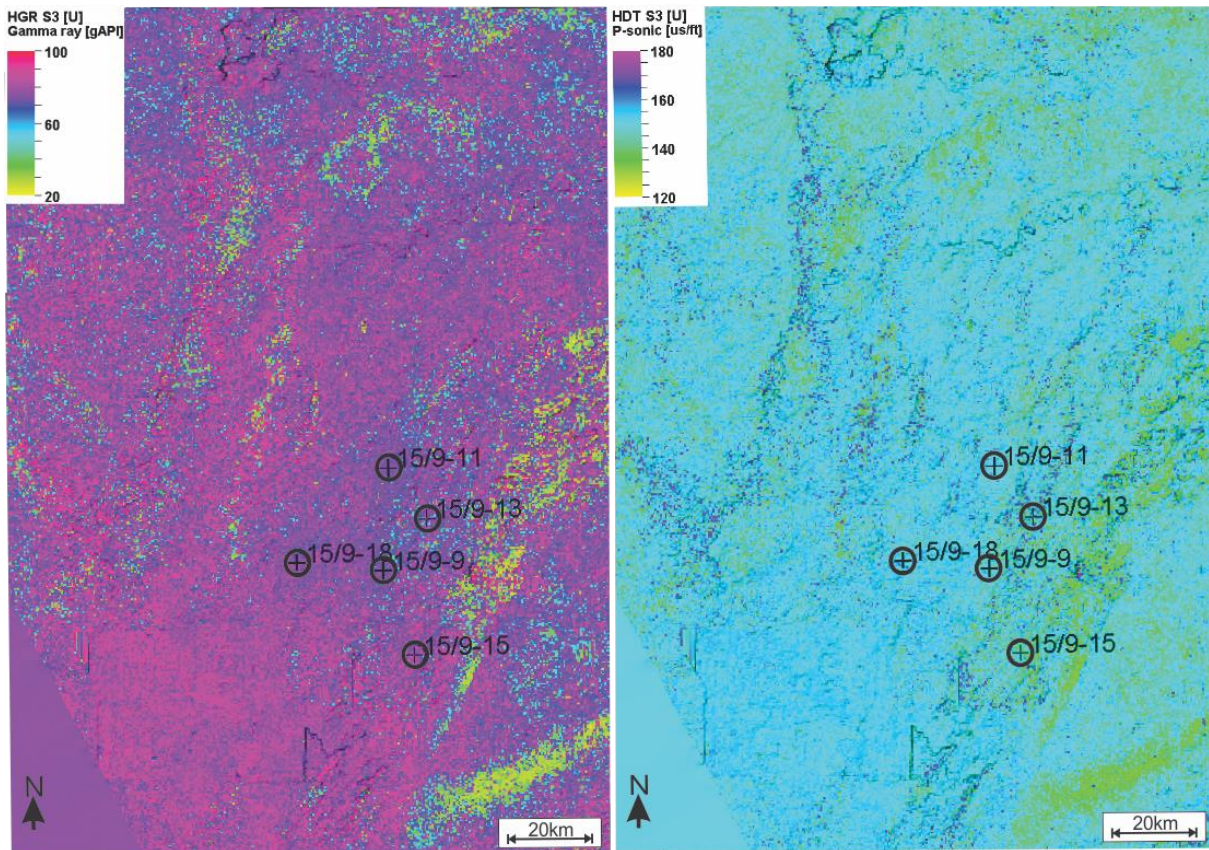


Figure 4.21: Co-kriging interpolation done on the third sequence, S3. The gamma ray distribution is shown to the left and the sonic to the right.

The distribution of density values after the co-kriging interpolation is indicated in figure 4.22. Values are distributed from 1.7 to 2.3 g/cm³. Areas with more specific values are observed. However, most of the sequence show a background density of 2.1 g/cm³. This might indicate a shale lithology, that has not been subjected to a high degree of mechanical compaction (Rider & Kennedy, 2011). The local elongated features seen in the bottom right corner of the sequence, show abnormal values in the three co-kriging results. These features are associated with lower values for the three logs. The gamma logs show values down to 20 API, the sonic logs down to 140 μ s/ft., and the density logs show values down 1.7 g/cm³.

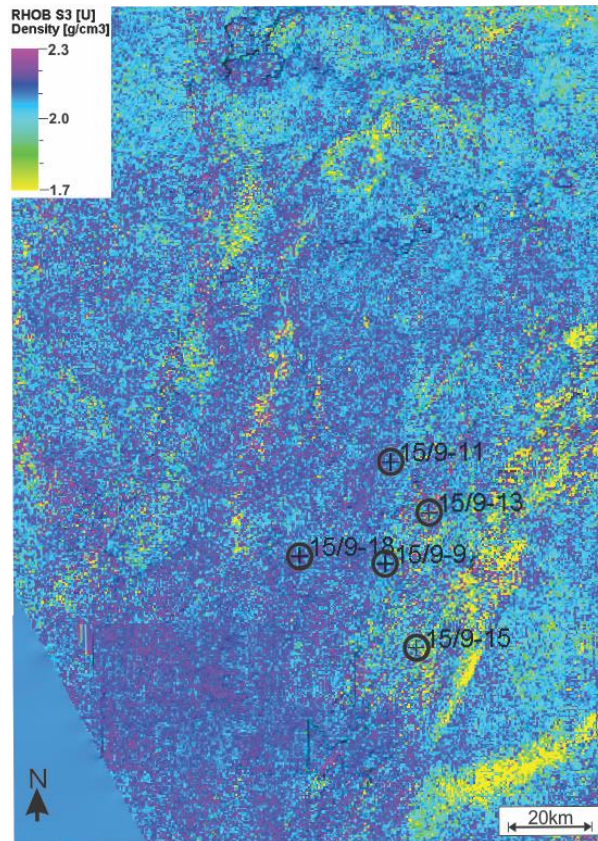


Figure 4.22: The distribution of density values in sequence S3, after co-kriging interpolation.

4.4.4 Sequence S4

Sequence S4 show generally low values after the co-kriging interpolation. Figure 4.23 show the co-kriging result between the gamma logs and corresponding seismic data. The distribution indicate that the sequence comprise mostly low gamma ray values. The sequence mainly show values around 30 API, but local areas with higher gamma values are observed.

The sonic values have been disturbed with the co-kriging interpolation method, and the sequence mostly show values in-between 150-160 μ s/ft. The density values have been disturbed and show generally low values for the whole sequence (Fig. 4.24). Larger areas show values down to 1.4g/cm³, but also higher local values are observed in the sequence. The elevated values might indicate that the Utsira Formation, have local changes in mineral composition.

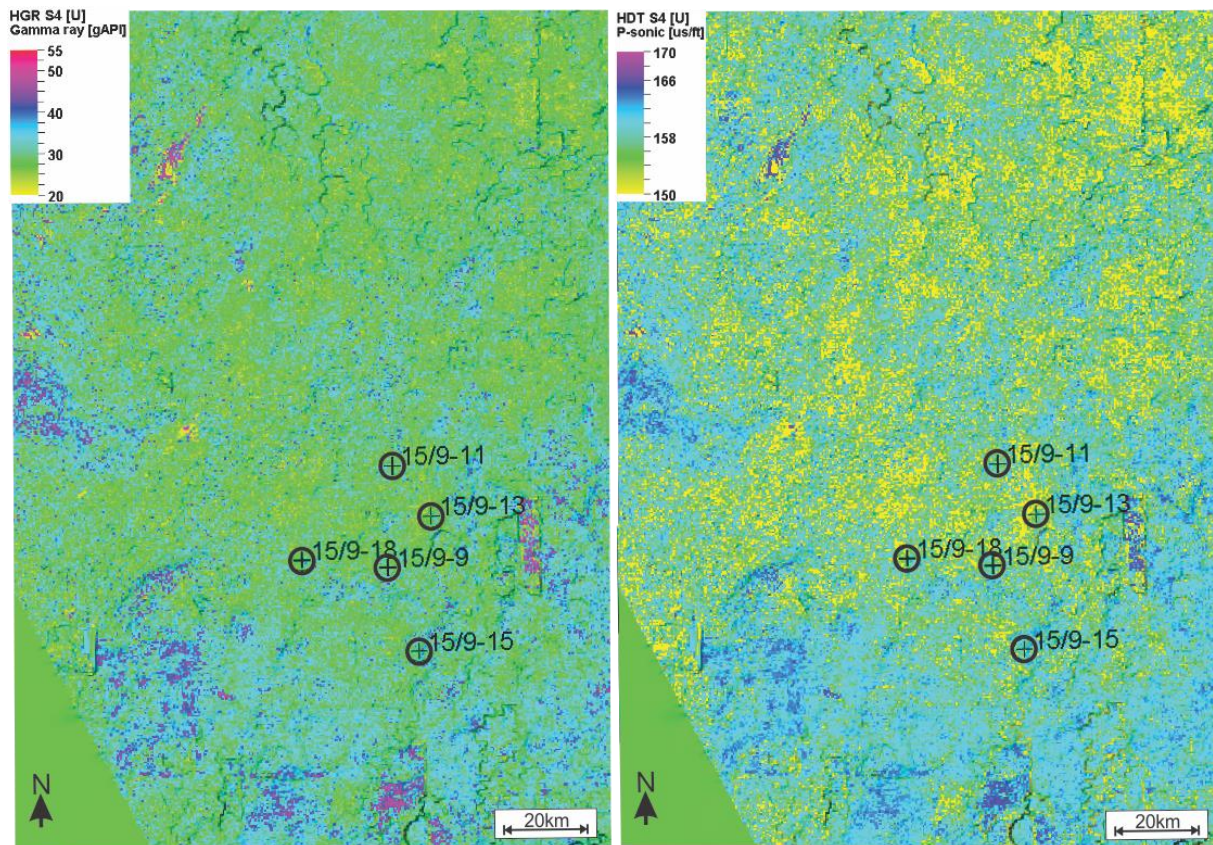


Figure 4.23: Co-kriging interpolation done on the fourth sequence, S4. The gamma ray distribution is shown to the left and the sonic to the right.

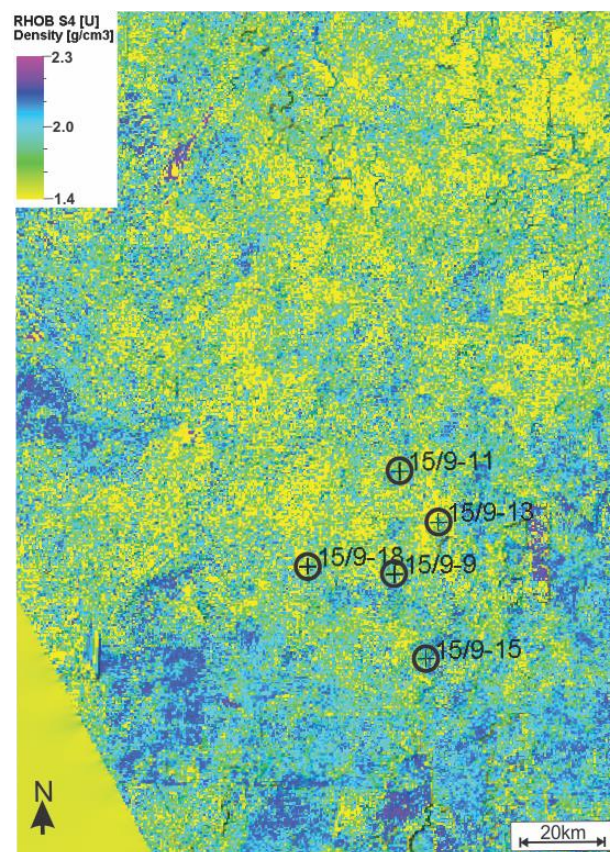


Figure 4.24: The density distribution in sequence S4, after co-kriging interpolation.

4.4.5 Sequence S5

Figure 4.25 indicate that the gamma and sonic values are generally uniform in the fifth sequence. The gamma values are relatively high, with most of the values occurring between 50-80 API. This is the same value ranges observed in the well logs. Lower gamma are located in the center of the elongated features with higher relief. These features might be related to the anticlinal features seen in figure 4.15 and 4.16. The sonic logs have a steady distribution of values in the sequence. Most of the values are observed to range from 120-150 μ s/ft. Lower values might be located in association with the elongated features (Fig. 4.25).

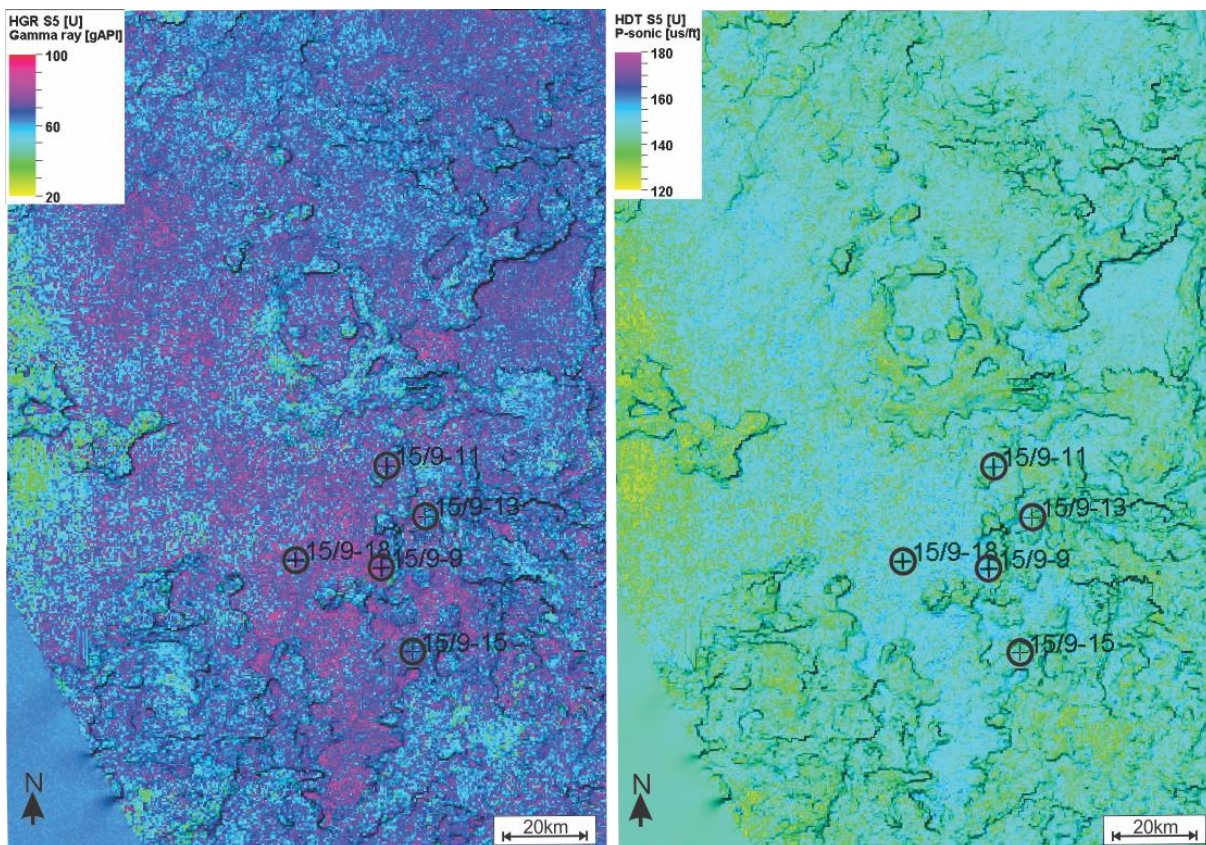


Figure 4.25: Co-kriging interpolation done on the fifth sequence, S5. The gamma ray distribution is shown to the left and the sonic to the right.

Figure 4.26 show the distribution of the density and the neutron logs in the model area. The density distribution, indicate that most values of the sequence varies between 1.7-2.1g/cm³. Local lower values are observed at the location of some of the elongated features, and to the east. The neutron distribution, show porosity fractions ranging from 0.48–0.60m³/m³. Lower values are observed on the elongated features.

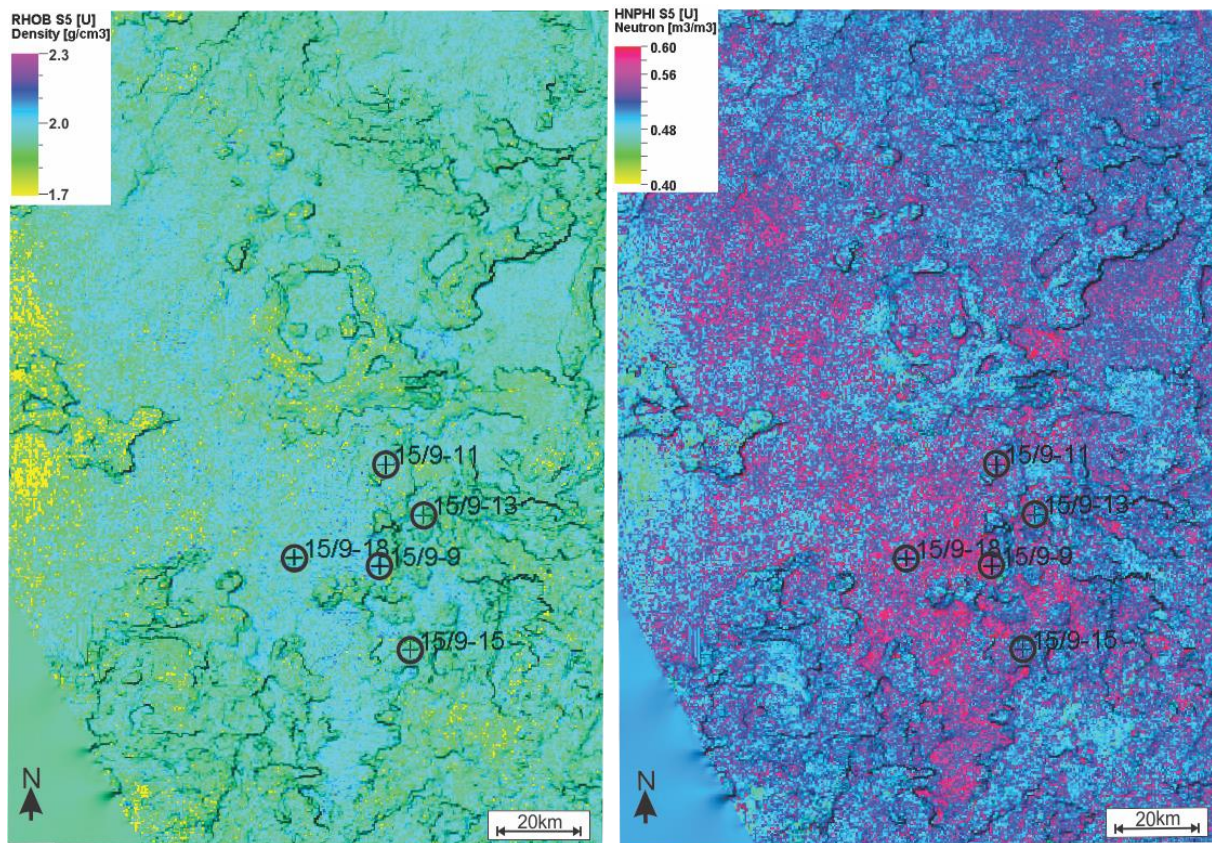


Figure 4.26: Co-kriging interpolation done on the fifth sequence S5. The density distribution is shown to the left, and the neutron to the right.

4.4.6 Sequence S6

Figure 4.27 show the distribution of gamma ray and sonic values in the model area. Sequence S6 have gamma ray values ranging from 80-100 API in the model area. Lower values are observed in the north-western parts. The lower values might be related to the extensive polygonal faulting, seen in this part of the study area. The area show gamma ray values down to 55 API, while the sonic log indicate values down to 140 $\mu\text{s}/\text{ft}$. The sonic log also show a value distribution that ranges from 140 $\mu\text{s}/\text{ft}$ in the north-western parts, to 160 $\mu\text{s}/\text{ft}$ in the central parts of the model area.

Figure 4.28 show the distribution of the density and the neutron logs in the model area. The co-kriging interpolation indicate that the sequence mostly consist of densities around 2.0 g/cm^3 . The neutron logs have been distributed and generally show values around 0.50 m^3/m^3 . Lower density values are observed to be located in the north-western parts.

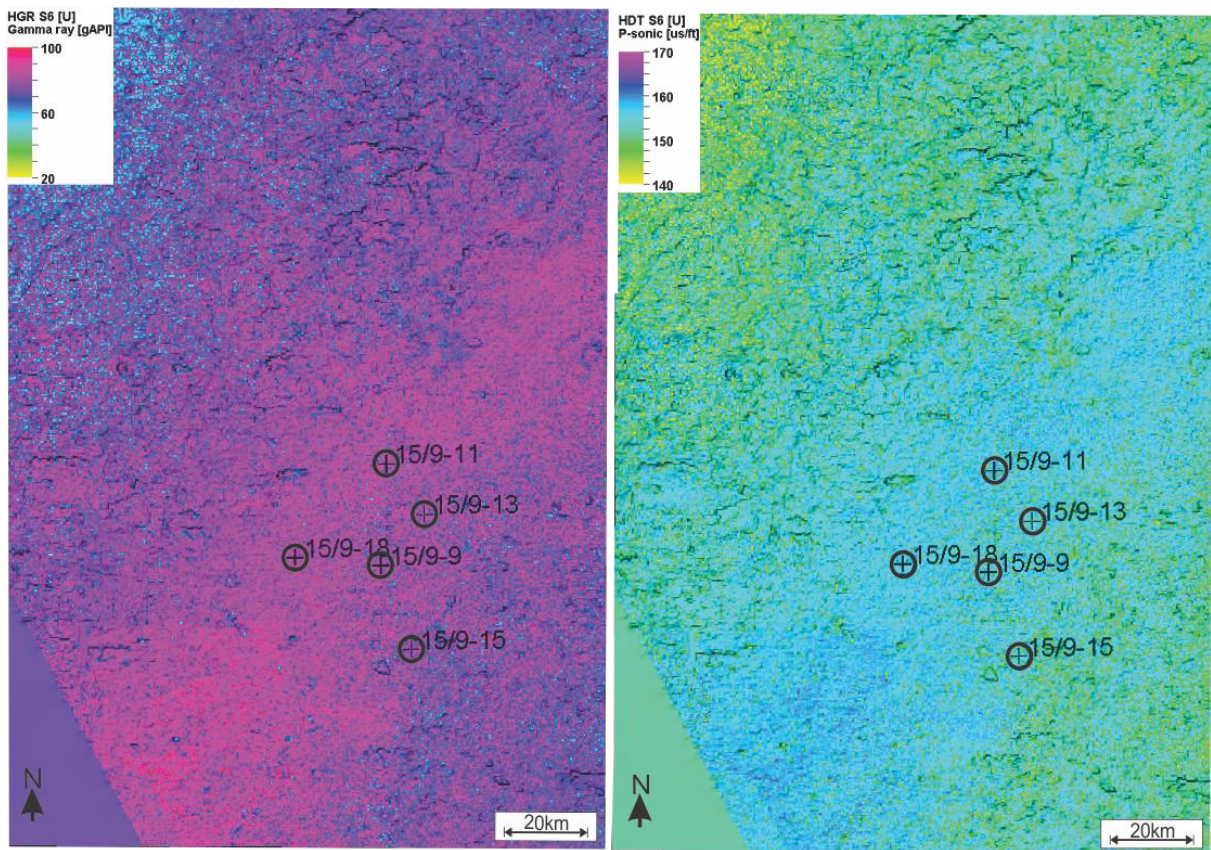


Figure 4.27: Co-kriging interpolation done on sequence S6. The gamma ray distribution is shown to the left and the sonic to the right.

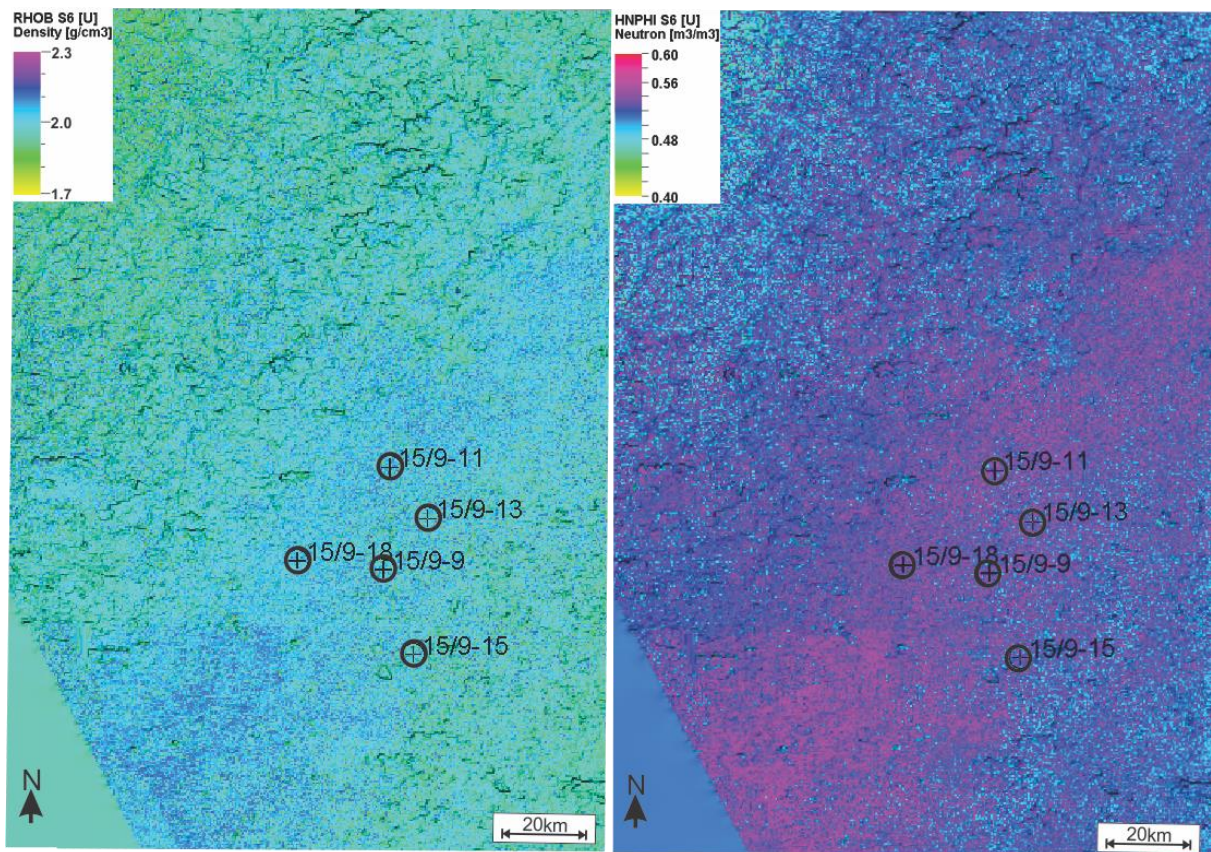


Figure 4.28: Co-kriging interpolation done on sequence S6. The density distribution to the left, neutron to the right.

4.5 Inserting hypothetical wells

Co-kriging interpolation have been used to distribute the petrophysical properties in the model. This gives the possibility to insert a hypothetical wells, and extract the interpolated well logs at any location. Figure 4.29 show the model after co-kriging have been applied to the entire model. The same semivariogram parameters have been used. The figure show the location of two hypothetical wells, indicated as Hypothetical well 1 (HW1) and hypothetical well 2 (HW2) HW1 is located approximately 19.3 km north-west from well 15/9-9, and HW2 is located in-between well 15/9-15 and 15/9-9. The hypothetical wells represent a sample point in the model, and can be used to indicate how the properties have been interpolated outside the range of the semivariogram.

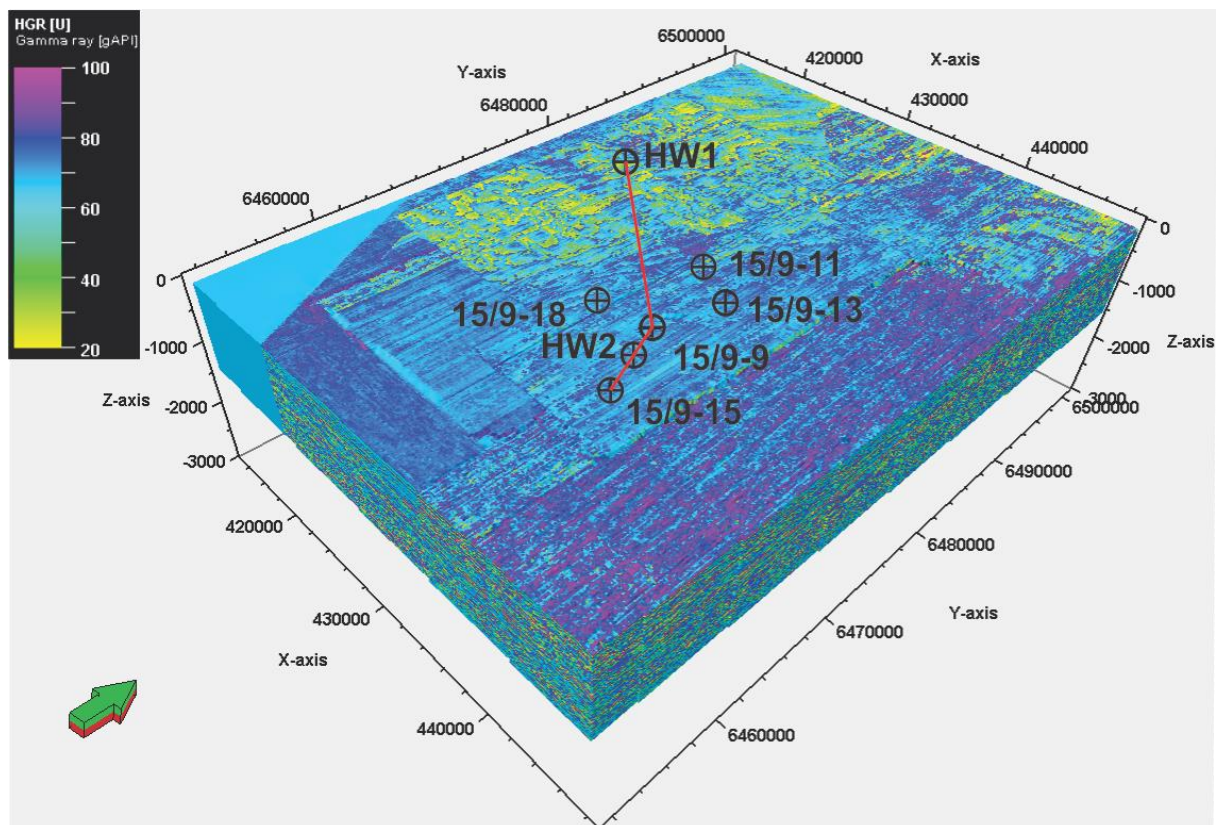


Figure 4.29: Simple model of the uppermost Cenozoic stratigraphy. The X and Y-axis is given in meters, Z-axis in TWT. Co-kriging have been used to distribute the gamma ray properties in the model. The wells are indicated. The red line show the well correlation between 15/9-15, 15/9-9 and the hypothetical wells HW1 and HW2 (Fig 4.30).

4.5.1 Predicting physical properties for hypothetical wells

The hypothetical wells have been placed some distance away from the other wells. This will give an indication on how the properties have been interpolated at this location. Figure 4.30 indicate the two hypothetical wells, in relation to the two original up-scaled well logs in 15/9-15 and 15/9-9. The outline of the well section window have been indicated in figure 4.29.

The well section window indicate that HW1 have some difficulties in interpolating trends in, some distance away from the other wells. HW1 is located outside the range of the semivariogram, and the Utsira Formation (S4) is not distinctively showing in HW1.

The gamma log show an average value of 75 API, with several spikes up to 100 API. There is also several low value intervals in the interpolated gamma log. These have values down to 30 API. The interpolated sonic log in HW1 have an average value of 155 $\mu\text{s}/\text{ft}$. Spikes up to 190 $\mu\text{s}/\text{ft}$ are observed. The density log have an average of 1.9 g/cm^3 . However, several intervals with lower density values, are observed in relation to the lower gamma ray log values. This intervals have densities down to 1.4 g/cm^3 . The neutron log show an average value of 0.50 m^3/m^3 , with spikes up to 0.60 m^3/m^3 . It is clear that the interpolated well logs in HW1 relies on correlation between the seismic data and the well log values, and have been interpolated based on the parameters within the semivariogram ranges.

HW2 is located close to the original well logs, and inside the range of the semivariogram. The hypothetical well show a strong correlation towards the other well logs, and the Utsira Formation is clearly visible (Fig. 4.30, See well HW2, S4). The original well logs show several distinctive trends, these trends can also be observed in HW2. The well logs in HW2 show some deviations in values, in relation to the original well logs. However, due to the close proximity towards the original wells, these values is considered valid. Hence, the petrophysical values for each interpret sequence can here be extracted.

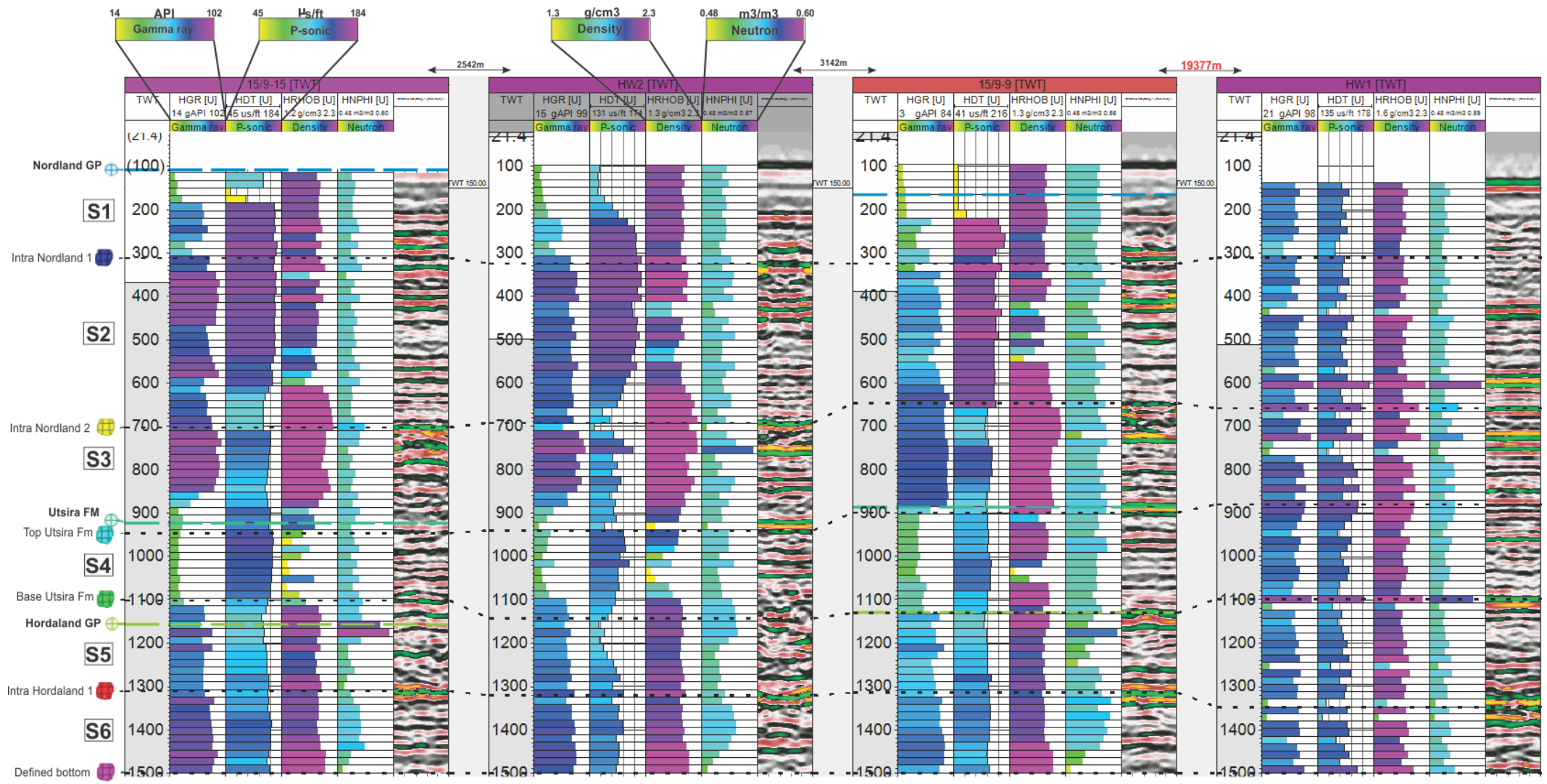


Figure 4.30: Well section window showing well 15/9-15, HW2, 15/9 and HW1. See figure 4.29 for direction and outline (red line between wells). The interpolated well logs for each corresponding well is indicated. Well seismic have been extracted for each well (see chapter 3.6.3). Notice that the density and neutron log have now been interpolated to cover the entire well. Also notice the distance between the wells. The value ranges with corresponding color templates, have been auto-adjusted.

5 Discussion

5.1 Sequence interpretation

The first authors to described and subdivided the uppermost Cenozoic succession in the northern North Sea was Deegan and Scrull (1977) and Isaksen and Tonstad (1989). Numerous authors have followed in the further work of subdivision and classification (Martini, 1971; Gradstein et al., 1994; Mudge & Bujak, 1994; Jordt et al., 1995; Eidvin et al., 1999; Eidvin et al., 2000; Rundberg & Eidvin, 2005; Eidvin & Rundberg, 2007). The sequences in this thesis can be seen in relation to the regional work done by Jordt et al. (1995), Faleide et al. (2002) and Rundberg and Eidvin (2005).

In order to map out seismic sequences, key seismic sections had to be used. The survey consist of 3297 inlines and 5026 crosslines, and in order to get a good representation of the reflection configuration adjacent to the wells, a central crossline (2875) and composite line (Composite line 1a) had to be used.

The traditional workflow in seismic sequence stratigraphy, is to divide the seismic into sequences based upon reflection terminations (Mitchum et al., 1977). However, the location and shallow view of the seismic data used in this thesis, makes it hard for such a classification. The Sleipner area is located in the middle of the North Sea towards the end of the Norwegian sector, and the shallow focus of the seismic don't provide a regional overview. However, indication of reflection terminations is seen in-between some of the horizons in the seismic sections.

The sequences have been classified based on reflection configuration with used of original seismic data and attributes. The wells have provided critical petrophysical insight, towards the lithology and subsurface conditions. And the co-kriging interpolation have given the possibility to distribute the well data in the sequences.

Table 5.1 summarizes the reflection configuration and the average well log values. The table also show the correlation towards previous work. The following chapters will focus on the results found in chapter 4.

Sequence interpretations				(Rundberg & Eidvin, 2005; Eidvin & Rundberg, 2007)	(Jordt et al., 1995; Jordt et al., 2000)	(Gregersen & Johannessen, 2007)
Sequence	Reflection configuration	Average well log values 15/9-9, 15/9-11, 15/9-13, 15/9-15, 15/9-18.				
S1	Discontinuous disrupted	HGR HDT	35-65API 60-165µs/ft.		CSS-10	Glaciomarine deposits.
S2	Continuous parallel	HGR HDT	75API 170µs/ft.		CSS-9	Prograding complex
S3	Continuous subparallel	HGR HDT HRHOB	90API 150 µs/ft. 2.0-2.2g/cm3		CSS-8	Shale drape
S4	Discontinuous disrupted	HGR HDT HRHOB	25-60API 145-155µs/ft. 1.3-2.0g/cm3	LN-2	CSS-7	
S5	Discontinuous disrupted	HGR HDT HRHOB HNPHI	50-80API 130-160µs/ft. 1.8-2.0g/cm3 0.40 m3/m3	LN-1	CSS-6 (?)	
S6	Discontinuous disrupted	HGR HDT HRHOB HNPHI	80-100API 160µs/ft. 1.8-2.0g/cm3 0.45-0.50m3/m3	UH-4	CSS-5	

Table 5.1: Summary table of the reflection configuration and average well log values, observed in each sequence. Possible correlation of sequence S1-S6 towards previous work is illustrated.

5.2 Sequence variability

The classification of sequences and paleo-environment, will be discussed mainly towards the work of Jordt et al. (1995) and Rundberg and Eidvin (2005). However, several authors are central in this discussion (Gregersen et al., 1997; Eidvin et al., 1999; Eidvin et al., 2000; Eidvin & Rundberg, 2001; Faleide et al., 2002; Eidvin & Rundberg, 2007; Gregersen & Johannessen, 2007; Eidvin et al., 2014). All the sequences have been deposited in a shelf to marine area, with variable processes, water depth and source areas.

5.2.1 Sequence S1

5.2.1.1 Reflection configuration and features

The reflection configuration of the upper most sequence was classified to be discontinuous, and to show several disrupted reflections (Table 5.1). The sequence show channel features and local chaotic reflections. The sequence also show numerous artifacts related to the processing of the 3D seismic cube. The age of the sequence is Late Pleistocene to Holocene.

The upper most sequence have been interpreted to be the regional sequence CSS-10 after (Jordt et al., 1995), and the sequence consist of mostly glacial deposits (Sejrup et al., 1991; Eidvin et al., 1999; Sejrup et al., 2000; Faleide et al., 2002). The North Sea was glaciated as early as 850 ka, and almost all of the Quaternary sediments in the northern North Sea, were deposited under arctic conditions (Sejrup et al., 1991; Sejrup et al., 2000). Figure 5.1 indicate that sequence CSS-10/S1 is regional distributed, with a maximum thickness occurring in the Norwegian trench.

According to Sejrup et al. (1991) there was a change in the sedimentary environment in the middle of Pleistocene. Consequently, overlying deposits appear less continuous and were highly influenced by glacial processes. There was also fluvial erosion and deposition, related to these glacial processes (Sejrup et al., 1991) The disrupted reflections indicate that the sediments might have been reworked and disturbed by different processes. This is supported by Eidvin et al. (1999), who interpret glacio-marine sediments to be characterized with discontinuous reflections, if they were subjected to strong glacial influence. This have been interpreted to be consistent with the reflection configuration for S1.

5.2.1.2 Petrophysical data and distribution

The well logs indicated that the uppermost sequence, had lower gamma and sonic values in the uppermost parts (Fig. 4.14). The lower gamma values is here interpreted to be unconsolidated sands (Rider & Kennedy, 2011). The lower parts of the sequence show higher

values, and the lithology here have been interpreted to be shale. The well logs provide a good indication of the lithology. This interpretation can be correlated between all the five wells (Fig 4.14).

The co-kriging results of the uppermost sequence S1 is highly disturbed by artifacts and noise (Fig 4.19). Survey merging and processing have given an irregular seafloor configuration. However, the values observed in the well logs suggest that sequence S1 consist of sands and underlying shales. This can be observe around the wells (Fig 4.19). The seismic data changes in character along the seafloor reflection, and might be considered unreliable as a secondary variable for co-kriging interpolation. Larger parts of the interpolated gamma logs, indicate that S1 consist of sands. However, higher values that indicate a shale lithology is observed.

5.2.1.3 Depositional environment

According to Jordt et al. (1995) the base of the CSS-10 is a pronounced regional angular unconformity. This is evident by the incline nature of S2, and the terminations of reflection seen from S2 upwards towards S1 (Fig.4.3, IH1). The IN1 horizon is interpreted according to the reflection configuration and the well logs of the sequences, In addition, the horizons fit the angular unconformity that marks the base of CSS-10. Reflection terminations may be seen located underneath the horizon (Fig.4.3). The substantial fall in sea-level associated with glaciation in Late Pleistocene, resulted in the in the unconformity that CSS-10 is deposited on (Gregersen & Johannessen, 2007).

Figure 5.4 indicate that ice sheet covered the North Sea in late Pleistocene times. Sequence CSS-10 /S1 is probably a result of uplift caused by isostatic rebound and glacial processes. The early initiation of glaciation led to a regional erosion before the deposition of S1. Boreal arctic to arctic conditions and glacial tills dominated, and an inner neritic environment (Up to 30m water depth) has been suggested by Eidvin et al. (1999). Deposition of the Pleistocene unit has varied from glacial to a fluvial environment. This is related to repeated glacial cycles, causing glaciomarine clays to be deposited under shallow marine conditions. This most likely explain the configuration of the reflections. Figure 5.1 show the regional extent of the sequence, and it is clear that a regional processes has dominated.

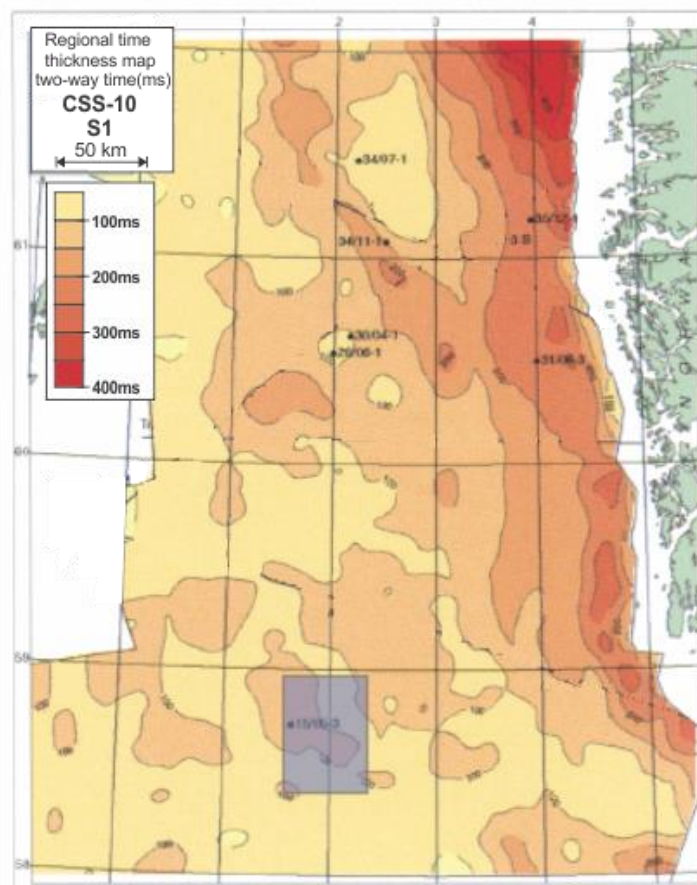


Figure 5.1: Time thickness map of CSS-10. Interpreted to be S1. The approximated position of the study area is shown in light shaded blue color. Figure is modified after Faleide et al. (2002).

5.2.2 Sequence S2

5.2.2.1 Reflection configuration and features

The overall reflection configuration of sequences S2, was classified as continuous, with a parallel configuration (Table 5.1). The sequence show a distinct thickening towards the south with incline reflections, indicate a divergent progradation configuration. Based upon the reflection configuration interpreted from seismic attributes, the sediments must have been deposited in a relative stable environment, as the reflections show good continuity. The distinctive dipping trend towards the south, might indicate that most of the sediments are sourced from the uplifted Scandinavia. According to Eidvin et al. (1999) the Pleistocene reflection patters are commonly continuous and parallel, typical for glacio-marine sediments. Furthermore, Jordt et al. (1995) suggest that the sequence is characterized by a high amplitude reflections with variable continuity. This is consistent with the description given here.

5.2.2.2 Petrophysical data and distribution

Both the gamma logs and the sonic logs show high values within the sequence. This indicate a shale lithology. The density log seen in the lower parts of the sequence, might support this interpretation. Correlation of the gamma ray logs, indicate that there is a distinctive block configuration within the sequences. Clearly seen in well 15/9.11, 15/9-13 and 15/9-15 (Fig.4.14, S2). The lower section show some indication of a gradual decrease in gamma ray values towards the middle of the sequence. This might indicate that water depths were gradual lowering in this period, possible related to repeated glacial cycles. Correlation of the sonic logs indicate elevated values, compared to the underlying units. This is most likely linked to the mineral composition within this interval.

The co-kriging interpolation done on the gamma ray and sonic logs for sequence S2 (Fig. 4.20), indicate that major parts of the sequence consist of shale. However, localized sands are present. These sands can be clearly seen at the location of well 15/9-18, in figure 5.2.

Long and thin elongated features can be vaguely seen in the co-kriging interpolation (Fig.4.20). These features might be rivers. Interpolated values from the gamma logs, indicate that these features contain sands. In addition, the interpolated sonic logs show lower values associated with these features.

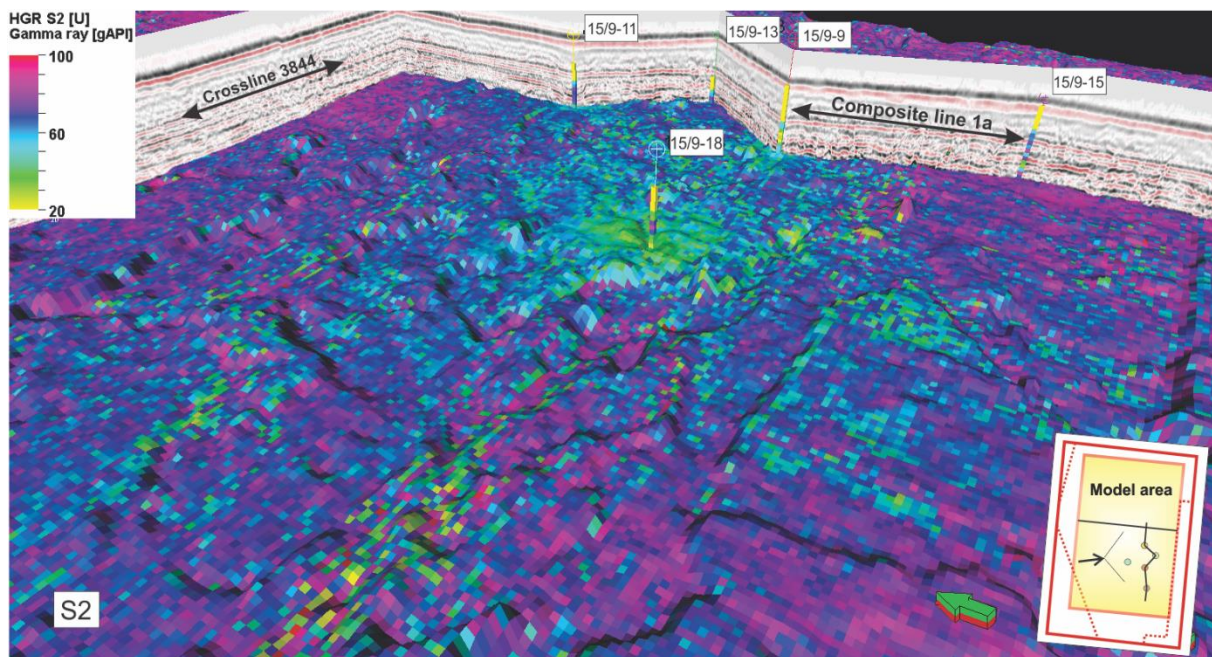


Figure 5.2: 3D illustration of the co-kriging result of gamma logs in S2, in relation to the seismic data and the up-scaled well logs. The sequence mostly consist of shale, but localized sands are located within the sequence. The survey figure in the bottom right corner, indicate the view direction towards the wells.

5.2.2.3 *Depositional environment*

The entire North Sea basin has been covered by ice sheets during Pleistocene. This is indicated in figure 5.4, which shows two glacial maximums, Weichselian glacial maximum (20 ka) and Late Saalian glacial maximum (160-140 ka) (Svendsen et al., 2004).

Sequence S2 most likely correlates to CSS-9 after Jordt et al. (1995). Gregersen and Johannessen (2007) identified CSS-9 as a prograding complex with incline reflections, that downlap onto the underlying unit. This is consistent with the observations done here. Figure 5.3 shows the thickness of the sequence CSS-9, after Faleide et al. (2002). Southwards from the study area, the thickness increases greatly (Fig. 5.3). This increase in thickness is consistent with the time thickness map produced for sequence S2 in figure 4.6.

The prograding nature of the sequence indicates a period of relative high supply and sedimentation rate, with a possible fall in sea-level. The massive input of sediments is therefore related to glacial processes that eroded the uplifted Scandinavia (Rokoengen et al., 1995; Henriksen & Vorren, 1996). Extensive glaciation of the Norwegian shelf is probably the main source for sediments, and has supplied the Sleipner area with high amounts of glacio-marine sediments. The depositional environment for the Pleistocene sequence has been suggested to be middle neritic (30-100m water depth) by Eidvin et al. (1999). This indicates a shallow marine environment with dominant glacial processes. The sediments have most likely been reworked in the shallow waters, and deposited in a prograding configuration. Based on the reflection configuration, well logs and the co-kriging results, this is a plausible setting.

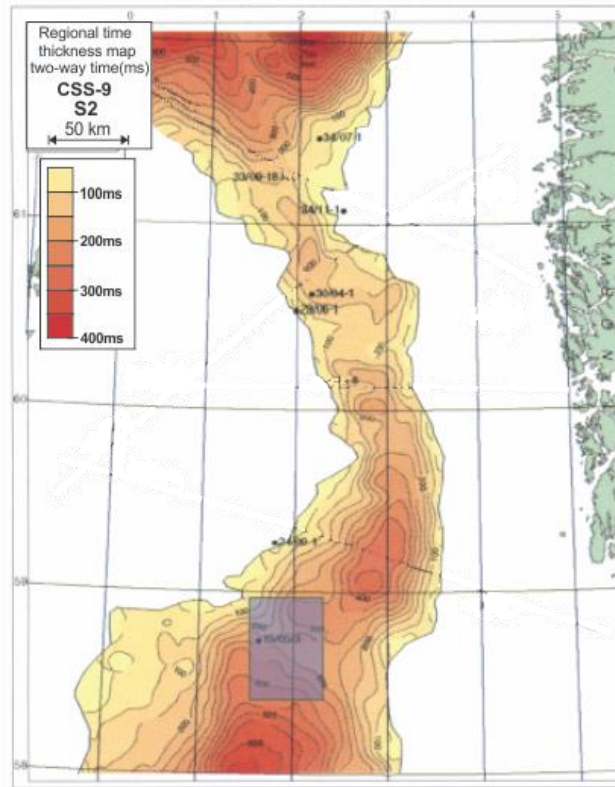


Figure 5.3: Regional time thickness map of CSS-9/S2. The figure show the outline of the sequence. The Study area is indicated as a blue rectangle. Figure is modified after Faleide et al. (2002).



Figure 5.4: Regional map showing the extent of the Late Weichselian glacial maximum (ca. 20 ka) (Red line), and Late Saalian (160-140 ka) (White line). The dotted green line, indicate the extent of older ice sheets Figure modified after Svendsen et al. (2004).

5.2.3 Sequence S3

5.2.3.1 Reflection configuration and features

Sequence S3 might correlate to CSS-8 after Jordt et al. (1995). The sequence was further interpreted by Gregersen and Johannessen (2007) to be a shale drape. The sequence is here classified with a parallel to subparallel reflection configuration (Table 5.1). The reflections show good continuity, with medium to high amplitudes. The sequence show a distinctive dipping trend towards the south with incline reflections. The high amplitudes found at the top and base of the sequence, most likely indicate a strong acoustic contrast. Based on the reflection configuration, the depositional environment has most likely been low energy, as the reflections show a good continuity and have medium to high amplitudes. In addition, there is no abnormal or irregular reflections observed in the sequence, which could indicate high energy depositional features.

Numerous bright spots with associated acoustic masking, have been observed within the sequence (Fig.4.15 and 4.16). The combination of the variance and envelope attribute, illustrates clearly the accumulation of high amplitudes in the upperparts of the sequence. Bright spots are seen at this depth, both in the composite line and crossline. This might suggest that IN2 marks the deposition of an impermeable layer, which act as a cap rock for the migrating shallow gas.

The RMS attribute highlights both the negative and the positive amplitudes. The bright spots seen in the RMS attribute, might indicate shallow gas accumulations, as gas appear as strong negative amplitudes in the subsurface (Andreassen et al., 2007). The associated acoustic masking, is seen extensively throughout the entire survey. These zones have been interpreted by Karstens and Berndt (2015) to be gas chimneys. The gas chimneys can be seen in relation to the anticlinal features, as most of the acoustic masking is located at the top of these. It is possible the sand injections and the underlying polygonal faulting, have given good migration routes for the shallow gas.

5.2.3.2 Petrophysical data and distribution

Interpretation of the well logs suggest that the sequence consist of shale (Fig.4.14). This is supported by Gregersen and Johannessen (2007), who investigate drill cuttings from the Sleipner area. The gamma ray log show indications of a bell shape configuration. With decreasing values towards a low interval, located approximately at IN2. This might indicate a gradual decreasing in shale content, towards a smaller sand interval. The well logs correlated

strongly within the sequence. Most of the logs show a serrated outline, that could indicate thin layers of slightly different mineral composition (Rider & Kennedy, 2011). The abrupt change in lithology found at the base of the sequence, most likely indicate a change in paleo-environment for the northern North Sea basin.

The co-kriging results seen in figure 4.21 and 4.22 show a relatively uniform distribution. Abnormal values have been observed along elongated irregular features. The features may be related to different depositional processes during Pliocene times. The elongated configuration and the low gamma values, might suggest that these are submarine channels. The incline morphology of the sequence and the co-kriging results, could indicate a drainage direction towards east. Figure 5.5 show a 3D illustration of sequence S3 towards the seismic data and up-scaled wells. Lower values can here be observed along S3. This could be localized sands, within the sequence.

The interpolated gamma ray logs, indicate that most of the sequence consist of high values (90-100 API). The density and sonic logs, also show relatively high values, throughout the sequence. These results most likely indicate that sequence S3, consist of shale in major parts of the study area (Fig 4.21 and 4.22).

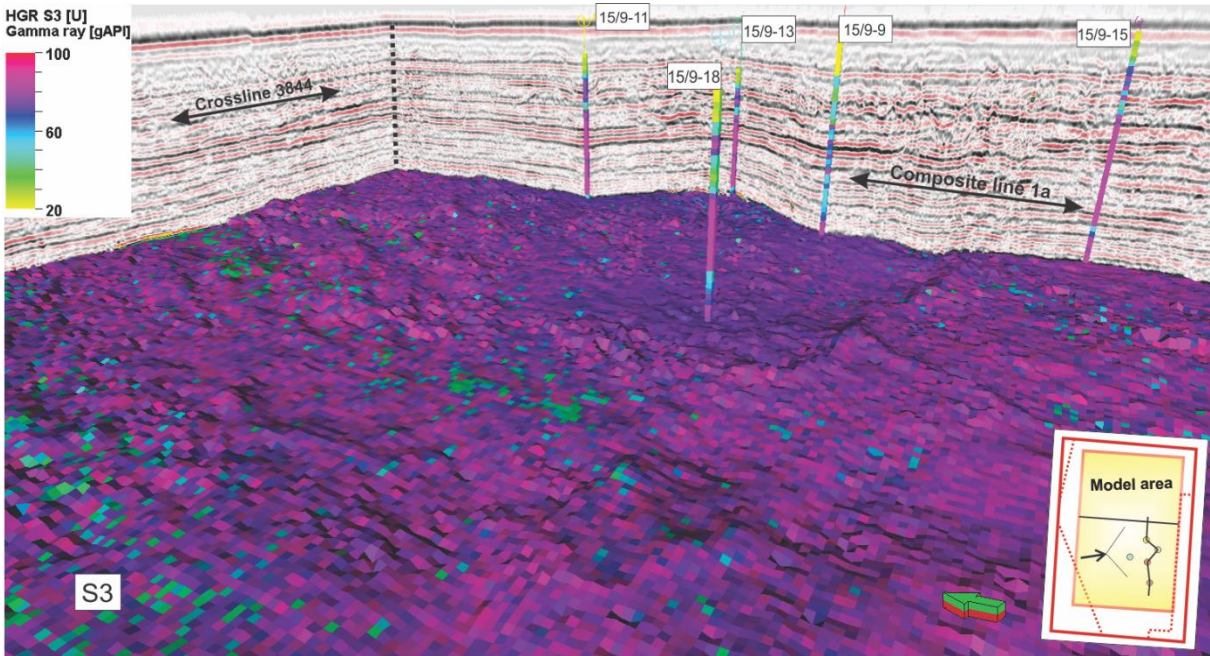


Figure 5.5: 3D illustration of the co-kriging result of gamma logs in S3, in relation to the seismic data and the up-scaled well logs. The sequence mostly consist of shale. The survey figure in the bottom right corner, indicate the view direction towards the wells.

5.2.3.3 Depositional environment

According to Jordt et al. (1995) the sequence is of mostly Pliocene age. The incline reflections of the sequence suggest an outbuilding of sediments from the shelf area. This is confirmed by Jordt et al. (1995), who suggest that sediments built out as prograding clinoforms north of the Viking graben. This outbuilding pattern suggest that the basin margins in the North Sea were uplifted. Jordt et al. (1995) suggest that most of the sediments built out form the southern parts of Fennoscandia. This is supported by Faleide et al. (2002), who suggest that the upper Pliocene sequence consist of glacial derived sediments, sources from the uplifted Norway. The outline of the sequence is shown in figure 5.6 and the thickness is shown in figure 5.7. It is clear from these figures that sequence S3 is thickest in the center of the basin.

The deposition of sequence S3, is most likely related to the late Pliocene cooling, which later led to extensive glaciation of both hemispheres (Knies et al., 2002). The major glaciation of the Northern Hemisphere in late Pliocene times, is seen in context to the deposition of S3. The sediments show a dominant transport direction form the Norwegian shelf margin, and built out into the northern North Sea (Faleide et al., 2002). This dominant direction is observed in the co-kriging results of S3. Lower values occur in elongated features, these could be drainage channels from the Norwegian shelf margin.

The strong lithological change from seen at the base of S3 and top of S4, is consistent with the major change in depositional environment, seen in late Pliocene. Faleide et al. (2002) suggest that the sequence have been deposited by rapid deposition of glacial processes, and that the clinoforms indicate a water depth of 500 meters. However, a middle to outer neritic environment (up to 200m water depth) have been suggest by Eidvin et al. (1999). Based on the configuration of the sequence, well log values, and the co-kriging interpolation, this could be a plausible depositional environment.

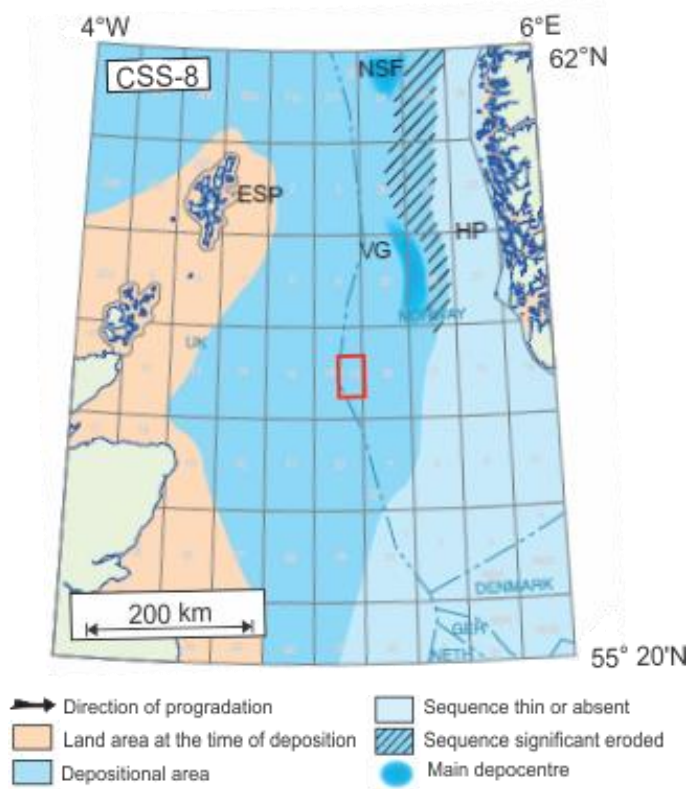


Figure 5.6: Paleo-geography showing the main depocentres of CSS-8, based on Jordt et al. (1995) and Isaksen and Tonstad (1989). ESP–East Shetland Platform. VG–Viking Graben. NSF–North Sea Fan. HP–Horda Platform. Figure is modified after Fyfe et al. (2003).

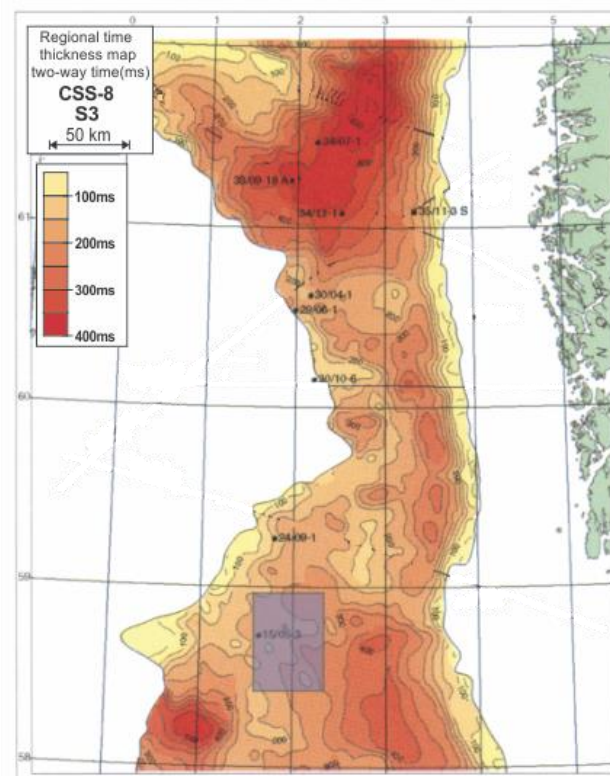


Figure 5.7: Regional time thickness map of CSS-8/S3. The figure show the thickness outline of the sequences. The Study area is indicated as a blue rectangle. Figure is modified after Faleide et al. (2002).

5.2.4 Sequence S4

5.2.4.1 Reflection configuration and features

The reflection configuration in sequence S4 was interpreted to be discontinuous with a disrupted configuration (Table 5.1). The sequence show zones with chaotic and contorted configuration. Based on this configuration, the sequence most likely have been subjected to processes that have affected the natural parallel bedding pattern. Low amplitude reflections is observed within the sequence, these are disrupted locally but can be traced laterally. A semi-continuous, sub-parallel configuration have been suggested by Gregersen et al. (1997). This is partly consistent with the observations done here. The reflections are cut into numerous intervals, making the classification of a disrupted configuration appropriate.

5.2.4.2 Petrophysical data and distribution

The well correlation done in figure 4.14, indicate a distinctive drop in gamma ray values within sequences S4. An average value of 35 API, with some spikes up to 65 API have been observed. This distinctive drop in values, can be correlated across all the wells in the study area (Fig.4.14). The distinctive low gamma ray values in S4, have been interpreted with some confidence to be a sand interval. The density logs show numerous spikes within the sequence. However, the density logs in well 15/9-9 and especially 15/9-18, show no drastic change in density compared to the other sequences. This most likely related to local differences in mineral composition. The sonic log seem to correlate in all the five wells, as there are no abrupt changes in the log pattern. The caliper log show elevated values within the sequence. This is most likely due to a change in borehole conditions, as the sandy formation is assumed to be less compacted than the adjacent shale sequences. The acoustic impedance logs show different responses in well 15/9-9 and 15/9-18, this is due to the different responses in the density logs. The configuration of the acoustic logs, strengthen the hypothesis of several thin layers of shale composition within the sequence.

Based on the co-kriging interpolation, sequence S4 consist of sands in the study area (Fig. 4.23 and 4.24). The Utsira Formation have a depocenter located in the Sleipner area (Riis & Halland, 2014), this is consistent with the result of the co-kriging interpolation. The interpolated gamma ray logs, indicated a relatively uniform distribution of low values (down to 30 API). The sonic logs show the same uniformity, with values ranging from 150-160 $\mu\text{s}/\text{ft}$. The interpolated density logs indicate that the sequence mostly consist of densities down to 1.4 g/cm^3 . However, larger areas with densities up to 2.1 g/cm^3 is observed (Fig. 4.24).

Low values can be observed for the three interpolated well logs (Fig 4.23). These are indicated as shallow depression in figure 5.8. The shallow depressions, have been interpreted to be localized areas with different mineral composition. Shales might be located in these areas.

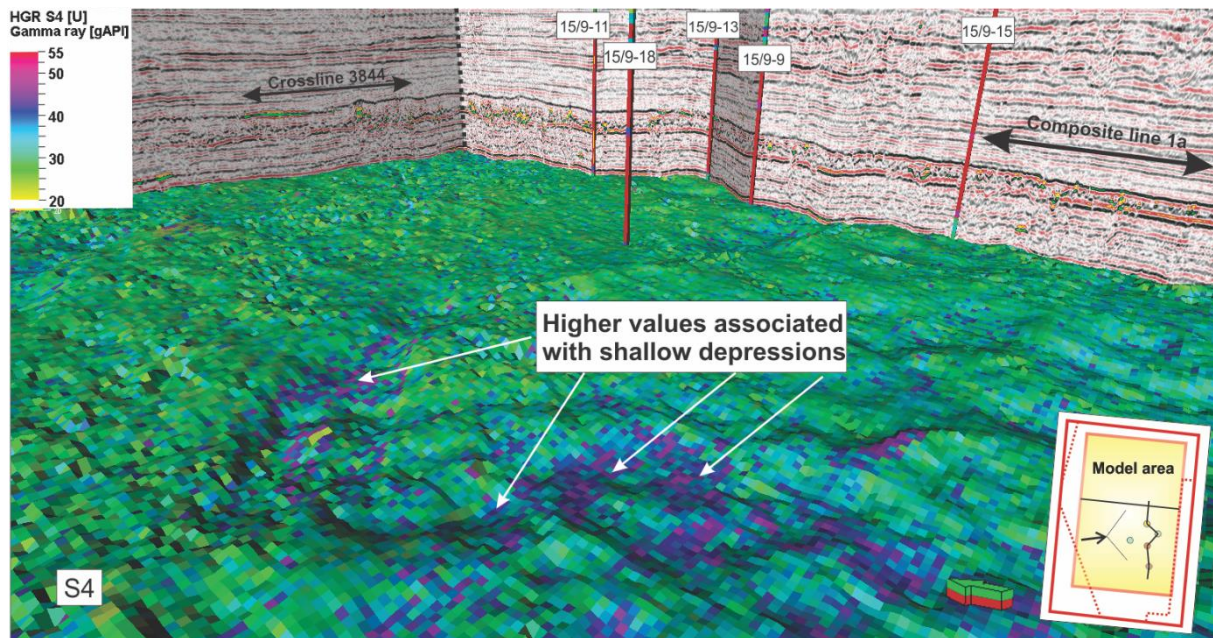


Figure 5.8: 3D illustration of the co-kriging result of gamma logs in S4, in relation to the seismic data and the up-scaled well logs. The sequence mostly consist of sands, but elevated values are seen in local shallow depressions. The survey figure in the bottom right corner, indicate the view direction towards the wells.

5.2.4.3 Depositional environment

Sequence S4 have been interpreted to be LN-2 after Rundberg and Eidvin (2005) and CSS-7 after (Jordt et al., 1995). The sequences comprise the Utsira Formation, first described by Deegan and Scrull (1977) and later Isaksen and Tonstad (1989). According to Eidvin and Rundberg (2007) the Utsira Formation consist of medium-grained sandstones. This is consistent with the co-kriging result shown in figure 4.23 and 4.24. The sandstones are mainly quartzose, but glauconite also occur (Eidvin & Rundberg, 2007). Based on recent biostratigraphic work, the age of the Utsira Formation have been estimated to be Upper Miocene to Lower Pliocene (Eidvin & Rundberg, 2007).

Figure 5.9 show the paleogeography in Upper Miocene times. According to Fyfe et al. (2003), the Utsira Formation consist of over 200 meters of mature, well-sorted, fine to medium grained sandstones. This is consistent with the thickness observed in the seismic sections, and the thickness map in figure 4.7. The sequence have most likely been deposited in response to uplift of the East Shetland Platform and the Norwegian North sea margin, this resulted in an

increased sedimentary input (Gregersen et al., 1997; Fyfe et al., 2003). The fossil assemblage indicate that the Utsira Formation was deposited in an inner neritic environment (up to 30m water depth) (Eidvin & Rundberg, 2007). This is consistent with Galloway (2001) and Galloway (2002), who have described the depositional environment in detail.

Figure 5.10 show the outline of the Utsira Formation. The figure indicate a deltaic outline of the sands. The Utsira Formation have most likely been deposited in a high energy, shelf environment. The sands were deposited in a narrow sea, named the Viking strait (Galloway, 2001, 2002). The elongated configuration of the Viking strait, amplified the oceanic and tidal currents that entered the basin from the north Atlantic (Fig.5.9) (Galloway, 2002). Consequently, the sand deposits were extensively reworked (Galloway, 2001, 2002). This most likely explain the discontinuous reflection configuration observed in the sequence.

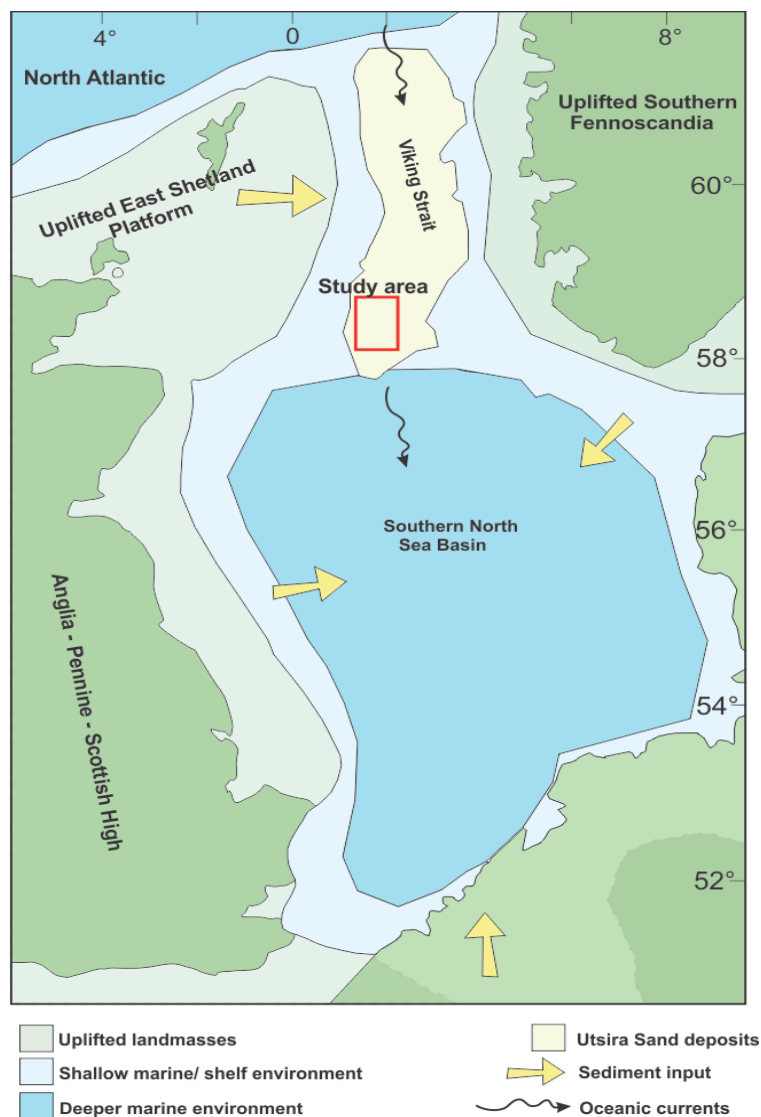


Figure 5.9: Regional Upper Miocene paleogeography of the North Sea Basin. The approximate position of the study area is indicated as a red rectangle. The figure is made after Galloway (2002) and Rundberg and Eidvin (2005).

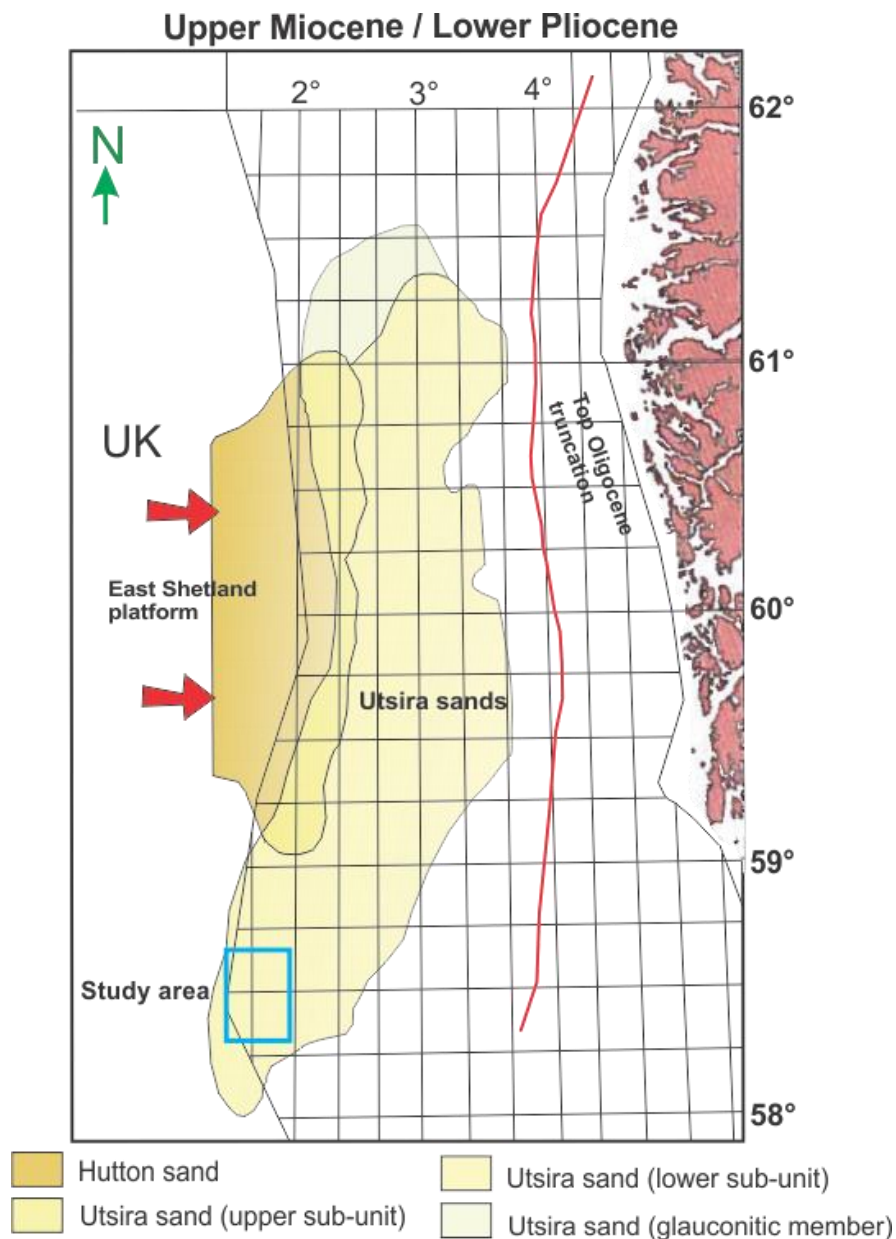


Figure 5.10: The deltaic distribution of the Utsira Formation in the northern North Sea. The red arrows show the direction of main sediment supply. The approximate position of the study area is here indicated with a blue rectangle. Figure is modified after Rundberg and Eidvin (2005).

5.2.5 Sequence S5

5.2.5.1 Reflection configuration and features

Sequence S5 have been interpreted to be the new unit LN-1, after Rundberg and Eidvin (2005). The sequence have discontinuous reflections, and have been classified with a disrupted configuration (Table 5.1). Based on the reflection configuration the sediments may have been subjected to local processes that have contorted the reflections. The continuity of the strata have been disrupted either by pre or post-depositional processes, and the reflections have generally a medium amplitude.

Rundberg and Eidvin (2005) performed a detailed biostratigraphic analysis of key wells in the Southern Viking Graben. This has proven the existence of a Middle Miocene unit. Rundberg and Eidvin (2005) included well 15/9-13 in their study, which is also used in this thesis. Rundberg and Eidvin (2005) further interpreted the top of the unit to be a high-amplitude reflector, this top reflector is here interpreted to be BUfm. The sequence clearly postdates the Mid-Miocene unconformity (Rundberg & Eidvin, 2005). The outline of the Middle Miocene unit is illustrated in figure 5.12.

Correlation of S5 towards Jordt et al. (1995) have proven difficult. The sequence located between CSS-5 and CSS-7, might be logically CSS-6, but Faleide et al. (2002) interpreted CSS-6 to be completely eroded in the study area. This could indicate that CSS-4 of Late Oligocene age is located within the study area, and that CSS-4 and CSS-5 correlate with S6 and S5. However, the stratigraphic location of LN-1 and CSS-6 is both of Middle Miocene age, which implies that CSS-6 might be located in the study area, making CSS-6 correlated to S5 and LN-1. Figure 5.13 indicate the outline of CSS-6. The main depocenter of CSS-6 is confined to the southern parts of the North Sea basin, indicating that the sequence is thin or absent within the study area (Fig.5.13). Caution is given to the correlation between CSS-6 and S5.

It is clear from the reflection configuration that the anticlinal features in the sequence, highly affects the reflectors. The anticlinal features have been interpreted by Rodrigues et al. (2009) and Løseth et al. (2012) to be the result of remobilized sands, injecting upwards through fractures. The remobilized sands cut and distort the natural bedding, within the mud dominated sequence. This have here been interpreted to explain the irregular reflections seen in the sequence S5.

5.2.5.2 Petrophysical data and distribution

Interpretation of the well logs, indicate a shale lithology. This interpretation is supported by Eidvin and Rundberg (2007), who states that the sequence LN-1 consist of mainly marine shales, where coarser shales are generally glauconitic. The gamma ray logs have some intervals with lower values, these intervals is most likely sand intervals. These intervals is clearly seen in well and 15/9-9 and 15/9-18 (Fig.4.14, S5). This observation is consistent with the correlation done by Rundberg and Eidvin (2005), who indicated that the sequence comprise mudstones with thin sands in some wells. It is possible that these sand intervals extend laterally over greater distances, and might be the ones that have been injected into the overlying unit.

The co-kriging interpolation indicate that the most of the sequence have uniform values, with some deviations (Fig 4.25 and 4.26). The co-kriging results indicate that most of sequence S5 consist of a shale lithology. However, the sequence have local variations. Several areas with lower values is observed in all the distributed well logs. These areas have been interpreted to be sands, and might occur in association with the elongated features.

The elongated features observed in the co-kriging results (Fig 4.25 and 4.26), have been established to correlate to the anticlinal features seen in the seismic sections (Fig. 4.15 and 4.16). This correlation is illustrated in figure 5.11. The elongated features have been observed to show low values along the tops of the features. The 3D illustration in figure 5.11 highlight these features, in relations to the seismic data and well logs. The lower values is here clearly observed on top of the elongated features. These lower values is most likely sands.

The observed elongated features and associated sands, have here been interpreted to be the mobilized and injected sands, studied by Rodrigues et al. (2009) and Løseth et al. (2012).

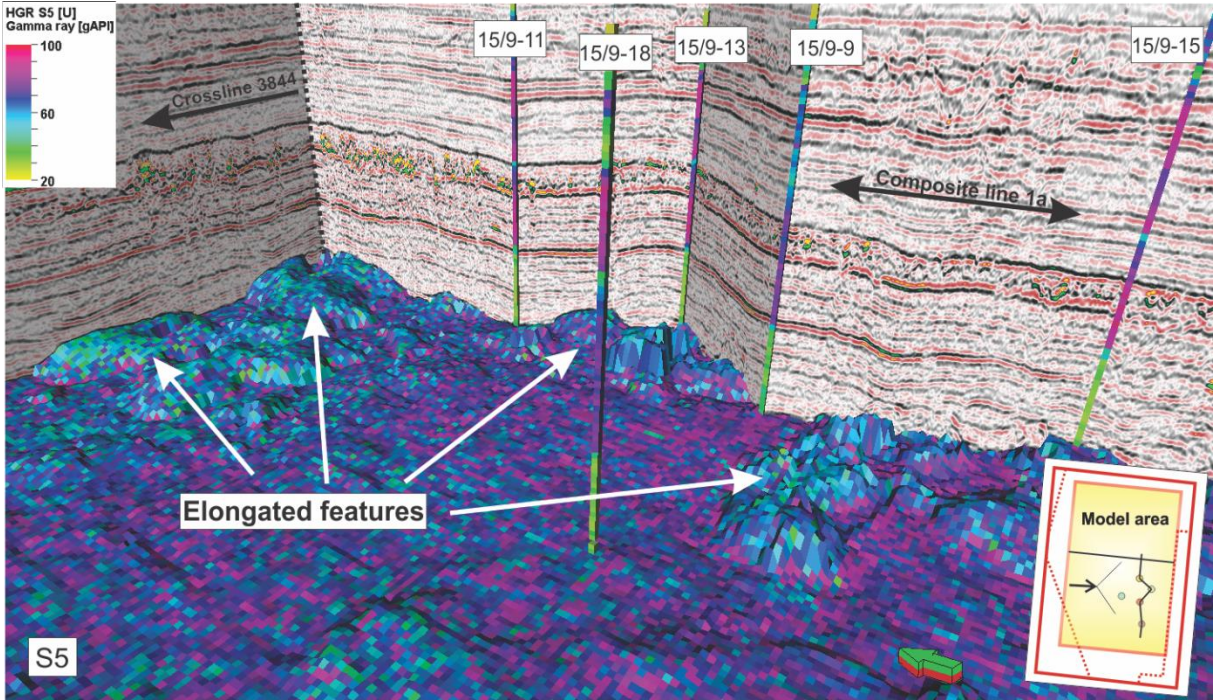


Figure 5.11: 3D illustration of the elongated features observed on top of the co-kriging result of S5. The sequence mostly consist of shale, but sands are located on top of the elongated features. The up-scaled well logs is shown. The survey figure in the bottom right corner, indicate the view direction towards the wells. The survey is oriented north.

5.2.5.3 Depositional environment

The attributes and the medium to low amplitudes observed in the sequence, might indicate that the layers are thin, and the configuration may indicate that the environment was low energy, distal from any source area. The continuity of the strata have been disturbed, but some

indications of lateral continuous reflections can be traced. The uplifted East Shetland Platform have most likely remained an important source for sediments during Mid-Miocene times.

Eidvin and Rundberg (2007) investigate the fossil assemblage in numerous wells in the study area, including well 15/9-13. Based on the fossil assemblage, the Middle Miocene sequence was deposited in an outer neritic environment (up to 200m water depth) (Eidvin & Rundberg, 2007). This might confirm the character of the reflections in the sequence. The deposited material came from a well-defined delta system that was developing to the west in Middle-Miocene times, this system was prograding rapidly towards the east (Eidvin et al., 2014). This most likely indicate that sequence S5 have been deposited just at the start of the uplifting of the East Shetland Platform. Due to the uplift of the northern North Sea in Early Miocene, the water depths were greater in the southern part of the Viking graben. This might explain the outer neritic environment, and the low energy setting S5 was deposited in. the outline of the Middle Miocene sequence shown in figure 4.12, the sequence is deposited in the basin center, with relatively high water depths. This have been interpreted to explain the dominant shale lithology.

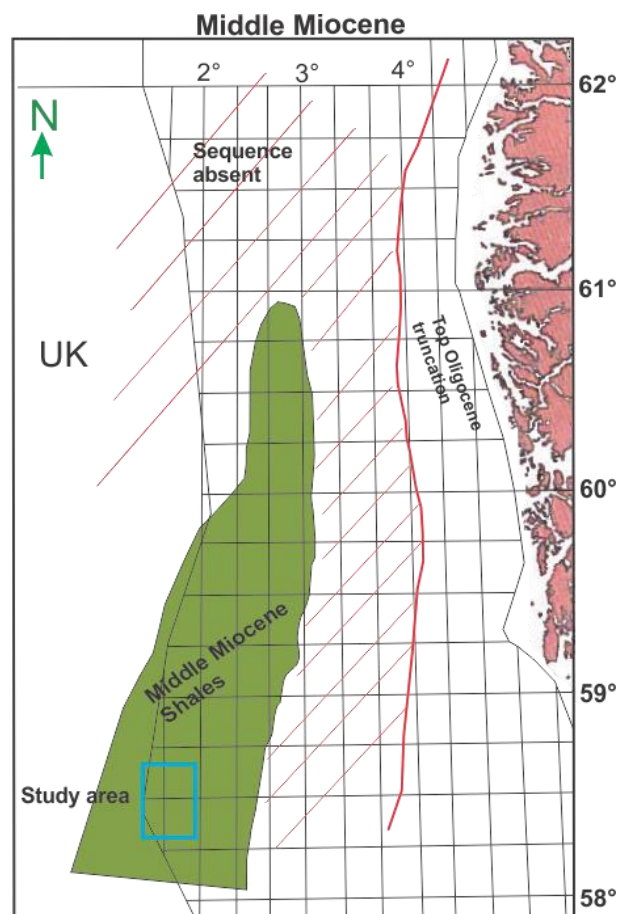


Figure 5.12: Distribution of Middle Miocene shales. The study area have been indicated with a blue rectangle. Figure modified after Rundberg and Eidvin (2005).

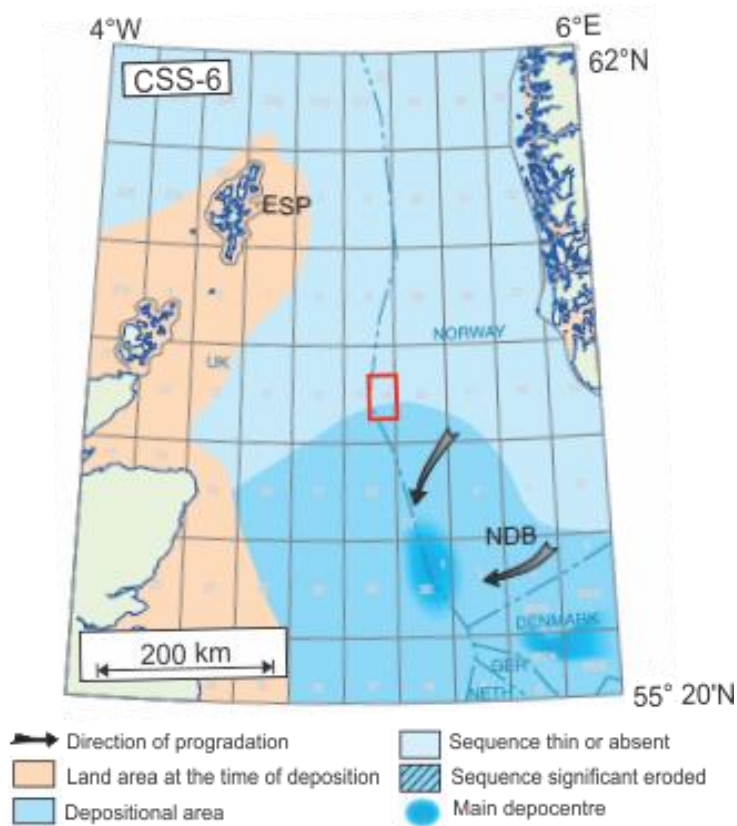


Figure 5.13: Paleo-geography showing the main depocentres of CSS-6, based on Jordt et al. (1995) and Isaksen and Tonstad (1989). Figure is modified after Fyfe et al. (2003).

5.2.6 Sequence S6

5.2.6.1 Reflection configuration and features

Based upon the reflection configuration (Table 5.1) and the nature of the top reflector, the sequence must have been subjected to strong post-depositional processes, which have strongly influence the character of the sediments. The reflections is observed in several areas to be highly disrupted and even chaotic. This configuration is most likely related to the migration of shallow gas and fluidization/mobilization of the sediments, injecting into the overlying units. The disrupted configuration of the sequence is most likely due to the dewatering and faulting of the sequence.

The top reflection show a very distinctive high amplitude reflection, which can be followed in the entire study area. The reflection is faulted in a series of segments, which has been interpreted as polygonal faulting (Fig 4.15 and 4.16). Cartwright (1994) was among the first authors to seismically map these faults in the study area, and proposed a three-stage model to explain their origin. However, the polygonal faults was later identified by Cartwright and Lonergan (1996), who interpreted them to be related to three-dimensional compaction of the

sediments during early burial. The polygonal faulting occurred in response to volumetric contractions. This contraction is related to pore fluid loss, giving extensional normal faulting. In contrast to tectonic faulting, polygonal faults have no systematic strike orientation (Cartwright & Lonergan, 1996). This is consistent with the findings in this thesis. The polygonal faulting seen in the study area, is indicated in figure 4.17. The faults show no dominant strike orientation, and the dip angle of most of the faults appear to be around 55°. The faults have been extensively mapped and classified by Lonergan et al. (1998).

5.2.6.2 Petrophysical data and distribution

Interpretation of the well logs gives an overall indication of a shale lithology. The gamma ray values are highest of all the sequences (80-100API), and according to Rider and Kennedy (2011) the average shale have a gamma ray value of 100 API. The sonic log varies considerably due to differences in acoustic properties, for different mineral content. Sequence S6 have an average slowness of 160µs/ft, and an interval velocity of 1,905m/s, this have been interpreted to support the gamma log in identification of a shale lithology. The density log show values between 1.8-2.0 g/cm³, this suggest a low quartz content (2.6 g/cm³). The neutron log indicate that the sequence have relative good porosities, this might indicate a less compacted shale.

The co-kriging interpolation indicated that the sequence have a uniform distribution of well log values in the model area (Fig. 4.27 and 4.28). The sequence has most likely been deposited with only minor changes in environment, as no larger changes is observed in the co kriging results. However, lower values have been observed in the area with extensive polygonal faulting. The polygonal faulting have probably acted as a migration route for shallow gas and for mobilized sediments. Mobilized sediments might have intruded into the sequence, this could explain the lower values associated with polygonal faulting. The interpolation of the density and neutron log indicate that the sequence have an average density of 2.0g/cm³ and porosities up to 0.50 m³/m³ in the area. The co-kriging interpolation indicate that entire sequence consist of shale, this is consistent with the interpretation done by Rundberg and Eidvin (2005), who states that sequence UH-4, contains mudstones in the Southern Viking Graben (Fig. 5.15). Figure 5.14 gives a 3D illustration of sequence S6 after co-kriging have been applied to the gamma ray logs. In addition, the up-scaled well logs is illustrated. The figure illustrates the irregular surface, most likely related to the polygonal faulting

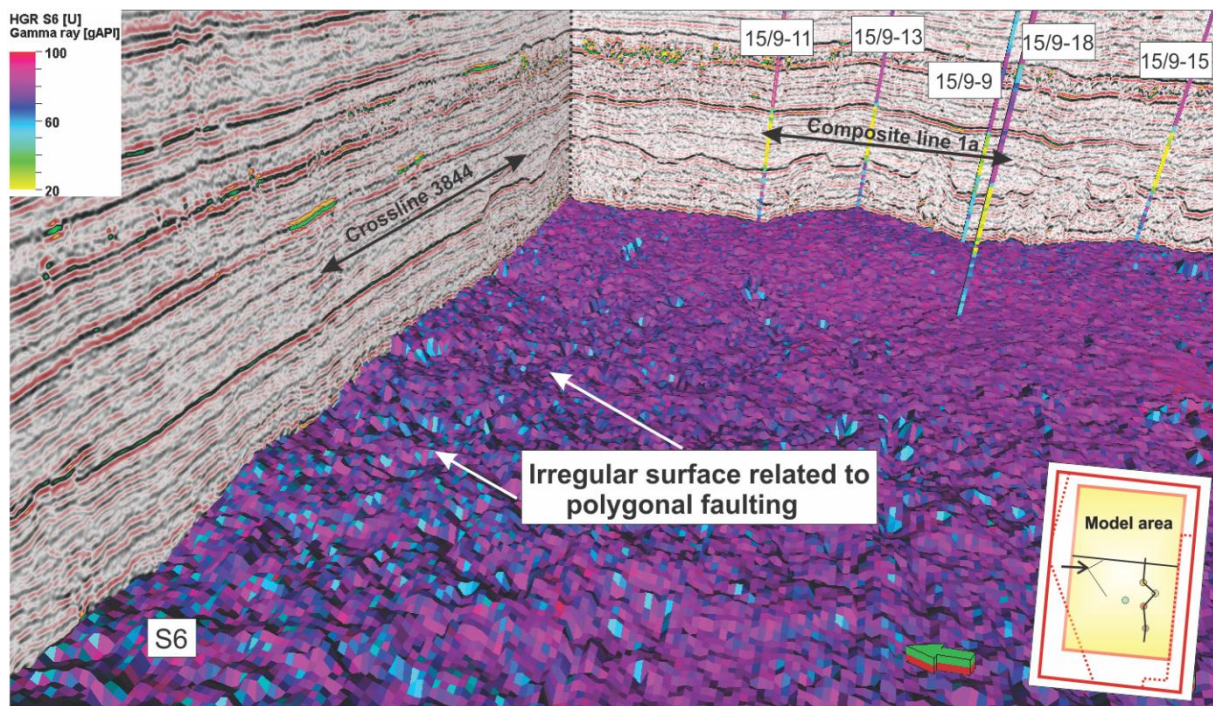


Figure 5.14: 3D illustration of sequence S6 after co-kriging have been applied to the gamma log. (See figure 4.27 for plane view). The sequence is illustrated in relation to the up-scaled well logs and the seismic data. The view angle is indicated in the survey figure in the bottom right corner.

5.2.6.3 Depositional environment

Sequence S6 have been correlated to UH-4 of Lower Miocene age, after Rundberg and Eidvin (2005). UH-4 have been interpreted by Rundberg and Eidvin (2005) to conformably overly Oligocene strata, and correspond to CSS-5 of Jordt et al. (1995). Figure 5.15 show the outline of the Lower Miocene sediments in the North Sea. The Lower Miocene succession, contains the Skade Formation. However, the sandy formation is located further north and is not present in the study area (Eidvin et al., 2014). This is confirmed by the co-kriging interpolation done for this sequence (Fig. 4.27). Figure 5.16 show the regional outline, with the main depocentres of CSS-5.

The lithology of sequence S6 is establish to be shale. Rundberg and Eidvin (2005) states that the sequences could also contain glauconitic and spiculite rich sediments. This would imply a marine shelf setting (Rundberg & Eidvin, 2005). The Skade Formation is deposited as turbidity currents (Rundberg & Eidvin, 2005). However, no sands are observed in sequence S6. This might indicate that the Sleipner area is located to far from the source area, and that only the fine particles from the turbidity currents were deposited in the more distal parts (Fig 5.16).

The Middle Miocene unconformity is interpreted to be located at the top of sequences S6, where IH1 marks the erosional surface. The Mid-Miocene unconformity developed in response to a larger sea level fall, and several authors have suggested that the sequence was subaerially exposed (Jordt et al., 1995; Michelsen et al., 1999). Løseth et al. (2013) suggested that the entire northern North Sea was exposed. However, the unconformity was most likely developed by submarine erosion (Rundberg & Eidvin, 2005). This implies that an increase in marine circulation and vigorous currents and associated erosion dominated. The climatic cooling may also have increased the oceanic circulation (Rundberg & Eidvin, 2005).

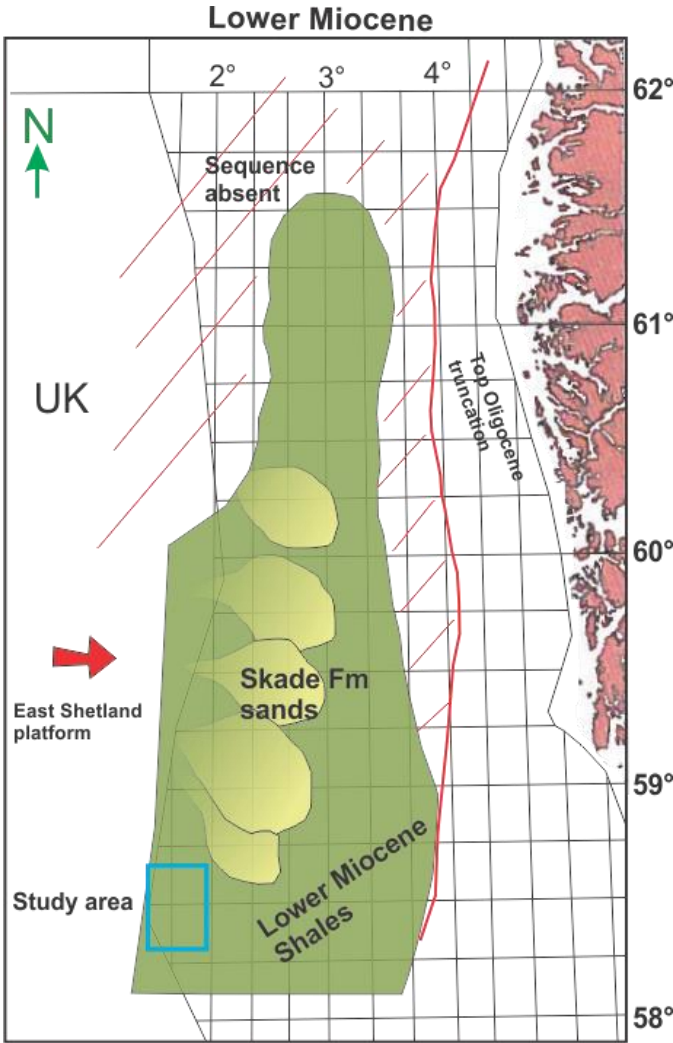


Figure 5.15: Distribution of Lower Miocene sediments. The sandy Skade Formation is located further north than the study area (blue rectangle) The figure is modified after Rundberg and Eidvin (2005).

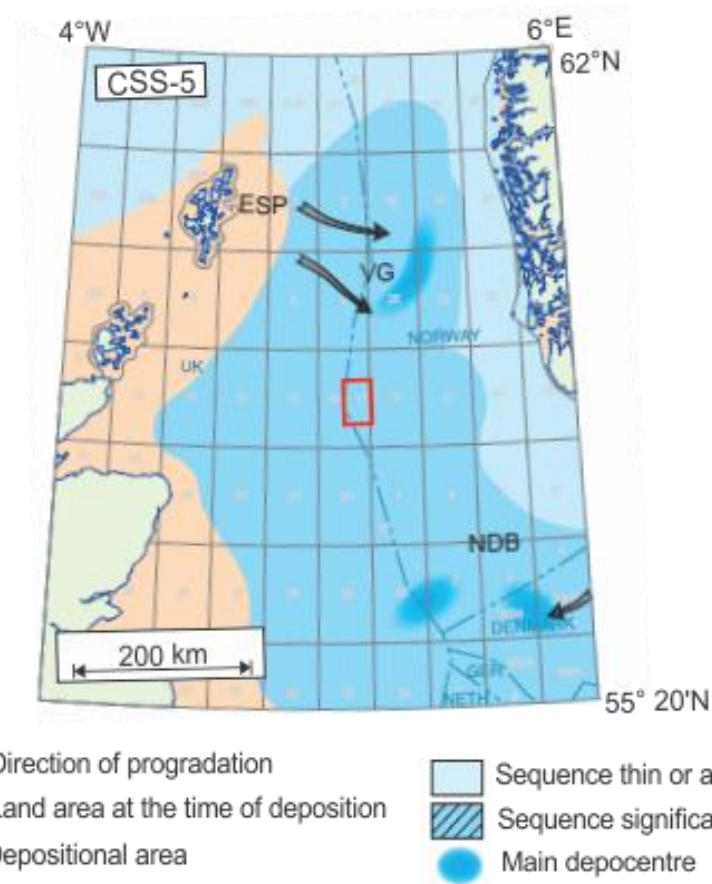


Figure 5.16: Paleo-geography showing the main depocentres, based on Jordt et al. (1995) and Isaksen and Tonstad (1989). Figure is modified after Fyfe et al. (2003).

5.3 Correlation between well logs and seismic horizons

The well logs have a substantial higher data resolution compared to the seismic. This is clear from the well section window presented in figure 4.14. The interpreted horizons don't interact with the well logs ideally. The horizons have been interpreted along some of the most continuous reflections in the study area, these reflections is either a strong lithological contrast or unconformity. The reflections correlated to the well logs strongly, but with deviations. The most distinctive deviation is seen in well 15/9-15 along IN2 (Fig 4.14).

IN2 follows the most continuous reflections in the survey. The well section window in figure 4.14, indicate that the IN2 is located just above 600m in the wells. However, in well 15/9-15 the horizon jumps down to about 650m. The well logs suggest that the horizon should be located higher in the well, but this is in conflict with the seismic data. The interpreted reflection is easy to trace across the survey, and the interpretation should not deviate.

The well tops also have vertical deviations across the well section window. The well top that marks the start of the Utsira Formation show some deviations, as some interpreters have excluded the uppermost thin-layers of shale in the Utsira Formation. The well top that marks the start of the Hordaland Group show greater deviations between the wells. Different interpreters have picked the start of the Hordaland Group to be at the base of the Utsira sand. However, deviations are observed for each well. New age estimates (Eidvin & Rundberg, 2007) suggest that the start of the Hordaland Group might be located at the IH1 horizon, which is the Middle Miocene Unconformity. This is shown clearly in well 15/9-11, where the interpreted horizon IH1 correlates strongly to the top of the Hordaland Group (Fig. 4.14).

5.4 The co-kriging interpolation method

The co-kriging interpolation technique, is highly depended on the number of sample points available (Taner, 2001). In order to increase the quality of the interpolated map, the density of the sample points should be increased (Hansen et al., 2010). However, the sample points here, are expensive exploration wells.

The assumption that two wells close to each other, have similar values, is central in the co-kriging interpolation method. The wells show a strong correlation in figure 4.14. Hence, the ranges of the semivariogram have been set to include all these wells (See chapter 3.7.2). The correlation between the two variables used in co-kriging should be high. Hence, a high correlation have been assumed for the extracted seismic data, and all the well logs.

It is important to differentiate between the co-kriging done in chapter 4.4 and 4.5. In chapter 4.4, co-kriging was applied to each individual sequence, and in chapter 4.5, co-kriging was used on the entire model. The same semivariogram parameters and well logs were used in each case.

The co-kriging done for each sequence show the most promising results. These are presented along the interpreted horizons, and represent the spatial interpolation between the seismic data and the up-scaled well logs in the entire sequence interval. The co-kriging done for the entire model, populate the entire volume of the model with properties from the well-logs. It is clear from this interpolation, that the range of the semivariogram highly affects the result (See chapter 5.4.2).

5.4.1 Correlation coefficient

When using the co-kriging interpolation method, Petrel estimates the correlation coefficient between the two variables (Seismic data and the well logs). The assumption that the

characteristic of the seismic data, and the values in the well logs can be correlated, is significant. The gamma ray logs especially, have no relation to the seismic data and could give unreliable results. Care should be taken when using co-kriging between seismic data and well logs that don't have any acoustic relation to the seismic.

The co-kriging interpolation method uses that well-log values close to the seismic data. This implies that the configuration of the seismic data is directly related to petrophysical data. This is most likely not an accurate representation for the gamma ray logs, as these measures the natural radiation from the formation, and has no correlation to the seismic data.

However, the co-kriging method has been primary used to give a lateral understanding of the distribution of well log data within each sequences. This is presented along the first layer of the sequences, corresponding to the interpreted horizons. This ensures that the seismic character in relation to the well log values, in each individual sequence is honored. In other words, the seismic character within a specific sequence is interpolated with the well-logs covering the same interval in the model. This ensures that dominant lithology in the sequence, remains dominant in the interpolation result.

5.4.2 Fitting the semivariogram

One of the most difficult aspects when fitting a model to a semivariogram, is that little reliable information exist for short sample distances. This leads to low confidence when estimating the range (Sinclair & Blackwell, 2002). There is also sparsity of information on which to base an estimate of the nugget effect. The difficulties in modeling semivariograms comes from (i) poor choice of distance classes, (ii) mixed population inadvertently grouped together, (iii) outliers and skewed distributions, and (iv) artifacts. Semivariograms can be fitted to semivariograms by eye, without the complexity of best-fit procedures, described by authors such as Cressie (1985) and Sinclair and Blackwell (2002)

By giving the wells higher ranges in the semivariogram fitting, would imply that they can be correlated in a larger part of the model. This could provide a more accurate representation of reality. However, the purpose of the co-kriging modeling was to interpolated the values from the well logs, and not assume that the sequences have the same values in the entire sequence. The range strongly affects the outcome of the co-kriging interpolation. The current ranges was used because there is no petrophysical data available outside the location of the wells. The interpolation, increase in uncertainty away from the semivariogram ranges and the original wells.

5.4.3 Hypothetical wells

The well logs from the hypothetical wells was extracted from the model, when co-kriging had been applied on the entire model (Fig. 4.29). The poor correlation between the original wells and HW1 is strongly affected by the range of the semivariogram. The semivariogram was set to have a range of 12000 meters in the major direction (y-axis) and 8600 meters in the minor direction (x-axis). This covers the original five exploration wells and hypothetical well 2. These ranges implies that there is a correlation between the original well logs inside these ranges. HW1 is located 19.3 km away from well 15/9-9, outside the semivariogram ranges. Hence, the petrophysical values seen in HW1, are all interpolated by co-kriging without the influence of original well data (Fig. 4.30).

The hypothetical well logs indicate a loss in detail for HW1 (Fig. 4.30). The original well logs have a several trends. The interpolated well log at HW1 show little to no trends. The effect of the correlation coefficient between the well logs and the seismic data can be clearly seen HW1, as the seismic characteristic is captured in the well logs (Fig. 4.30).

Although the sequences can be traced to HW1, the petrophysical values seen in the original well logs cannot. The petrophysical properties have to be interpolated using co-kriging or other geostatistical methods, in order to sate with some certainty that the specific values occur in the same interval. In order to correct HW1, the ranges of the semivariogram could be adjusted to include a larger part of the model. However, this should only be done if a known well, is located near the hypothetical well. Hence, in order to improve quality of the interpolation, more sample points/wells are needed.

HW2 is located inside the ranges of the semivariogram and in close proximity to the original data, the well logs show a strong correlation towards the original data. The interpolated well logs at this location is considered valid, as the hypothetical well is located inside the range of the semivariogram and close to the primary variable (original up-scaled well logs).

Constrains of co-kriging interpolation is clearly identifiable. In order increase quality, expensive exploration wells have to be drilled. This will increase the number of data points and improve the interpolation. If more data points are available, this could allow the ranges of the semivariogram to be increased, allowing the interpolation of the primary variable to influence a greater area. The conclusion here would be, the more data points available, the higher the quality of the interpolation. In addition, the closer the hypothetical wells are to the original data, the higher the confidence in the interpolation.

6 Summary and conclusion

The objective for this thesis was to investigate and map the upper Cenozoic sequences in the Sleipner area. These sequences have been classified according to reflection configuration, and well log characteristics. This has provided information about the depositional environment for each individual sequence. Co-kriging interpolation have been used to interpolate the petrophysical data from the well logs. This has given a good indication about how the lithology change laterally in the study area.

- Sequence S1 have several discontinuous reflections, with a disrupted reflection configuration. This configuration is related to glacial processes, which have reworked the sediments. A few channel features have been observed, these have been interpreted to be related to glacial processes. Investigation of the well logs have established the uppermost sediments to consist of unconsolidated sands with underlying shales. These sediments have been deposited in a glacio-marine environment. The co-kriging interpolation method have established that the uppermost sequence consist of a sand to shale lithology in the entire Sleipner area.
- Sequence S2 have an incline continuous parallel reflection configuration. The sequence show a distinctive thickening towards the south. The prograding nature of the sequence indicate a period of high sediment supply. The sediments was derived from glacio-marine processes, sourced from the uplifted Scandinavia. Investigation of the well logs indicate a shale lithology. The co-kriging interpolation method suggest that this lithology is dominant for the entire Sleipner area.
- Sequence S3 have incline reflections with a continuous parallel to subparallel reflection configuration. The sequence have numerous bright spots along the top reflector (IN2). These have been interpreted to be shallow gas accumulations. Interpretation of the well logs indicate a shale lithology. This lithology have been established to be dominant in the entire Sleipner area, using co-kriging interpolation. Sequence S3 was deposited as a response of the Late Pliocene cooling and glaciation of the northern hemisphere. The sediments built out from the Norwegian shelf margin.

- Sequence S4 correspond to the Utsira Formation. The sequence have discontinuous reflections with a disrupted configuration. Interpretation of the well logs have established a sand dominated lithology, with thin-layers of shale. The co-kriging interpolation confirms a sand dominated lithology in the study area. Sequence S4 have been deposited by in a shallow marine environment, sourced from the uplifted East Shetland Platform. The sands have been extensively reworked by tidal and oceanic currents in a narrow strait, this have given the discontinuous reflection configuration.
- Sequence S5 have been classified with a disrupted reflection configuration. Several elongated features have been observed at the base of the sequence. These are caused by underlying mobilized sediments, injection into the sequence. These features highly affects the reflection configuration of the sequence. Correlation of the well logs have established that the sequence consist of shale, with a few thin layers of sand. The co-kriging interpolation indicate that sequence S5 is shale dominated in the entire study area. Sands occur in relation to the elongated features. Sequence S5 was deposited in a marine environment, sediments were sourced from the developing delta system located on the East Shetland Platform.
- Sequence S6 consist of several high amplitude, discontinuous reflections. Classified as disrupted. This configuration is related to the extensive polygonal faulting seen in the sequence. The polygonal faulting is formed due to dewatering by compaction. The faults have given good migration routes for shallow gas and fluids. Correlation of the well logs suggest a shale dominated lithology. The co-kriging results confirms that sequence S6 consist of shale in major parts of the study area. Sequence S6 has been deposited in a marine shelf setting, were sediments was sourced from the East Shetland Platform.
- The co-kriging interpolation method has provided a useful geostatistical tool, for predicting well log values in the study area. This has given insight on how the values distribute laterally in each individual sequence. By applying co-kriging to each individual sequence, the character of the seismic data towards the original well logs is

honored, giving a more reliable result. Hypothetical wells has been placed in the study area, giving the possibility to extract interpolated well logs. This has given a good indication on how the well log values is distributed in three-dimension. It is clear that the constraints of co-kriging method, lies in the number of available data points, and the uncertainty in the interpolation done at further distances away from the primary variable.

7 References

- Abreu, V. S., & Anderson, J. B. (1998). Glacial eustasy during the Cenozoic: Sequence stratigraphic implications. *Aapg Bulletin-American Association of Petroleum Geologists*, 82(7), 1385-1400.
- Ahmadi, Z. M., Sawyers, M., Kenyon-Roberts, S., Stanworth, C. W., Kugler, A., Kristiansen, J., & Fugelli, E. M. (2003). Paleocene. In D. Evans, C. Graham, A. Armour, & P. Bathurst (Eds.), *The Millennium Atlas: Petroleum geology of the central and northern North Sea* (pp. 235-259): The Geological Society of London.
- Andreassen, K., Nilssen, E. G., & Odegaard, C. M. (2007). Analysis of shallow gas and fluid migration within the Plio-Pleistocene sedimentary succession of the SW Barents Sea continental margin using 3D seismic data. *Geo-Marine Letters*, 27(2-4), 155-171. doi: 10.1007/s00367-007-0071-5
- Bachmaier, M., & Backes, M. (2008). Variogram or semivariogram? Understanding the variances in a variogram. *Precision Agriculture*, 9(3), 173-175. doi: 10.1007/s11119-008-9056-2
- Balch, A. H. (1971). Color Sonagrams - New Dimension in Seismic Data Interpretation. *Geophysics*, 36(6), 1074-&. doi: Doi 10.1190/1.1440233
- Barnes, A. E. (1993). Instantaneous Spectral Bandwidth and Dominant Frequency with Applications to Seismic-Reflection Data. *Geophysics*, 58(3), 419-428. doi: Doi 10.1190/1.1443425
- Barnes, A. E. (2000). Weighted average seismic attributes. *Geophysics*, 65(1), 275-285. doi: Doi 10.1190/1.1444718
- Basu, S., Dalei, S. N., & Sinha, D. P. (2008). 3D Seismic data Merging -A Case History in Indian Context. *Geohorizons*, 7-13.
- Boait, F. C., White, N. J., Bickle, M. J., Chadwick, R. A., Neufeld, J. A., & Huppert, H. E. (2012). Spatial and temporal evolution of injected CO₂ at the Sleipner Field, North Sea. *Journal of Geophysical Research-Solid Earth*, 117.
- Bohling, G. (2005). Introduction to Geostatistics and Variogram analysis. Retrieved March, 2016, from <http://people.ku.edu/~gbohling/cpe940/Variograms.pdf>
- Brown, A. R. (1999). *Interpretation of three-dimensional seismic data* (5th ed.). Tulsa, Okla.: American Association of Petroleum Geologists.
- Brown, A. R. (2001). Understanding seismic attributes. *Geophysics*, 66(1), 47-48. doi: Doi 10.1190/1.1444919
- Brown, L. F., & Fisher, W. L. (1977). Seismic-Stratigraphic Interpretation of Depositional Systems: Examples from Brazilian Rift and Pull-Apart Basins: Section 2. Application of Seismic

- Reflection Configuration to Stratigraphic Interpretation. In E. C. Payton (Ed.), *Seismic Stratigraphy--Applications to Hydrocarbon Exploration* (Vol. 26, pp. 213-248): American Association of Petroleum Geologist.
- Bruce, D. R. S., & Stemmrik, L. (2003). Carboniferous. In D. Evans, C. Graham, A. Armour, & P. Bathurst (Eds.), *The Millennium Atlas: petroleum geology of the central and northern North Sea* (pp. 83-89): The Geological Society of London.
- Cartwright, J. A. (1994). Episodic basin-wide fluid expulsion from geopressured shale sequences in the North Sea basin. *Geology*, 22(5), 447-450. doi: 10.1130/0091-7613(1994)022<0447:ebwfef>2.3.co;2
- Cartwright, J. A., & Lonergan, L. (1996). Volumetric contraction during the compaction of mudrocks: A mechanism for the development of regional-scale polygonal fault systems. *Basin Research*, 8(2), 183-193.
- Catuneanu, O., Galloway, W. E., Kendall, C. G. S., Miall, A. D., Posamentier, H. W., Strasser, A., & Tucker, M. E. (2011). Sequence Stratigraphy: Methodology and Nomenclature. *Newsletters on Stratigraphy*, 44(3), 173-245. doi: 10.1127/0078-0421/2011/0011
- Chadwick, R. A., & Noy, D. J. (2015). Underground CO₂ storage: demonstrating regulatory conformance by convergence of history-matched modeled and observed CO₂ plume behavior using Sleipner time-lapse seismics. *Greenhouse Gases-Science and Technology*, 5(3), 305-322.
- Chadwick, R. A., Zweigel, P., Gregersen, U., Kirby, G. A., Holloway, S., & Johannessen, P. N. (2004). Geological reservoir characterization of a CO₂ storage site: The Utsira Sand, Sleipner, Northern North Sea. *Energy*, 29(9-10), 1371-1381.
- Chiles, J.-P. (2012). *Geostatistics : modeling spatial uncertainty* (2nd ed. ed.). Oxford: Wiley-Blackwell.
- Chopra, S., & Larsen, G. (2000). Acquisition footprint - Its detection and removal. *CSEG Recorder*, 16-20(25).
- Chopra, S., & Marfurt, K. J. (2005). Seismic attributes - A historical perspective. *Geophysics*, 70(5), 3s0-28s0. doi: 10.1190/1.2098670
- Christiansson, e. a. (2000). Crustal structure in the northern North Sea: An integrated geophysical study. *Journal of the Geological Society*, 167, 15-40.
- Copetake, P., Sims, A. P., Crittenden, S., Hamar, G. P., Ineson, J. R., Rose, P. T., & Tringham, M. E. (2003). Lower Cretaceous. In D. Evans, A. Armour, & P. Bathurst (Eds.), *The Millennium Atlas: petroleum geology of the central and northern North Sea* (pp. 191-211): The Geological Society of London.
- Coward, M. P. (1995). Structural and tectonic setting of the Permo-Triassic basins of northwest Europe. *Geological Society Special Publication*(91), 7-39.

- Coward, M. P., Dewey, J. F., Hempton, M., Holroyd, J., & Mange, M. A. (2003). Tectonic evolution. In D. Evans, C. Graham, A. Armour, & P. Bathurst (Eds.), *The Millennium Atlas: petroleum geology of the central and northern North Sea* (pp. 17-33): The Geological Society of London.
- Cressie, N. (1985). Fitting Variogram Models by Weighted Least-Squares. *Journal of the International Association for Mathematical Geology*, 17(5), 563-586. doi: Doi 10.1007/Bf01032109
- Deegan, C. E., & Scrull, B. J. (1977). A standard lithostratigraphic nomenclature for the Central and Northern North Sea. *Institute of Geological Sciences Report 77/25(1)*, 0-36.
- Diggle, P., & Ribeiro, P. J. (2007). *Model-based geostatistics*.
- Eidvin, T., Jansen, E., Rundberg, Y., Brekke, H., & Grogan, P. (2000). The upper Cainozoic of the Norwegian continental shelf correlated with the deep sea record of the Norwegian Sea and the North Atlantic. *Marine and Petroleum Geology*, 17(5), 579-600.
- Eidvin, T., Riis, F., & Rasmussen, E. S. (2014). Oligocene to Lower Pliocene deposits of the Norwegian continental shelf, Norwegian Sea, Svalbard, Denmark and their relation to the uplift of Fennoscandia: A synthesis. *Marine and Petroleum Geology*, 56, 184-221.
- Eidvin, T., Riis, F., & Rundberg, Y. (1999). Upper Cainozoic stratigraphy in the central North Sea (Ekofisk and Sleipner fields). *Norsk Geologisk Tidsskrift*, 79(2), 97-127.
- Eidvin, T., & Rundberg, Y. (2001). Late Cainozoic stratigraphy of the Tampen area (Snorre and Visund fields) in the northern North Sea, with emphasis on the chronology of early Neogene sands. *Norsk Geologisk Tidsskrift*, 81(2), 119-160.
- Eidvin, T., & Rundberg, Y. (2007). Post-Eocene strata of the southern Viking Graben, northern North Sea; integrated biostratigraphic, strontium isotopic and lithostratigraphic study. *Norwegian Journal of Geology*, 87(4), 391-450.
- Factmap, N. (2016). Norwegian Petroleum Directorate factpages. from [Online] Accesed: Jan. 2016 http://gis.npd.no/factmaps/html_20/
- Faerseth, R. B. (1996). Interaction of Permo-Triassic and Jurassic extensional fault-blocks during the development of the northern North Sea. *Journal of the Geological Society*, 153, 931-944. doi: DOI 10.1144/gsjgs.153.6.0931
- Faleide, J. I., Kyrkjebø, R., Kjennerud, T., Gabrielsen, R. H., Jordt, H., Fanavoll, S., & Bjerke, M. D. (2002). Tectonic impact on sedimentary processes during Cenozoic evolution of the northern North Sea and surrounding areas. *Geological Society, London, Special Publications(196)*, 235-269.
- Fyfe, J. A., Gregersen, U., Jordt, H., Rundberg, Y., Eidvin, T., Evans, D., . . . Andreasen, P. (2003). Oligocene to Holocene In D. Evans, C. Graham, A. Armour, & P. Bathurst (Eds.), *The Millennium Atlas: petroleum geology of the central and northern North Sea* (pp. 279-287): The Geological Society of London.

- Gabrielsen, R. H., Kyrkjebo, R., Faleide, J. I., Fjeldskaar, W., & Kjennerud, T. (2001). The Cretaceous post-rift basin configuration of the northern North Sea. *Petroleum Geoscience*, 7(2), 137-154. doi: DOI 10.1144/petgeo.7.2.137
- Galloway, W. E. (2001). Seismic expressions of deep-shelf depositional and erosional morphologies, Miocene Utsira formation, North Sea Basin. *Marine Geophysical Researches*, 22(5-6), 309-321. doi: Doi 10.1023/A:1016339330477
- Galloway, W. E. (2002). Paleogeographic setting and depositional architecture of a sand-dominated shelf depositional system, Miocene Utsira formation, North Sea Basin. *Journal of Sedimentary Research*, 72(4), 476-490. doi: Doi 10.1306/110801720476
- Gawthorpe, R. L., & Leeder, M. R. (2000). Tectono-sedimentary evolution of active extensional basins. *Basin Research*, 12(3-4), 195-218. doi: DOI 10.1046/j.1365-2117.2000.00121.x
- Glennie, K. W. (1998). *Petroleum geology of the North Sea : basic concepts and recent advances* (4th ed.). Oxford: Blackwell Science.
- Glennie, K. W., Higham, J., & Stemmerik, L. (2003). Permian. In D. Evans, C. Graham, A. Armour, & P. Bathurst (Eds.), *The Millennium Atlas: petroleum geology of the central and northern North Sea* (pp. 91-103): The Geological Society of London.
- Goldsmith, P. J., Hudson, G., & Van Veen, P. (2003). Triassic. In D. Evans, C. Graham, A. Armour, & P. Bathurst (Eds.), *The Millennium Atlas: petroleum geology of the central and northern North Sea* (pp. 105-127): The Geological Society of London.
- Goovaerts, P. (1998). Ordinary cokriging revisited. *Mathematical Geology*, 30(1), 21-42. doi: Doi 10.1023/A:1021757104135
- Gradstein, F. M., Kaminski, M. A., Berggren, W. A., Kristiansen, I. L., & Diorio, M. A. (1994). Cenozoic Biostratigraphy of the North-Sea and Labrador Shelf. *Micropaleontology*, 40, 1-+.
- Gregersen, U., & Johannessen, P. N. (2007). Distribution of the Neogene Utsira Sand and the succeeding deposits in the Viking Graben area, North Sea. *Marine and Petroleum Geology*, 24(10), 591-606.
- Gregersen, U., Michelsen, O., & Sorensen, J. C. (1997). Stratigraphy and facies distribution of the Utsira formation and the Pliocene sequences in the northern North Sea. *Marine and Petroleum Geology*, 14(7-8), 893-914. doi: Doi 10.1016/S0264-8172(97)00036-6
- Hansen, T. M., Mosegaard, K., & Schiott, C. R. (2010). Kriging interpolation in seismic attribute space applied to the South Arne Field, North Sea. *Geophysics*, 75(6), P31-P41. doi: 10.1190/1.3494280

- Henriksen, S., & Vorren, T. O. (1996). Late Cenozoic sedimentation and uplift history on the mid-Norwegian continental shelf. *Global and Planetary Change*, 12(1-4), 171-199. doi: Doi 10.1016/0921-8181(95)00019-4
- Husmo, T., Hamar, G. P., Høiland, O., Johannessen, E. P., Rømuld, A., Spencer, A. M., & Titterton, R. (2002). Lower and Middle Jurassic. In D. Evans, C. Graham, A. Armour, & P. Bathurst (Eds.), *The Millennium Atlas: petroleum geology of the central and northern North Sea* (pp. 129-155): The Geological Society of London.
- Isaksen, D., & Tonstad, K. (1989). A revised Cretaceous and Tertiary lithostratigraphic nomenclature for the Norwegian North Sea. *NPD-Bulletin No. 5*, 0-59.
- Jones, E., Jones, R., Ebdon, C., Ewen, D., Milner, P., Plunkett, J., . . . Slatern, P. (2003). Eocene. In D. Evans, C. Graham, A. Armour, & P. Bathurst (Eds.), *The Millennium Atlas: Petroleum geology of the central and northern North Sea* (pp. 261-277): The Geological Society of London.
- Jordt, H., Faleide, J. I., Bjorlykke, K., & Ibrahim, M. T. (1995). Cenozoic Sequence Stratigraphy of the Central and Northern North-Sea Basin - Tectonic Development, Sediment Distribution and Provenance Areas. *Marine and Petroleum Geology*, 12(8), 845-879.
- Jordt, H., Thyberg, B. I., & Nøttvedt, A. (2000). Cenozoic evolution of the central and northern North Sea with focus on differential vertical movements of the basin floor and surrounding clastic source areas. *Geological Society, London, Special Publications*(167), 219-243.
- Karstens, J., & Berndt, C. (2015). Seismic chimneys in the Southern Viking Graben - Implications for palaeo fluid migration and overpressure evolution. *Earth and Planetary Science Letters*, 412, 88-100. doi: 10.1016/j.epsl.2014.12.017
- Knies, J., Matthiessen, J., Vogt, C., & Stein, R. (2002). Evidence of 'Mid-Pliocene (similar to 3 Ma) global warmth' in the eastern Arctic Ocean and implications for the Svalbard/Barents Sea ice sheet during the late Pliocene and early Pleistocene (similar to 3-1.7 Ma). *Boreas*, 31(1), 82-93.
- Knott, S. D., Burchell, M. T., Jolley, E. J., & Fraser, A. J. (1993). Mesozoic to Cenozoic Plate Reconstructions of the North-Atlantic and Hydrocarbon Plays of the Atlantic Margins. *Petroleum Geology of Northwest Europe: Proceedings of the 4th Conference*, 953-974. doi: Doi 10.1144/0040953
- Knox, R. W. O. B., & Holloway, S. (1992). Paleogene of the Central and Northern North Sea. In R. W. O. B. Knox & W. G. Cordey (Eds.), *Lithostratigraphy nomenclature of the UK North Sea* (Vol. 1). Nottingham: British Geological Survey.
- Krivoruchko, K., Esri, Wood, N., & Company, C. E. (2014). Using Multivariate Interpolation for Estimating Well Performance. Retrieved February, 2016, from <http://www.esri.com/esri-news/arcuser/summer-2014/using-multivariate-interpolation-for-estimating-well-performance>

- Lonergan, L., Cartwright, J., & Jolly, R. (1998). The geometry of polygonal fault systems in Tertiary mudrocks of the North Sea. *Journal of Structural Geology*, 20(5), 529-548. doi: Doi 10.1016/S0191-8141(97)00113-2
- Lundin, E., & Dore, A. G. (2002). Mid-Cenozoic post-breakup deformation in the 'passive' margins bordering the Norwegian-Greenland Sea. *Marine and Petroleum Geology*, 19(1), 79-93. doi: Pii S0264-8172(01)00046-0Doi 10.1016/S0264-8172(01)00046-0
- Løseth, H., & Henriksen, S. (2005). *A Middle to Late Miocene compression phase along the Norwegian passive margin*. Paper presented at the Petroleum Geology: North-West Europe and Global Perspectives - Proceedings of the 6th Petroleum Geology Conference.
- Løseth, H., Raulline, B., & Nygard, A. (2013). Late Cenozoic geological evolution of the northern North Sea: development of a Miocene unconformity reshaped by large-scale Pleistocene sand intrusion. *Journal of the Geological Society*, 170(1), 133-145. doi: 10.1144/jgs2011-165
- Løseth, H., Rodrigues, N., & Cobbold, P. R. (2012). World's largest extrusive body of sand? *Geology*, 40(5), 467-470.
- Løvås, G. G. (2013). *Statistikk for universiteter og høyskoler* (3. utg. ed.). Oslo: Universitetsforl.
- Marshall, J. E. A., & Hewett, A. J. (2003). Devonian. In D. Evans, C. Graham, A. Armour, & P. Bathurst (Eds.), *The Millennium Atlas: petroleum geology of the central and northern North Sea* (pp. 65-81): The Geological Society of London.
- Martini, E. (1971). Standard Tertiary and Quaternary Calcareous Nannoplankton Zonation. *Proceeding of the 2nd Planktonic Conference Roma, 2*, 739-785.
- Matheron, G. (1963). Principles of geostatistics. *Economic Geology*, 58, 1246-1266.
- Michelsen, O., Thomsen, E., Danilsen, M., Heilmann-Clausen, C., Jordt, H., & Laursen, G. V. (1999). Cenozoic Sequence Stratigraphy in the eastern North sea. In P.-C. De Graciansky, J. Hardenbol, T. Jacquin, & P. R. Vail (Eds.), *Mesozoic and Cenozoic Sequence Stratigraphy of European Basins* (pp. 91-118): Special Publication of the Society of Economic Paleontologist and Mineralogists.
- Mitchum, R. M., Vail, P. R., & Sangree, J. B. (1977). Seismic Stratigraphy and global changes of sea level, Part 6: Stratigraphic interpretation of seismic reflection patterns in depositional sequences. In E. C. Payton (Ed.), *Seismic Stratigraphy - Application to Hydrocarbon exploration* (Vol. 26, pp. 117-133): American Association of Petroleum Geologist.
- Mudge, D. C., & Bujak, J. P. (1994). Eocene Stratigraphy of the North-Sea Basin. *Marine and Petroleum Geology*, 11(2), 166-181. doi: Doi 10.1016/0264-8172(94)90093-0
- Nichols, G. (2009). *Sedimentology and stratigraphy*. Oxford: Wiley-Blackwell,.

- NPD. (2014). *CO2 Storage Atlas of the Norwegian Continental Shelf* (E. K. Halland, J. Mujezinovic, & F. Riis Eds.): Norwegian Petroleum Directorate
- NPD. (2016). Norwegian Petroleum Directorate factpages. from [Online] Accessed: Jan. 2016
<http://factpages.npd.no/factpages/Default.aspx?culture=en>
- Odoherly, R. F., & Anstey, N. A. (1970). Reflections on Amplitudes. *Geophysics*, 35(6), 1151-&.
- Prosser, S. (1993). Rift-related linked depositional systems and their seismic expression. Williams, G. D. and Dobb, A. (eds). *Tectonic and Seismic Sequence Stratigraphy. Geological Society Special publications*(71), 35-66.
- Reynolds, J. M. (2011). *An introduction to applied and environmental geophysics*. Chichester: Wiley-Blackwell.
- Rider, M. H. (1990). Gamma-ray log shape used as a facies indicator: critical analysis of an oversimplified methodology. *Geological Society, London, Special Publications*, 48(1), 27-37. doi: 10.1144/gsl.sp.1990.048.01.04
- Rider, M. H., & Kennedy, M. (2011). *The geological interpretation of well logs*. Scotland: Rider-French.
- Riis, F., & Halland, E. (2014). CO2 storage atlas of the Norwegian Continental shelf: Methods used to evaluate capacity and maturity of the CO2 storage potential. *12th International Conference on Greenhouse Gas Control Technologies, Ghgt-12*, 63, 5258-5265. doi: 10.1016/j.egypro.2014.11.557
- Rodrigues, N., Cobbold, P. R., & Loseth, H. (2009). Physical modelling of sand injectites. *Tectonophysics*, 474(3-4), 610-632.
- Rokoengen, K., Rise, L., Bryn, P., Frengstad, B., Gustavsen, B., Nygaard, E., & Sættem, J. (1995). Upper Cenozoic Stratigraphy on the Mid-Norwegian Continental-Shelf. *Norsk Geologisk Tidsskrift*, 75(2-3), 88-104.
- Rundberg, Y., & Eidvin, T. (2005). Controls on depositional history and architecture of the Oligocene-Miocene succession, northern North Sea Basin. *Onshore-Offshore Relationships on the North Atlantic Margin*, 12, 207-239.
- Rundberg, Y., & Smalley, P. C. (1989). High-Resolution Dating of Cenozoic Sediments from Northern North-Sea Using Sr-87 Sr-86 Stratigraphy. *Aapg Bulletin-American Association of Petroleum Geologists*, 73(3), 298-308.
- Schlumberger. (2014). Petrel Help Center (Version 2014.1 (64-bit)).
- Sejrup, H. P., Aarseth, I., & Hafliðason, H. (1991). The Quaternary Succession in the Northern North-Sea. *Marine Geology*, 101(1-4), 103-111. doi: Doi 10.1016/0025-3227(91)90065-C

- Sejrup, H. P., Larsen, E., Landvik, J., King, E. L., Hafliðason, H., & Nesje, A. (2000). Quaternary glaciations in southern Fennoscandia: evidence from southwestern Norway and the northern North Sea region. *Quaternary Science Reviews*, 19(7), 667-685. doi: Doi 10.1016/S0277-3791(99)00016-5
- Selley, R. C. (1998). *Elements of petroleum geology* (2nd ed.). San Diego: Academic.
- Sheriff, R. E. (1980). Nomogram for Fresnel-Zone Calculation. *Geophysics*, 45(5), 968-972. doi: Doi 10.1190/1.1441101
- Sheriff, R. E. (1985). Aspects of Seismic Resolution. *Seismic Stratigraphy II: American Association of Petroleum Geologists, Memoir 39*, 1-10.
- Sheriff, R. E. (2006). *Encyclopedic dictionary of applied geophysics* (5th ed.). Tulsa: Society of Exploration Geophysicists.
- Sinclair, A. J., & Blackwell, G. H. (2002). *Applied mineral inventory estimation*. Cambridge ; New York: Cambridge University Press.
- Spencer, A. M., & Larsen, V. B. (1990). Fault Traps in the Northern North-Sea. *Tectonic Events Responsible for Britains Oil and Gas Reserves*, 55, 281-298.
- Subrahmanyam, D., & Rao, P. H. (2008). Seismic Attributes- A Review. *7th International Conference & Exposition of Petroleum Geophysics*, 398.
- Surlyk, F., Dons, T., Clausen, C. K., & Higham, J. (2003). Upper Cretaceous. In D. Evans, C. Graham, A. Armour, & P. Bathurst (Eds.), *The Millennium Atlas: petroleum geology of the central and northern North Sea* (pp. 213-233): The Geological Society of London.
- Svendsen, J. I., Alexanderson, H., Astakhov, V. I., Demidov, I., Dowdeswell, J. A., Funder, S., . . . Stein, R. (2004). Late quaternary ice sheet history of northern Eurasia. *Quaternary Science Reviews*, 23(11-13), 1229-1271.
- Taner, M. T. (2001). Seismic Attributes. *Canadian Society of Exploration Geophysics Recorder (CSEG)*, 48-56.
- Twiss, R. J., & Moores, E. M. (2007). *Structural geology*.
- Vail, P. R. (1987). Seismic stratigraphy interpretation using sequence stratigraphy (pp. 1-10).
- Veeken, P. C. H. (1996). The Cenozoic fill of the North Sea basin (UK sector 56-62 degrees N), a seismic stratigraphic study with emphasis on Paleogene massflow deposits. *Geologie En Mijnbouw*, 75(4), 317-340.
- Veeken, P. C. H. (2007). *Seismic stratigraphy, basin analysis and reservoir characterisation*. Amsterdam: Elsevier.

- Veeken, P. C. H., Moerkerken, B. v., & ScienceDirect. (2013). *Seismic stratigraphy and depositional facies models*.
- Zanella, E., & Coward, M. P. (2003). Structural framework. In D. Evans, C. Graham, A. Armour, & P. Bathurst (Eds.), *The Millennium Atlas: petroleum geology of central and northern North Sea* (pp. 45-59): The Geological Society of London.
- Ziegler, P. A. (1975). Geologic Evolution of North-Sea and Its Tectonic Framework. *Aapg Bulletin-American Association of Petroleum Geologists*, 59(7), 1073-1097.
- Ziegler, P. A. (1989). Evolution of the Arctic - North-Atlantic Rift System. *Earthquakes at North-Atlantic Passive Margins : Neotectonics and Postglacial Rebound*, 266, 37-38.
- Ziegler, P. A. (1992). North-Sea Rift System. *Tectonophysics*, 208(1-3), 55-75. doi: Doi 10.1016/0040-1951(92)90336-5

8 Appendix A

8.1 Attributes composite line 1a

8.1.1 Envelope

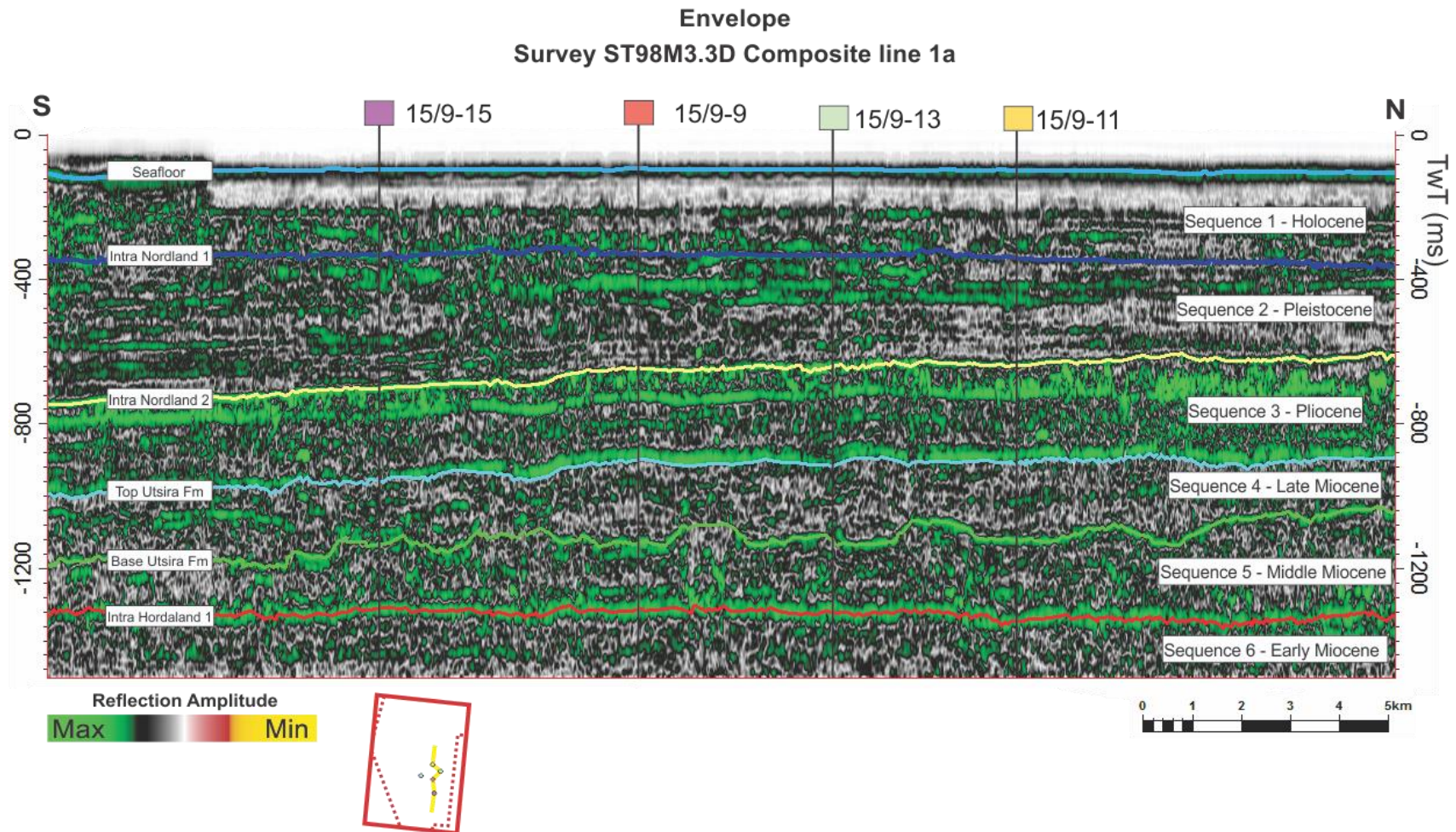


Figure 8.1: Envelope attribute on composite line 1a. The interpreted horizons is indicated to the left, and sequences to the right in the seismic section.

8.1.2 Cosine of phase

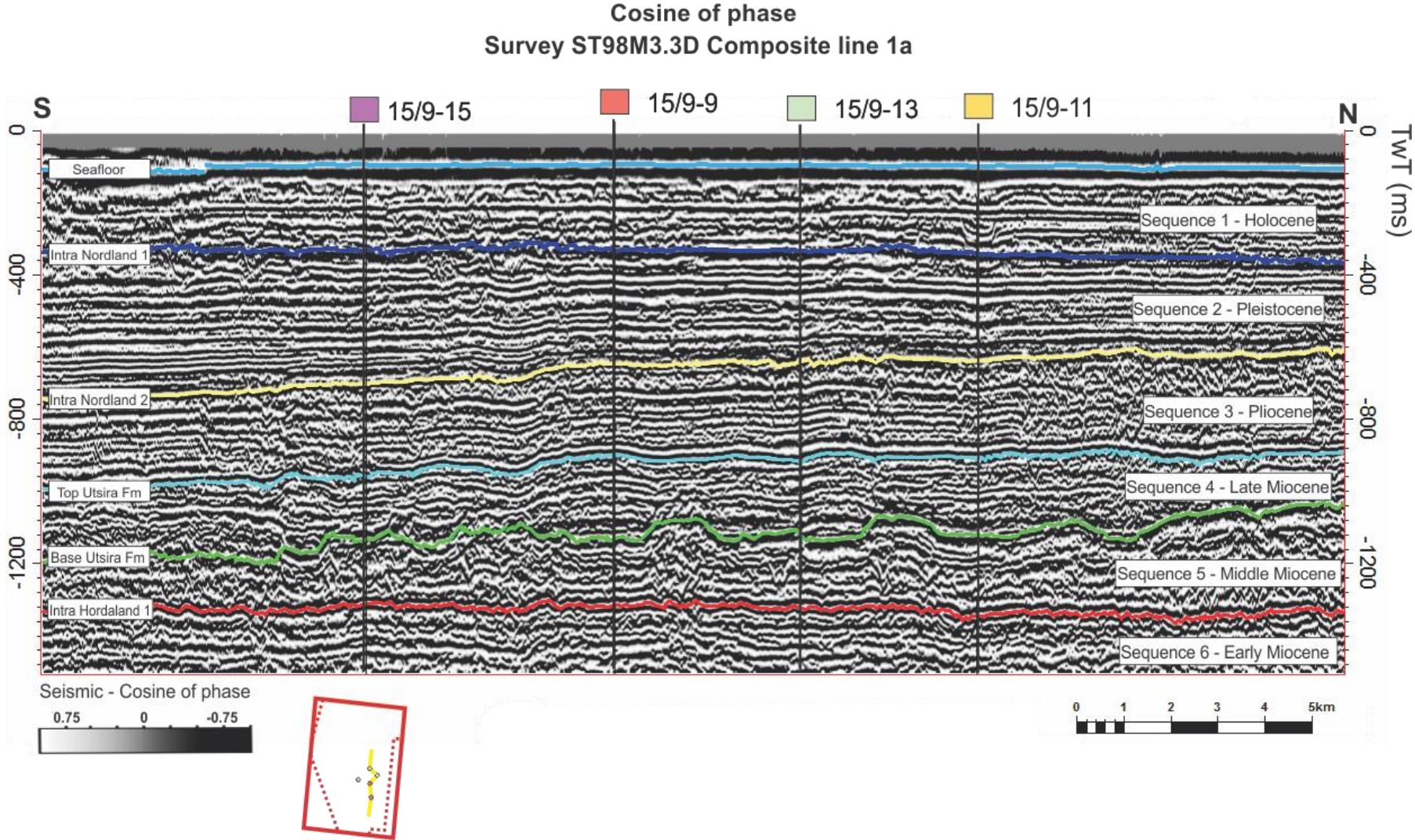


Figure 8.2: Cosine of phase attribute on composite line 1a. The interpreted horizons is indicated to the left, and sequences to the right in the seismic section.

8.1.3 Dominant frequency

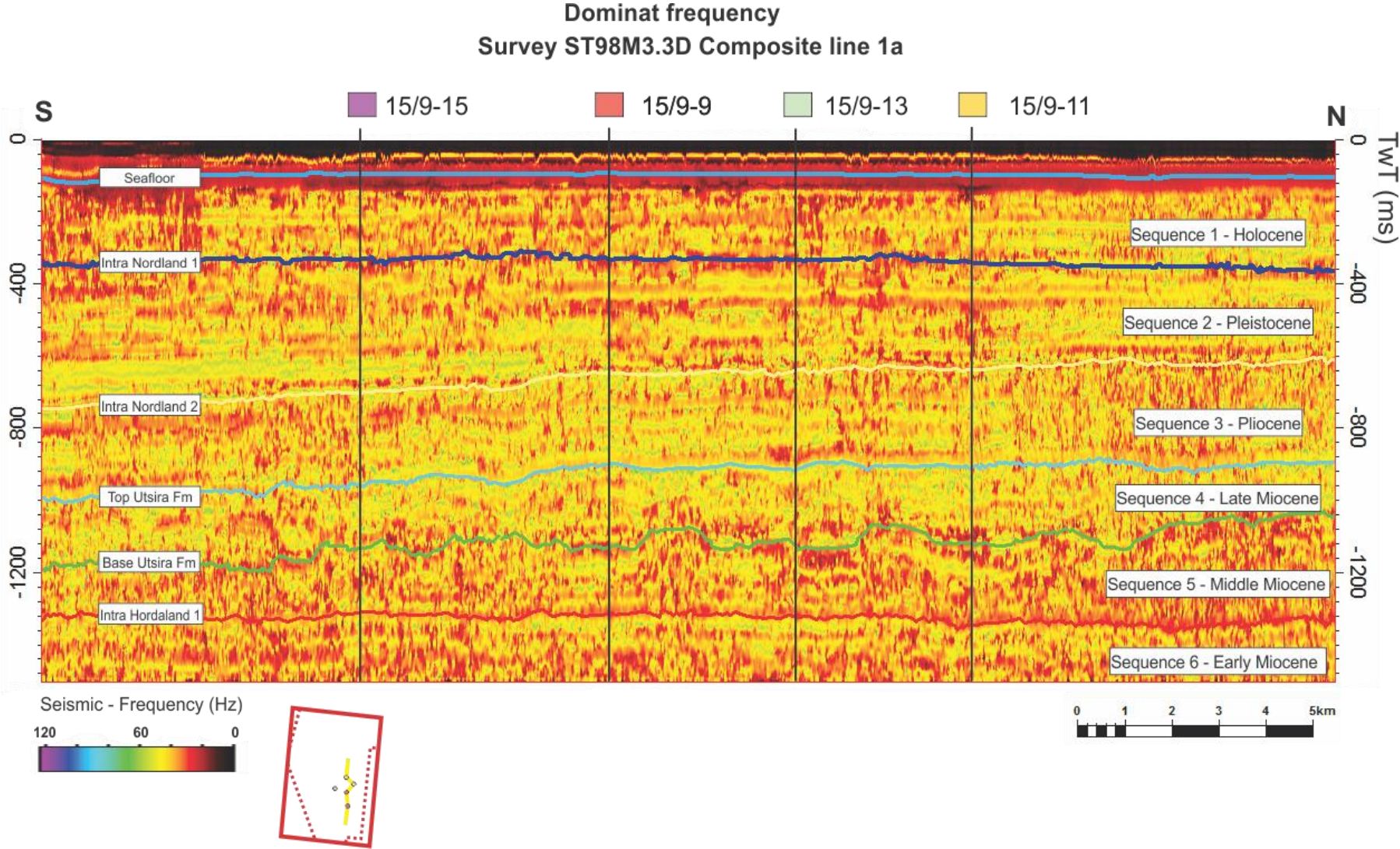


Figure 8.3: Dominant frequency attribute on composite line 1a. The interpreted horizons is indicated to the left, and sequences to the right in the seismic section.

8.1.4 Variance

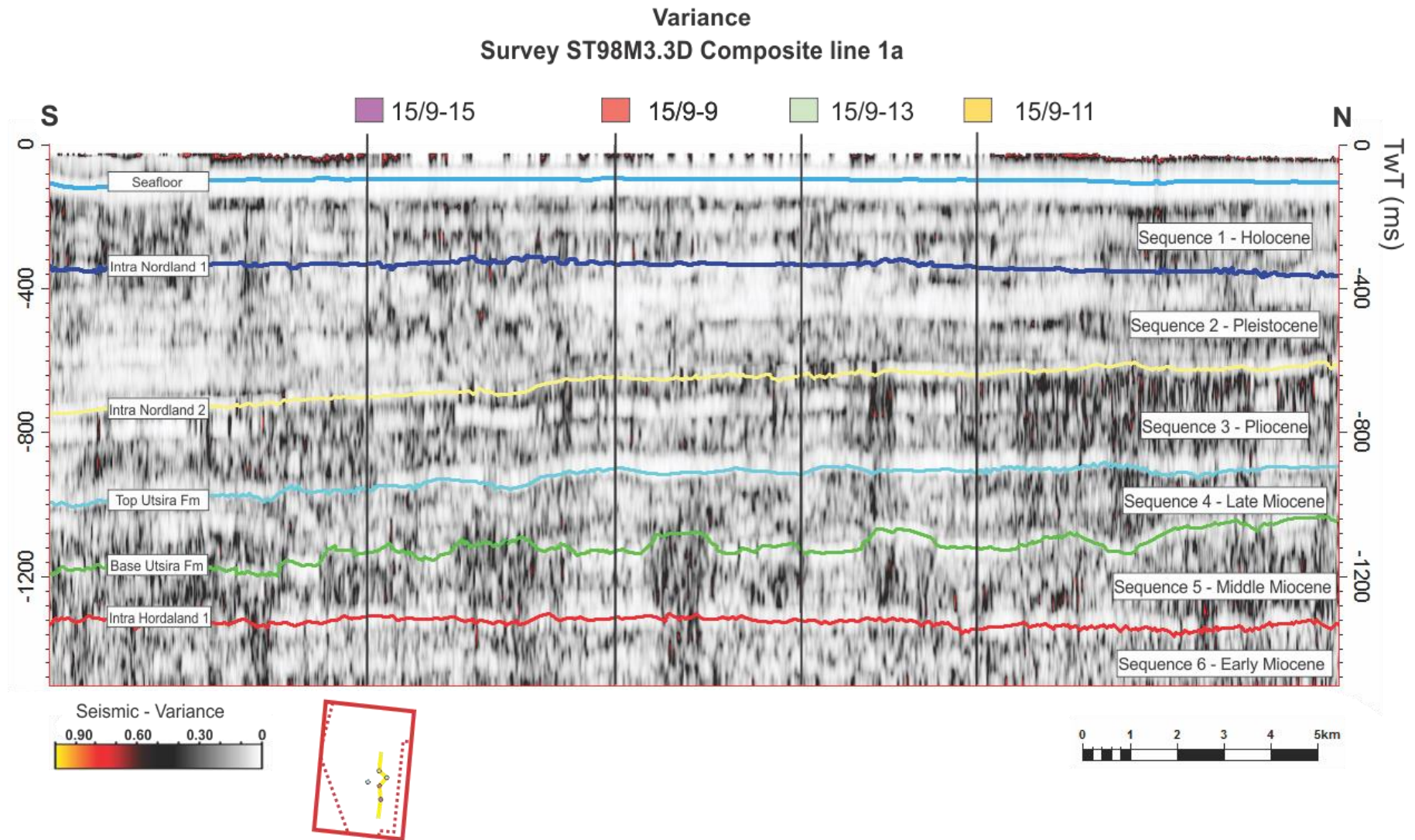


Figure 8.4: Variance attribute on composite line 1a. The interpreted horizons is indicated to the left, and sequences to the right in the seismic section.

8.1.5 Variance with envelope

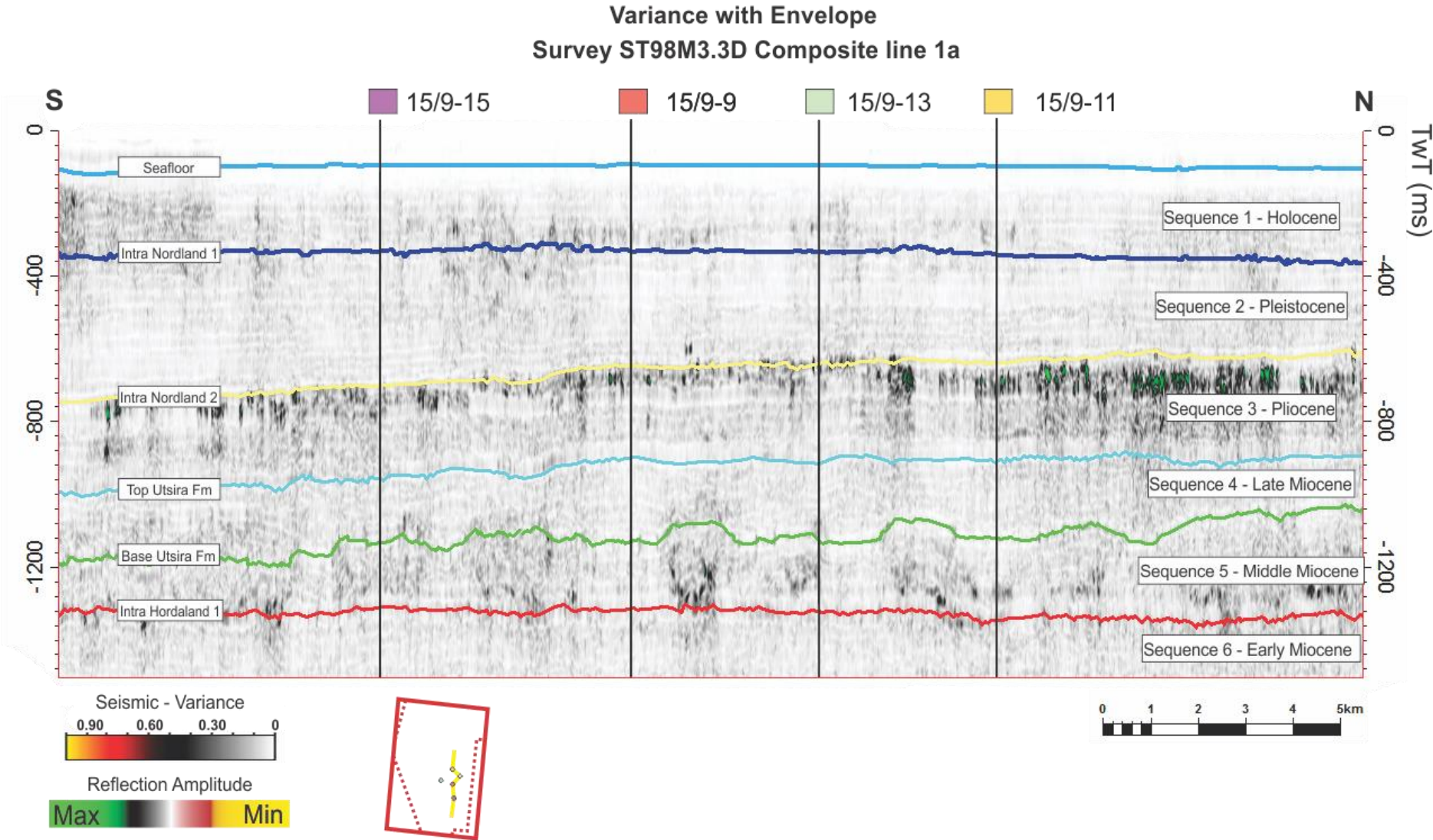


Figure 8.5: Variance with the envelope attribute on composite line 1a. The interpreted horizons is indicated to the left, and sequences to the right in the seismic section.

8.1.6 RMS amplitude

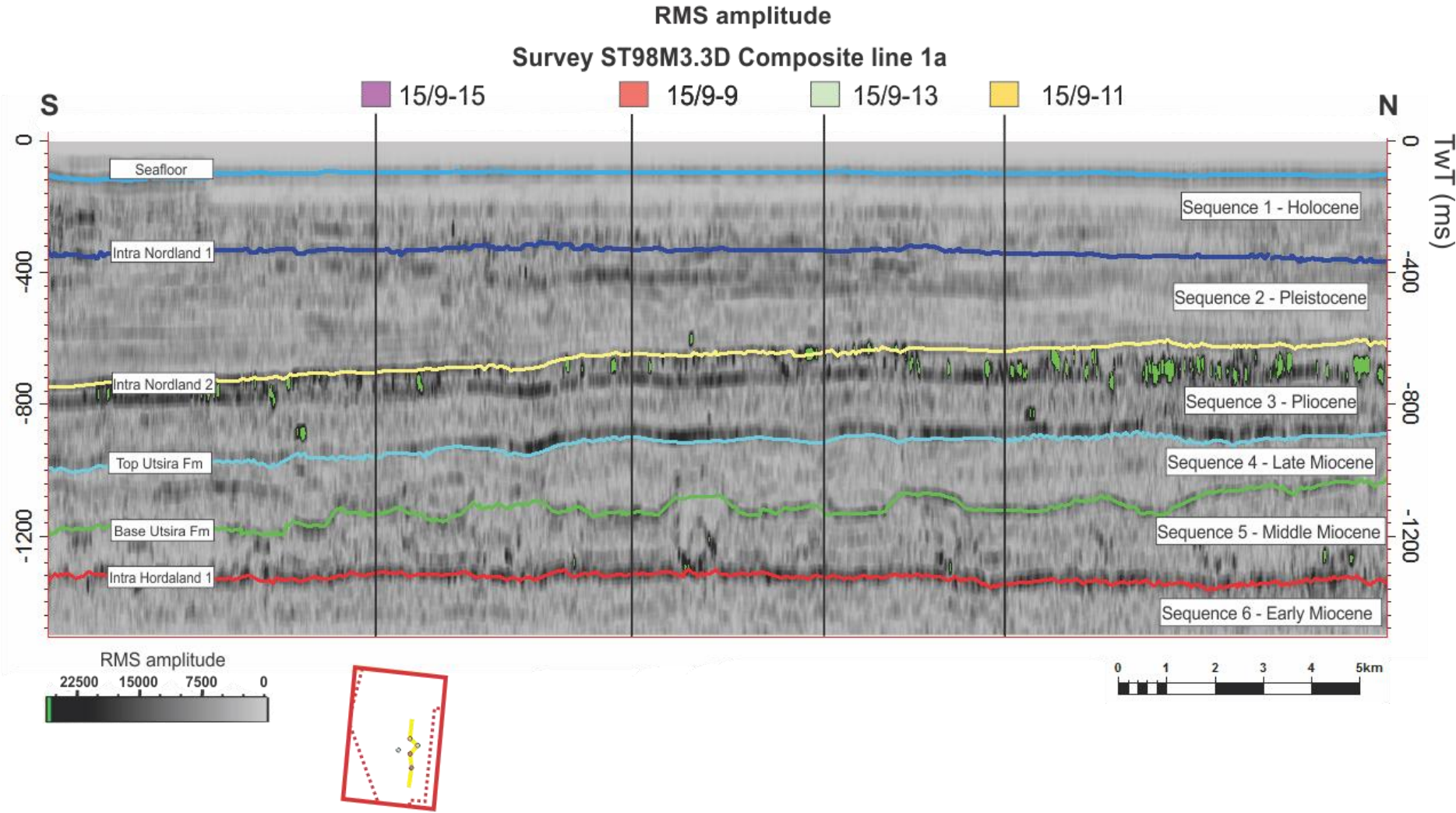


Figure 8.6: RMS attribute on composite line 1a. The interpreted horizons is indicated to the left, and sequences to the right in the seismic section.

8.2 Attributes crossline 2875

8.2.1 Envelope

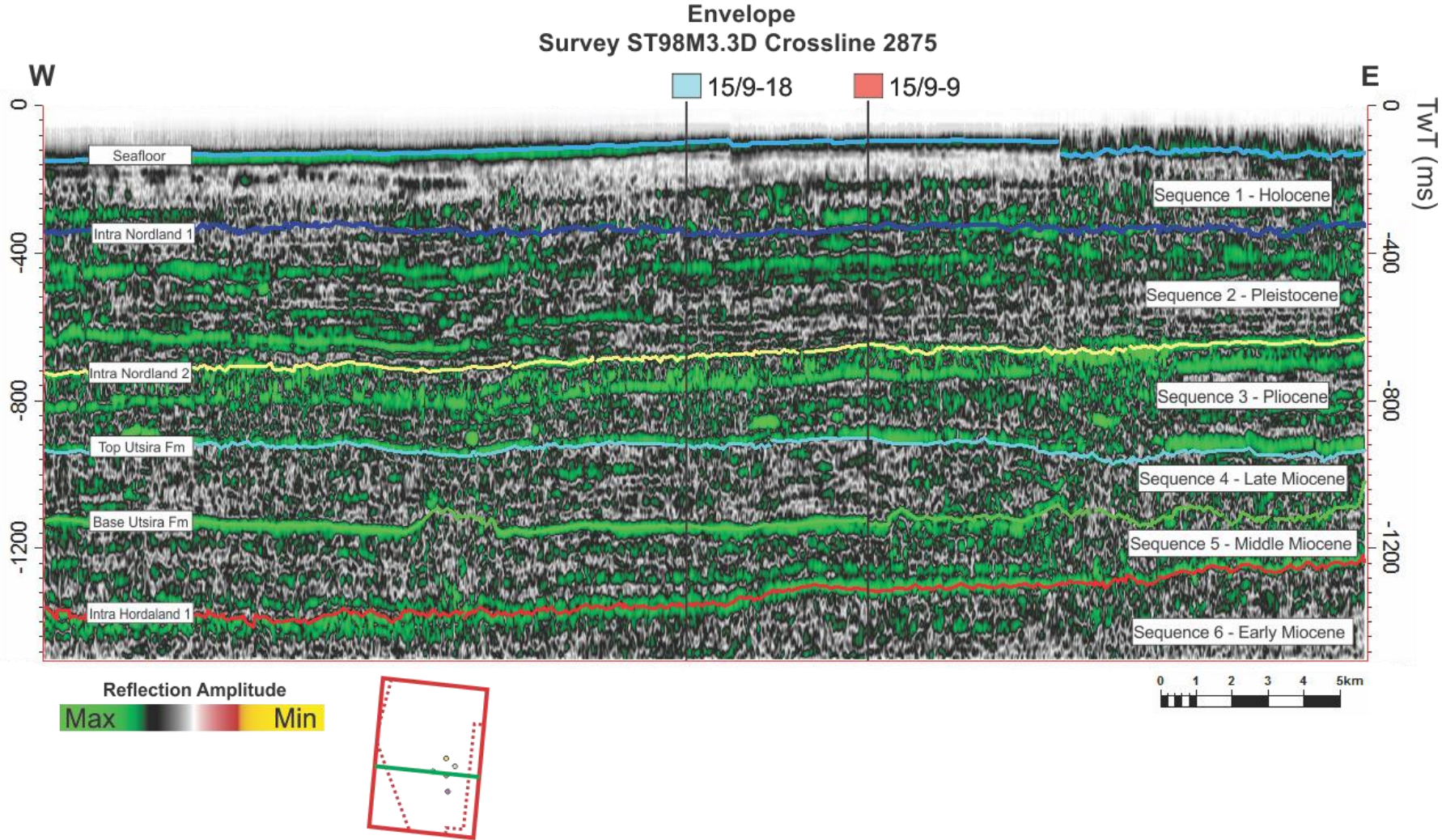


Figure 8.7: Envelope attribute on crossline 2875. The interpreted horizons is indicated to the left, and sequences to the right in the seismic section.

8.2.2 Cosine of phase

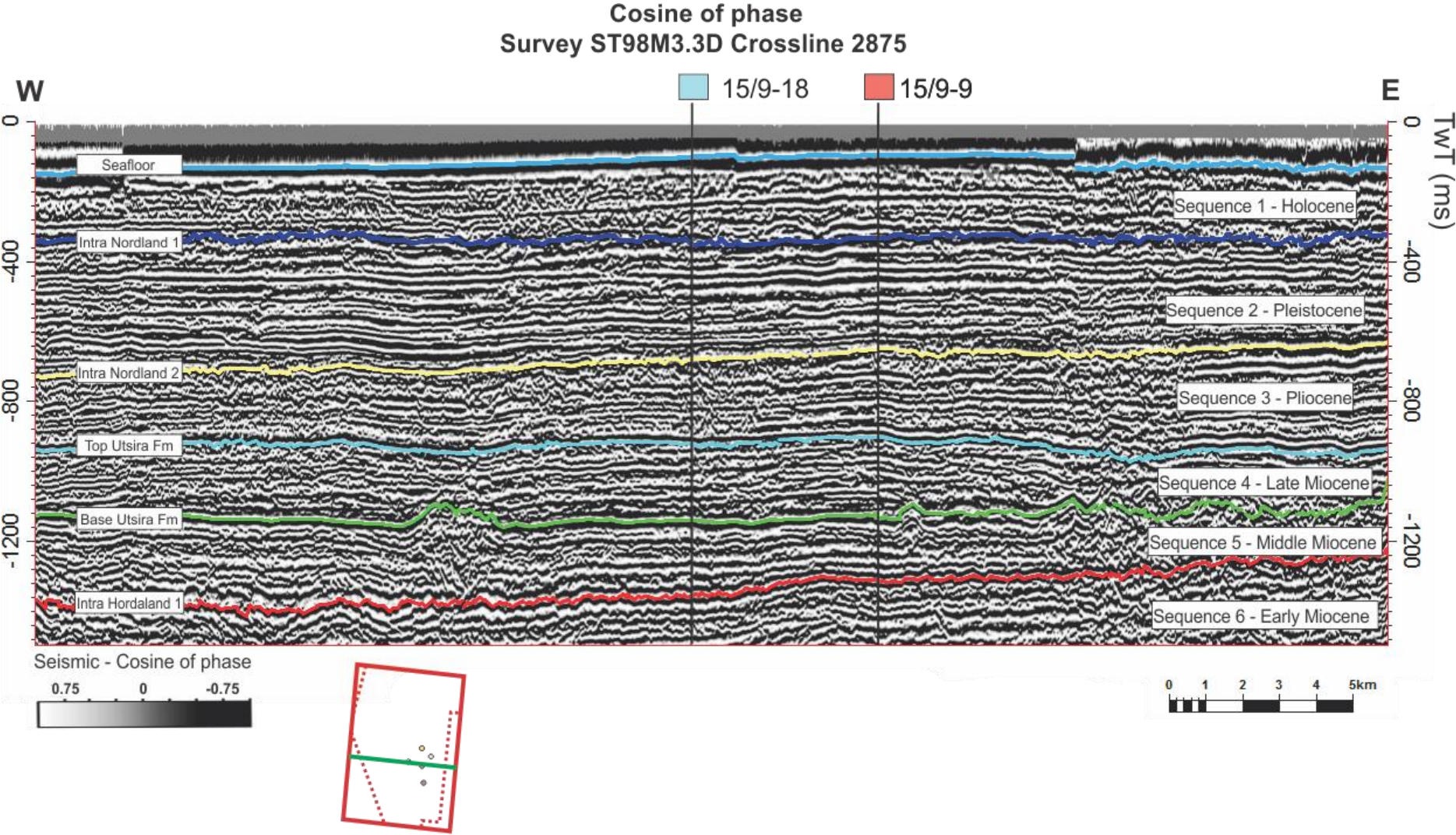


Figure 8.8: Cosine of phase attribute on crossline 2875. The interpreted horizons is indicated to the left, and sequences to the right in the seismic section.

8.2.3 Dominant frequency

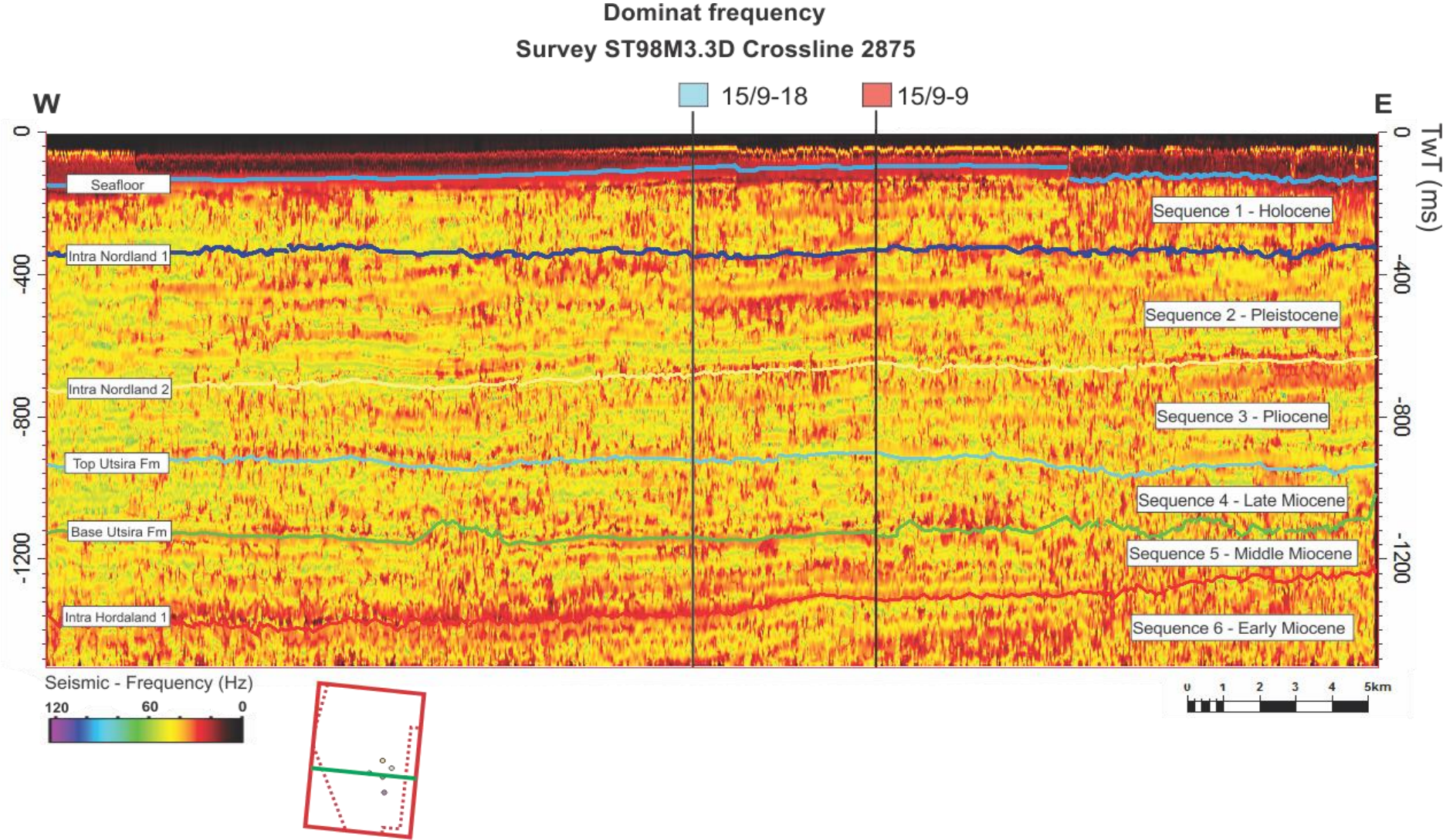


Figure 8.9: Dominant frequency attribute on crossline 2875. The interpreted horizons is indicated to the left, and sequences to the right in the seismic section.

8.2.5 Variance with envelope

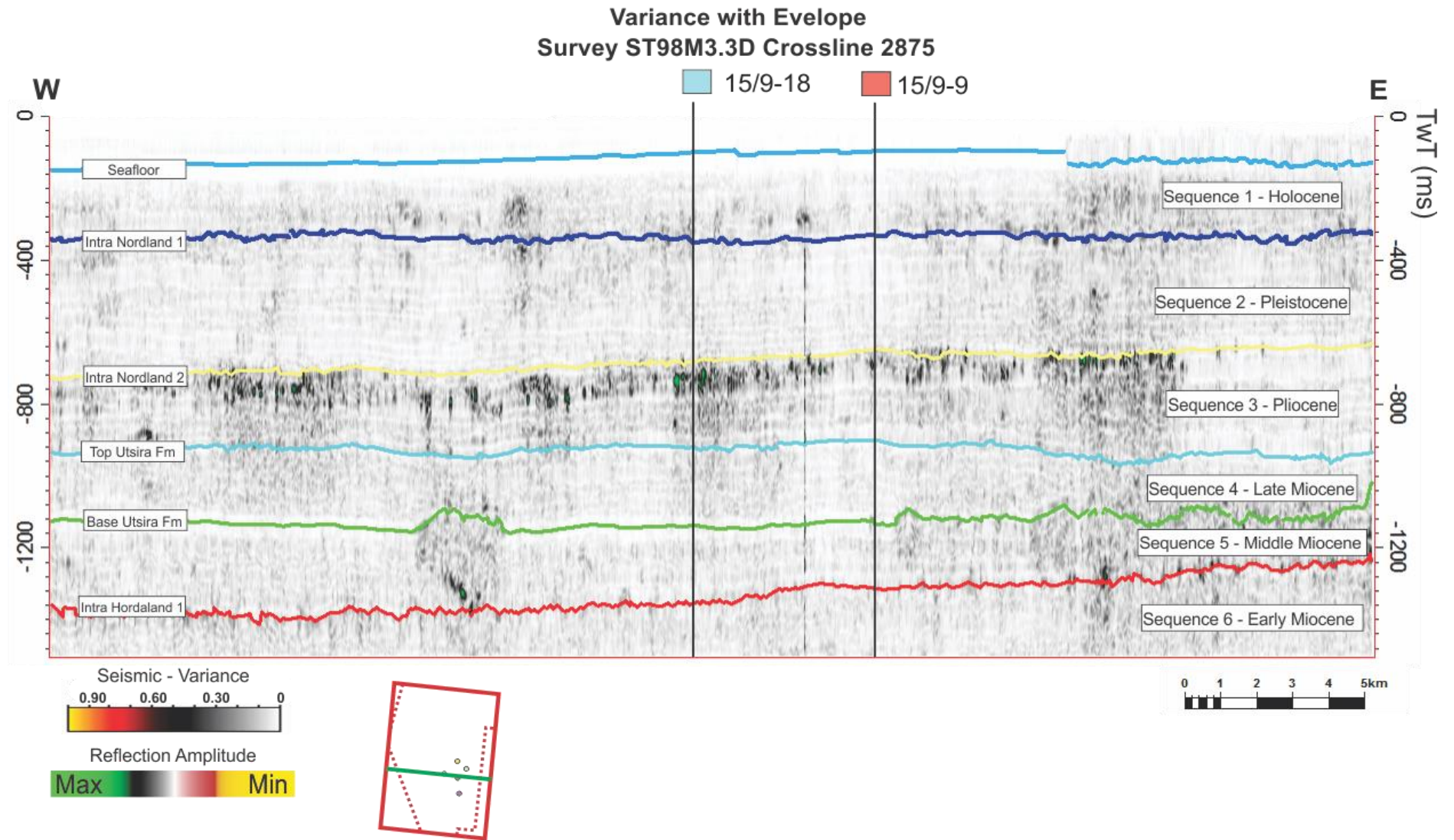


Figure 8.11: Variance with envelope attribute on crossline 2875. The interpreted horizons is indicated to the left, and sequences to the right in the seismic section.

8.2.6 RMS amplitude

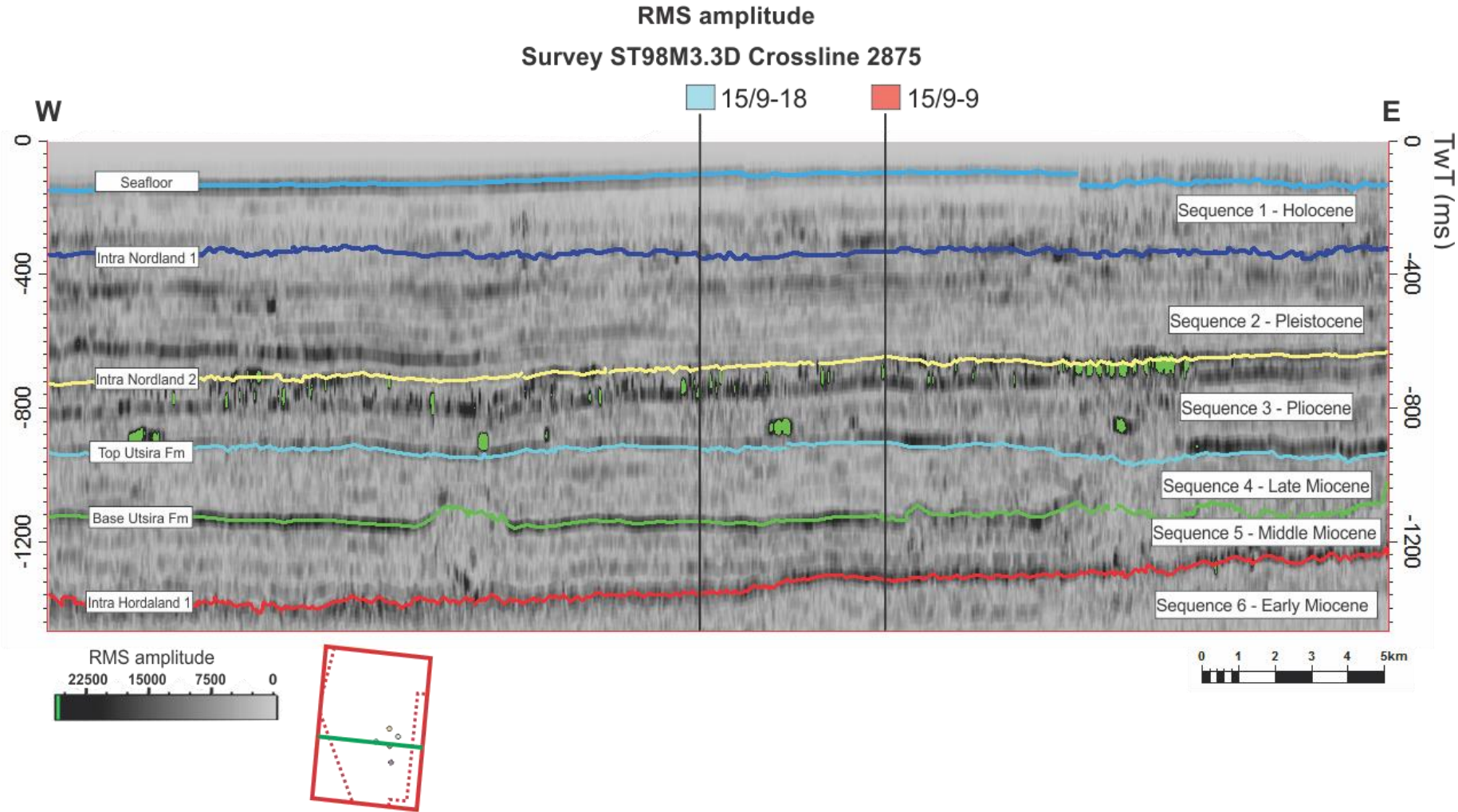


Figure 8.12: RMS attribute on crossline 2875. The interpreted horizons is indicated to the left, and sequences to the right in the seismic section.

